CONSEJO SUPERIOR DE INVESTIGACIONES CIENTÍFICAS

ESTACIÓN EXPERIMENTAL DEL ZAIDÍN

UNIVERSIDAD DE GRANADA

PROGRAMA DE DOCTORADO EN BIOLOGÍA FUNDAMENTAL Y DE SISTEMAS

DOCTORAL THESIS

C-DI-GMP REGULATION OF CYTOPLASMIC AND EXTRACELLULAR PROTEINS IN PLANT-ASSOCIATED BACTERIA

ARIANA CASAS ROMÁN

2024

Thesis supervisors:

Dr. Juan Sanjuán Pinilla

Dra. Mª Trinidad Gallegos Fernández

Editor: Universidad de Granada. Tesis Doctorales
Autor: Ariana Casas Román
ISBN: 978-84-1195-407-5
URI: https://hdl.handle.net/10481/94656

Esta Tesis Doctoral ha sido realizada en el Departamento del Suelo y de la Planta (Grupo de investigación 'Interacciones Planta-Bacteria') de la Estación Experimental del Zaidín (CSIC).

Para su realización, se contó con la financiación de la 'Ayuda para contratos predoctorales para la formación de doctores' PRE2018-083387, adscrita al proyecto BIO2017-83533-P (ambos financiados por el Ministerio de Ciencia, Innovación y Universidades, la Agencia Estatal de Investigación y el Fondo Social Europeo).

Durante la tesis doctoral se realizó una estancia breve en el grupo de investigación coordinado por la Dra. Laura Baldomà Llavinés en la Facultat de Farmàcia i Ciencies de l'Alimentació de la Universitat de Barcelona (septiembre-diciembre 2020).

Parte de los resultados expuestos en esta Tesis Doctoral han sido presentados en los siguientes congresos y publicaciones:

Publicaciones

Casas-Román, A., Lorite, M.J., Werner, M., Muñoz, S., Gallegos, M.T., Sanjuán, J. 2024. The *gap* gene of *Rhizobium etli* is required for both free life and symbiosis with common beans. Accepted for publication in *Microbiological Research*, https://doi.org/10.1016/j.micres.2024.127737

Casas-Román, A., Lorite, M.J., Sanjuán, J., Gallegos, M.T. 2024. Two glyceraldehyde-3-phosphate dehydrogenases with distinctive roles in *Pseudomonas syringae* pv. tomato DC3000. *Microbiological Research* 278, 127530. https://doi.org/10.1016/j.micres.2023.127530

Lorite, M.J., Casas-Román, A., Girard, L., Encarnación, S., Díaz-Garrido, N., Badía, J., Baldomá, L., Pérez-Mendoza, D., Sanjuán, J. 2023. Impact of c-di-GMP on the Extracellular Proteome of *Rhizobium etli*. *Biology (Basel)* 12, 44. https://doi.org/10.3390/biology12010044

Congresos

Casas-Román, A., Lorite, M.J., Gallegos, M.T., Sanjuán, J. 2024. Roles of glyceraldehyde-3-phosphate dehydrogenases in plant-interacting bacteria (comunicación oral). *I Meeting of the "Andalucía AGRO-HUB" PhD students*, Málaga, España.

Casas-Román, A., Lorite, M.J., Gallegos, M.T., Sanjuán, J. 2023. Two glyceraldehyde-3-phosphate dehydrogenases with distinctive roles in *Pseudomonas syringae* pv. tomato DC3000 (póster). *II Jornada de la Juventud Investigadora de la Estación Experimental del Zaidín*, Granada, España.

Casas-Román, A., Lorite, M.J., Muñoz, S., Gallegos, M.T., Sanjuán, J. 2022. Characterization of the glyceraldehyde-3-phosphate dehydrogenase protein in *Rhizobium etli*" (comunicación oral). *I Spanish-Portuguese Congress on Beneficial Plant-Microbe Interactions and XVIII National Meeting of the Spanish Society of Nitrogen Fixation*, Oeiras, Portugal.

Casas-Román, A., Lorite, M.J., Muñoz, S., Gallegos, M.T., Sanjuán, J. 2022. Funciones de la gliceraldehído-3-fosfato deshidrogenasa en bacterias que interaccionan con plantas (comunicación oral y póster). *XIII Reunión de Microbiología molecular - SEM*, Granada, España.

Casas-Román A., Werner, M., Lorite, M.J., Muñoz, S., Ferreiro, M.D., Gallegos, M.T., Sanjuán, J. 2021. Papel de la gliceraldehído-3-fosfato deshidrogenasa en las interacciones planta- bacteria (comunicación oral). *IX Reunión de Microbiología de Plantas - SEM*, formato virtual.

Casas-Román, A., Werner, M., Lorite, M.J., Muñoz, S., Pérez-Mendoza, D., Girard, L., Sanjuán, J. 2019. Importancia del gen *gap* de *Rhizobium etli* para la simbiosis con *Phaseolus vulgaris* (póster). *XVII National Meeting of the Spanish Society of Nitrogen Fixation (SEFIN*), Madrid, España.

RESUMEN

La agricultura es uno de los factores predominantes que contribuyen a la crisis medioambiental actual. En este contexto, la fijación biológica de nitrógeno (FBN) aparece como un proceso crucial que ofrece ventajas tanto ecológicas como económicas al fomentar la producción agrícola sostenible mediante la reducción de la dependencia en fertilizantes nitrogenados. La simbiosis entre bacterias rizobiales y plantas leguminosas ejemplifica esto, proporcionando una vía ambientalmente sostenible para el cultivo agrícola. Por otro lado, las enfermedades producidas por bacterias fitopatógenas representan una amenaza cada vez mayor para el rendimiento de los cultivos, lo que resulta en pérdidas agrícolas sustanciales. Aunque el resultado es completamente diferente para los dos tipos de interacciones, los mecanismos moleculares implicados en la comunicación entre ambas bacterias y sus plantas huésped parecen ser similares. La presente tesis doctoral se centra en dos bacterias que representan estas interacciones: el simbionte de la judía común *Rhizobium etli* CE3 (Ret), y la bacteria fitopatógena *Pseudomonas syringae* pv. tomato DC3000 (Pto).

El segundo mensajero diguanilato cíclico (c-di-GMP) actúa como un mensajero bacteriano que controla la transición entre diferentes tipos de vida, estando involucrado en motilidad, formación de biopelículas y en la secreción de exopolisacáridos (EPS) y proteínas. Este trabajo se centra en proteínas que están diferencialmente reguladas por c-di-GMP en bacterias simbióticas y patógenas, siguiendo un estudio previo realizado por Lorite *et al*. (2023) sobre el impacto de este mensajero en el proteoma extracelular de *R. etli*. En un primer enfoque se realizó una comparativa entre niveles fisiológicos y elevados de c-di-GMP de las proteínas encontradas intracelular y extracelularmente en cultivos de Pto. Además de reforzar su implicación en la formación de biopelículas, la producción de EPS y la movilidad, las proteínas exportadas diferencialmente abundantes presentaron tendencias diferentes en las dos bacterias, lo que resalta la complejidad de sus proteomas y su regulación diferencial.

Un hallazgo destacado del estudio sobre Ret fue que una gran parte de las proteínas citoplasmáticas cuya exportación parecía ser promovida por c-di-GMP habían sido reportadas previamente como proteínas *moonlighting* o multifunción en otros organismos. En el caso de Pto, apareció una tendencia opuesta: la exportación de enzimas metabólicas citoplasmáticas parece disminuir con altos niveles de c-di-GMP. Esto resalta la importancia de la presencia de proteínas citoplasmáticas *moonlighting* fuera de la célula y la regulación de su exportación. Entre las potenciales proteínas *moonlighting* citoplasmáticas, el estudio de la gliceraldehído-3-fosfato deshidrogenasa (Gap) resulta interesante ya que el c-di-GMP promueve su exportación en Ret. Como proteína *housekeeping* ampliamente conservada y

para la que se han descrito funciones *moonlightin*g en una gran variedad de bacterias, Gap aparece como una candidata prometedora para poseer funciones *moonlighting* similares en los dos tipos de bacterias. Sin embargo, nuestros resultados en Pto han mostrado que la exportación de Gap1 y Gap2 no experimenta cambios significativos bajo niveles altos de c-di-GMP. Sin embargo, su estudio continuó siendo interesante ya que ambas proteínas Gap se encontraron en el extrasoma en diferentes condiciones de cultivo, lo que sugiere la existencia de posibles funciones *moonlighting* en esta bacteria.

La caracterización genética y funcional de las proteínas Gap presentes en Pto y Ret desveló diversas implicaciones en ambas bacterias. A nivel metabólico, hay una clara disparidad ya que Ret posee una sola proteína Gap responsable de la actividad tanto glucolítica como gluconeogénica, mientras que Pto posee dos enzimas diferentes y no intercambiables para cada actividad, siendo Gap1 glucolítica y Gap2 gluconeogénica. Se ha demostrado que el tercer gen páralogo (*gap3/epd*) presente en Pto carece de actividad Gap, pero es indispensable para el metabolismo de la vitamina B6, mostrando actividad eritrosa-4-fosfato deshidrogenasa, por lo que se denominó *epd*. En Pto, ambas enzimas Gap exhibieron características funcionales distintas dependiendo del estado fisiológico de la bacteria. Gap1 ejerce un papel importante en motilidad, producción de biosurfactantes y formación de biopelículas, mientras que únicamente Gap2 parece ser esencial para el crecimiento de la bacteria en plantas de tomate. En Ret, se observó que se necesita una proteína Gap activa en todas las etapas de la simbiosis con su planta huésped, *Phaseolus vulgaris*. Ambas actividades metabólicas parecen contribuir a la aptitud bacteriana durante las etapas tempranas e intermedias de la interacción, mientras que la actividad gluconeogénica de Gap parece ser crítica para la invasión del nódulo y la fijación de nitrógeno. Aunque la proteína Gap de Ret se secreta de manera relacionada con el c-di-GMP, no se observó ningún efecto en fenotipos relacionados, como la floculación, la formación de biopelículas o la producción de EPS. Curiosamente, a pesar de las diferencias en las proteínas Gap entre las dos bacterias, la similitud de sus genes *gap* permitió una restauración casi completa del fenotipo silvestre cuando se complementaron intercambiándolas.

El estudio de la exportación de Gap aparece como especialmente interesante ya que su translocación fuera de la célula, que no puede atribuirse únicamente a sus funciones metabólicas primarias, sugiere posibles roles multifuncionales. En el caso de Pto, Gap1 apareció consistentemente exportada independientemente de la composición del medio y de los niveles de c-di-GMP. Por otro lado, Gap2 solo se exportaba en medios específicos y dependiendo de su abundancia intracelular. Estos hallazgos sugieren la probabilidad de roles *moonlighting* para ambas proteínas; sin embargo, los mecanismos que promueven su exportación siguen siendo desconocidos. En el caso de Ret ya se había detectado

que Gap se exportaba diferencialmente bajo altos niveles de c-di-GMP, lo que impulsó al examen de sus posibles mecanismos de exportación. No se encontraron evidencias de la exportación de Gap a través de lisis celular o vesículas de membrana en Ret. Sin embargo, Gap se encontró localizada en el citoplasma y asociada tanto a las membranas internas como externas de la bacteria. Esto, junto con la observación de un aumento en el número de proteoformas extracelulares inducido por c-di-GMP, sugiere la participación de mecanismos de exportación no clásicos o no canónicos. Dado que las modificaciones post-traduccionales (PTM) desempeñan un papel crucial en la exportación y la emergencia de funciones *mooonlighting* en proteínas citoplasmáticas, se realizaron investigaciones preliminares sobre posibles PTMs presentes en la proteína Gap de Ret, que revelaron la presencia de residuos fosforilados en la proteína Gap intracelular. Estos resultados sugieren un posible vínculo entre el diguanilato cíclico, las PTMs y la exportación de proteínas citoplasmáticas, lo que abre vías para el estudio de otras PTMs que también podrían estar implicadas en los roles *moonlighting* de la proteína Gap.

En conclusión, esta tesis doctoral aporta nuevos conocimientos sobre el papel del c-di-GMP en la regulación y exportación de proteínas, tanto en bacterias simbióticas como fitopatógenas. Centrándose en las proteínas Gap y sus posibles funciones *moonlighting*, se destacan las principales similitudes y diferencias entre los dos tipos de bacterias.

SUMMARY

Agriculture is a predominant factor contributing to the ongoing environmental crisis. In this context, biological nitrogen fixation (BNF) emerges as a pivotal process offering economic and ecological advantages by fostering sustainable agricultural production through reduced dependence on nitrogen fertilizers. The symbiotic bond between *Rhizobium* bacteria and leguminous plants embodies this, providing an environmentally sustainable avenue for agricultural cultivation. Conversely, the threat posed by phytopathogenic bacteria-induced diseases increasingly endangers crop yields, resulting in substantial agricultural losses. Although the outcome is completely different for the two types of interactions, common molecular mechanisms that mediate communication between the interacting partners appear to be involved. The present thesis is centered in two bacteria representing these interactions: the common bean symbiont *Rhizobium etli* CE3 (Ret), and the phytopathogen *Pseudomonas syringae* pv. tomato DC3000 (Pto).

The second messenger cyclic diguanylate (c-di-GMP) acts as a bacterial messenger that controls the transition between different lifestyles, being involved in motility, biofilm formation or exopolysaccharide (EPS) and protein secretion. This work is focused on proteins differentially regulated by c-di-GMP in symbiotic and pathogenic bacteria following a previous study about its impact on the extracellular proteome of Ret by Lorite *et al.* (2023). In a first approach, a study of the proteins found in the intracellular and extracellular environments of Pto under physiological *versus* increased c-di-GMP levels was performed. Asides from reinforcing its implication in biofilm formation, EPS production and motility, the differentially abundant exported proteins presented different trends between the two bacteria, which highlights the complexity of their proteomes and the differential regulation therein.

A notable finding from the study on Ret was that a large fraction of the cytoplasmic proteins whose export appeared to be promoted by c-di-GMP had been previously reported as moonlighting or multifunctional proteins in other organisms. In the case of Pto, an opposed contrasting trend emerged: the export of a larger number of cytoplasmic metabolic enzymes appeared to be downregulated by c-di-GMP. Overall, this highlights the importance of the presence of potential moonlighting cytoplasmic proteins outside the cell, and the regulation of their export. Among the potential moonlighting proteins, glyceraldehyde-3-phosphate dehydrogenase (Gap) was a compelling candidate for involvement of c-di-GMP in its regulation in plant-interacting bacteria, since this second messenger had been found to promote its exportation in Ret. As a widely conserved housekeeping protein with moonlighting functions described in a diverse array of bacteria, Gap appeared as promising candidate for similar functional roles in the two bacteria under

study. Nevertheless, our results with Pto evidenced that the export of Gap1 and Gap2 did not experience significant changes under high c-di-GMP levels. Its study remained interesting, however, as both Gap proteins were found to be exported under different culture conditions, suggesting the existence of potential moonlighting roles also in this bacterium.

The genetic and functional characterization of the Gap proteins present in Pto and Ret uncovered diverse implications in both bacteria. On a metabolic level, there is a clear disparity between the two bacteria since Ret harbours a single Gap protein responsible for both glycolytic and gluconeogenic activities, whereas Pto possesses distinct and non-interchangeable enzymes for each activity, being Gap1 glycolytic and Gap2 gluconeogenic. A third potential paralogue gene (*gap3/epd*) present in Pto was proved to lack Gap activity but be indispensable for vitamin B6 metabolism displaying erythrose-4-phosphate dehydrogenase activity, thus referred as *epd*. In Pto, both Gap enzymes exhibited distinct functional characteristics depending on the bacterium physiological state. Gap1 presented a substantial role in motility, biosurfactant production and biofilm formation, whereas only Gap2 appeared to be essential for growth on tomato plants. In Ret, an active Gap protein was found to be required throughout all stages of the symbiosis with its host plant *Phaseolus vulgaris*. Both metabolic activities appeared to contribute to bacterial fitness during early and intermediate stages of the interaction, whereas Gap gluconeogenic activity appeared to be critical for nodule invasion and nitrogen fixation. Although the Ret Gap protein is secreted in a c-di-GMP related manner, no involvement in free-living c-di-GMP related phenotypes, such as flocculation, biofilm formation or EPS production, was observed. Interestingly, despite the differences in Gap proteins between the two bacteria, the similarity of their *gap* genes enabled almost complete restoration of the wild type phenotype when interchangeably complemented.

Exploring Gap export presented a compelling research direction since its translocation outside the cell, which cannot be solely attributed to its primary metabolic functions, suggests potential moonlighting roles. In the case of Pto, Gap1 consistently appeared to be exported independently of the medium composition and c-di-GMP levels. Gap2, on the other hand, was only exported in specific media and correlated with its intracellular abundance. These findings underscore the likelihood of moonlighting roles for both proteins, yet, the mechanisms driving their exportation remain elusive. In the case of Ret, Gap had already been detected to be differentially exported under high c-di-GMP levels, which prompted an examination of potential export mechanisms. No evidence of Gap export through cell lysis or membrane vesicles in Ret was obtained. Instead, Gap was located in the cytoplasm but also associated to both the inner and outer membranes, which together with the observed increased number of extracellular Gap proteoforms induced by c-di-GMP, support the involvement of an active mechanism for Gap exportation in Ret.

Since post-translational modifications (PTMs) can determine proteoform number and diversity, preliminary investigations into potential PTMs present in the Ret Gap protein were performed, revealing the presence of phosphorylated residues in the intracellular Gap protein. The results suggest a link between c-di-GMP, PTMs and the export of cytoplasmic proteins, which could thereby impact the moonlighting roles of the Gap protein.

Overall, this thesis provides insight into the role of c-di-GMP in protein exportation and regulation in both symbiotic and plant-pathogenic bacteria. Focusing on Gap proteins and their possible moonlighting roles, it highlights the similarities and major differences between the two types of bacteria.

TABLE OF CONTENTS

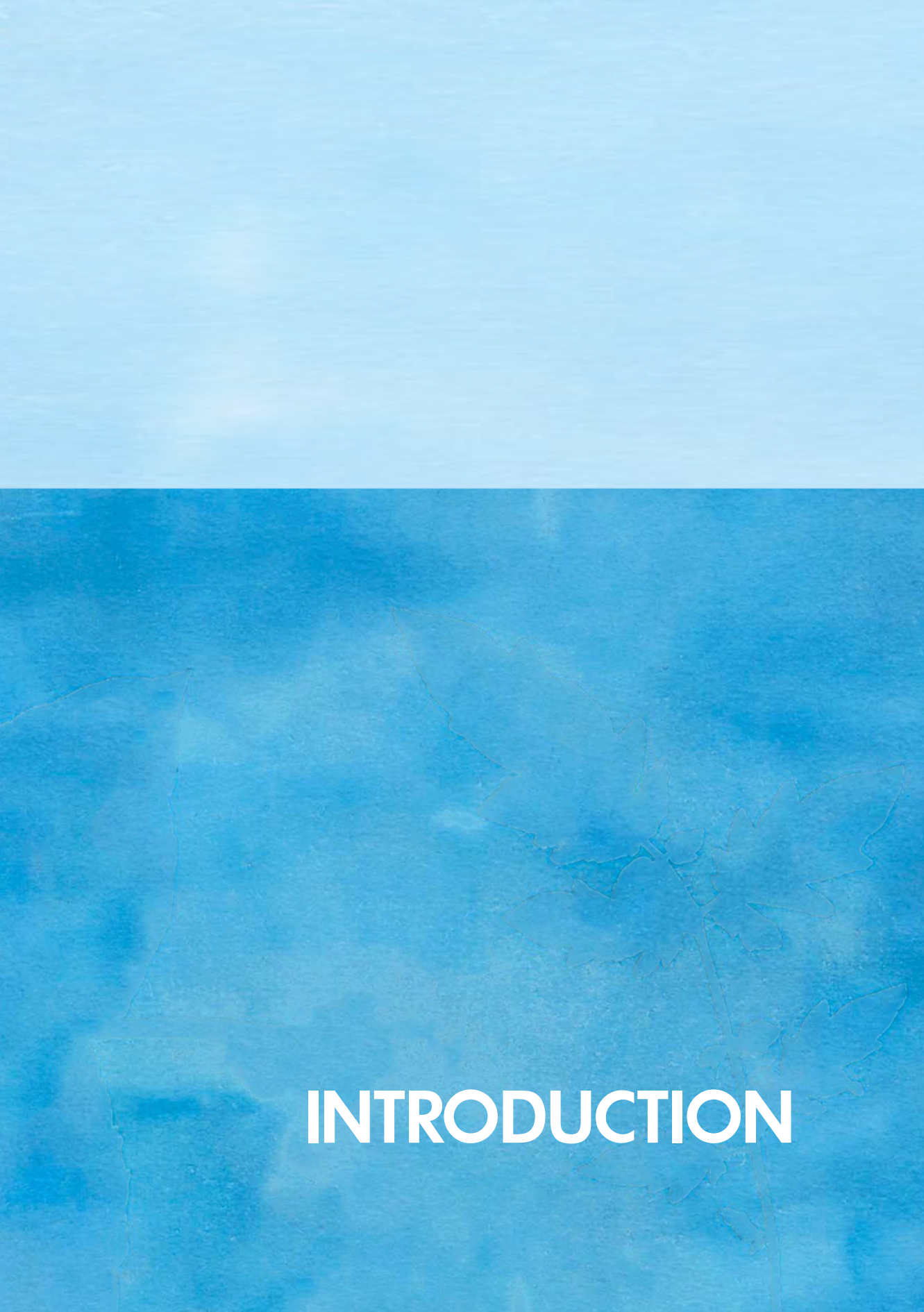

INTRODUCTION

INTRODUCTION

1. GLOBAL PERSPECTIVE ON THE AGROECOLOGICAL CRISIS

In today's context of global change, most of the established "safety planetary boundaries" – that is, limits to Earth system processes that, if crossed, can generate unacceptable environmental changes – have already been transgressed beyond the threshold of uncertainty or high risk. Agriculture stands as a prevailing factor contributing to numerous environmental threats, encompassing climate change, biodiversity loss, degradation of land and freshwater and perturbation of the biogeochemical cycles of nitrogen and phosphorous (Fig. I.1) (Foley *et al*., 2011; Steffen *et al*., 2015; Campbell *et al*., 2017; Richardson *et al*., 2023; Rockström *et al*., 2023). To meet the world's population food security and sustainability needs, the environmental footprint of the agri-food sector must diminish dramatically by halting agricultural expansion and reducing agrochemical inputs while increasing cropping efficiency, shifting diets, and reducing waste (Foley et *al*., 2011).

Agricultural ecosystems were created by humans approximately 12 000 years ago during the development of agriculture to generate a reliable food supply, thereby contributing to the rise of major civilizations. Since their emergence in the Fertile Crescent, agro-ecosystems have proliferated worldwide, covering around 40% of the land surface, with most of this expansion occurring within the last three centuries. In tropical regions, the establishment of new agricultural land has come at the expense of rainforests, savannahs, and other ecosystems, with future expansion poised to exacerbate this trend. Consequently, agriculture stands as the single most extensive form of land use on the planet (Foley *et al*., 2011; McDonald & Stukenbrock, 2016; Campbell *et al*., 2017). However, only 62% of crop production is directed towards human food, whereas 35% is designated for animal feed, resulting in an indirect and notably less efficient conversion to human food, predominantly in the form of meat and dairy products. The remaining 3% is allocated for bioenergy, seed production, and other industrial purpuses (Foley *et al*., 2011). A large part of the increased food supply production in modern society stems from enhancing productivity through substantial resource inputs, such as water and fertilizers, increased cultivation frequency (multiple cropping), and the use of genetically uniform plant varieties with superior yield and quality (monocultures) (Zhan *et al*., 2015).

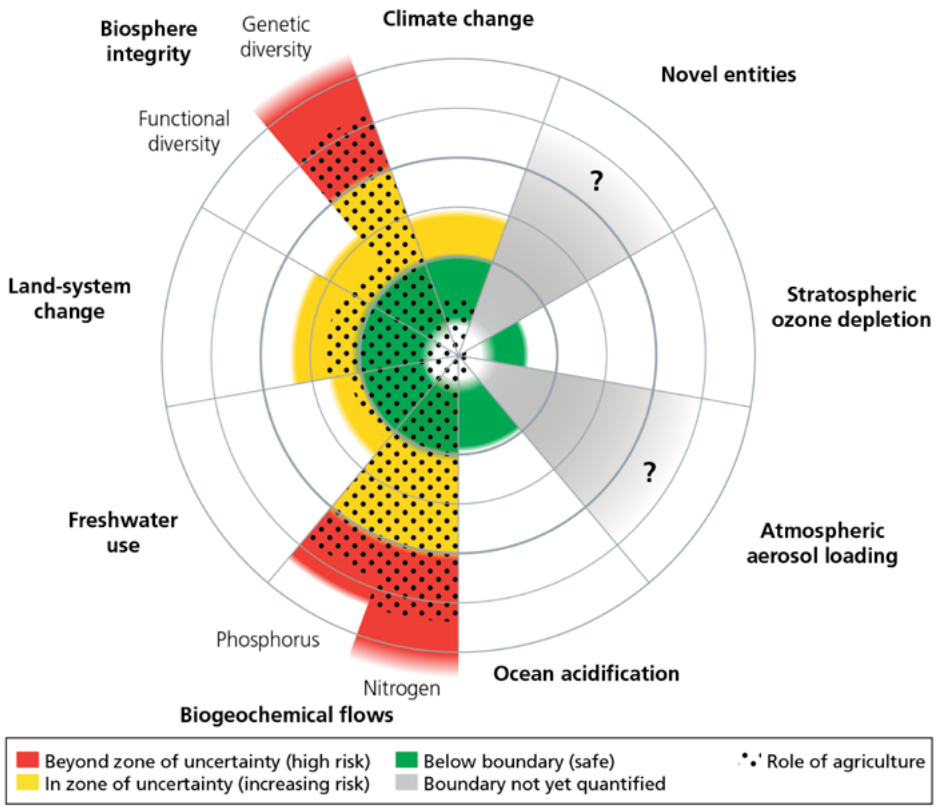

Figure I.1. Status of nine established planetary boundaries.
Overlaid in dots is the estimate of agriculture's role in that status. Over half of the limits appear at high risk or increasing risk beyond or in the zone of uncertainty (Campbell *et al*., 2017).

1.1. Nitrogen as a limiting factor in agriculture

Plant biomass and productivity of many ecosystems are limited by the availability of nitrogen, an essential nutrient for all forms of life. Although nitrogen is an abundant element on Earth, accounting for 78% of the atmospheric gases, a majority of it is in the form of molecular nitrogen (N_2) which is largely unusable by most living organisms. N_2 must be chemically or biologically converted (nitrogen fixation) into reactive forms (N_r) to be accessible for plants (Elser *et al*., 2007; Olivares *et al*., 2013; Stevens, 2019).

The "green revolution" of the 1960s brought about increased crop yields through the utilization of enhanced plant varieties and the widespread application of chemically synthesized nitrogen fertilizers, made possible by the development of the Haber-Bosch process. Despite its success in mitigation famine worldwide, paralleled by an unprece-

dented growth of the world's human population, the extensive use of nitrogen fertilizers has significant environmental repercussions. The Haber-Bosch process generates high amounts of CO_2 (approximately 275 million tons per year) by consuming fossil fuels such as natural gas and coal (Robertson & Vitousek, 2009; Olivares *et al.*, 2013). Moreover, chemical fertilizers are very inefficient, with a considerable portion of the applied nitrogen being lost to the environment (Galloway & Cowling, 2002). This results in contamination of aquatic, terrestrial and atmospheric systems, therefore increasing global acidification (Erisman *et al.*, 2015). Additionally, the release of nitrous oxide by denitrifying bacteria exacerbates the greenhouse effect (Maaz *et al.*, 2021; Snapp *et al.*, 2023).

Despite being a longstanding component of many global farming systems, with over 60% of fixed nitrogen on Earth attributed to it, the significance of biological nitrogen fixation (BNF) as the primary nitrogen source for agriculture has diminished with the increased reliance on fertilizer-N (Fig. I.2). Recognizing the potential of BNF in enhancing nitrogen use efficiency is crucial for future food security and environmental sustainability. However, optimizing BNF in agriculture requires a comprehensive understanding of the diversity of nitrogen-fixing microorganisms, the mechanisms of fixation, and the selection and formulation of efficient N-fixing microorganisms as biofertilizers (Peoples *et al.*, 1995; Olivares *et al.*, 2013; Fowler *et al.*, 2013; Soumare *et al.*, 2020).

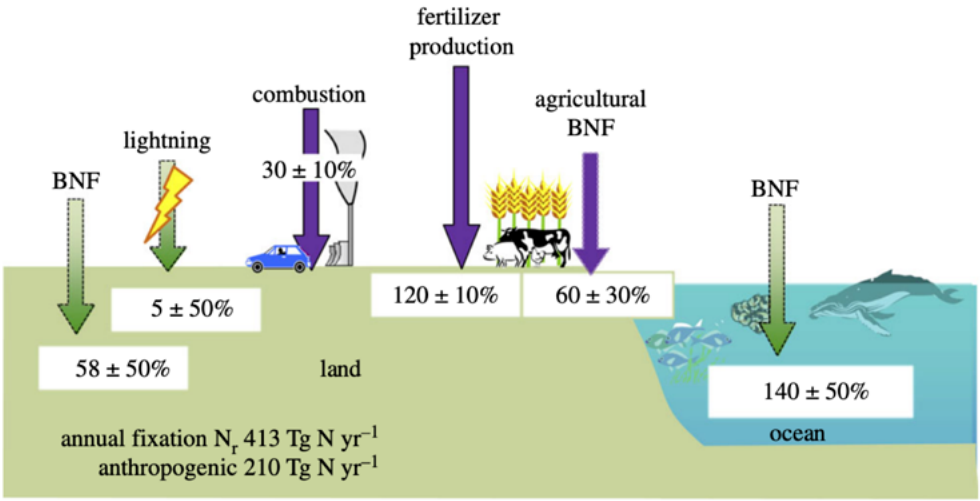

Figure I.2. Global nitrogen fixation, through natural and anthropogenic processes (2010). The arrows indicate a transfer from the atmospheric N_2 reservoir to terrestrial and marine ecosystems, regardless of the subsequent fate of the N_r. Green arrows represent natural sources, purple arrows represent anthropogenic sources. Industrial production is accomplished through the Haber-Bosch process (Fowler *et al.*, 2013).

1.2. Pathogens as a threat to agricultural sustainability

Another consequence of the agricultural expansion is an enormous reduction in plant and animal diversity, as species-rich natural ecosystems have been converted to species-poor agro-ecosystems (McDonald & Stukenbrock, 2016). The vast majority of agricultural lands, on which locally adapted but genetically diverse land races grew for thousands of years, are now mono- or oligocultures. However, since the "green revolution", these diverse cultures were largely replaced by genetically uniform, broadly adapted and high-yielding cultivars. This transformation has led to fields typically composed of a single clone or a population of nearly identical clones, resulting in minimal genetic diversity. Consequently, these practices have greatly increased the risk of substantial losses to plant diseases. Therefore, in terms of both disease management and resource conservation, these practices are unsustainable in the long term (Wouw *et al*., 2010; Zhan *et al*., 2015; McDonald & Stukenbrock, 2016).

Throughout millennia, wild plants and their associated pathogens have been engaged in continuous interactions shaped by coevolutionary processes, which have constrained the spatial extent and temporal duration of disease epidemics. However, modern agricultural practices, coupled with intensive resource inputs and widespread application of agrochemicals, disrupt those natural interactions, creating conditions that significantly enhance the spread of plant disease epidemics and contribute to rapid pathogen evolution (Zhan *et al*., 2015). Furthermore, global change is promoting the emergence of new etiological agents by altering the equilibrium within ecological habitats. In this context, the number of epidemics is expected to increase dramatically in the next coming decades, both in wild and crop plants (Bartoli & Roux, 2017).

Considering that around 15% of the total current crop production is lost to disease, diminishing these losses is an obvious strategy to increase food production without further exacerbating the degradation of natural ecosystems. But protecting crops from pathogens is likely to require a significant re-engineering of agro-ecosystems globally to enhance their resilience against disease, and establish less favourable conditions for the emergence and evolution of pathogens. The development of sustainable plant protection strategies requires a deeper understanding of the biology and evolution of the corresponding pathogens (McDonald & Stukenbrock, 2016; Savary *et al*., 2019; He & Creasey Krainer, 2020).

2. PLANT-INTERACTING BACTERIA

Plants are naturally associated with a great diversity of microorganisms. These interactions have developed over the course of their evolutionary history and remain an essential part of the ecological landscape, impacting plant health, productivity and long-term fitness (Reinhold-Hurek & Hurek, 2011; Plett & Martin, 2018). A great diversity of microorganisms inhabit within their aerial tissues (phyllosphere), root tissues (rhizosphere) and inner tissues (endosphere), with which they establish a broad range of beneficial, neutral, and harmful interactions (Reinhold-Hurek & Hurek, 2011; Plett & Martin, 2018; Santos & Olivares, 2021). On one hand, endosymbiotic beneficial interactions with microorganisms, such as soil bacteria collectively known as rhizobia or the arbuscular mycorrhiza fungi, result in an overall benefit to both partners based on nutrient exchange. At the other extreme are pathogenic interactions, in which bacterial pathogens establish compatible interactions with plants that cause variable damages and affect plant growth and reproduction. Although the outcome is completely different, shared molecular mechanisms facilitating communication between the interacting partners appear to be involved (Fig. I.3). Specifically, nitrogen-fixing bacterial symbionts of legume plants and phytopathogenic bacteria have embraced analogous strategies and genetic traits to colonize, invade and establish chronic infections within the plant host (Grant *et al*., 2006; Soto *et al*., 2006; Reinhold-Hurek & Hurek, 2011; Soto *et al*., 2011).

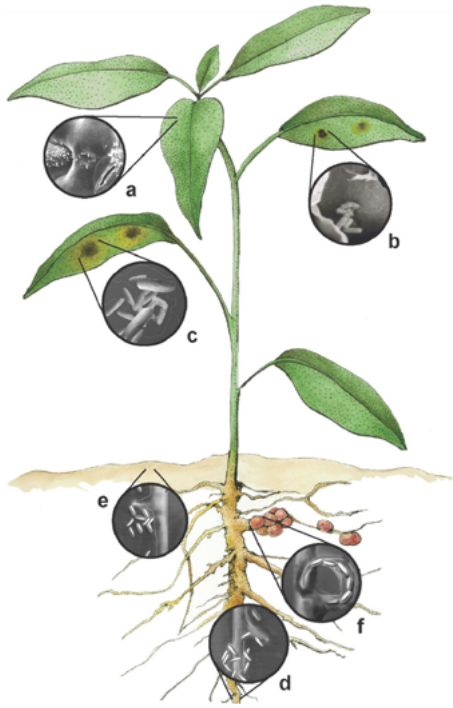

Figure I.3. Bacteria interact with plants in a great diversity of manners.
Sites of infection and plant symptoms caused by pathogenic or symbiotic bacteria are represented on an idealized plant. Pictures are not to scale. **a**. *Pseudomonas syringae* growing as an epiphyte on a leaf surface next to a stoma. **b**. *P. syringae* in apoplastic space within an infected leaf. **c**. *Erwinia carotovora* subesp. atroseptica in an infected leaf. **d**. *Ralstonia solanacearum* associated with a root. **e**. *Pseudomonas fluorescens* on a root. **f**. *Rhizobium* spp. in a curling root hair (Grant *et al*., 2006).

2.1. Beneficial symbiotic interactions: rhizobia

Microbial communities play an important role in the functioning of plants by positively influencing their physiology and development. Soil microbial communities represent one of the greatest reservoirs of biological diversity. The rhizosphere, which is the soil area that surrounds the plant and is under the direct influence of the bio-physicochemical characteristics of the roots can contain up to 10^{11} microbial cells per gram of root and more than 30000 prokaryotic species. Moreover, plants are able to shape their rhizosphere microbiome, as evidenced by the fact that different plant species host specific microbial communities (Berendsen *et al*., 2012; Mendes *et al*., 2013; Dries *et al*., 2021). The majority of land plants, including cereals, can establish symbiotic associations with arbuscular mycorrhizal fungi, which improve nutrient acquisition (particularly phosphate and nitrogen) and also contribute to protect them from various biotic and abiotic stresses. A much more specific symbiotic association is the one legumes establish with rhizobia, which induce the formation of root nodules in the host plant allowing for atmospheric nitrogen fixation (Govindarajulu *et al*., 2005; Berendsen *et al*., 2012; Venkateshwaran *et al*., 2013).

Rhizobia are soil and rhizospheric bacteria able to form nitrogen fixing symbioses with leguminous plants. They belong to more than 15 genera of α- and β-proteobacteria in the families Rhizobiaceae, Phyllobacteriaceae, Brucellaceae, Methylobacteriaceae, Bradyrhizobiaceae, Xanthobacteraceae, Hyphomicrobiaceae and Burkholderiaceae (Fig. I.4). The genus *Rhizobium*, accommodating 112 species, is the largest genus of rhizobia (Ormeño-Orrillo *et al*., 2015; Lindström & Mousavi, 2020).

2.1.1. Biological Nitrogen Fixation

Biological nitrogen fixation is a natural process that transforms atmospheric nitrogen (N_2) into a plant-accessible reduced form (NH_4^+ primarily). In nature, all organisms eukaryotes and prokaryotes, directly or indirectly depend on BNF for their N supply. This N serves as the primary component for the synthesis of nucleic acids, proteins, and other organic nitrogenous compounds. BNF is an ancient innovation exclusively achieved by some Bacteria and Archaea. For Bacteria, different groups are involved, including free-living bacteria like *Azotobacter*, *Azospirillum*, *Bacillus* or *Clostridium*; symbiotic bacteria like *Rhizobium* associated with legumes, whereas *Frankia* associate with the so-called actinorhizal plants (Soumare *et al*., 2020).

Root nodule symbiosis is one of the most effective and studied mutualistic relationships between plants and nitrogen-fixing organisms. These symbioses are characterized

by the development of specialized root (or occasionally stem) structures, the nodules, that are massively colonized by bacteria and act as nitrogen-fixing organs for the plant. The evolutionary origins of nodulation in plants dates back approximately 100 million years, resulting in the development of nodulation capacity in 70% of legume species, as well as in various lineages of actinorhizal plants. Concurrently, the ability to fix nitrogen with legumes has spread to hundreds of species in α- and β-Proteobacteria including the genera *Rhizobium*, *Sinorhizobium*, *Bradyrhizobium*, *Mesorhizobium*, *Azorhizobium*, *Paraburkholderia*, etc. (Sawana *et al*., 2014; Masson-Boivin & Sachs, 2018; Soumare *et al*., 2020).

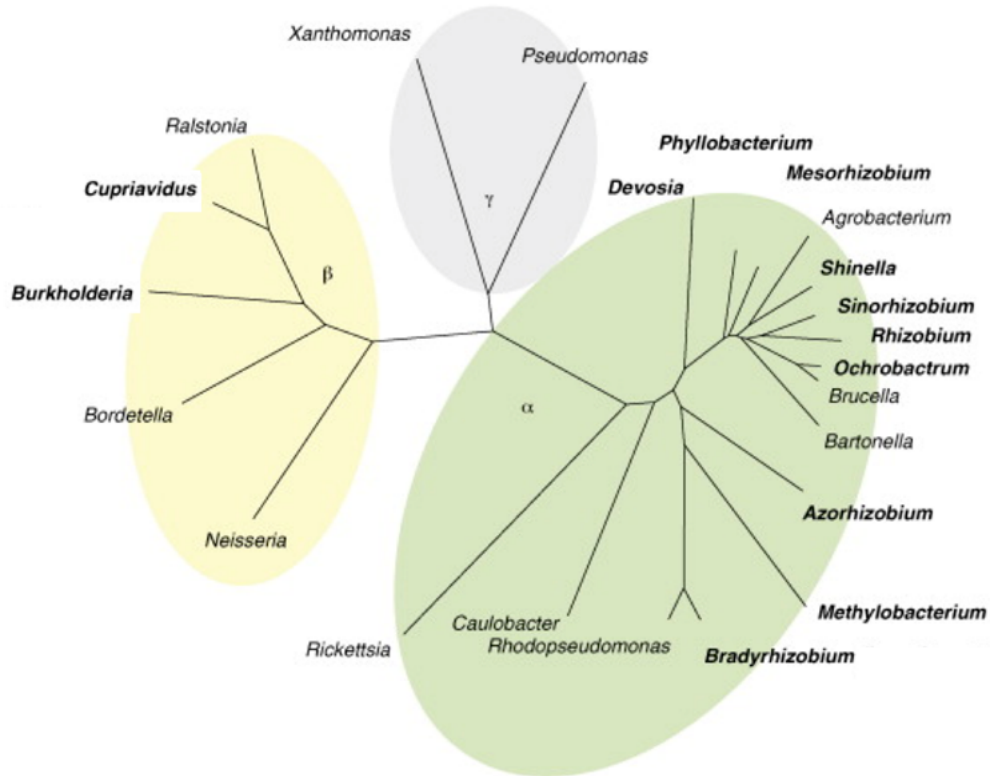

Figure I.4. Unrooted phylogenetic tree of 16S rDNA sequences from selected α-, β-, and γ-proteobacteria.
Genera in bold font contain rhizobia. Rhizobial species or strains whose genomes have been fully sequenced are indicated in parentheses. Rhizobial genomes with sequencing projects in progress are indicated in square brackets (Masson-Boivin *et al*., 2009).

The formation of nitrogen-fixing nodules is a complex process that requires a continuous and adequate signal exchange between plant and bacteria. Differentiated forms of the bacteria within the root nodule (bacteroids) reduce atmospheric nitrogen into ammonia which can be then used by the plant. In return, bacteria receive carbon sources from the plant in a protected niche (Soto *et al.*, 2006; Soto *et al.*, 2011). The initiation of the infection process in legumes involves the secretion of flavonoids, which act as signalling molecules that prompt the rhizobial bacteria to produce Nod factors and symbiotic exopolysaccharides. These bacterial compounds, in turn, activate multiple responses in the host plant, including the formation of infection threads (Fig. I.5a). These infection threads serve as conduits through which rhizospheric bacteria reach their endocellular niche (Fig. I.5b). Remarkably, during the invasion process and symbiosis, rhizobial bacteria possess the ability to evade the host plant innate immune response. Plant cells in the inner cortex internalize the invading bacteria within host-membrane-bound compartments, which subsequently mature into structures known as symbiosomes (Fig. I.5c). The internalized bacteria then develop into bacteroids, a differentiated form with the unique capability of nitrogen fixation (K. M. Jones *et al.*, 2007; Masson-Boivin *et al.*, 2009; Oldroyd, 2013).

All rhizobia rely on the most common form of nitrogenase, molybdenum (Mo)-nitrogenase, to accomplish nitrogen fixation. Mo-nitrogenase demands a substantial amount of energy with a minimal stoichiometry of 16 mol of ATP for each mole of N_2 reduced. Additionally, it displays extreme sensitivity to oxygen, which is in contradiction with the strict aerobic nature of rhizobia. To overcome these challenges, legume plants supply the endosymbiotic bacteria with photosynthetic products and create a nearly anoxygenic environment required for N_2 fixation within nodule cells. Among various mechanisms, nodule leg-haemoglobins play a crucial role in controlling the flux of oxygen towards the bacteroids, ensuring compatibility of bacteroid respiration and nitrogen fixation (Masson-Boivin *et al.*, 2009; Larrainzar *et al.*, 2020).

The study of the rhizobia-legume symbiosis is of great importance as a paradigm of the microbial-plant interaction, highlighting the significance of the understanding of BNF as a cost-effective way to improve soil fertility and crop production. Delving into the mechanisms underlying the symbiosis between plants and bacteria not only advances our knowledge of this specific interaction but also contributes to improve the understanding of other eukaryotic-bacterial interactions, like those involving pathogens responsible for causing crop damages.

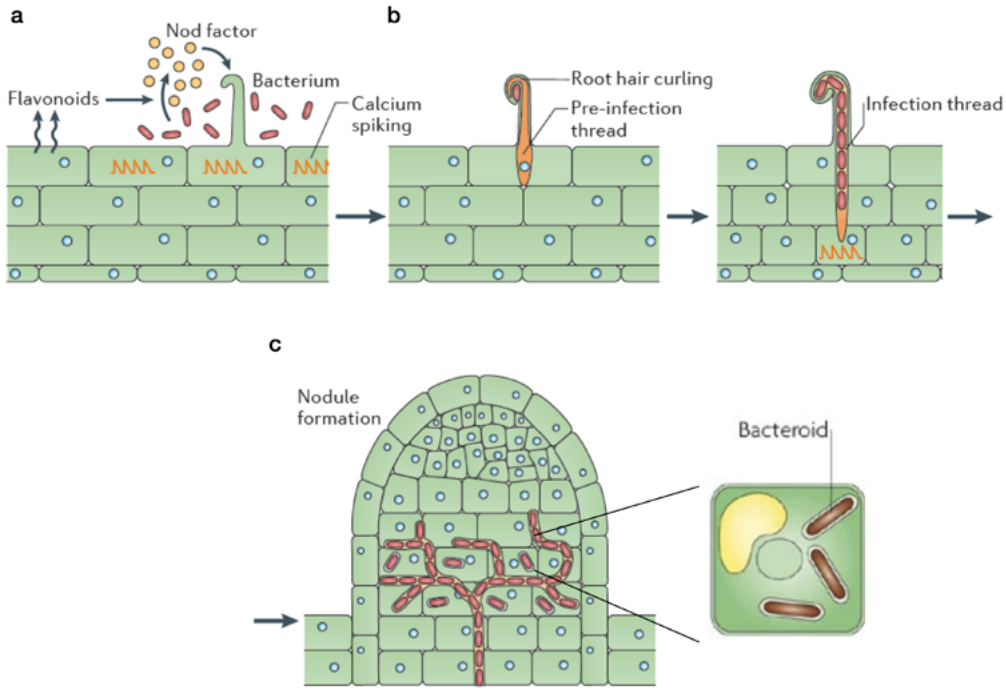

Figure I.5. Rhizobia-legume symbiosis infection process.
a. Initial flavonoid and Nod factor signalling. **b**. Root hair curling and infection thread extension and penetration. **c**. Nodule formation and bacterial differentiation into bacteroids. Modified from Oldroyd (2013) and K. M. Jones *et al.* (2007).

2.1.2. Carbon metabolism in Rhizobia

The bacterial lifestyle, whether as saprophytes in soil in the absence of plants or flourishing in the rhizosphere, is significantly shaped by their ability to obtain energy from available carbon compounds. Therefore, the versatility in utilizing a broad range of carbon sources is important for these organisms to thrive in diverse habitats, both *ex planta* and *in planta*. Thus, rhizobia are able to catabolize different carbon sources, including a wide range of mono, di-, and polysaccharides, organic acids and even certain aromatic compounds (Stowers, 1985; Geddes & Oresnik, 2014).

The great size and complexity of rhizobial genomes reflects a great metabolic diversity that can be advantageous in adapting to the changeable soil conditions. Consistent with this idea, the metabolic potential of rhizobial strains has been correlated with increased competitiveness. Therefore, it is not surprising that these bacteria possess a substantial

proportion of genes dedicated to carbon metabolism and substrate transport. Catabolism of most hexoses in rhizobia is described to occur through the Entner-Doudoroff (ED) pathway, alternative to the Embden-Meyerhof-Parnas (EMP) route present in *E. coli* (Stowers, 1985; Conway, 1992a). Instead, rhizobia are able to use the EMP pathway in a gluconeogenic manner, leading to a functional cyclic ED pathway (Fig. I.6) (Portais *et al.*, 1999; Gosselin *et al.*, 2001).

The catabolism through the ED pathway in rhizobia involves the oxidation of glucose-6-phosphate (G6P) to 6-phosphogluconate (6PG). Subsequently, 6PG is converted to 2-keto-3-deoxy-6-phosphogluconate (KDPG), which is then cleaved by the KDPG aldolase into glyceraldehyde-3-phospate (G3P) and pyruvate (Conway, 1992). Galactose catabolism does not follow this scheme nor does it enter glycolysis through the Leloir pathway as in *E. coli*. Instead, galactose is catabolized through a route analogous to the ED pathway, known as the De Ley-Doudoroff pathway, resulting in the formation of glyceraldehyde-3-phosphate and pyruvate (Fig. I.6) (Arias & Cerveñansky, 1986; Geddes & Oresnik, 2014).

Evidence supports that in rhizobia, the EMP pathway is used in a gluconeogenic manner rather than glycolytic. This inference is drawn from the absence of the phosphofructokinase-encoding gene *pfk* and its enzymatic activity, which catalyses the ATP-dependent conversion of fructose-6-phosphate into fructose-1,6-biphosphate (Irigoyen *et al.*, 1990; Capela *et al.*, 2001). Growth on intermediates or carbon sources entering metabolism through the tricarboxylic acid (TCA) cycle is carried out through the gluconeogenic pathway that requires the EMP route. This pathway serves multiple functions in central metabolism. In addition to being required for gluconeogenesis, it also participates in the cycling of glyceraldehyde-3-phosphate synthesized by the ED pathway during growth on hexoses, as well as in the conversion of pentoses and hexoses that enter central metabolism through fructose-6-phosphate into glucose-6-phosphate for glycolysis through the ED pathway (Fig. I.6) (Fuhrer *et al.*, 2005; Geddes & Oresnik, 2014).

Carbon metabolism of the bacteroid

Nitrogen fixation inside the nodules results from a metabolic exchange between the bacteroids, enclosed in the symbiosome, and the host plant. The primary carbon sources for bacteroids are dicarboxylic acids supplied by the plant, such as malate and succinate. They are derived from the sucrose photosynthesized by the plant and transported to the bacteroid. The membranes of both the symbiosome and the bacteroid play a crucial role in regulating metabolite exchange between the two organisms. Within the bacteroid, tricarboxylic acids are catabolized through the TCA cycle (Lodwig & Poole, 2003; Udvardi & Poole, 2013).

In the symbiosome, bacteroids are surrounded by the peribacteroid or symbiosome space, forming an inter-kingdom environment populated by proteins from both symbionts. Most proteins associated with the symbiosome membrane are annotated as being of plant origin and non-metabolic in nature. It has been suggested that symbiosome membrane proteins may participate in the transport of carbon, nitrogen and other nutrients between the plant and the bacteroid. In contrast, the identified proteins in the symbiosome space are predominantly metabolic enzymes of bacterial origin (Geddes & Oresnik, 2014; Emerich & Krishnan, 2014).

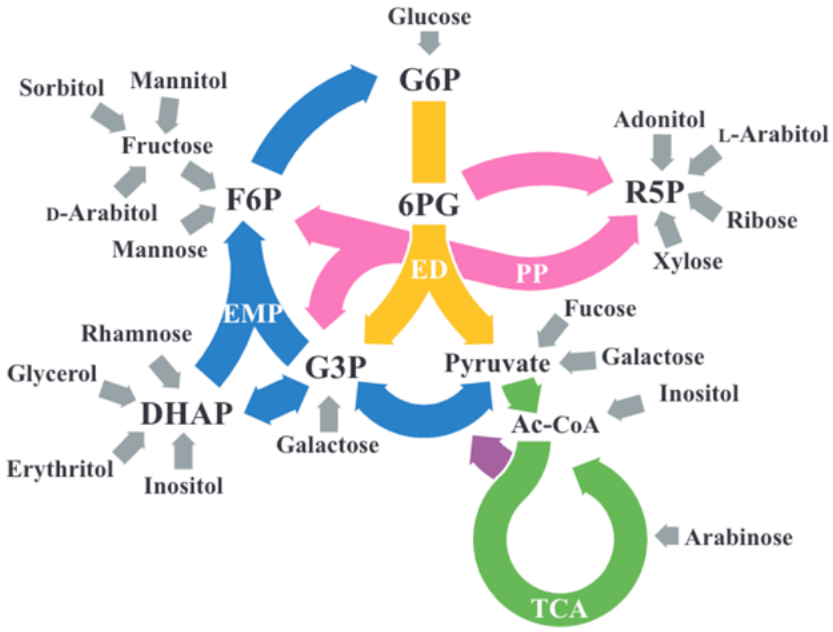

Figure I.6. Metabolic network of central carbon metabolism in rhizobia.
Coloured arrows represent the cyclic central metabolism of *S. meliloti*. Different colours represent the Embden-Meyerhof-Parnas (EMP), Entner-Doudoroff (ED), pentose phosphate (PP) pathways, and tricarboxylic acid (TCA) cycle. Grey arrows indicate entry points for different compounds into central metabolism and coloured arrows indicate the direction of carbon flow, as described in literature. Abbreviations: G6P, glucose-6-P; F6P, fructose-6-P; 6PG, 6-phosphogluconate; R5P, ribose-5-P; G3P, glyceraldehyde-3-P; Ac-CoA, acetyl-coenzyme A (Geddes & Oresnik, 2014).

2.1.3. Rhizobium etli

Rhizobium etli (Ret), is one of the two bacteria (along with *Pseudomonas syringae*) object of study in this doctoral thesis. It is a Gram-negative, aerobic, α-proteobacteria of *Rhizobiaceae* family which establishes a symbiotic interaction with *Phaseolus vulgaris* (common bean) (Aguilar *et al*., 2004). The work has been carried out with the specific strain Ret CE3 (Quinto *et al*., 1982), a derivative of strain CFN42 resistant to nalidixic acid and streptomycin.

The genome of *R. etli* CE3 is 6.5 Mb in size, comprising a chromosome of 4.38 Mb and 6 plasmids ranging from 184 to 600 Kb, known as pRetCFN42a, b, c, d, e and f. Collectively, these plasmids constitute one-third of the total genome. Notably, one of these plasmids, pRetCFN42d, is considered as the symbiotic plasmid or pSym, since it carries the majority of the genes responsible for nodulation and BNF (*nod*, *nif* and *fix*) (González *et al*., 2003; González *et al*., 2006).

Ret is able to synthesize various structural polysaccharides, including exo-polysaccharides (EPS). These EPS confer an adaptive advantage by protecting the cell from abiotic and biotic stresses. They are the main component of the extracellular matrix, participating in cell signalling, surface adhesion and biofilm formation (Schmid *et al*., 2015; Pérez-Mendoza and Sanjuán, 2016). The structural polysaccharides synthesized by Ret are the lipopolysaccharide (LPS), a capsular polysaccharide (CPS), periplasmic β-(1-2)-cyclic glucan, an acid exopolysaccharide (EPS), as well as a glucomannan, cellulose and mixed-linkage β-glucan (MLG) (Forsberg & Carlson, 1998; Forsberg *et al*., 2000; D'Haeze *et al*., 2007; Pérez-Mendoza *et al*., 2022).

2.2. Bacterial pathogens

Similar to rhizobia, pathogenic bacteria establish compatible interactions with plants which enable them to acquire nutrients from the host upon colonisation; however, the plant is harmed as a result of that interaction. Pathogenic bacteria typically enter plant tissues either through wounds or natural openings, occupying the apoplast of plant tissues or the xylem, where they multiply and spread. During this process, bacteria often inject effector proteins into plant host cells to overcome defence responses, mechanisms that are also utilized by symbionts. Infection by pathogenic bacteria often involves the deployment of hydrolytic enzymes and toxins which provoke plant injury, disease development, and, in severe cases, plant death (Soto *et al*., 2006; Soto *et al*., 2009; Reinhold-Hurek & Hurek, 2011).

2.2.1. *Pseudomonas syringae*

Pseudomonas is a genus of Gram-negative γ-proteobacteria with an aerobic and chemoheterotrophic metabolism. It is one of the most diverse and ubiquitous bacterial genera whose species have been isolated in all kinds of environments, which proves their great metabolic versatility (Palleroni, 1993; Jun *et al*., 2016). It includes important pathogenic species for both animals and plants (*P. aeruginosa* and *P. syringae*), whereas others greatly contribute to the turnover of organic matter and positively affect plant health and nutrition (e.g., *P. fluorescens*, *P. protegens* or *P. putida*) (Silby *et al*., 2009; Peix *et al*., 2009).

Pseudomonas syringae is one of the most studied plant pathogens since it serves as a model for the investigation of bacterial pathogenicity, molecular mechanisms underlying plant-microorganism interactions, microbial ecology and epidemiology. Within the *P. syringae* species, a remarkable diversity is observed with over 60 distinct pathovars documented, each of them displaying specificity to different groups of host plants (Xin *et al*., 2018). Originally isolated from *Syringa vulgaris* (Young, 1991), *P. syringae* pathovars infect nearly all economically important crop species, which makes this species one of the most prevalent plant pathogens. Interestingly, many isolates of *P. syringae* are non-pathogenic and exist as commensals in plants and in environments linked to fresh waters which act as reservoirs, transmission routes and sources of genetic diversity (Fig. I.7A) (Hirano & Upper, 2000; Morris *et al*., 2013; Xin *et al*., 2018).

The infection process

P. syringae bacteria undergo two interconnected growth phases. The epiphytic phase involves the bacteria living on the surface of plant tissues, usually the above ground parts, such as leaves, stems, flowers and fruits (collectively known as the phyllosphere). Conversely, during the endophytic phase, bacteria penetrate the plant tissue and colonize the intercellular apoplast space (Xin *et al*., 2018). The infection cycle starts when bacteria arrive to the phyllosphere of a compatible host, forming aggregates in protected areas, like trichome bases. Then, as opportunistic pathogens, take advantage of wounds and stomatal openings to invade the intercellular spaces inside the leaves (apoplast), where they multiply using the available nutrients (Fig. I.7B) (Melotto *et al*., 2008). Afterwards, bacteria synthesize different compounds that manipulate the metabolism and immune response of the host, ultimately resulting in tissue necrosis. The infection typically occurs locally but can be transmitted to other areas or other plants from the necrotic lesions.

The ability of *P. syringae* to gain entry to and proliferate inside the plant depends on its ability to synthesize toxins, grow factors and a type III secretion system (T3SS) that delivers proteins, known as type III effectors, into the plant cell. The main virulence factors of

P. syringae are the T3SS and phytotoxins, with the contributions of other cellular functions such as motility, siderophore synthesis and EPS production (Rico *et al*., 2011; Xin and He, 2013). The T3SS is a specialized secretion system present in numerous Gram-negative plant and animal pathogens and symbionts, which behaves as a molecular syringe that allows the bacteria to inject effector proteins directly into the host cell or into the intercellular space. The effectors can interfere with the plant's defence response at different levels (Alfano & Collmer, 2004). The T3SS is formed by a cytoplasmic ATPase complex and C ring, an export apparatus linked to the inner membrane, an intermembrane basal body, an extracellular pili and a translocation port that is situated in the host membrane (Galán *et al*., 2014). Phytotoxins are not essential for *P. syringae*'s pathogenicity, but their production results in increased disease severity, contributing to systemic movement of bacteria in planta, lesion size, and multiplication of the pathogen in the host. They vary in their specificity and chemical structure. Syringomycin, syringopeptin and syringafactin are lipopeptides with surfactant activity that contribute to necrosis. Phaseolotoxin, tabtoxin and mangotoxin, on the other hand, are antimetabolite toxins, produced by some pathovars, that are able to inhibit enzymes of aminoacid biosynthesis routes (Bender *et al*., 1999). Coronatine is another toxin produced by certain strains that affects jasmonic acid signalling and promotes stomatal opening allowing bacterial entry (Melotto *et al*., 2008; Melotto *et al*., 2017).

Motility and EPS synthesis

Motility is also crucial for *P. syringae* as it facilitates bacterial responses to environmental stimuli, increasing its competitiveness. During the infection process, it permits invasion of the apoplast and dissemination into other host plants. *P. syringae* strains are motile thanks to the presence of multiple polar flagella that propel them individually in liquid media (swimming) and through the surface or viscous media (swarming). Moreover, flagella are important for surface adhesion, biofilm formation and contribute to virulence (Jarrell & McBride, 2008; Melotto *et al*., 2008). Motility, however, not only relies on flagella, as it also depends on biosurfactant production. These amphipathic molecules reduce surface tension for the bacteria, facilitating its movement (Burch *et al*., 2010; Nogales *et al*., 2015).

Bacterial exopolysaccharides (EPS) confer an adaptive advantage as they protect the cell from abiotic and biotic stresses, including defence responses from the host. They are the main component of the extracellular matrix, participating in cell signalling, surface adhesion and biofilm formation (Schmid *et al*., 2015; Pérez-Mendoza &Sanjuán, 2016). The *Pseudomonas* genus are prolific EPS producers, with strains that usually synthesize several, such as alginate, cellulose, levan, Pea, Peb, Pel and Psl.

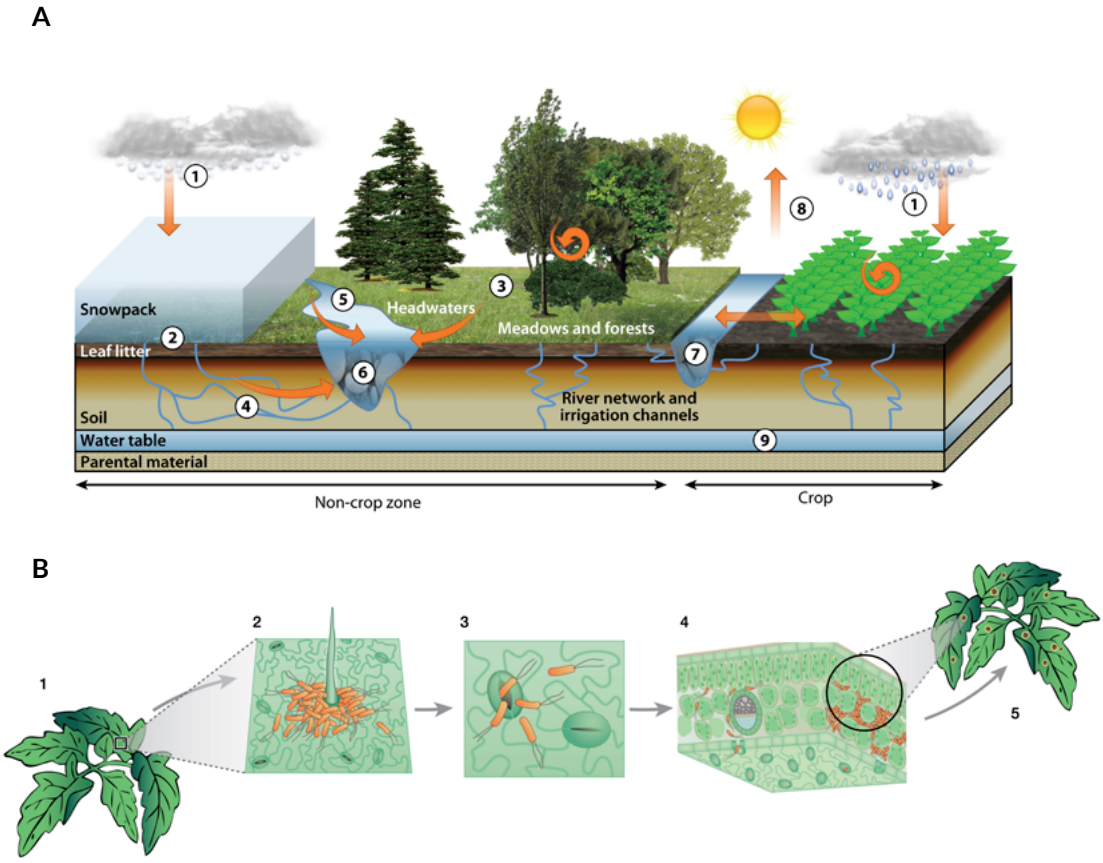

Figure I.7. Life cycle of *P. syringae* in the environment and during the infection process.
A. *P. syringae* reaches the soil and plant surfaces through atmospheric precipitation (1). It survives in accumulated snow (2), leaf litter, and grasses (3). During thawing and rainfall, a portion of these populations follows the underground (4) or surface (5) water flows until reaching the river network (6). Epiphytic populations of *P. syringae* on wild plants or in agricultural ecosystems can also follow those routes, reaching the crop surface through precipitation (1) or irrigation (7). Finally, leaf surface populations can form aerosols (8) and reach the troposphere or even penetrate the soil to reach the groundwater (9) (Morris *et al*., 2013).
B. *P. syringae* begins its infective cycle when it reaches the leaf of a healthy plant (1), forming aggregates in protected areas, such as the base of the trichomes (2). Bacteria take advantage of the presence of wounds and the opening of the stomata (3) to reach the apoplast (4), where they multiply and express virulence factors causing strain-specific symptoms (5). Modified from Xin and He (2013).

Capsular polysaccharides (levan, alginate) are present on the cell surface and have a protective role, whereas the aggregative ones (cellulose, Pel, Psl) provide structural integrity and interact with other components of the matrix. However, the presence and roles of EPS are highly variable, even between strains from the same species (Mann & Wozniak, 2012).

2.2.2. Carbon metabolism in *Pseudomonas*

Similar to rhizobia, pseudomonads, including *P. syringae*, exhibit the capacity to catabolize and grow in diverse carbon sources. This versatility in utilizing a wide range of carbon sources is crucial for their survival, especially during infection when they rely on the nutrients present in the plant apoplast. Interestingly, an analogous central carbon metabolism to that of rhizobia has been described for *Pseudomonas*, with a similar utilization of the Entner-Doudoroff (ED) and Embden-Meyerhof-Parnas (EMP) pathways (Rico *et al*., 2011; Kohlstedt & Wittmann, 2019).

Pseudomonads operate a so-called EDEMP cycle, which merges activities of the EMP, the ED (previously described in rhizobia), and the pentose phosphate (PP) pathways, as it has been demonstrated for *P. putida* KT2440 (Fig. I.8) (Nikel *et al*., 2015). Its genome encodes the enzymes of these three pathways for glucose catabolism, however, it lacks the glycolytic enzyme 6-phosphofructo-1-kinase (Pfk), which catalyses the ATP-dependent conversion of fructose-6-phosphate into fructose-1,6-biphosphate. The lack of Pfk explains why *P. putida* uses almost exclusively the ED pathway for hexose degradation (Lessie and Phibbs, 1984; del Castillo *et al*., 2007; del Castillo *et al*., 2008; Sudarsan *et al*., 2014; Nikel *et al*., 2015; Kohlstedt and Wittmann, 2019). The EDEMP cycle forces part of the triose phosphates, which would otherwise be further oxidized to acetyl-CoA and downwards, to be recycled back to hexose phosphates. Furthermore, the EDEMP cycle operates under both glycolytic and gluconeogenic regimes being an essential distributor of carbon through the central metabolism (Fig. I.8) (Nikel *et al*., 2015; Kohlstedt & Wittmann, 2019; Wilkes *et al*., 2021).

2.2.3. Pto DC3000

Pseudomonas syringae pv. tomato (Pto) causes bacterial speck disease, an economically important disease on tomato, particularly in greenhouse-grown plants. Symptoms of infection are brown-black leaf spots surrounded by a chlorotic halo and dark speck on green fruits. Disease development can result in extended chlorosis followed by desiccation, with yield loss. Serious disease outbreaks are favoured by high leaf wetness, cool temperatures and cultural practices that allow bacteria to be disseminated to host plants (Hirano & Upper, 2000; Preston, 2000).

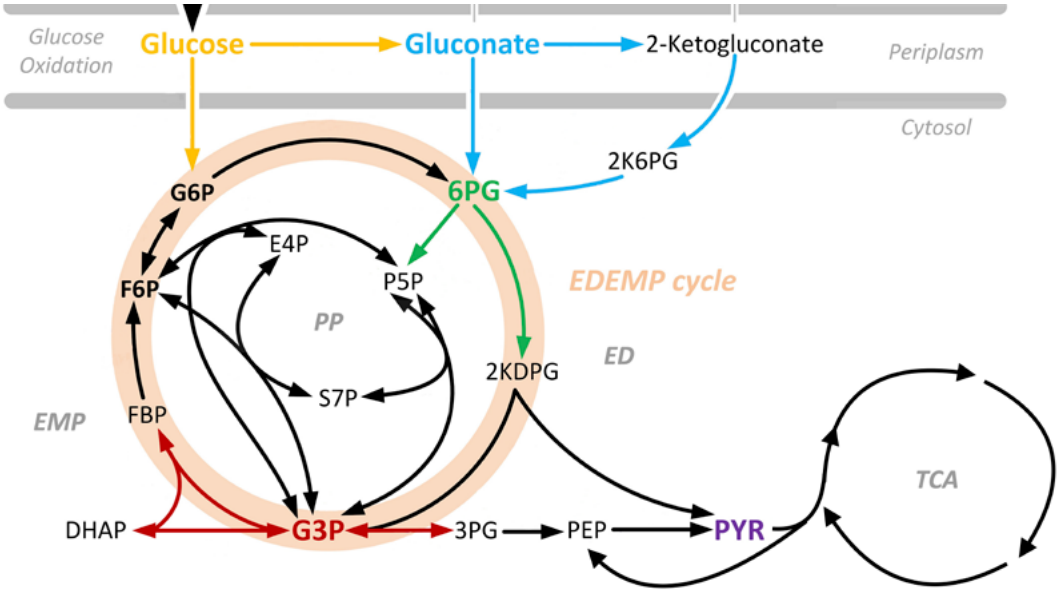

Figure I.8. Metabolic network of central carbon metabolism in *Pseudomonas*.
The reactions are merged into the EDEMP cycle, which assembles enzymes from the ED, the EMP and the PP pathways into a unique metabolic architecture. Arrow heads indicate the direction of carbon flow as reported. Abbreviations: G6P, glucose-6-P; F6P, fructose-6-P; FBP, fructose-1,6-bisphosphate; DHAP, dihydroxyacetone-P; 6PG, 6-phosphogluconate; 2KDPG, 2-keto-3-deoxy-6-phosphogluconate; 2K6PG, 6-phospho-2-ketogluconate; P5P, pentose-5-P; S7P, sedoheptulose-7-P; E4P, erythrose-4-P; G3P, glyceraldehyde-3-P; 3PG, 3-phosphoglycerate; PEP, phosphoenolpyruvate; PYR, pyruvate. Modified from Kohlstedt & Wittmann (2019).

Pto DC3000 is a rifampicin resistant strain derived from NCPPB1106. It is a model pathogen for study as it is able to accept foreign DNA and can infect *Arabidopsis* as well as tomato. It also provokes and hypersensitive response (HR) in non-compatible hosts like *Nicotiana tabacum* and *Phaseolus vulgaris* (Cuppels, 1986; Whalen *et al*., 1991). Its genome is composed of a circular chromosome of 6.4 Mb and two plasmids, pDC3000A and pDC3000B, of 73 and 67 kb respectively. It encodes for numerous proteins involved in virulence, as those related to the T3SS, toxin production, host immune response suppression, motility or adhesion (Buell *et al*., 2003). Unlike other *P. syringae* strains, it is a weak epiphyte, it does not have a replication phase on the leaf surface and depends on a rapid entry into the apoplast (Boureau *et al*., 2002; Melotto *et al*., 2008; Xin & He, 2013; Nogales *et al*., 2015).

In Pto DC3000 protein secretion has an important role for bacterial interaction with the host plant, being the type III secretion system (T3SS), responsible for the release of effector proteins, essential for virulence. The effectors interact with the cell wall and plasma membrane, or are directly translocated into the host cells cytoplasm. Moreover, specific secreted proteins are also involved in processes such as nutrient acquisition, stress responses or metabolic adaptation. Their synthesis and secretion are regulated in response to environmental cues, allowing the pathogen to adapt to changing conditions and, at the same time, to modulate plant functions and metabolism creating an environment that favours Pto growth in plant tissues (Preston, 2000; Petnicki-Ocwieja *et al*., 2002; Filloux, 2011; Rico *et al*., 2011; Schumacher *et al*., 2014). The most abundant proteins in the extracellular fraction of Pto DC3000 grown in fructose medium, commonly used to induce T3SS expression and effector secretion, were those directly associated with T3SS mediated pathogenicity, and the translation elongation factor Tu (EF-Tu). Other proteins identified were the coronafacic acid and coronafacic acid polyketide synthases, both required for the synthesis of the phytotoxin coronatine, some ribosomal proteins, and metabolic enzymes of the Krebs cycle (Schumacher *et al*., 2014).

3. CYCLIC DIGUANYLATE AS A SECOND MESSENGER

Living organisms including bacteria continuously receive environmental stimuli which are integrated through complex signal transduction cascades, allowing them to respond and adapt to their changing ecological niches (Römling, 2023). Second messengers are small molecules that transmit specific signals from sensory domains to effector proteins. They allow virtually immediate and often amplified cellular responses (Hengge, 2009; Yan & Chen, 2010).

Bis-(3′,5′)-cyclic dimeric guanosine monophosphate (c-di-GMP, cdG) is a cyclic dinucleotide bacterial second messenger. It was first identified as an allosteric regulator of the cellulose synthase in *Gluconacetobacter xylinus* (Ross *et al*., 1987), but it is now recognized as one of the most widespread and versatile bacterial second messengers. It has been involved in numerous biological processes, such as motility, biofilm formation, polysaccharide biosynthesis, virulence and cell cycle progression (Yan & Chen, 2010; Krol *et al*., 2020; Hengge *et al*., 2023).

3.1. The c-di-GMP control module

A second messenger control module typically consists of four components: two enzymes responsible of producing and degrading the second messenger upon specific signals, an

effector molecule that binds it and is allosterically regulated by the second messenger and a target component that generates a molecular output upon direct interaction with the effector. Cellular c-di-GMP concentration is regulated by two class of enzymes, diguanylate cyclases (DGC), which synthesize c-di-GMP from two molecules of GTP, and phosphodiesterases (PDE), which degrade it into 5'-phosphoguanylyl-(3'-5')-guanosine (pGpG); pGpG is subsequently split into two GMP molecules (Fig. I.9) (Hengge, 2009; Yan & Chen, 2010; Sondermann *et al*., 2012).

3.1.1. Biosynthesis by diguanylate cyclases

DGC activity is linked to the GGDEF domain, named after the critical amino acid sequence motif of the enzyme's active site. DGCs usually assemble into homodimers, with each monomer harboring a GTP molecule in antiparallel position for the formation of a phosphodiester bond, resulting in the synthesis of c-di-GMP. Most DGCs are subject to allosteric product inhibition, involving the binding of c-di-GMP to a secondary site (I site) with an RXXD motif. This feedback control prevents excessive GTP consumption, sets an upper limit for c-di-GMP accumulation, and could dampen stochastic variations in cellular c-di-GMP content (Hengge, 2009; Römling *et al*., 2013).

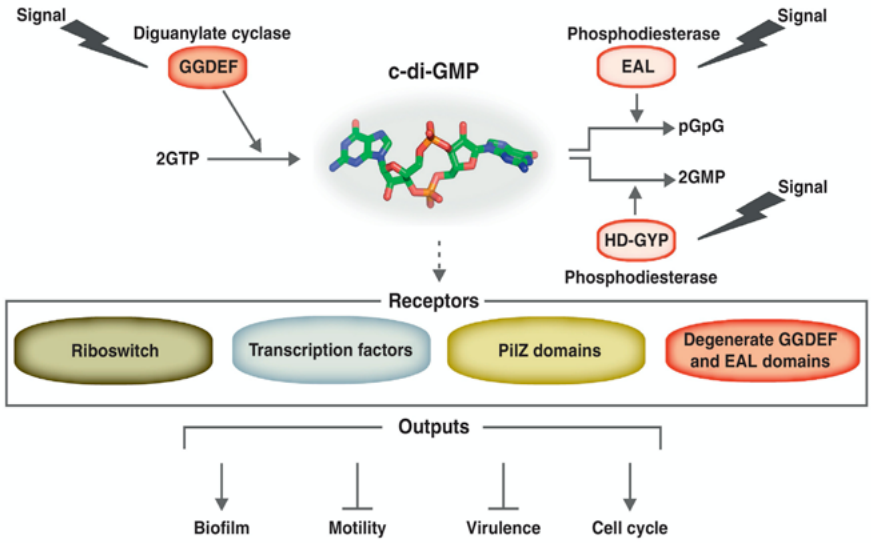

Figure I.9. The c-di-GMP control module.
C-di-GMP is produced by DGC proteins containing the GGDEF domain and degraded by PDE proteins bearing EAL or HD-GYP domains. C-di-GMP is sensed by receptor proteins or RNAs through the PilZ, degenerate GGDEF or EAL domain, transcriptional factors or riboswitch families. Typically, receptor proteins then interact with a downstream target to affect a particular cellular function. Modified from Sondermann *et al*. (2012).

The PleD diguanylate cyclase from *Caulobacter crescentus* is a response regulator from a two-component system with a crucial role in cell division and differentiation (Aldridge et al., 2003). The phosphorylation of PleD facilitates the formation of the enzymatically active dimers, ultimately leading to the synthesis of c-di-GMP. A modified variant of PleD, denoted as PleD*, has been used in this work to augment c-di-GMP production. PleD* possesses constitutive DGC activity independent of phosphorylation due to a series of amino acid shifts. It still exhibits, however, allosteric product inhibition (Chan *et al*., 2004; Paul *et al*., 2007).

3.1.2. Degradation by phosphodiesterases

There are two types of specific PDEs which can degrade c-di-GMP: EAL domain proteins and HD-GYP domain proteins. EAL domain proteins are enzymes that linearize c-di-GMP to 5'-pGpG, which is subsequently degraded by nonspecific cellular PDEs. They exhibit high specificity for c-di-GMP and require Mg^{2+} and Mn^{2+}, whereas they are inhibited by Ca^{2+} and Zn^{2+}. HD-GYP domain proteins constitute a subfamily within the HD superfamily of metal-dependent phosphohydrolases and are unrelated to the EAL proteins. HD-GYP proteins break the phosphodiester bond and further degrade c-di-GMP into GMP. Although GGDEF domains for DGCs and both PDE domains occur separately, composite proteins in which a GGDEF domain and either an EAL or a HD-GYP domain coexist, are frequently found (Hengge, 2009; Römling *et al*., 2013).The environmental regulation of DGC and PDE activity is most likely accomplished by the diverse sensory and regulatory domains often associated with these proteins, such as PAS, HAMP and REC domains. These domains have been implicated in responding to diverse environmental and intracellular signals, including redox potential, light, oxygen, osmolarity and antibiotics, among others. However, only a limited number of activator signals have been conclusively demonstrated to interact with these predicted sensing domains so far (Mills *et al*., 2011; Römling *et al*., 2013).

3.1.3. Effector molecules

To exert its function, c-di-GMP has to bind to and allosterically alter the structure and output function of an effector component. The ability of c-di-GMP to regulate multiple cellular functions is directly linked to the extensive diversity of sensing components, that cannot be recognized by a single common domain or c-di-GMP-binding site. Currently, four types of c-di-GMP effector proteins have been identified: PilZ domains, transcription factors, riboswitches and degenerate GGDEF and EAL domains (Fig. I.9) (Hengge, 2009; Sondermann *et al*., 2012). However, the variety of proteins and protein domains able to bind c-di-GMP is constantly increasing (Hengge *et al*., 2016; Pérez-Mendoza *et al*., 2017; Hengge *et al*., 2023).

The PilZ family of proteins represents the best studied class and displays a broad phylogenetic distribution. PilZ domains are found either as single domain proteins or in conjunction with other domains predicted to possess enzymatic, regulatory or transport functions. The majority of genomes encode multiple of these potential receptors, among which YcgR from *E. coli* and BcsA from *Gluconacetobacter xylinus* were the first experimentally validated c-di-GMP receptors within this family. Notably, the PilZ-like proteins studied so far seem to be activated by c-di-GMP and to function at the post-translational level through protein-protein interactions (Hengge, 2009; Sondermann *et al*., 2012).

Different transcription factors able to bind c-di-GMP have also been described. FleQ from *P. aeruginosa* was one of the first c-di-GMP-responsive transcription regulators identified. It oppositely regulates the genes required for flagellar motility and surface adhesion in response to fluctuating intracellular levels of that second messenger, since c-di-GMP binding to FleQ results in the rearrangement of FleQ-DNA complexes (Hickman and Harwood, 2008; Baraquet *et al*., 2012; Matsuyama *et al*., 2016; Baraquet and Harwood, 2015). Another example is the *S. meliloti* transcriptional regulator CuxR, which has been recently shown to bind c-di-GMP to activate transcription of genes involved in biosynthesis of an arabinose-rich polysaccharide (Schäper *et al*., 2017).

Mounting evidence suggests that GGDEF domains with a degenerate active site function as c-di-GMP receptors. Among this subset of degenerate GGDEF-containing proteins are PelD from *P. aeruginosa* and the PleD paralogue PopA, both exhibiting strong c-di-GMP affinity despite differences in their domain organizations and functions. Thus, a molecular feature that mediates feedback inhibition (I site) in active DGCs is used for c-di-GMP sensing in these proteins. Likewise, the degenerate and catalytically inert EAL domain of LapD from *P. fluorescens* has been shown to act as c-di-GMP-binding effector module to control biofilm formation (Li et al., 2012; Schirmer & Jenal, 2009).

In addition to the proteins that bind c-di-GMP, riboswitches have also been identified as effector molecules. Riboswitches are regulatory elements located in the untranslated regions (UTRs) of certain mRNAs that recognize small molecule ligands with high affinity and specificity (Sudarsan et al., 2008; Shanahan and Strobel, 2012). Upon c-di-GMP binding, the mRNA undergo alterations in its secondary structures, consequently influencing transcription, mRNA stability, or translation of the downstream genes (Römling *et al*., 2013).

Despite the advancements in understanding of c-di-GMP signaling, numerous receptors linked to c-di-GMP remain unidentified, which can be deduced from the fact that several cellular processes mediated by c-di-GMP operate independently of known effectors (Schirmer & Jenal, 2009). As an example, the MLG synthase BgsA of *S. meliloti* does not contain any predictable c-di-GMP binding domains, but it has been demonstrated to bind c-di-GMP (Pérez-Mendoza *et al*., 2017).

3.2. Cellular functions regulated by c-di-GMP

Upon the emergence of c-di-GMP as a novel second messenger, initial phenotypes associated with c-di-GMP signalling included cell differentiation in *C. crescentus* and biofilm formation in *G. xylinus*, *Salmonella enterica*, *Vibrio cholerae* and *P. aeruginosa*. Since then, the list of bacteria relying on c-di-GMP signalling has significantly expanded, accompanied by a broadened range of phenotypes affected by it. This spectrum now includes such diverse phenomena as survival and transmission of obligate intracellular pathogens, virulence, antibiotic production and long-term nutritional stress survival (Römling *et al*., 2013; Hengge, 2021; Junkermeier & Hengge, 2023; Wang *et al*., 2023).

3.2.1. Exopolysaccharides (EPS)

Bacterial biosynthesis and secretion of extracellular polysaccharides is a physiological process that occurs under diverse environmental conditions. These polysaccharides play essential roles maintaining the structural integrity of the cell envelope or preventing cellular desiccation, and participate in more complex activities, such as interactions within bacterial communities and biofilm formation, or interaction with eukaryote hosts (Whitney & Howell, 2013). A great variety of cellular and environmental signals regulate the production of bacterial exopolysaccharides. Among them, cellulose, alginate, mixed-linkage β-glucan (MLG), curdlan, or xanthan, are known to be regulated by c-di-GMP (Römling *et al*., 2013; Pérez-Mendoza & Sanjuán, 2016).

To date, four mechanisms governing the synthesis and secretion of bacterial EPS have been identified: the Wzx/Wzy-dependent pathway, the ATP-binding cassette (ABC) transporter-dependent pathway, the synthase-dependent pathway, and the extracellular synthesis facilitated by a single sucrase protein (Schmid *et al*., 2015). It has been proved that c-di-GMP regulates EPS production that use the Wzx/Wzy or the synthase-dependent pathways (Liang, 2015; Pérez-Mendoza & Sanjuán, 2016).

3.2.2. Motility and biofilm formation

In nature, bacteria are usually found living in multicellular communities or biofilms adhered to biotic or abiotic surfaces. The structural integrity of bacterial biofilms significantly relies on a self-produced extracellular matrix that comprise exopolysaccharides, nucleic acids, and proteins. The major components of the biofilm matrix differ, depending on the bacterial species and strain, the stage of biofilm development and the environmental conditions (Gloag *et al*., 2013; Whitney & Howell, 2013). Beyond immobilizing bacteria, the extracellular components of biofilm contribute to enhanced liquid retention,

facilitate nutrient acquisition and provide protection against mechanical stress and toxic compounds, with biofilm bacteria exhibiting increased tolerance to antibiotics and host immune responses (Römling & Balsalobre, 2012; Krol *et al*., 2020).

Many of the extracellular compounds that contribute to biofilm formation are subject to regulation by c-di-GMP. As described previously, the production of many EPS is governed by this second messenger, but other molecules necessary for biofilm formation, like adhesin proteins which intervene in the irreversible union of bacteria to surfaces, can also be modulated by intracellular c-di-GMP levels (Pérez-Mendoza *et al*., 2011b; Duque *et al*., 2013; Espinosa-Urgel & Ramos-González, 2023). Another important c-di-GMP-controlled mechanism for biofilm formation involves the inhibition of various types of bacterial motility, including swimming, swarming, twitching and gliding. Diverse transcription factors are able to regulate those processes with c-di-GMP acting at a transcriptional, posttranscriptional, and post-translational levels (Wolfe & Visick, 2008; Whitney & Howell, 2013; Pérez-Mendoza *et al*., 2014). Also, some PilZ domain proteins have been shown to work as molecular brakes and/or clutches of flagellar rotation upon binding c-di-GMP, such as YcgR in enterobacteria (Paul *et al*., 2010), MotI in *Bacillus* (Subramanian *et al*., 2017), FlgZ in Pseudomonads (Martínez-Granero *et al*., 2014) and likely McrA in rhizobia (Schäper *et al*., 2016).

3.2.3. Virulence

Genetic screens have revealed the impact of c-di-GMP signalling pathways on virulence in numerous animal and plant pathogens. The initial insights emerged from studies on *V. cholerae*. *In vitro* assays indicated that reduced c-di-GMP levels triggered an elevated expression of the cholera toxin, a major virulence factor. Conversely, elevated c-di-GMP levels were associated with reduced virulence in the infant mouse model of cholera (Davies *et al*., 2012; Römling *et al*., 2013).

Distinct c-di-GMP signalling pathways exert both positive and negative regulation on various aspects of virulence (Krol *et al*., 2020). In the phytopathogenic bacterium *Pectobacterium atrosepticum*, c-di-GMP has been found to regulate biofilm formation as well as the secretion of a proteinaceous multi-repeat adhesin, required for binding to the host plant (Pérez-Mendoza *et al*., 2011a; 2011b). In *Pectobacterium carotovorum*, c-di-GMP has been shown to be involved in the synthesis of multiple bacterocins (Lagitnay *et al*., 2022). In *Erwinia amylovora*, c-di-GMP promotes virulence by enhancing amylovoran production and biofilm formation. In contrast, motility and the type III secretion system are and functional when c-di-GMP is absent (Kharadi *et al*., 2018). In addition, c-di-GMP represses the production of plant cell wall lytic enzymes in the soft rot pathogen *Dickeya dadantii* (Yuan *et al*., 2020).

3.3. C-di-GMP signalling in plant-interacting bacteria

The establishment of pathogenic or mutualistic interactions between plant and bacteria requires the continuous exchange of multiple signals that need to be integrated to coordinate, in time and space and upon environmental conditions, the expression of determinants for colonisation and eventual invasion of the host (Pérez-Mendoza *et al*., 2014). In the initial stages, bacterial motility and chemotaxis, exopolysaccharide (EPS) production, biofilm formation and secretion of adhesion and effector proteins are crucial for the success of the interaction. Complex regulatory networks involving inter and intracellular signalling, finely tune all those bacterial traits (Pérez-Mendoza *et al*., 2014; López-Baena *et al*., 2019). The second messenger c-di-GMP emerges as a key molecule in orchestrating these processes, since it allows the internalisation of the perceived environmental signals through regulatory networks and cascades that results in specific responses controlling lifestyle transitions (Krol *et al*., 2020).

In various plant-beneficial bacteria, such as *Azospirillum brasilense*, c-di-GMP has been involved in processes primarily related to exopolysaccharide production and biofilm formation (Ramírez-Mata *et al*., 2016). In *Azospirillum baldaniorum*, the diguanylate cyclase CdgC was shown to be required for optimal colonisation of wheat roots, so it has been proposed that participates in a cascade leading to bacterial attachment to the roots (Sierra Cacho *et al*., 2021). In *Pseudomonas putida*, the CfcA/CfcR two-component system appears to regulate c-di-GMP levels and biofilm formation in response to salts (Tagua *et al*., 2022). Furthermore, both arginine biosynthesis and uptake influence intracellular concentration of the second messenger, and thereby the associated phenotypes (Barrientos-Moreno *et al*., 2022). Additionally, AmrZ is involved in the regulation of c-di-GMP levels. In *Pseudomonas ogarae*, it participates in the regulation of a complex network of genes encoding DGCs and PDEs (Muriel *et al*., 2018), with AmrZ having a prominent role in the regulation of extracellular matrix components by c-di-GMP (Blanco-Romero *et al*., 2022).

3.3.1. Role of c-di-GMP in plant symbiotic *rhizobia*

Rhizobial strains with enhanced of intracellular c-di-GMP levels exhibit common free-living phenotypes, including reduced motility, increased EPS production, and enhanced biofilm formation. The importance of cellulose in c-di-GMP-dependent biofilm formation has been demonstrated in *R. etli*, since a *cel* mutant was unable produce it (Pérez-Mendoza *et al*., 2014; Krol *et al*., 2020).

In α-rhizobia, only adverse effects of elevated c-di-GMP levels on symbiotic performance have been described. Increased c-di-GMP levels in *R. etli* and *R. leguminosarum* strains favoured the early stages of the interaction, exhibiting enhanced adhesion to

plant roots; however, it impaired symbiotic efficiency, as plant growth and nitrogen contents were reduced. The high intracellular c-di-GMP levels appeared to impose a strong pressure against progression of the symbiosis (Pérez-Mendoza *et al*., 2014). In *Sinorhizobium fredii* elevated c-di-GMP levels caused symbiotic defects, whereas quenching of c-di-GMP had no detectable effects (Y. Li *et al*., 2021). Likewise, removal of c-di-GMP in *S. meliloti* did not affect its symbiotic efficiency (Schäper *et al*., 2016).

Proteins also play a crucial role in maintaining the structural integrity of bacterial biofilm matrices, including actively secreted proteins, adhesins, and motility organelles (such as flagella and pili) and their secretion can be directly or indirectly regulated by c-di-GMP (Fong & Yildiz, 2015). A study of the extracellular proteome of a *Rhizobium etli* strain under artificially elevated intracellular levels of c-di-GMP (Lorite *et al*., 2023) revealed that those high levels not only facilitated the secretion of various extracellular proteins potentially involved in adhesion and biofilm formation, but also promoted the export of cytoplasmic proteins (ECP) to the external environment of the cell. Remarkably, most of these cytoplasmic proteins had been previously characterized as multifunctional proteins in other organisms, often found extracellularly or associated with the bacterial cell surface.

3.3.2. Role of c-di-GMP in phytopathogenic *Pseudomonas*

In numerous *Pseudomonas* species, second messenger c-di-GMP regulates biofilm formation, motility and virulence. In *P. syringae* strains, c-di-GMP intricately controls virulence since it inhibits T3SS by downregulating the expression of numerous genes, represses bacterial motility by inhibiting the expression of several flagellar operons, and inhibits PAMPs by downregulating *fliC* transcription (Wang *et al*., 2019; Wang *et al*., 2023) *P. syringae* EPS production is regulated by multiple environmental signals. Thus, nutrient availability, temperature, and surface association strongly affect the expression of different polysaccharides under the control of c-di-GMP and the signalling proteins LadS and CbrB (Krishna *et al*., 2022). Specifically, the formation of c-di-GMP dependent air-liquid pellicles in which the main EPS is cellulose has been documented (Pérez-Mendoza *et al*., 2014; Farias *et al*., 2019; Pérez-Mendoza *et al*., 2019).

In several phytopathogenic *Pseudomonas*, elevated c-di-GMP levels have different effects on disease symptom development. For instance, overexpressing the DGC PleD* in Pto and *P. savastanoi* pv. phaseolicola (Pph) did not induce changes in virulence, despite important alteration in phenotypes such as motility or EPS production. Conversely, high levels of c-di-GMP in *Pseudomonas savastanoi* pv. savastanoi (Psv) noticeably impacted the disease symptomatology, leading to an increased knot size in olive plants (Aragón *et al*., 2015a; Aragón *et al*., 2015b).

In summary, phytopathogenic *Pseudomonas* and symbiotic *Rhizobium* strains with enhanced intracellular levels of c-di-GMP displayed common free-living responses: reduction of motility, increased production of extracellular polysaccharides and enhanced biofilm formation. However, differential outcomes were observed in the interaction with their corresponding host plants. Increased c-di-GMP levels in symbiotic *R. etli* and *R. leguminosarum* strains favoured the early stages of the interaction, but impaired further steps in the symbiotic process. In contrast, development of disease symptoms in Pto-tomato or Pph-bean interactions did not seem significantly affected by high c-di-GMP (Pérez-Mendoza *et al.*, 2014).

4. MOONLIGHTING PROTEINS

Moonlighting or multifunctional proteins comprise an interesting subset of proteins in which a function, in addition to the one typically ascribed to it, is found in a single polypeptide chain. In this way, moonlighting proteins possess two or more separate roles that cannot be ascribed to gene fusions, splice variants, or protein fragments expressing different roles after proteolysis (Jeffery, 2009). This term suggests a mechanism by which the cell (with a finite number of genes) increases its functional repertoire and goes against the general one protein-one function paradigm (Seidler, 2013; Kainulainen & Korhonen, 2014; Jeffery, 2020).

Protein moonlighting describes the process that involves acquiring and maintaining new, additional functions without complete cellular loss of the original primary function for that gene product. The process was initially described by Piatigorsky *et al.* (1988) and Wistow *et al.* (1988) in eukaryotes. Jeffery (1999), coined the term "moonlighting" to better describe these proteins with multiple jobs in a cell or organism. She observed that the set of moonlighting proteins that had been identified at that point seemed enriched for ubiquitous proteins like metabolic enzymes, implying that these ancient, widely conserved proteins, served as foundation elements for evolution and function diversification. Over time, it has become evident that moonlighting proteins are fairly common, providing molecular links between seemingly distinct biological processes (Jeffery, 2004). Indeed, a study in budding yeast showed that one-third of the tested enzymes, upon deletion, exhibited phenotypes restorable by catalytically inactive versions of the protein, indicating those proteins played additional roles aside from catalysis (Espinosa-Cantú *et al.*, 2018; Singh & Bhalla, 2020).

As moonlighting proteins are often randomly identified and are difficult to find through biological experiments, some prediction tools have been developed (Shirafkan *et al.*, 2021; M. L. Li *et al.*, 2021; Chen *et al.*, 2022) and different databases

created. Among the available databases are MoonProt (Mani *et al*., 2015; Chen *et al*., 2018; Chen *et al*., 2021), MoonDB (Ribeiro *et al*., 2019) or MultitaskProtDB (Franco-Serrano *et al*., 2018).

4.1. Moonlighting mechanisms

Different mechanisms have been described for a protein to be able to combine or switch between different moonlighting functions (Fig. I.10). One of the most frequently observed phenomena is subcellular localization changes, where proteins exhibit one function in the cell cytosol but a different one outside the cell or inside an organelle (Jeffery, 2004). Indeed, intracellular enzymes and chaperones that play a different role outside the cell constitute one of the largest subgroups of moonlighting proteins identified to date. Therefore, the dual cellular localization of a protein suggests the existence of moonlighting functions. Although this is a limited criterion, it has remained prevalent in the identification of bacterial moonlighting proteins, particularly in proteomic studies (Turnbull *et al*., 2016; Jeffery, 2017; Jeffery, 2018). Proteins can also exhibit moonlighting functions through various mechanisms. They can be expressed by a different cell type or make use of different solvent-exposed surface areas for different functions. Other mechanisms involve binding to a small molecule or another protein, or becoming part of a multiprotein complex. Evolving new binding partners is not a cumbersome process, as binding specificity can be significantly altered with just a few amino acid changes. If the primary function of the protein does not involve a large part of its surface, a new binding activity can evolve anywhere on that surface by modifying seemingly unused regions. These mechanisms are not mutually exclusive, and a combination of them is likely to be involved (Liu & Jeffery, 2020; Singh & Bhalla, 2020).

4.1.1. Post-translational modifications

Post-translational modifications (PTMs) represent another widespread mechanism influencing catalytic activity and enabling interaction with new binding partners. PTMs are chemical modifications that increase the complexity of the proteome by regulating activity, increasing or decreasing enzyme catalysis rates, controlling protein localization or interactions with other molecules, and altering information flows through signalling pathways. They can occur throughout a protein's lifespan and be reversible or permanent (Jeffery, 2016; Macek *et al*., 2019; Forrest & Welch, 2020). Phosphorylation, glycosylation, acylation or methylation are the most commonly described PTMs, but various other types have been identified. For moonlighting proteins that function in two different pathways, PTMs can serve as crucial regulatory mechanisms, acting as a switch between activities. The dynamic and often reversible nature of PTMs, coupled

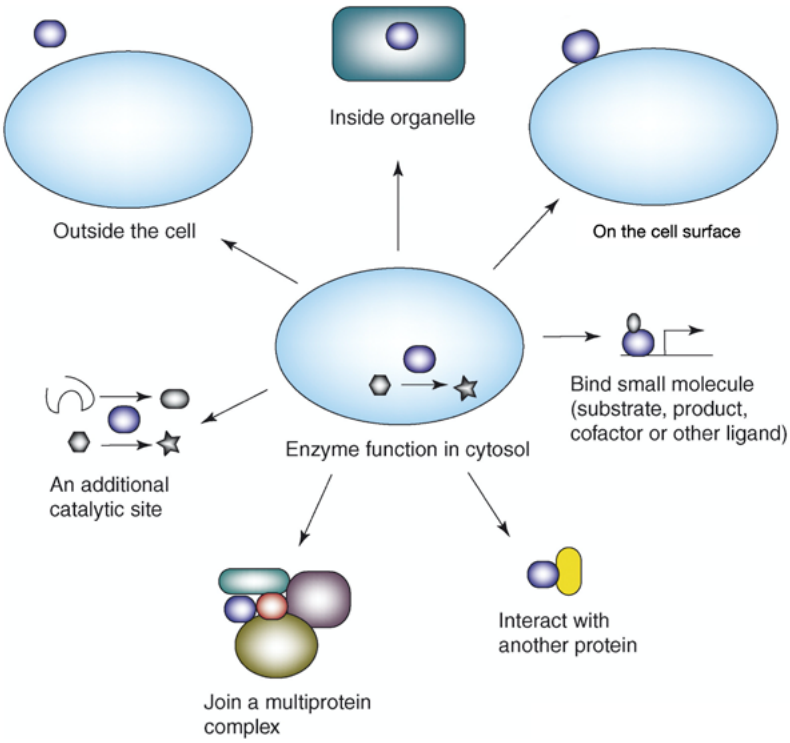

Figure I.10. Protein moonlighting.
There are diverse ways by which a protein can exhibit moonlighting functions. An enzyme is depicted in the cell cytosol catalysing a specific chemical reaction (represented by the hexagon and star symbols). However, the same protein may have an entirely different function when located outside the cell, on the cell surface, or within an organelle. A protein can also have different roles due to an additional catalytic site or when it binds to a cofactor or other ligand. New functions can also arise from interaction with another protein, or when it becomes part of a larger multiprotein complex. Modified from Jeffery (2004).

with their rapid addition/removal compared to synthesizing new proteins, significantly contribute to the cell's ability to adapt quickly to environmental fluctuations (Jeffery, 2016). One example is the elongation factor thermal unstable Tu (EF-Tu), a G protein that catalyses the binding of aminoacyl-tRNA to the A-site of the ribosome in living cells. Bacterial EF-Tus have been identified as targets for reversible PTMs such as phosphorylation, which reduces their binding affinity to GTP, methylation and acetylation in different bacteria (Sajid *et al.*, 2011; Harvey *et al.*, 2019).

4.1.2. Translocation mechanisms

Moonlighting proteins often perform their canonical and moonlighting functions in different cell compartments. However, the mechanisms governing their translocation to the cell exterior have remained elusive. Their secretion occurs without the involvement of well-characterized sorting mechanisms targeting extracellular localization, leading to their occasional designation as anchorless surface proteins or surface-associated housekeeping enzymes (Jeffery, 2018).

One of most straightforward explanations for the presence of cytoplasmic proteins in the extracellular media is that they originate from cell lysis and subsequently associate to the surface of neighbouring cells (Fig. I.11A) (Wang *et al*., 2013, Turnbull *et al*., 2016). In group B streptococci (*Streptococcus agalactiae*), GAPDH levels detected on the cell surface and extracellular media decreased in mutants that displayed a lower level of cell lysis, and a similar trend was described for *Streptococcus pneumoniae* (Oliveira *et al*., 2012; Terrasse *et al*., 2015). Cell lysis or defective cell division also appear to be involved in the release of cytoplasmic proteins by *Staphylococcus aureus*, as described in an *atlA* (major autolysin) mutant, where the release of GAPDH and FbaA (fructose-bisphosphate aldolase) was severely affected (Pasztor *et al*., 2010). Nevertheless, other studies propose that at least certain moonlighting proteins require a secretion system (Ebner *et al*., 2016).

Another exportation mechanism involves their packaging into membrane-derived vesicles (MVs). These consist of various types of lipids derived from cellular membranes along with other molecules, such as proteins, nucleic acids and low molecular mass organic compounds with various biological functions. MVs allow their enclosed content to be transported away from the cell while providing protection from the external environment. At their destination, the contents can be delivered by fusing with target membranes or by contact with a surface that can trigger its lysis (Fig. I.11B) (Nagakubo *et al*., 2020). Many Gram-negative bacteria produce outer-membrane derived vesicles (OMVs), with an average diameter of 20-200 nm, which often encapsulate cytoplasmic proteins (CPs). For instance, *Cronobacter sakazakii* generates OMVs containing different proteins, including classically secreted and outer-membrane proteins, but also CPs such as GroEL, DnaK, or EF-Tu (Kothary *et al*., 2017). Similarly, an analysis of OMVs from pathogenic and non-toxic strains of *Bacteroides fragilis* revealed a significant content of CPs involved in carbohydrate and amino acid metabolism (Zakharzhevskaya *et al*., 2017). Furthermore, the identification of proteins associated with the extracellular matrix of *Pseudomonas aeruginosa* biofilms revealed that the large majority of those proteins originated from OMVs (Toyofuku *et al*., 2012).

An alternate hypothesis suggests the secretion of moonlighting proteins onto the cell surface through yet unknown so-called non-classical or non-canonical secretion pathways (Fig. I.11D). There is evidence supporting the involvement of a secretion system for some individual proteins (Götz *et al.*, 2015; Chen *et al.*, 2016; Wang *et al.*, 2016). For instance, in *Bacillus subtilis*, the release of GroEL, DnaK and enolase is not due to cell lysis, or MVs. Moreover, there was no N-terminal cleavage, and a mutant form of enolase with a hydrophobic helix replaced with a more neutral helix, was retained inside the cell when the wild type protein was detected in the media (Yang *et al.*, 2011). Also, a modified T3SS

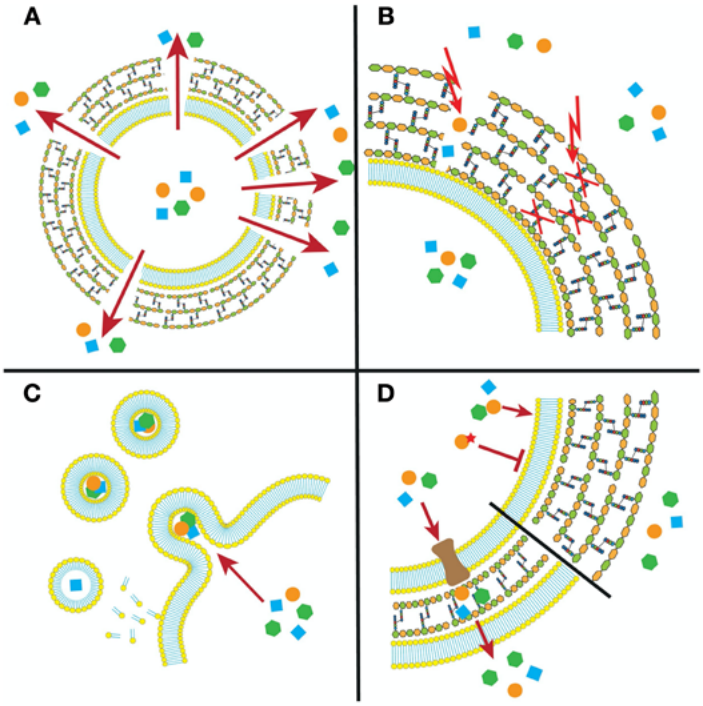

Figure I.11. Secretion and release routes for cytoplasmic proteins (CPs).
A. Cell lysis, due to environmental or cellular factors, is a major contributor to the release of CPs in many bacteria.
B. Weakening of the cytoplasmic membrane or cell wall by autolysins or membrane-acting agents diminish cell integrity and cause CP release.
C. Formation of membrane-vesicles with CPs as cargo.
D. Biochemical properties such as hydrophobicity, or structural features like intramolecular helices influence the secretion process of CP (upper part). Additionally, translational and osmotic stress can induce the synthesis of mechanosensitive channels and increase membrane permeabilisation, leading to the release of CPs. Modified from Ebner & Götz (2019).

appears to be used for GAPDH exportation in an enteropathogenic *E. coli* (Aguilera *et al*., 2012). As secretion of these proteins may involve unknown pathways, PTMs could render some proteins to be passable substrates; additionally, unidentified chaperones might be required for this process (Jeffery, 2018). Several studies have also identified peptides on the cell surface resulting from the proteolytic cleavage of intracellular proteins, including EF-Tu, suggesting that cleavage might yield peptides with improved binding capabilities to certain host structures compared to the original protein (Widjaja *et al*., 2017). Therefore, although experimental evidence has been presented for the different hypotheses, the overall data remains scattered and only suggestive. Similarly, the mechanisms governing their attachment to the cell surface are not well understood (Wang & Jeffery, 2016; Ebner & Götz, 2019).

4.2. Moonlighting proteins in bacteria

In bacteria, the first identified moonlighting enzyme was glyceraldehyde-3-phosphate dehydrogenase (Gap or GAPDH). It was found on the cell surface as well as in the cytoplasm of group A streptococci, and was reported to exhibit multiple adhesive functions *in vitro*, potentially contributing to increased bacterial virulence (Pancholi & Fischetti, 1992). Since then, numerous moonlighting proteins have been identified or suggested in prokaryotic organisms, with almost all enzymes of the EMP glycolytic pathway associated with an adhesive moonlighting function (Kainulainen & Korhonen, 2014).

A large number of moonlighting proteins have been found to contribute to the virulence of bacterial pathogens. They are often highly conserved housekeeping proteins involved in chaperone function, stress response or metabolism, that play additional roles during pathogenesis, relying on their secretion. Once outside the pathogen cell, these proteins mediate cell signalling, adhesion and even act as toxins. As of 2018, one-fourth of the around 700 proteins with known moonlighting functions have been found to be pathogen virulence proteins. One hypothesis suggested to explain this apparent prevalence of moonlighting proteins in virulence is that, due to their primary functions in core metabolic pathways, they exhibit sequence homology with host proteins. This similarity may hinder the host's ability to recognize these virulence factors as exogenous, impeding the production of protective antibodies (Singh & Bhalla, 2020; Franco-Serrano *et al*., 2021).

While moonlighting proteins were initially identified in pathogenic Gram-positive bacteria, posterior research has revealed their presence in Gram-negative bacteria as well as in non-pathogenic or commensal bacteria, highlighting the common occurrence of moonlighting. For instance, *E. coli* GAPDH has been found to be secreted outside the cell, where it plays a role in signal transduction (Ferreira *et al*., 2013). Additionally,

Lactobacillus plantarum surface located enolase has the ability to bind to fibronectin, a major component of the host extracellular matrix (Castaldo *et al*., 2009).

The majority of the currently known bacterial moonlighting proteins fulfil essential roles within the cell, such as glycolysis, chaperone activity, protein synthesis, or nucleic acid stability. Consequently, silencing of a moonlighting-associated gene most likely has broad phenotypic effects, making it challenging to interpret its implications for both the canonical and the moonlighting function. The recognised adhesive moonlighting functions are diverse and include binding to secreted mucins, epithelial cells, lymphocytes and monocytes, extracellular matrices, circulating effector molecules, and other microbes. However, the physiological significance and biological consequences of those interactions are only well understood in a limited number of cases. Thus, the EF-Tu exhibits diverse functionalities in the cell surface, interacting with membrane receptors and the extracellular matrix of plant and animal cells (Harvey *et al*., 2019). The structures of most bacterial moonlighting proteins, such as EF-Tu, enolase and GAPDH, exhibit substantial conservation across kingdoms and do not significantly differ between prokaryotes and eukaryotes. This conservation is understandable given their essential metabolic functions and their ability to moonlight in multiple organisms (Kainulainen & Korhonen, 2014; Jeffery, 2018; Liu & Jeffery, 2020).

Some recently documented moonlighting functions include those observed for ribosomal proteins, usually involved in assembly and protein translation, that also exhibit antimicrobial activities. For example, certain ribosomal proteins from lactic acid bacteria were effective as antimicrobials against *Listeria monocytogenes*, *Streptococcus pyogenes*, *Streptococcus uberis*, and *Enterococcus faecium (*de Carvalho *et al*., *2010;* Pidutti *et al*., 2018; Hurtado-Rios *et al*., 2022). Furthermore, in *P. aeruginosa*, a single gene of the accessory genome encoding a VirB4 homolog of an element of a type IV secretion system, has been shown to become essential for the regulation of core genome-encoded metabolism and virulence features, probably functioning as a metabolic sensor of virulence and quorum sensing (Wiehlmann *et al*., 2023).

4.3. Glyceraldehyde-3-phosphate dehydrogenase

Glyceraldehyde-3-phosphate dehydrogenase (GAPDH or Gap; EC 1.2.1.12) is an ancient and ubiquitously distributed enzyme of sugar metabolism with key roles in the glycolytic and gluconeogenic pathways. It catalyses the conversion of glyceraldehyde-3-phosphate to 1,3-bisphosphoglycerate and *vice versa*. The early discoveries about GAPDH date back to the first half of 20th century, and the early works (1930-1970) on this enzyme significantly contributed to establish the fundamental principles of biochemistry, particularly enzymology (Seidler, 2013). More recently, additional

roles unrelated to its enzymatic function have been described for GAPDH in diverse organisms (bacteria, fungi, mammals, plants), which make it a prototype for multifunctional proteins (Giménez *et al*., 2014; Sirover, 2014; Yang & Zhai, 2017).

4.3.1. Basic biology of GAPDH

Sequence and structure

GAPDH is present in virtually all organisms and the *gap* gene is highly conserved among prokaryotes and eukaryotes. When comparing the sequence of the human GAPDH to that of invertebrates, the degree of identity varies from 72 to 75%, whereas compared to that of microorganisms, a 45-46% identity is observed, with homology based on similarity increasing up to 65%. This is not surprising, given GAPDH's "housekeeping" role and its essential biological activity for cellular existence.

The *gap* gene codes for a single polypeptide of 34-38 KDa (Seidler, 2013) that possesses two main domains: the N-terminal nucleotide-binding domain (NBD) and the catalytic domain, which contains a cysteine at the active site. The NBD consists of a parallel β-sheet surrounded by α-helices in a classical *Rossmann* fold. On the other hand, the catalytic domain is composed of an antiparallel β-sheet surrounded by α-helices and contains the active site residues, as well as the so-called S-loop (Fig. I.12A) (Malay *et al*., 2009; Sirover, 2014). The folded protein chain assembles into a homotetrameric enzyme, which is the usual form of the protein in the cytosol. Functionally and structurally, the GAPDH tetramer is a dimer of dimers, and the pair of dimers relate to each other across the Q-axis, the only true 2-fold axis of symmetry (Fig. I.12B) (Seidler, 2013; Sirover, 2014; Querol-García *et al*., 2017).

Enzymatic activity

Glycolysis, a vital metabolic pathway in central carbon metabolism associated with energy production, consists of two main stages. The first stage starts with glucose, a ubiquitous hexose that is converted to the molar equivalent of two triose-phosphates. The second stage transform D-glyceraldehyde 3-phosphate into pyruvate, with the first reaction requiring GAPDH (Fig. I.13A). Moreover, glyceraldehyde-3-phosphate is a product of several other important metabolic pathways, including gluconeogenesis, pentose phosphate pathway, fructose catabolism, and glycerol metabolism (Kim & Dang, 2005; Seidler, 2013).

GAPDH catalyses the oxidative phosphorylation of the substrate D-glyceraldehyde 3-phosphate, which is converted to the product, 1,3-bisphospho-D-glycerate. In this process, inorganic phosphate acts a co-substrate, and becomes incorporated into the

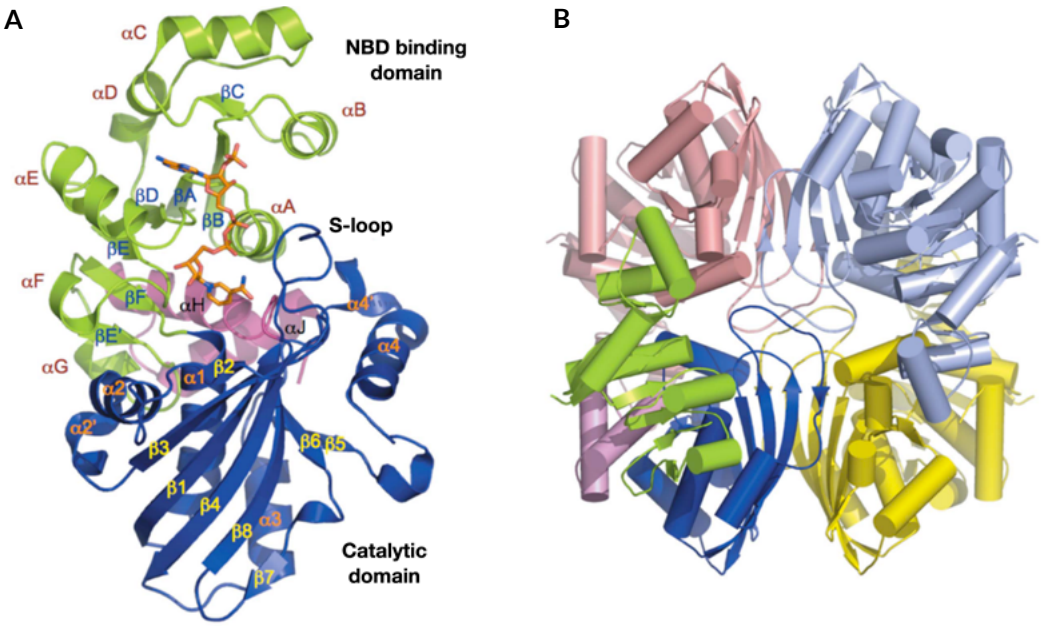

Figure I.12. Overall structure of GAPDH (*M. jannaschi*).
A. Structure of the GAPDH monomer. The nucleotide-binding domain (NBD) is displayed in green, the catalytic domain in blue and the C-terminal domain in pink. Bound $NADP^+$ is depicted in orange. Secondary-structure elements are indicated.
B. Quaternary structure of the GAPDH tetramer. Modified from Malay *et al.* (2009).

final product, thus requiring the presence of two anion binding pockets within the enzyme active site. The cofactor, nicotinamide adenine dinucleotide-oxidized (NAD^+ or $NADP^+$), receives two electrons during the catalytic event, creating the reduced form of the dinucleotide, NADH or NADPH. The enzyme, therefore, features a dinucleotide-binding site (Fig. I.13B). This reaction is fully reversible, with 1,3-bisphospho-D-glycerate serving as the substrate in the opposite direction, and NADH or NADPH as the cofactor, which becomes oxidized to NAD^+ or $NADP^+$. Inorganic phosphate and D-glyceraldehyde 3-phosphate become the products of the reverse reaction (Fothergill-Gilmore & Michels, 1993; Butterfield *et al.*, 2010; Seidler, 2013).

GAPDH IN PROKARYOTES

Based on homology, GAPDH family members can be categorised into three classes: class I enzymes, the most common, which utilize NAD^+ and/or $NADP^+$; class II enzymes, which include archaeal NAD(P)-dependent GAPDHs; and class III bifunctional enzymes (erythrose-4-phosphate dehydrogenase/GAPDH) that are more common in γ-proteobacteria (Figge *et al.*, 1999; Elkhalfi *et al.*, 2013).

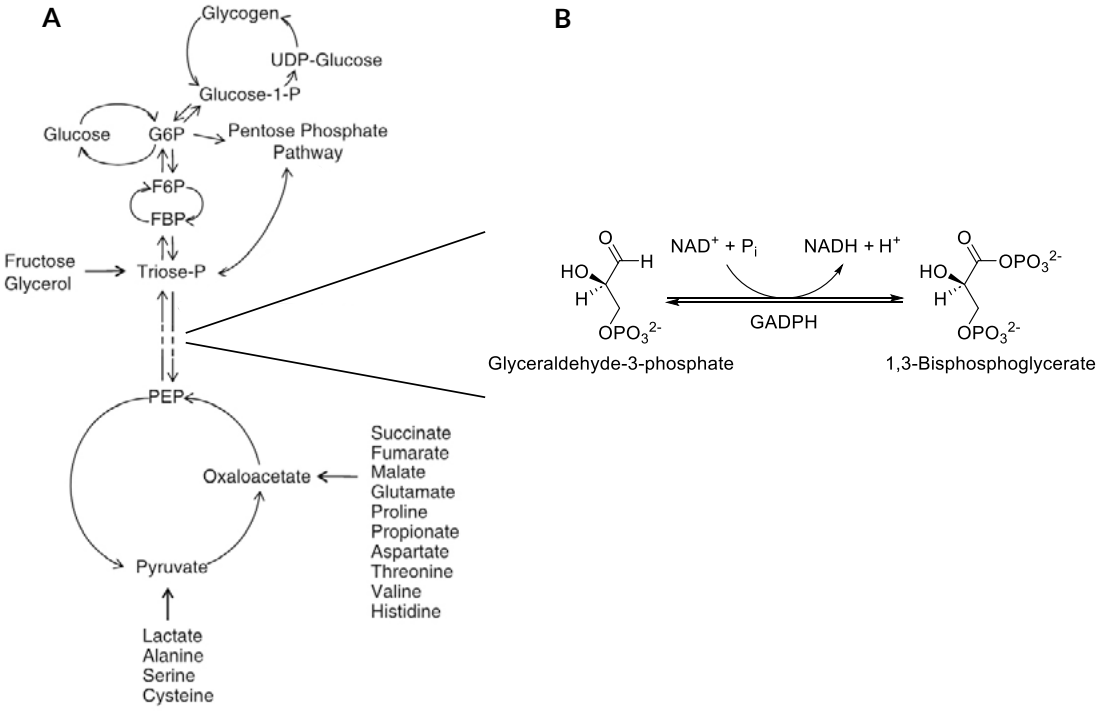

Figure I.13. GAPDH role in metabolism.
A. Central carbon metabolism main pathways (glycolysis, gluconeogenesis, pentose phosphate pathway and tricarboxylic acid cycle) where GAPDH plays an essential role. Modified from Seidler (2013).
B. Reaction catalysed by GAPDH, oxidative phosphorylation of glyceraldehyde-3-phosphate to 1,3-bisphosphoglycerate and *vice versa*.

Although many bacteria contain a single GAPDH protein capable of performing both glycolytic and gluconeogenic activities, as seen in *E. coli* (Seta *et al*., 1997), there is no universal layout for this enzymatic activity in bacteria. For instance, in the Gram-positive *Bacillus subtilis* and *Staphylococcus aureus* a NAD-dependent and a NADPH-dependent GAPDH specialized in glycolysis and in gluconeogenesis, respectively, coexist (Fillinger *et al*., 2000; Purves *et al*., 2010; Commichau *et al*., 2013). This configuration may grant certain advantages for the functioning of particular metabolic pathways under specific environmental conditions (Nikel *et al*., 2015).

4.3.2. GAPDH as a moonlighting protein

GAPDH has been recognised as a moonlighting protein since early studies. Numerous investigations have described GAPDH as a multifunctional protein involved in various biological processes in pathogens (Pancholi & Fischetti, 1992), probiotics (Kinoshita *et al*., 2008), mammals (Sirover, 2011) and plants (Zaffagnini *et al*., 2013). Indeed, GAPDH can be considered a model of a moonlighting protein that displays a wide array of cellular functions attributable to its capacity to engage in complex interactions (Giménez *et al*., 2014).

The multifunctionality of GAPDH has been extensively documented in human cells, where it is involved in numerous cellular processes, such as transcriptional and post-transcriptional gene regulation, chromatin structure, intracellular trafficking, DNA replication and DNA repair (Sirover, 2011). Each moonlighting function requires the integration of GAPDH into specific protein complexes and may implicate different regions of the protein's structure. Moreover, the diverse moonlighting functions of GAPDH may rely on specific PTMs, which can define its oligomeric state, subcellular localization, or different binding partners (Copley, 2012; Giménez *et al*., 2014). GAPDH can undergo several covalent modifications, such as S-glutathionylation, S-nitrosylation, phosphorylation, acetylation and ADP-ribosylation, among others (Sirover, 2014). These alterations give rise to different protein forms, which differ in their isoelectric point, and therefore can be separated by two-dimensional gel electrophoresis. Most of those modifications are linked to oxidative stress responses and may have important physiological consequences (Giménez *et al*., 2014; Sirover, 2021).

Moonlighting functions of GAPDH in bacteria

In bacteria, as stated above, the initial identification of GAPDH as a moonlighting protein occurred on the surface of the pathogen *Streptococcus pyogenes*, a Gram-positive bacterium that causes pharyngitis and skin infections. This surface-located GAPDH is enzymatically active and able to bind several human proteins, such as fibronectin, lysozyme, laminin or cytoskeletal proteins (Pancholi & Fischetti, 1992; Jin *et al*., 2005). GAPDH has also been found on the surface of other streptococci, like *Streptococcus suis* and *Streptococcus pneumoniae* (Bergmann *et al*., 2004; Brassard *et al*., 2004), and other Gram-positive pathogens, such as *Bacillus anthracis* (Matta *et al*., 2010) or *Staphylococcus aureus* (Ebner *et al*., 2016). Various roles have been attributed to these surface-exposed GAPDH proteins. For instance, in *Mycoplasma pneumoniae* it mediates interactions with the extracellular matrix proteins of the human host and contributes to respiratory tract colonisation (Dumke *et al*., 2011). In *Listeria monocytogenes*, cell wall-associated GAPDH was shown to catalyse the ADP-ribosylation of Rab5a, a protein involved in endosome maturation (Schaumburg *et al*., 2004).

The description of moonlighting roles for GAPDH in Gram-negative pathogens emerged more than a decade later. GAPDH has been detected on the surface and secreted into the medium by enteropathogenic or enterohemorrhagic *E. coli* strains in a soluble and active form (Egea *et al*., 2007). Besides *E. coli*, GAPDH has been found on the surface of other Gram-negative pathogens, such as *Neisseria meningitidis*, *Edwardsiella tarda* and *Francisella tularensis* (Liu *et al*., 2005; Dumke *et al*., 2011; Kopeckova *et al*., 2020a). Specific extracellular activities are advantageous for the colonisation of the intestinal mucosa. In this regard, certain housekeeping proteins initially associated with pathogenesis mechanisms, have also been identified in the secretome of probiotic strains. Notably, secretion of GAPDH by several Gram-positive probiotic *Lactobacillus* species (Sánchez *et al*., 2009a; Sánchez *et al*., 2009b), as well as by the Gram-negative probiotic *Escherichia coli* Nissle 1917 (Aguilera *et al*., 2012) has been reported.

These alternative roles usually rely on the ability of GAPDH to modify its subcellular location, as they depend on the presence of the protein on the cell surface or in the extracellular media (Sirover, 2014; Yang and Zhai, 2017). Nevertheless, as other multifunctional proteins, the GAPDH sequence lacks any known motif for extracytosolic trafficking. In the case of *Lactobacillus plantarum*, export of GAPDH to the bacterial cell surface has been linked to plasma membrane permeability *(*Saad *et al*., 2009), whereas in *E. coli* Nissle 1917, GAPDH was found to use a modified T3SS (Aguilera *et al*., 2012). Nevertheless, the precise translocation mechanism remains unclear (Kopeckova *et al*., 2020b).

4.3.3. GAPDH in plant-interacting bacteria

As mentioned earlier, GAPDH has been shown to engage with various host components in both pathogenic and beneficial bacteria, participating in adhesion and binding to extracellular matrices. However, its potential roles in plant-interacting bacteria remain largely unexplored.

GAPDH in rhizobia

In rhizobia, glyceraldehyde-3-phosphate dehydrogenase (GAPDH) is encoded by a single *gap* gene, resulting in a protein of approximately 37 kDa. Typically, the *gap* gene is positioned downstream of *tkt*, which encodes another metabolic protein known as transketolase. The *tkt-gap* genetic arrangement is conserved in many rhizobia, as well as other α- and β-proteobacteria. The specific location or type of promoter that regulates their expression, as well as whether those genes are transcribed as a single operon, remains unknown. This GAPDH is predicted to possess both glycolytic and gluconeogenic activities. *S. meliloti* mutants lacking GAPDH activity obtained after Tn5 transposon

mutagenesis were unable to grow on gluconeogenic carbon sources and displayed significantly reduced growth on glycolytic carbon sources (Finan *et al.* 1988).

Regarding possible indications of moonlighting functions, the Gap protein of *R. etli* has been found as an extracellular protein under normal growth conditions (Meneses et al., 2017). Also, in a more recent work, Lorite *et al.* (2023) have observed that secretion of the *R. etli* Gap protein was enhanced by high intracellular levels of c-di-GMP. The presence of PTMs has also been detected, as the GAPDH protein of *S. fredii* has been observed to be phosphorylated at two adjacent residues (Thr^{210} and Ser^{211}), which suggests that other rhizobial Gap proteins could also bear this type of PTM (Liu *et al*., 2015).

In relation to symbiosis, different phenotypes have been observed concerning the role of gluconeogenic enzymes: while *pckA* (encoding phosphoenolpyruvate carboxykinase) mutants of *S. meliloti* and *R. leguminosarum* form N-fixing nodules (Finan *et al*., 1991; Mulley *et al*., 2010), a *pckA* mutant of *R. etli* formed only nodule-like structures with undeveloped infection threads (Tatè *et al*., 2004), whereas *pckA* mutants of the NGR234 *Sinorhizobium* strain exhibited a variable symbiotic phenotype depending on the host plant (Østerås *et al*., 1991). In the rhizobia-legume symbiosis, nitrogen fixation is possible thanks to the cooperative interaction of proteins from both symbionts, potentially engaged in roles different from those performed in the individual organisms. Moreover, symbiosis requires the coordinated secretion of plant and bacterial proteins into the symbiosome (Simonsen & Rosendahl, 1999; Liu *et al*., 2006; D. Wang *et al*., 2010). Analysis of the symbiosome membrane and space have revealed a mixture of proteins of both plant and bacteroid origin, suggesting directed transport of proteins from each symbiont. The majority of the approximately 150 proteins associated with the symbiosome membrane are of plant origin and non-metabolic in nature, whereas the identified symbiosome space proteins are mostly metabolic enzymes of bacterial origin (Panter *et al*., 2000; Saalbach *et al*., 2002; Catalano *et al*., 2004). These observations support the concept that the symbiosome is an inter-kingdom domain, hosting proteins from both plant and bacteroid origins. Furthermore, these proteins are functioning in a novel 'extracellular' environment, and thus could be considered moonlighting. Interestingly, about one-fourth of the identified proteins in the symbiosome membrane and space have been recognized as moonlighting proteins, including GAPDH of plant origin. This suggests that the symbiosome is not only unique in facilitating symbiotic nitrogen fixation, but also in its protein composition and molecular architecture, where different metabolic proteins like GAPDH may be playing undiscovered roles (Emerich & Krishnan, 2014).

GAPDH in Pseudomonas

Unlike rhizobia, most *Pseudomonas* display at least two putative *gap* alleles. The *gap1* or *gapA* gene is the most common and ubiquitous, encoding a class I GAPDH where the classical structural domains are clearly recognised. Another *gap* gene, referred as *gap2* or *gapB*, is present in many *Pseudomonas* strains, like *P. putida* and *P. syringae* (Elkhalfi *et al*., 2013; Nikel *et al*., 2015). The Gap2 protein possesses an extra N-terminal unstructured region which makes it larger than the canonical GAPDHs. It would belong to the subgroup of ATP-insensitive class I GAPDHs, which have been proposed to participate in the gluconeogenic pathway (Elkhalfi *et al*., 2013). A third putative *gap* gene, referred as *gap/epd*, is present in the genome of several *Pseudomonas* strains, with *P. fluorescens* and *P. syringae* among them (Elkhalfi *et al*., 2013). The enzyme encoded by *gap/epd* belongs to the class III of Gap/Erythrose-4-phosphate dehydrogenase (E4PDH or Epd) bifunctional enzymes, also found in other proteobacterial groups. Epd catalyses the conversion of D-erythrose 4-phosphate (E4P) to 4-phosphoerythronate (4-PE), the first step of the vitamin B6 or pyridoxal 5'-phosphate (PLP) biosynthesis pathway, which makes this enzyme essential when uptake of B6 vitamers from the environment is not possible (Richts *et al*., 2019; Nimma *et al*., 2023).

Limited information is currently available regarding the potential moonlighting functions of GAPDH in *Pseudomonas*. However, in the case of Pto DC3000, a specific GAPDH isoform (Gap1) has been found to be exported extracellularly in a T3SS-inducing medium (Elkhalfi *et al*., 2014; Schumacher *et al*., 2014), suggesting a putative extracellular role of this protein.

OBJECTIVES

OBJECTIVES

The agricultural sector significantly contributes to the ongoing environmental crisis. However, amidst this challenge, biological nitrogen fixation stands out as a crucial process with both economic and ecological benefits, since it promotes sustainable agriculture by reducing the reliance on nitrogenous fertilizers. Specifically, the symbiotic relationship between *Rhizobium* bacteria and leguminous plants exemplifies this, offering an environmentally sustainable approach to agricultural production. On the other hand, diseases caused by phytopathogenic bacteria pose a substantial threat to crop yields, leading to significant losses. By comprehensively understanding the dynamics of both types of plant-bacteria interactions, we can leverage them in various ways. This includes developing agricultural biotechnologies that support sustainable crop production and exploring industrial biotechnologies for producing valuable bacterial compounds, like polymers or secondary metabolites.

The background and working hypothesis of this PhD thesis conceive the second messenger c-di-GMP playing a pivotal role at the crossroad of two important and underexplored aspects of bacterial physiology: surface moonlighting proteins and non-classical secretion mechanisms, suggesting a genetic and programmed control of both processes in bacteria. Following the previous study about the impact c-di-GMP on the extracellular proteome of *Rhizobium etli* by Lorite *et al*. (2023), this doctoral thesis is based on the hypothesis that c-di-GMP controls the export of cytoplasmic proteins to the cell exterior, and this process is relevant for the colonization and infection of plants by phytobacteria, both pathogenic and beneficial.

The main objective of this doctoral thesis is to investigate moonlighting proteins whose exportation is potentially regulated by c-di-GMP in plant-associated bacteria. To achieve this, the following specific objectives will be addressed:

1. Determination of c-di-GMP-dependent protein profiles in *Pseudomonas syringae* pv. tomato (Chapter I).

2. Assessment of the roles of Gap, a moonlighting protein, in plant-associated bacteria: *Pseudomonas syringae* pv. tomato and *Rhizobium etli* (Chapters II and III).

3. Investigation of the mechanisms involved in the export of cytoplasmic proteins, focusing on the c-di-GMP-dependent Gap protein of *R. etli* (Chapter IV).

MATERIALS AND METHODS

MATERIALS and METHODS

1. BACTERIAL STRAINS AND PLASMIDS

1.1. Bacterial strains

Bacterial strains used in this work and their main characteristics are listed in Table M.1. *Rhizobium etli* CE3 (Quinto *et al*., 1982) and *Pseudomonas syringae* pv. tomato DC3000 (Cuppels, 1986) were the two strains object of study in this doctoral thesis. *Escherichia coli* strains were used as plasmid vector hosts.

1.2. Plasmids

Plasmids used and constructed in this work are listed in Table M.2. For direct cloning of PCR products, the high copy number commercial plasmids pGEM-T and pCR2.1-TOPO were used. Mutants were constructed using the mobilizable vector pK18*mobsacB* which behaves as a non-replicative, suicide plasmid in *Rhizobium* and *Pseudomonas*. The pJB3Tc19 plasmid was routinely used as a mobilizable, broad host-range expression vector for complementation and/or overexpression of different genes. The pTD-NTwin-Strep plasmid was used for expression of tagged recombinant proteins. In this plasmid, the sequence of interest is fused with the Twin-strep and 6xHis tag sequences, and expressed from a P_{trc} synthetic promoter which responds to IPTG. On the other hand, the pME6016 plasmid was used for transcriptional activity analysis of gene promoters. This vector contains a promoterless *lacZ* gene encoding β-galactosidase which serves as a reporter of gene expression. Genetic maps of the non-commercial plasmids used are shown in Appendix A.

2. MEDIA AND CULTURE CONDITIONS

2.1. Rich media

Escherichia coli and Pto DC3000 strains were routinely grown in Luria-Bertani broth (LB) (Sambrook *et al*., 1989) at 37ºC and 28ºC or 20ºC , respectively. Liquid cultures were grown in shaking conditions (170 rpm). For solid media bacteriological agar was added to a final concentration of 1% (w/v). LB composition: 10 g/l tryptone, 5 g/l yeast extract and 5 g/l NaCl.

Table M.1. Bacterial strains.

Strain	Characteristics	Reference
P. syringae pv. tomato		
Pto DC3000	Pto; Wild type; Rif^R	Cuppels (1986)
Pto ΔwssBC	DC3000 Cel^-, ΔwssBC; Rif^R	Pérez-Mendoza *et al.* (2014)
Pto ΔG1	DC3000 Δ*gap1*; Rif^R	Casas-Román *et al.* (2024)
Pto ΔG2	DC3000 Δ*gap2*; Rif^R	Casas-Román *et al.* (2024)
Pto ΔG1/2	DC3000 Δ*gap1* Δ*gap2*; Rif^R	Casas-Román *et al.* (2024)
Pto Δepd	DC3000 Δ*epd*; Rif^R	Casas-Román *et al.* (2024)
Rhizobium etli		
CE3	Ret; CFN42 derivative; Nx^R, Sm^R	Quinto *et al.* (1982)
AC1D	CE3 Δ*gap*; Nx^R, Sm^R	This work
Ret Tn7Km	CE3 with a mini-Tn7Km transposon; Km^R, Nx^R, Sm^R	Romero-Jiménez *et al.* (2015)
Ret Tn7pleD*Km	CE3 with a mini-Tn7*pleD**Km transposon; Km^R, Nx^R, Sm^R	Romero-Jiménez *et al.* (2015)
AC1D Tn7Km	AC1D with a mini-Tn7Km transposon; Km^R, Nx^R, Sm^R	This work
AC1D Tn7pleD*Km	AC1D with a mini-Tn7*pleD**Km transposon; Km^R, Nx^R, Sm^R	This work
LR102	Ret Cel^- Tn7Km; CE3 Δ*celAB* with a mini-Tn7Km transposon; Km^R, Nx^R, Sm^R	Pérez-Mendoza *et al.* (2022)
LR101	Ret Cel^- Tn7pleD*Km; CE3 Δ*celAB* with a mini-Tn-7*pleD**Km transposon; Km^R, Nx^R, Sm^R	Pérez-Mendoza *et al.* (2022)
Escherichia coli		
DH5α	*supE44 recA1 endA1 gyrA96 thi1 relA1 hsdR17* Δ*lacU169* ϕ80dlacZΔM15; Nx^R	Hanahan (1983)
S17.1	*thi*, *pro*, *recA*, *hsdR*, *hsdM*, Rp4Tc::Mu, Km::Tn7; Sm^R, Sp^R, Tmp^R	Simon *et al.* (1983)
β2163	RP4-2-Tc::Mu Δ*dapA*::(erm-pir); Em^R, Km^R, $DAPA^{aux}$	Demarre *et al.* (2005)
OmniMAX™	F´{*proAB lacI*^{q} lacZΔM15 Tn10 Δ(*ccdAB*)} mcrA Δ(*mrr hsdRMS-mcrBC*) ϕ80(lacZ)ΔM15 Δ(*lacZYA-argF*)*U169 endA1 recA1 supE44 thi-1 gyrA96 relA1 tonA panD*; Nx^R, Tc^R	Invitrogen

Ap: ampicillin, DAPA: diaminopimelic acid, Em: erythromycin, Km: kanamycin, Nx: nalidixic acid, Rif: rifampicin, Sm: Streptomycin, Tc: tetracycline, Tmp: trimethoprim, ^{aux}: auxotroph, ^{R}: resistant.

Table M.2. Plasmids.

Plasmid	Characteristics	Reference
pGEM-T	Cloning vector; Ap^R	Promega
pCR2.1-TOPO	Cloning vector; Ap^R	Invitrogen
PUX-BF13	Plasmid bearing transposase genes tnsABCDE, ori R6K; Ap^R	Bao *et al*. (1991)
pK18mobsacB	Suicide vector; Km^R	Schäfer *et al*. (2024)
pK18ΔG1	pK18*mobsacB* derivative bearing a 1221 bp EcoRI fragment containing a deleted version of gap1; Km^R	Casas-Román *et al*. (2024)
pK18ΔG2	pK18*mobsacB* derivative bearing a 1157 bp EcoRI fragment containing a deleted version of gap2; Km^R	Casas-Román *et al*. (2024)
pK18Δepd	pK18*mobsacB* derivative bearing a 1112 bp BamH1/HindIII fragment containing a deleted version of epd from Pto DC3000; Km^R	Casas-Román *et al*. (2024)
pK18Δgap	pK18*mobsacB* derivative bearing a 1279 bp PstI fragment containing a deleted version of gap from R. etli; Km^R	This work
pJB3Tc19	IncP Cloning vector, Plac promoter; $Ap^{R,}$, Tc^R	Blatny *et al*. (1997)
pJBpleD*	pJB3Tc19 derivative bearing a 1400 bp EcoRI/XbaI fragment containing the pleD* gene from *Caulobacter crescentus*; $Ap^{R,}$, Tc^R	Pérez-Mendoza *et al*. (2014)
pJG1	pJB3Tc19 derivative bearing a 1330 bp HindIII/BamHI fragment containing *gap1* from Pto DC3000; $Ap^{R,}$, Tc^R	Casas-Román *et al*. (2024)
pJG2	pJB3Tc19 derivative bearing a 1718 bp SphI/XbaI fragment containing *gap2* from Pto DC3000; $Ap^{R,}$, Tc^R	Casas-Román *et al*. (2024)
pJepd	pJB3Tc19 derivative bearing a 1253 bp HindIII/BamHI fragment containing *epd* from Pto DC3000; $Ap^{R,}$, Tc^R	Casas-Román *et al*. (2024)
pJGap	pJB3Tc19 derivative bearing a 1070 bp PstI/XbaI fragment containing gap from *R. etli*; $Ap^{R,}$, Tc^R	This work
pJMCy	pJB3Tc19 derivative bearing a 1070 bp PstI/XbaI fragment containing gap from *R. etli* with a G->C mutation in position 508; $Ap^{R,}$, Tc^R	This work
pTD-NTwinStrep	IncP TwinStrep/His6 expression vector; Sm^R, Spc^R	Dammeyer *et al*. (2013)
pGap12	pTD-NTwinStrep bearing a 1006 bp fragment containing the gap gene from *R. etli* with TwinStrep and His_6 tags; Sm^R, Spc^R	This work
pUC18T-mini-Tn7pleD*Km	pUC18 derivate bearing a mini-Tn7 transposon which contains the *pleD** gene and a kanamycin resistance gene; Ap^R, Km^R	Romero-Jiménez *et al*. (2015)
pUC18T-mini-Tn7Km	pUC18T-mini-Tn7*pleD**Km derivate with a 1114 bp NcoI internal deletion of *pleD** gene; Ap^R, Km^R	Romero-Jiménez *et al*. (2015)
pME6016	pVS1-p15A shuttle vector for transcriptional lacZ fusions; Tc^R	Schnider-Keel *et al*. (2000)
pME6016-PG1	P_{gap1}::'lacZ transcriptional fusion, 233 bp EcoRI/PstI fragment bearing the *gap1* promoter cloned in pME6016; Tc^R	Casas-Román *et al*. (2024)
pME6016-PG2	P_{gap1}::'lacZ transcriptional fusion, 219 bp EcoRI/PstI fragment bearing the *gap2* promoter cloned in pME6016; Tc^R	Casas-Román *et al*. (2024)

Ap: ampicillin, Km: kanamycin, Rif: rifampicin, Sm: Streptomycin, Spc: Spectinomycin, Tc: tetracycline, ^{R}: resistant.

PG-agar media 0.5% (w/v) (Matilla *et al*., 2007) was used for Pto swarming and syringafactin assays. PG-agar composition: 5 g/l protease-peptone No.3 (Difco 211693), 2 g/l glucose and 5 g/l bacto-agar (Difco 214010).

Rhizobium etli strains were routinely grown in TY broth (Beringer, 1974) at 28°C. Liquid cultures were grown in shaking conditions (170 rpm). For solid media bacteriological agar was added to a final concentration of 1.5% (w/v). TY composition: 5 g/l tryptone (PanReac 403682.1210), 3 g/l yeast extract (PanReac 403687.1210), and 0.9 g/l $CaCl_2$ ($2H_2O$).

Every media, solid or liquid, was sterilized in an autoclave at 120° and 1 atm for 20 min.

2.2. Minimal media

Different minimal media were used for Pto and Ret strains. For solid media purified agar (Conda 1806.00) was added to a final concentration of 1.3% (w/v). Every media, solid and liquid, was sterilized in an autoclave at 120° and 1 atm for 20 min.

M9 medium (Sambrook *et al*., 1989) was used for Pto growth assays. Macroelement composition: 47.76 mM Na_2HPO4, 22 mM KH_2PO_4, 8.55 mM NaCl, 18.7 mM NH_4Cl, 24.5 µM Fe-citrate and 1 mM $MgSO_4$. Fe-citrate and $MgSO_4$ were separately prepared in 1000× solutions, sterilized by filtration and added to the medium prior to use. Microelement composition: 0.915 µM $ZnCl_2$, 3.8 µM $MnCl_2$, 9.64 µM HBO_3, 38.5 µM $CoCl_2$, 0.15 µM $CuCl_2$, 0.2 µM $NiCl_2$, and 0.343 µM $NaMoO_4$. Microelements were prepared in a 400× solution, sterilized by filtration and added to the medium prior to use. Different carbon sources were added to the media according to the performed assay.

MMY medium (Meneses *et al*., 2010) was used for Ret growth assays. Composition: 0.41 mM $MgSO_4$, 1.26 mM K_2HPO_4, 10 mM NH_4Cl, 1.49 mM $CaCl_2$, 0.0184 mM $FeCl_3$, 0.818 µM biotin, 0.296 µM thiamine and 0.209 µM pantothenate. $CaCl_2$ and $FeCl_3$ were prepared in 100× and 1000× solution respectively, sterilized by filtration and added to the medium prior to use. Carbon sources were added to the media according to the performed assay. Vitamins (biotin, thiamine and pantothenate) were prepared together in a 1000× solution, sterilized by filtration and added to the medium prior to use.

T3SS-inducing minimal medium (Huynh *et al*., 1989) with modified carbon source (MMPM) was used for Pto proteomic and expression assays. Composition: 50 mM K-phosphate buffer pH 5.7, 7.6 mM $(NH_4)_2SO_4$, 1.7 mM $MgCl_2$, 1.7 mM NaCl, 10 mM mannitol, and 10 mM pyruvate. The different elements were prepared in stock solutions of 1 M (except 500 mM for K-phosphate) and combined at the established proportions to prepare this medium.

MMR media (Robertsen *et al.*, 1981) was used for EPS production assays. Composition: 7 mM Na-glutamate, 55 mM mannitol, 1.31 mM K_2HPO_4, 2.2 mM KH_2PO_4, 0.61 mM $MgSO_4$, 0.34 mM $CaCl_2$, 0.022 mM $FeCl_3$, 0.85 mM NaCl, 0.818 µM biotin, 0.296 µM thiamine and 0.209 µM pantothenate. $CaCl_2$ and $FeCl_3$ were prepared in 100× and 1000× solutions respectively, sterilized by filtration and added to the medium prior to use. Vitamins (biotin, thiamine and pantothenate) were prepared together in a 1000× solution, sterilized by filtration and added to the medium prior to use.

2.3. Antibiotics and media supplementation

Antibiotics were prepared in concentrated solutions in deionized water and sterilized by filtration, except rifampicin and tetracycline that were dissolved in methanol. Antibiotics were added when required to the cultures/plates (Table M.3). All free-living assays with strains carrying pJB3Tc19 or derived plasmids were done in media supplemented with tetracycline to prevent plasmid loss, while those carrying pTD-NTwinStrep or derived plasmids were supplemented with spectinomycin.

Table M.3. Antibiotic concentration (µg/ml)

Antibiotic	*E. coli*	Pto	Ret
Ampicillin	100	100	100
Kanamycin	50	50	25-50
Nalidixic acid	-	-	20
Rifampicin	-	10	-
Streptomycin	100	-	50
Spectinomycin	100	-	100

When necessary, media were supplemented with:

- 5-bromo-4-chloro-3-indolyl-β-d-galactopyranoside (X-Gal) dissolved in N,N-dimethylformamide at 1 mg/ml stock concentration to a final concentration of 2 µg/ml in the media.

- Isopropyl β-D-1-thiogalactopyranoside (IPTG) dissolved in water at 500 mM stock concentration and sterilized by filtration, used at a final concentration of 0.5 mM in the media.

- Diaminopimelic acid (DAPA) dissolved in water at 30 mM stock concentration and sterilized by filtration, used at a final concentration of 0.3 mM in the media.

- Sucrose at a final concentration of 15% (w/v). Sucrose was sterilized in an autoclave at 115°C and 1 atm. for 30 min., then mixed with the corresponding media before use.

2.4. Conservation of bacterial strains

For long term conservation of bacterial strains, glycerol was used as a cryoprotector. Sterile glycerol was added to bacterial cultures to a 20% final concentration in cryotubes that were preserved at -80ºC.

3. MOLECULAR BIOLOGY METHODS

3.1. Isolation and quantification of nucleic acids

3.1.1. Isolation and purification of total DNA

Chromosomal DNA isolation was performed using the commercial kit *Realpure Genomic DNA Extraction kit* (Real RBME15), following the manufacturer instructions. For Ret, 2-5 ml of culture grown in TY medium for 24-48h at 28ºC were used. For Pto 1-2 ml of culture grown in LB medium for 16-24 h were used. Sample rehydration after purification was performed using milliQ water to avoid interference with subsequent techniques.

3.1.2. Isolation and purification of plasmid DNA

Plasmid DNA isolation was performed using the commercial kit *GenEluteTM Plasmid Miniprep Kit* (Sigma PLN70). 1-5 ml of culture were used depending on the plasmid copy number, and manufacturer instructions were followed. Sample elution after purification was performed using milliQ water to avoid interference with subsequent techniques.

3.1.3. Rapid isolation of total DNA by thermal lysis

In situations when a rapid DNA extraction was required over purity of the sample, total DNA (both chromosomal and plasmid) was obtained through thermal lysis of bacteria grown in solid media. A colony of the strain of interest was suspended in 50-100 µl of milliQ water and incubated at 95ºC for 5 min.

3.1.4. Isolation and purification of total RNA

RNA isolation and manipulation were performed in RNAse-free conditions. Diethyl pyrocarbonate (DEPC)-treated water was used in all steps to inactivate RNAses. Cell pellets from bacterial suspensions were obtained by centrifugation and preserved at -80ºC. After defrosting, 1.5 ml of TRI Reagent LS (Molecular Research Center) preheated at 70ºC were added to the samples. After 10 min incubation at 65ºC, samples were centrifuged for 10 min at 12000×*g* and 4ºC, and the supernatant was transferred to a new tube. 1/10 v of 1-bromo-3-chloropropane (BCP) were added

followed by vortex for 30 s, then, samples were incubated for 5 min at room-temperature (RT) before centrifugation for 15 min at 12000×*g* and 4°C. The superior aqueous phase was transferred to another tube and 1 v of isopropanol was added to precipitate the RNA. After a 10 min incubation, the sample was centrifuged again for 10 min and the obtained pellet was washed with 70% ethanol. After centrifugation, the RNA pellet was incubated at 50°C until dryness and then suspended in 50-100 µl of DEPC water at 50°C.

To remove remaining DNA, samples were treated with DNAse. To 100 µl of RNA sample, 5 U of DNAse (DNase I recombinant RNase-free Roche), 40 U of RNAse inhibitor (Ambion) and water to a final volume of 150 µl were added. The reaction was incubated for 1 h at 37°C and a phenol-chloroform extraction was performed. To do so, 1 v of phenol:chloroform:isoamilic alcohol (25:24:1 v/v) was added and vortexed for 30 s before centrifugation for 10 min at 12000×*g* and 4°C. The superior aqueous phase was transferred to another tube and 1/10 v of 3 M sodium acetate pH 4.8, and 3 v of cold absolute ethanol were added to precipitate the RNA. The sample was incubated overnight at -20°C, then centrifuged for 15 min at 12000×*g* and 4°C and the obtained pellet was washed with 70% ethanol and centrifuged under the same conditions for 5 min. The supernatant was eliminated and the RNA pellet was incubated at 50°C until dryness, and then suspended in 25-100 µl of DEPC water at 50°C. Samples were preserved at -20°C or -80°C.

3.1.5. Determination of nucleic acids concentration and purity

Concentration and purity of nucleic acids was quantified by spectrophotometry using the NanoDrop ND-1000 (Bio-Rad). Absorbance was measured at 260 nm and concentration was calculated using the corresponding factor (for double-stranded DNA an OD_{260} of 1 = 50 ng/µl, and for single-stranded RNA an OD_{260} of 1 = 40 ng/µl). Purity was estimated by calculating the 260/280 absorbance ratio, considering 1.8 for DNA and 2 for RNA as the optimal ratios.

3.2. Nucleic acid electrophoresis in agarose gels

Separation and visualization of DNA and RNA fragments was performed by horizontal gel electrophoresis on agarose gels in TBE buffer (50 mM Tris, 2.5 mM EDTA-Na_2, 50 mM BO_3H_2, pH 8.2). Agarose concentration was adjusted between 0.8-1.5 (w/v) depending on the fragment size, using a higher concentration for smaller fragments. Sample buffer (6×) was made of 30% glycerol (v/v), 0.25% bromophenol blue dye (w/v), and 0.25% xylene cyanol dye (w/v). Different commercial DNA ladders were used as molecular weight markers to estimate fragment sizes (Molecular Weight Marker II and III

from Merck, and 100bp DNA ladder from New England Biolabs). Electrophoresis was performed at 70-100 V, and gels were stained with ethidium bromide afterwards. Gels were visualized under UV light and images captured with a Bio-Rad Molecular Imager Gel Doc System analysed using the Quantity One software (Bio-Rad).

3.3. Polymerase chain reaction (PCR)

Polymerase chain reaction was employed to amplify specific genome segments from Ret CE3 and Pto DC3000, to generate fragments with restriction sites and mutations, and to detect plasmid and genome inserts. Specific oligonucleotide used as primers are described in the corresponding chapters.

3.3.1. Standard PCR method

Reactions were adjusted according to the polymerase used.

For amplicons to be cloned, a high fidelity *Accuprime Taq* DNA polymerase was used (Invitrogen), with an extension temperature of 68ºC. The reaction was carried out in a volume of 25 µl, with a final concentration of the commercial buffer composition of: 60 mM Tris-SO_4 (pH 8.9), 18 mM $(NH_4)_2SO_4$, 2 mM $MgSO_4$, 2 mM dNTP, and 10% glycerol. The final concentrations of the rest of the compounds were: 0.04 U/µl thermostable AccuPrime™ enzyme, 0.2 µM each (forward and reverse) primer, and 40 ng of genomic DNA or 10-20 ng of purified plasmid DNA.

For detection of cloned or deleted sequences/fragments in plasmids and chromosomes, a *DreamTaq* DNA polymerase (Thermo Scientific) was used, with an extension temperature of 72ºC. The final compound concentration was: 0.04 U/µl polymerase, 0.2 µM each (forward and reverse) primer, recommended concentration of commercial buffer and 1-2 µl of bacterial lysate.

PCR reactions were performed in an T100 thermocycler (Bio-Rad). Standard reaction conditions were: (i) initial denaturalization at 94ºC for 3 min, (ii) 30-35 cycles of: denaturalization for 30 s at 94ºC, annealing for 30 s at 50-58ºC and extensions for 30 s/kb at the optimal polymerase temperature and (iii) final elongation for 5 min.

3.3.2. Overlapping PCR

Overlap extension PCR (or splicing by overlap extension PCR) was used to generate deletions in a DNA fragment (Lee *et al*., 2004). For deletion mutagenesis four primers were used: one primer for each end and two splicing chimeric primers which contained nucleotide sequences derived from each of the two regions immediately flanking the sequence to be deleted plus overlapping 5' sequences. In a first step, two separate

PCRs were performed (Fig. M.1: PCR 1 and PCR 2), obtaining two amplicons with complementary 5' overhangs. In a second step, the two amplicons were combined and a final PCR reaction was performed after an initial denaturation and subsequent annealing of the two flanking regions. The final PCR with the outermost primer pair resulted in the final product which lacks the deleted region (Fig. M.1).

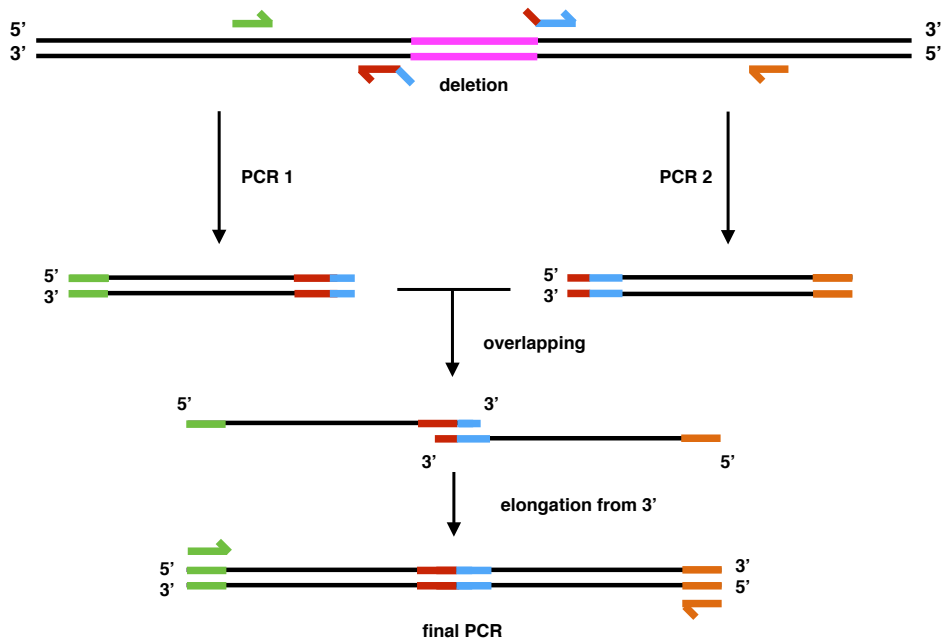

Figure M.1. Deletion by overlap extension PCR.
Two PCR products (PCR1 and PCR2) representing the flanking regions of the sequence to be deleted are prepared by using one non-chimeric (depicted in green and orange) and one chimeric primer (depicted in red and blue). In a second step, the two PCR products are used as the template for a ligation PCR that contains the outermost primer pair.

3.4. Cloning of DNA fragments on a vector

3.4.1. DNA digestion by restriction endonucleases

Digestion reactions were performed following manufacturer indications (Sigma-Aldrich and New England Biolabs). Digestions with multiple enzymes were performed simultaneously when the buffer and reaction temperature were compatible. When necessary, enzymes were deactivated by heat or removed by DNA purification after agarose gel electrophoresis.

3.4.2. DNA band purification from agarose gels

To isolate restriction fragments and PCR products, an agarose gel electrophoresis was performed, and the gel stained with ethidium bromide for DNA visualization under UV. The desired fragment was sliced with a scalpel and purified using the commercial kit NucleoSpin Gel and PCR Clean-up (Macherey-Nagel 740609.50), following the manufacturer indications.

3.4.3. Ligation of DNA fragments in cloning vectors

The covalent union of two lineal DNA molecules with compatible ends was performed using T4 DNA ligase enzyme (NEB, MO202S). The reaction was performed in final volume of 15 µl with the provided buffer using 1 µl (400 U) of ligase and a 1:3 vector:insert ratio, at 16ºC overnight.

3.4.4. Sequencing and sequence analysis

DNA sequencing was performed by de Genomic Unit of the Instituto de Parasitología y Biomedicina López Neyra – CSIC. It was performed with BigDyeTerminator v3.1 chemistry and automated multicapillary electrophoresis system. Sequence results were aligned and compared using the MUSCLE software by EMBL-EBI (Madeira *et al*., 2022).

3.5. Gene expression analysis

3.5.1. cDNA synthesis

Synthesis of the complementary DNA strand (cDNA) from total RNA samples was performed using the SuperScript II reverse-transcriptase enzyme (Invitrogen) following the manufacturer's indications. 1 µg of total RNA was mixed with 2 µl of First Strand Buffer (5×) and 100 ng of random hexamers (primers) in RNAse-free water to a final volume of 10 µl. The reaction was incubated for 5 min at 65ºC, cooled in ice, and 9 µl of mix solution (2 µl of First Strand Buffer 5×, 20 mM dithiothreitol (DTT), 1 mM dNTPs and water) were added. After 2 min incubation at RT, the reverse transcriptase (SSII Invitrogen) was added and the reaction was incubated for 10 min at 25ºC, 2 h at 42ºC, and was inactivated at 65ºC for 15 min. Samples were preserved at -20ºC.

3.5.2. Gene expression quantification by real-time PCR (qRT-PCR)

Quantitative PCR allows quantification of nucleic acids by monitorization of their amplification by fluorescence in real-time. The copy number of DNA at the start of the reaction can be quantified thanks to the cycle threshold (Ct) value, which represents the number of PCR cycles needed to produce a significative fluorescence increase. For

oligonucleotide design, gene sequences were obtained through the Kyoto Encyclopedia of Genes and Genomes (KEGG) and the software Oligo 6 (Molecular Biology Insights) was used following the recommendations by Pueyo *et al*. (2002).

RT-PCR reactions contained 50 ng cDNA, 300 nM oligonucleotides, and a commercial mix (2× iTaq Universal SYBR Green Supermix, BioRad) in a final volume of 25 µl. Standard reaction conditions were an initial denaturalization at 95ºC for 2 min, followed by 40 cycles of: denaturalization for 20 s at 95ºC and annealing and extension for 30 s at 70ºC. After amplification, a melting curve was obtained under the following conditions: 1 min at 95ºC and 30 cycles of 10 s, starting at 95ºC and diminishing 1ºC every cycle until 66ºC.

Relative gene expression was performed following the ΔΔCt method (Livak and Schmittgen, 2001). The genes of interest were amplified with the reference gene *gyrA*, and its relative variation was calculated as $2^{-\Delta\Delta Ct}$.

4. GENETIC MANIPULATION METHODS

4.1. E. coli competent cells preparation

E. coli competent cells were prepared following the method described by Lederberg & Cohen (1974). A 100 ml culture flask was inoculated with 1 ml of *E. coli* pre-culture and incubated at 37ºC at 180 rpm to an OD_{600}~0.4. Cultures were cooled on ice for 10 min, centrifuged for 10 min at 4ºC and 10000×*g*, and the supernatant was discarded. Afterwards, cells were suspended in one volume of sterile 0.1 M $MgCl_2$ at 4ºC, and centrifuged for 5 min at 4ºC and 5000×*g*. The supernatant was discarded again, the cells were suspended in 1/2 volume of sterile 0.1 M $CaCl_2$ at 4ºC, and kept on ice for 30 min. A last centrifugation step for 5 min at 4ºC and 5000×*g* was performed before suspension of the cells in a 1/10 volume of sterile solution containing 0.1 M $CaCl_2$ and 20% glycerol at 4ºC. The cell suspension was divided into 100 µl aliquots and stored at -80ºC until use.

4.2. Thermal shock bacterial transformation

Transformation of competent *E. coli* cells with plasmid DNA was performed according to the method described by Nishimura *et al*. (1990). After thawing an aliquot of competent cells on ice, 10-50 ng of plasmid DNA were added and gently mixed before incubation for 45 min on ice. A thermic shock was performed at 42ºC for 2 min followed by a 5 min incubation on ice. Afterwards, 1 ml of LB medium was added and the cells were incubated for 1 h at 37ºC with shaking. Cells that have acquired the plasmid were selected by plating dilutions on LB agar plates with the appropriate antibiotics and

incubated for 24 h at 37°C. When the plasmid allowed for white/blue colony selection by complementation of β-galactosidase activity (Sambrook *et al*., 1989), the media was supplemented with 2 µg/ml X-gal and 0.5 mM IPTG.

4.3. Electrocompetent cells preparation

E. coli electrocompetent cells were prepared following the method described by Sambrook *et al*. (1989). An exponential phase 100 ml culture (OD_{600}=0.4-0.6) was cooled on ice before three successive centrifugation rounds (10 min at 4°C and 10000×*g*) with suspension of the cells in decreasing volumes (100 ml, 50 ml and 5 ml) of sterile deionized water. The final suspension of 5 ml was divided into 100 µl aliquots stored at -80°C until use.

Pto electrocompetent cells were prepared following the method described by Choi et al. (2006). Cells were suspended from fresh cultured plates in 300 µl of sterile sucrose 300 mM solution and centrifuged for 1 min at 12000×*g*. Pelleted cells were washed two times with 300 µl of the same sucrose solution and suspended in a final volume of 100 µl of sucrose 300 mM. Electrocompetent cells were kept on ice until use, performing electroporation immediately after preparation.

4.4. Electroporation

For electrocompetent cell transformation, 10-50 ng for replicative vectors and 300-500 ng for suicide vectors of DNA suspended in milliQ water were added to the cells kept on ice. After gentle agitation, the mixture was transferred into an electroporation cuvette (1 mm BridgeTM), previously cooled at 4°C. The cuvette was subjected to a 1.8 kV electric pulse in an electroporator (Eporator, Eppendorf). Cells were immediately recovered by adding 1 ml of LB medium and incubated for 1 h at 37°C for *E. coli* or 2-3 h at 28°C in the case of Pto. Cells that acquired the plasmid were selected by plating dilutions on LB agar plates with the appropriate antibiotics, following incubation at the adequate temperature for 24-48 h.

4.5. Bacterial conjugation

Bacterial conjugations were performed to introduce plasmids into Ret strains following the method described by Schäfer *et al*. (1994). Cells from cultures in exponential phase (OD_{600}~0.4) of the *E. coli* donor strains were mixed with late exponential phase cells (OD_{600}~0.8) of the Ret receptor strain in a 1:1 proportion. 1 ml of each culture was centrifuged in the same 1.5 ml tube and the supernatant was discarded. The culture mixture was washed two times with TY liquid medium, and the pellet resuspended in 40 µl of media, which were placed on top of a sterile Millipore 0.45 µm filter previously laid on a TY medium plate (supplemented with DAPA for the β2163 donor strain). Filters

were then incubated overnight at 28°C. The following day, the conjugation mixture was suspended from the filter into liquid media, and cells that acquired the plasmid were selected by plating dilutions on selective medium.

4.6. Directed mutagenesis by integration and allele exchange

Loss-of-function genetic mutations were generated by deletion of the corresponding gene. To achieve the deletion, the DNA amplicon with the modified sequence obtained (3.3.2.) was cloned into an integrative vector (non-replicative or suicide). Regions of at least 500 bp at each side of the target gene allow for homologous recombination and integration in the chromosome. The integrative vector pK18*mobsacB* was used. It carries the gene *sacB* (which confers sensitivity to sucrose, sucrose^S), and kanamycin resistance gene. After introduction of the plasmid into the designated strains by electroporation or bacterial conjugation, colonies that had integrated the plasmid (Km^R/sucrose^S) were selected. Afterwards, tranconjugants were grown in liquid rich media in the absence of kanamycin to force plasmid loss (shaking at 28°C for Ret strains, and static at 4°C for Pto strains). Cells were then plated on rich medium with sucrose (15% w/v) and the Km^S/sucrose^R colonies (potential double-recombinants) were selected and checked by PCR and sequencing.

5. IN-VIVO ASSAYS

5.1. Growth assays

5.1.1. Solid media growth assays

Solid media growth assays were carried out in square 50 ml plates. Bacterial cells grown in rich media with the appropriate antibiotics were adjusted to an OD_{600} of 1. Serial 1/10 dilutions were performed and 10 µl drops of each dilution and strain were placed in rich medium or minimal medium plates supplemented with different carbon sources. The concentration of the carbon sources was adjusted according to the carbon molar content of each compound, being glucose 10 mM, galactose 10 mM, succinate 15 mM and glucose and succinate (5 mM and 7.5 mM, respectively). Plates were incubated at the appropriate temperature and growth was monitored for 7 days. The experiment was repeated with three independent cultures.

5.1.2. Growth curves

Growth curves were carried out in standard culture conditions. Bacterial cells grown in rich media with the appropriate antibiotics were resuspended in sterile milliQ water and adjusted to an OD_{600} of 1. The bacterial suspensions were washed and diluted 1/100

in the appropriate medium and 200 µl were dispensed in a 100-well Honeycomb plate (Bioscreen). The concentration of defined carbon sources were the same as described for the solid media assays above. The plates were incubated at the appropriate temperature with continuous shaking in a Bioscreen C equipment (MBR). The absorbance was measured every hour at 600 nm to determine the turbidity of the culture until the stationary phase was reached. Each strain counted with 4 replicates per plate and the assay was carried out at least 2 times for each condition.

5.2. Motility experiments

5.2.1. Swimming assays

For swimming motility assays, bacterial strains were grown on LB plates at 28ºC for 48 h, resuspended in sterile milliQ water and adjusted to an OD_{600} of 2.0. Then, 0.3% agar LB plates were stabbed with 2 µl aliquots of that suspension and incubated for 48 h at 20ºC. Diameters of the swimming halos were photographed and measured using ImageJ (Schneider *et al.*, 2012). Motility was expressed as the average diameter of the swimming halo ± standard deviation. Three motility plates were used for each strain, and the experiment was repeated with three independent cultures.

5.2.2. Swarming assays

For swarming motility assays, bacterial strains were grown on LB plates at 28ºC for 48 h, resuspended in sterile milliQ water and adjusted to an OD_{600} of 2.0. Two µl aliquots of the suspensions were placed in the centre of peptone-glucose (PG)-agar plates, incubated at 20ºC and observed after 24 h. The swarming surface on each plate was determined using ImageJ (Schneider *et al.*, 2012). Motility was expressed as the average surface of the swarming area ± standard deviation. Three motility plates were used for each strain, and the experiment was repeated with three independent cultures.

5.3. Biosurfactant production assays

An atomized oil assay was used to detect syringafactin as described by Burch *et al.*, (2010). Pto strains were grown on LB plates for 48 h, resuspended in sterile milliQ water and adjusted to an OD_{600}=1.0. 10 µl aliquots were pipetted onto the surface of LB plates, incubated for 48 h at 20ºC and then sprayed with a mist of mineral oil (Sigma M5904) using a sprayer with an air flow of 6 l/min. The diameter of the visible halo of brighter oil drops (surfactant halo) and the area of the producing bacterial colony were measured using ImageJ (Schneider *et al.*, 2012). The normalized halo area was calculated by subtracting the colony area from that of the surfactant halo.

Generally, larger halos in the atomized oil assay indicate higher surfactant production levels. Three plates were used for each strain, and the experiment was repeated with three independent cultures.

5.4. Biofilm and flocculation assays

5.4.1. Biofilm formation assays

For solid-liquid (S-L) biofilm quantification bacterial cells grown in rich media at 28°C with the appropriate antibiotics were adjusted to an OD_{600} of 1. The bacterial suspensions were diluted up to an OD_{600}=0.1 in MMR medium with the appropriate supplements. 150-200 µl were dispensed into a sterile polystyrene multi-well plate (Greiner Cellstar 96 round bottom). Plates were incubated in the appropriate conditions depending on the strains, and after incubation the medium was removed and the wells carefully washed with deionised water before incubation with crystal violet (CV) (240 µl 0.1% in water) for 1 hour. After removal of CV washing with deionised water, 150 µl of 80% ethanol were added to each well and incubated for 1 h. Coloration was quantified by measurement of OD_{570} with an Eon Biotek plate reader with the Gen5 software. Each strain counted with 8 replicates per plate and the experiment was repeated with three independent cultures.

5.4.2. Flocculation assays

Flocculation assays were conducted by growing bacterial strains in rich medium supplemented with glucose and MMR medium supplemented with glucose and succinate in culture tubes. Bacterial cells grown in rich media plates at 28°C with the appropriate antibiotics were adjusted to an OD_{600} of 1. Culture tubes with 4 ml of medium were inoculated with the bacterial suspensions up to an OD_{600}=0.1. Tubes were incubated at 28°C with continuous shaking and photographs were taken at 24 h and 48 h to observe the flocs.

5.5. β-galactosidase activity assays

β-galactosidase activity was measured in permeabilized cells following the method described by Miller (1972) based on the colorimetric reaction produced by the hydrolysis of *o*-nitrophenyl-β-D-galactopyranoside (ONPG) into galactose and *o*-nitrophenol by the enzyme β-galactosidase. The concentration of *o*-nitrophenol can be measured by the Beer-Lambert-Bouger law in which Abs = ε (molar extinction coefficient) x c (molar concentration) x l (optical path length).

Bacterial strains were grown on rich medium plates at 28°C and cells pelleted and resuspended in sterile milliQ water, washed and resuspended in the corresponding medium. The suspensions were adjusted to an OD_{600}≈4.0–8.0 and 150 µl were dispensed in a multi-well plate (Greiner Cellstar 96 round bottom) in which 1:2 serial dilutions were made. The plates were incubated at 20°C with constant shaking at 600 rpm on an IKA MS 3 Basic shaker for 5 h (in the case of LB) or 24 h (in the case of minimal media). OD of the cultures was measured at 600 nm before performing the enzymatic reactions, which were carried out in polypropylene DeepWell plates (VWR 732–3323, well volume 2 ml) kept at 30°C in a water bath. 30-50 µl of culture were added to the plate followed by 10 µl of SDS 0.1% and 10 µl of chloroform. Plates were incubated for 30 min at room temperature. 400 µl of Z buffer pH 7.0 (60 mM Na_2HPO_4, 40 mM NaH_2PO_4,10 mM KCl 10, 1 mM $MgSO_4$ and β-mercaptoetanol 0,27% (v/v)) were added to the wells followed by 100 µl of ONPG (0.4 mg/ml in sodium phosphate buffer 0,1 M pH 7,0). The reaction mixture was incubated at 30°C until yellow coloration was clearly visible (5-30 min) and the reaction was stopped by adding 1 ml of 0.5 M Na_2CO_3. Measurements were performed by transferring 100 µl of the reaction into flat bottom multi-well plates (Greiner Cellstar 96 flat bottom) and absorbance at 420 nm and 550 nm was measured in an Aeon Biotek plate reader with the Gen5 software. At least 3 replicates were performed for each measurement. β-galactosidase activity was expressed in Miller units (MU) and determined using the following equation: (*t* represents reaction time in minutes and *v* the volume of bacterial culture in ml):

$$\text{β-galactosidase activity} = 1000 \times (OD_{420} - (1.7 \times OD_{550})) / (t \times v \times OD_{600})$$

5.6. Exopolysaccharide production determination

Polysaccharide production determination was performed in solid media by Congo Red (CR) and Calcofluor (CF) colony staining. Exopolysaccharide production can be detected by bacterial growth in media supplemented with CR and CF. CR binds D-glycopyranosyl units from neutral or basic polysaccharides as well as certain proteins. CF is more specific, binding glycosidic bonds β(1-3) and β(1-4), present in cellulose or curdlan (Teather & Wood, 1982; Spiers *et al*., 2002).

CR was prepared in distilled water at 5 mg/ml and sterilized by filtration. It was added to solid media to a final concentration of 50 µg/ml. CF was added into hot melted medium to a final concentration of 200 µg/ml. After bacterial growth, CR plates were photographed under natural light and CF plates were observed and photographed under UV light.

5.7. Cell viability determination

A live/dead staining method based on two nucleic acid probes was followed to differentiate and quantify live and dead cells in bacterial cultures, as previously described (Masco *et al*., 2007). The dyes used were propidium iodide (PI), red-colored, which only enters membrane-compromised cells, and SYTO13 (Invitrogen), green-coloured, which is membrane-permeant and stains both viable and non-viable cells. Exponential or stationary phase cells were harvested by centrifugation, washed and adjusted to an OD_{600} of 0.1. Then, the cell suspensions were incubated with 10 mM NaCl for live cells or 70% isopropyl alcohol for dead cells. A standard curve with various proportions of live/dead cells was prepared, and both the standards and the samples were stained according to the manufacturer indications. The staining solution (0.01 mM SYTO13 and 0.06 mM PI) was mixed with the bacterial suspensions in a 1:1 ratio in a 96-well microplate (Greiner). The samples were incubated in the dark for 15 min before measuring fluorescence in a multiplate reader VarioskanLUX (ThermoScientific, Waltham, MA, USA). Intensities of green (510 nm) and red (630 nm) emission were recorded after excitation at 485 nm and 530 nm, respectively. The green to red fluorescence emission ratio, which is proportional to the relative number of live bacteria, was calculated. Each strain counted with 2 replicates and the assay was carried out at least 3 times for each condition.

5.8. Membrane vesicle isolation and quantification

5.8.1. Membrane vesicle isolation

Membrane vesicles (MVs) were isolated from culture supernatants following previously described methodology (Pérez-Cruz *et al*., 2016). Bacterial cells were grown in MMY cultures with the pertinent antibiotics to an OD_{600} of 0.6-0.8, then pelleted by centrifugation at 10,000× g for 30 min at 4°C. The supernatants were filtered through a 0.45 µm-pore-size filter (Millipore) and concentrated by centrifugation through a 100 KDa Centricon® Plus-70 filter device (Millipore). The MVs were collected by ultracentrifugation at 100,000× g for 2 h at 4°C, washed with phosphate buffered saline (PBS) (137 mM NaCl, 2.7 mM KCl, 1.76 mM KH_2PO_4, 10 mM Na_2HPO_4, pH 7.4) to eliminate excess polysaccharide and again pelleted at 100,000× g for 2 h at 4°C. The pellet containing the MVs was resuspended in an appropriate volume of PBS and stored at -20°C.

5.8.2. Membrane vesicle quantification

MVs were indirectly quantified by measuring the lipid content, which was determined using the lipophilic fluorescent dye FM4-64 (Thermofisher, Waltham, MA, USA) as previously described (Frias *et al*., 2010). A fraction of PBS resuspended MVs was incubated with FM4-64 (final concentration of 5 µg/ml in PBS) for 5 min in darkness at

room temperature. Vesicles alone and the FM4-64 probe alone were used as negative controls. After excitation at 515 nm, emission at 635 nm was measured with the multiplate reader Varioskan TM LUX (ThermoScientific, Waltham, MA, USA). Fluorescence was normalized for the culture volume from which MVs were isolated.

6. IN PLANTA ASSAYS

6.1. Pseudomonas syringae plant assays

6.1.1. Tomato plant infection assays

Seeds of *Solanum lycopersicum* cv. Moneymaker (a PtoR line, i.e., a compatible host for Pto DC3000) were germinated and grown in a plant growth chamber with 16/8-h light/dark cycles at 24/16°C day/night and 70% relative humidity.

Pto strains were grown on LB plates for 48 h at 28°C, then suspended in sterile milliQ water and the concentration adjusted to 10^8 cfu/ml (OD_{600} =0.1) before application to one leaf of different 4-week-old plants with an airbrush until the leaf (adaxial and abaxial) surface was uniformly wet.

The analysis of symptom development and sampling was performed 3 h after inoculation (0 dpi), and several days after inoculation (3, 6 and 10 dpi) to monitor bacterial growth in plant. Bacteria were recovered from the infected leaves using a 10 mm-diameter cork-borer, sampling 10 disks per leaf. Five disks (3.9 cm^2) were homogenized by mechanical disruption using a stirrer (IKA RW16 basic) into 1 ml of milliQ water and counted after plating serial dilutions onto LB plates with the corresponding antibiotics. Population levels were expressed in cfu/cm^2 and symptom severity (necrotic area per leaflet induced by the inoculated strains) was photographed at 3, 6 and 10 dpi.

6.2. Phaseolus symbiosis assays

6.2.1. Seed sterilization and germination

Bean (*Phaseolus vulgaris* cv. Contender) seeds were surface-sterilized by washing abundantly with deionized water followed by a 2 min treatment with ethanol 100%, which was removed by washing three times with deionized water. A second treatment adding 5% sodium hypochlorite for 5 min was applied and seeds were washed again 5 times with sterile deionized water, then soaked in water for 2 h in darkness. Bean seeds were germinated on purified agar:water (1% w/v) for 72 h at 28°C in the dark.

6.2.2. Nutrient solution

A nitrogen-free nutrient solution was used, modified from Rigaud and Puppo (1975). The solution was adjusted to pH 7.2 with KOH and sterilized at 120ºC for 20 min. Macroelement composition: 0.73 mM KH_2PO_4, 1.34 mM KCl, 0.4 mM $MgSO_4$, 0.35 mM $CaSO_4$, 0.034 mM $Na_2FeEDTA$. Microelement composition: 0.45 µM Na_2MoO_4, 46 µM H_3BO_3, 0.8 µM $CuSO_4$, 1.91 µM $ZnSO_4$, and 11.11 µM $MnSO_4$. Microelements were prepared in a 1000× stock solution, and added to the final nutrient solution before sterilization.

6.2.3. Nodulation kinetics

To analyse nodulation kinetics of individual rhizobial strains, seedlings were carefully placed in 18 cm × 16.5 cm CYG germination pouches (Mega International, USA), and the root of each seedling was inoculated with approximately 10^5 bacterial cfu. Sixteen seedlings per strain were inoculated, and water-inoculated plants were used as negative controls. Plants were cultivated in a growth chamber with 16/8-h light/dark photoperiod at 24/16ºC day/night and 75% relative humidity. Pouches were replenished with 50 ml of nitrogen-free nutrient solution when necessary. Visible nodules were daily counted until 21 days post-inoculation.

6.2.4. Symbiotic efficiency assays

To test the symbiotic efficiency of rhizobial strains, 12 bean seedlings were sown in autoclaved Leonard-type jars assemblies. The system consists of an upper pot containing a 3:1 mix of vermiculite:perlite and a lower container with and nitrogen-free nutrient solution. Plants were cultivated in the same conditions as above for 28 days, when the shoot fresh weight and the number of nodules were determined. Shoot dry weights were determined after desiccating the samples in an oven at 65ºC for 3 days. Dry shoots were ground and total nitrogen content was determined following the *Dumas* method with an elemental analyzer Leco TruSpec CN, at the Nitrogen and Carbon Analysis Service of the Estación Experimental del Zaidín - CSIC (Granada, Spain).

7. BIOCHEMICAL TECHNIQUES / PROTEIN ANALYSIS

7.1. Total protein samples preparation

7.1.1. Sample collection

Bacterial strains were grown on rich medium plates and resuspended in sterile milliQ water. The suspensions were used to inoculate 250-500 ml M9, or MMPM media flasks to an initial OD_{600}=0.01. Cultures were grown overnight with continuous shaking (180 rpm),

to an OD_{600}=0.7-0.9. Cultures were centrifuged 2× 30 min at 7500×*g* at 4ºC. After the second centrifugation, supernatants were collected, filtered through a 0.45 µm pore-size filter (Millipore) and immediately frozen at -20ºC. Cell pellets were washed with saline solution and kept at -80ºC until use.

7.1.2. Protein isolation by lyophilization and phenol extraction

For extracellular protein sample preparation, supernatants of 500 ml cultures were lyophilized in a freeze-dryer Thermo Savant ModulyoD and then resuspended in 15 ml of extraction buffer (0.7 M sucrose, 0.5 M Tris-HCl pH 8.2, 0.1 M KCl, 50 mM EDTA, 2% β-mercaptoethanol) (Hurkman & Tanaka, 1986) supplemented with protease inhibitor (cOmplete Mini, EDTA-free, Roche).

For cell-associated protein sample preparation, cell pellets were resuspended in 1 ml of extraction buffer, sonicated for 5 cycles of 30 s (C = 4, 20%) in a Branson Sonicator 250, centrifuged at 15,000×*g* for 2 min and the supernatant extract was collected.

The phenol extraction protocol (Hurkman & Tanaka, 1986) was followed for protein isolation. 12 g/l (w/v) of polyvinylpolypyrrolidone (PVPP) were added to the sample, followed by one volume of saturated phenol pH 6.4. After gentle shaking for 10 min at room temperature, the samples were centrifuged at 4000×*g* for 20 min at 4ºC, then the phenolic phase was recovered. A second phenolic extraction was performed following the same procedure and, after the phenolic phase was recovered, 4 volumes of ammonium acetate in methanol kept at -20ºC were added and the samples were incubated overnight at -20ºC. The samples were centrifuged at 10000×*g* for 20 min at 4ºC and the pellet sample was conserved. Two more washes were performed with a 2 ml volume of ammonium acetate in methanol, and a final one with 2 ml of acetone. The resulting pellets were dried under vacuum for 20 min. Final protein samples were suspended in protein solubilisation buffer [7 M urea, 2 M thiourea, 4% CHAPS detergent, 30 mM Tris(2-carboxyethyl) phosphine hydrochloride (TCEP)].

7.1.3. Supernatant protein extraction by concentration

For proteomic analysis, supernatants of 250 ml cultures were concentrated using Amicon® Ultra-15 Centrifugal Filter Devices with 3000 MWCO, which allow recovery of highly concentrated sample. A protease inhibitor (1/4 of a tablet, cOmplete Mini, EDTA-free, Roche) was added to the supernatants prior to concentration. Fifteen ml of supernatant were sequentially centrifuged through filter devices at 5000×*g* for 20 min at room temperature (20ºC) until 250 ml were concentrated into 300 µl of final sample. Samples were kept at -20ºC until use.

7.2. Protein purification by gravity columns

Protein purification was performed using the Strep-Tactin®XT (IBA Lifesciences GmbH) system. It is composed of an engineered streptavidin with four biotin binding pockets, which it is able to bind recombinant proteins tagged with Strep-tag®II or Twin-Strep-tag®. The purification was performed following the manufacturer's indications in 1 ml column bed volume (CV) columns at 4ºC to ensure stability of the protein. Bof bacterial cultures (100 ml) were centrifuged and the pellets were suspended in 2 ml of extraction buffer (100 mM Tris pH 8.0, 150 mM NaCl, 1 mM EDTA) supplemented with protease inhibitor (cOmplete Mini, EDTA-free, Roche). Cell extracts were obtained using a French press followed by centrifugation of the lysate for 2 min at 12000*xg* and 4ºC and recovery of the supernatants. After equilibration of the columns with 2 CV of extraction buffer, the cell extracts were applied, followed by washing with 5 CV of extraction buffer. Then, 6 fractions of 0.5 ml of elution buffer (100 mM Tris/HCl pH 8.0, 150 mM NaCl, 1 mM EDTA, 50 mM biotin) were applied and the 0.5 ml eluates were sequentially recovered. Columns were washed with 6 CV of regeneration buffer (3 M $MgCl_2$) prior to equilibration with 8 CV of extraction buffer and stored at 4ºC.

7.3. Total protein quantification

Protein contents were determined by the Bradford method (Bradford, 1976) or with PierceTM 660 nm Protein Assay from Thermo Scientific. A standard curve with Bovin serum albumin (BSA) protein was performed with concentrations from 5 to 25 µg/ml.

For the Bradford method, samples were diluted in H_2O to a final volume of 800 µl and 200 µl of Bradford solution were added. After incubation for 5 min, 200 µl of sample were transferred into flat-bottom multi-well plates (Greiner Cellstar 96 flat bottom) and absorbance at 595 nm was measured in an Aeon Biotek plate reader with the Gen5 software. At least 3 replicates were performed for each sample.

For the Pierce method, samples were diluted in H_2O to a final volume of 60 µl and 900 µl of Pierce solution were added. After 5 min of incubation in darkness, 160 µl of sample were transferred into flat-bottom multi-well plates (Greiner Cellstar 96 flat bottom) and absorbance at 660 nm was measured in an Aeon Biotek plate reader with the Gen5 software. At least 3 replicates were performed for each sample.

7.4. Denaturalising protein electrophoresis (SDS-PAGE)

7.4.1. Mono-dimensional protein electrophoresis

Protein electrophoresis was performed using discontinuous 10% denaturalising sodium dodecyl-sulfate (SDS) polyacrylamide gels according to the method described by Laemmli (1970). Each gel consisted of an upper stacking layer [125 mM Tris-HCl,

pH 6.8, polyacrylamide 5% (w/v), SDS 0.1% (w/v)] and a separating lower layer [375 mM Tris-HCl pH 8.9, polyacrylamide 10% (w/v), SDS 0.1% (w/v)]. Both layers were polymerized by adding 0.42 ml of 10% (w/v) ammonium persulfate (APS) and 0.12 ml of tetramethylethylethylendiamine (TEMED) per 100ml of solution.

Samples were mixed with 2× or 6× sample buffer (350 mM Tris-HCl pH 6.8, 6% SDS, 30% glycerol, 0.603 M DTT, 6% bromophenol blue). Gels were run in 25 mM Tris-HCl pH 8.3, 192 mM glycine and 0.1% SDS buffer in a Mini-Protean tetra vertical electrophoresis cell (Bio-Rad) at 70-90 V for 1-2h. Staining was performed with 0.25% Coomassie Brilliant Blue R-250, 40% methanol and 10% acetic acid solution. Precision Plus Protein pre-stained standard (Bio-Rad) from 10 to 250 kDa was used as a molecular mass marker.

7.4.2. Two-dimensional protein electrophoresis (2DE-GE)

Two-dimensional electrophoresis protein separation for Western blots (WB) were carried out at the Proteomics facility of University of Córdoba. For 2D-GE WB, 80 µg protein samples were used. The first dimension was run in a 7 cm IPG (Immobilized pH gradient) strip pH 3-10 from Bio-Rad, with a lineal increase of voltage (2 h of passive rehydration; 10 h at 50 V of active rehydration; 30 min at 250 V; 1 h at 1000 V; 30 min at 4000 V; and 4000 V until 20,000 Vh). Strips were equilibrated for two periods of 15 min in Tris-urea buffer (375 mM Tris-HCl, pH 8.8, 6 M urea, 2% SDS, 20% glycerol), with 2% DTT added the first time and 2.5% of iodoacetamide added secondly. For the second dimension, the strips were transferred into a vertical 10% SDS-PAGE and run at 50 V in a MiniProtean Tetra Cell System (BioRad, Hercules, CA, USA). Then, 2D SDS-PAGE gels were stained with imidazole and scanned in a GS-800 Calibrated Densitometer (Bio-Rad). Gels were washed for 10 min with 100 mM EDTA and equilibrated for 15 min in a Towbin buffer (25 mM Tris-HCl pH 8.3, 192 mM glycine, 20% methanol, 0.02% SDS). Finally, gels were transferred to nitrocellulose membranes for 20 h at 30 V and 2°C in a Trans-Blot Plus Electrophoretic Transfer Cell (BioRad).

7.4.3. Phos-tag protein electrophoresis

Phos-tag SDS-PAGE is a specialised electrophoresis technique that separates different forms of a protein based on its phosphorylation levels. This method provides characteristic separation patterns of phosphoprotein isoforms according to the number and/or site of the attached phosphate groups (Kinoshita *et al*., 2006).

For Phos-tag SDS gel preparation, 8% SDS polyacrylamide gels were supplemented with 50 μM Phos-tag™ (NARD Chemicals, Hiroshima), and 0.1 mM $MnCl_2$. Prior to gel loading, samples were treated with 20% tricholoracetic acid (TCA) (1/1 volume), precipitated at 4°C for 5 min, centrifuged for 10 min at 12000*xg* and 4°C, and washed with acetone twice before resuspending them in loading buffer.

7.5. Immunodetection by Western blot

For Western blots (WB), protein samples (20-40 μg) were loaded onto 10% SDS-PAGE gels and electrophoresis were performed in Tris-Glycine-SDS buffer in a Mini-Protean Tetra Cell (BioRad) (Laemmli, 1970). Proteins were transferred from gels to PVDF membranes using the Trans-Blot Turbo Transfer System (Bio-Rad) at 1.3 A, 25 V, 7-12 min. PVDF membranes were activated with methanol and blocked in PBS-T buffer (137 mM NaCl, 2.7 mM KCl, 1.76 mM KH_2PO_4, 10 mM Na_2HPO_4, 0.1% Tween 20, pH 7.4) with 2% skimmed milk. Blocked PVDF membranes were incubated overnight at 4°C in the same buffer with the primary antibody. After washing with PBS-T buffer, the membranes were incubated with a 1:10,000 dilution of the peroxidase-linked secondary antibody. Detection was done with ECL Prime Western Blotting (Amersham) in a Chemidoc XRS System (Bio-Rad). Band analysis was performed with the Quantity-One software (Bio-Rad). Precision Plus Protein All Blue pre-stained standard (Bio-Rad) from 10 to 250 kDa was used as a molecular mass marker. TBS-T buffer (50 mM Tris-HCl, 140 mM NaCl, 0.1% Tween 20, pH 7.4) and bovin serum albumin (BSA) were used instead of PBS-T and skimmed milk respectively with anti-phosphorylation antibodies.

7.6. Protein dephosphorylation

Protein dephosphorylation was carried out on proteins fixed on a PVDF membrane after transfer, but before the blocking step. Two phosphatases were used: lambda phosphatase and alkaline phosphatase. Alkaline phosphatases are significantly more potent enzymes than the lambda phosphatase; however, they only dephosphorylate phosphate groups from threonine and serine amino acids. The Lambda phosphatase, on the other hand, specifically targets phosphate groups from threonine, serine, and tyrosine amino acids.

First, treatment with lambda-phosphatase (sc-200312, SantaCruz Biotechnology) was performed. Membranes were incubated in the provided buffer with 5 μl (2000 U) of lambda-phosphatase rocking at 25°C overnight. Then 20 U of calf-intestinal alkaline phosphatase (18009-027, Invitrogen) were added, and the membranes were incubated for an additional hour. After digestion, membranes were rinsed with deionized water before proceeding with the blocking step.

7.7. Proteomic analysis

Quantitative proteomics was performed by liquid chromatography with tandem mass spectrometry (LC-MS-MS), a powerful analytical technique that combines the separation ability of liquid chromatography (LC) with selective mass analysis by mass spectrometry (MS). Samples analyses were performed at the Proteomics Facility from the Research Support Central Service, University of Córdoba.

Samples were acidified with 0.5 % trifluoroacetic acid. A desalting and concentration step were performed with Sample Prep Pipette tips ZipTip C18 (Millipore), and the samples were dried under vacuum conditions using a Speedvac system (200 ng per sample).

LC-MS-MS was carried out using a nanoElute nanoflow ultrahigh-pressure LC system (Bruker Daltonics, Bremen, Germany) coupled to a timsTOF Pro 2 mass spectrometer, equipped with a CaptiveSpray nanoelectrospray ion source (Bruker Daltonics). For most analyses, 200 ng of peptide digest was loaded onto a Bruker FIFTEEN C18 capillary column (15 cm length, 75 µm ID, 1.9 µm particle size, 120 Å pore size; Bruker Daltonics). Peptides were separated at 30°C using a 20 min gradient at a flow rate of 300 nl/min (mobile phase A (MPA): 0.1% FA; mobile phase B (MPB): 0.1% FA in acetonitrile). A step gradient from 0 to 35% MPB was applied over 13 min, followed by a second step gradient from 35 to 90% MPB of 13 to 15 min, and finished with a 90% MPB wash for an additional 5 min. The total run time was of 20 min per analysis. The timsTOF Pro 2 was run in DIA-PASEF mode with isolation windows of 25 Da in a mass range of 450-950 Da without mass overlapping. Ion mobility resolution was set to 0.85–1.30 V s/cm^2 over a ramp time of 100 ms. The collision energy was increased stepwise as a function of the ion mobility ramp, from 27 to 45 eV. A polygonal filter was applied on the m/z space and ion mobility to exclude low m/z, mainly single-charged ions from the selection of PASEF precursors.

Raw data was analyzed in Spectronaut (see 15.1.210713.50606 – Rubin) (Biognosys). The reference library is acquired from QilexProteomeDB. The directDIA algorithm was used for raw data analysis and library generation was created with the Pulsar search algorithm using the database itself. All settings were set to default (BGS factory settings). To account for post-translational modifications and chemical labelling, the following adjustments were used: carbamidomethylation of cysteine residues was set as fixed modification, methionine oxidation and acetylation (N-terminal protein) were set as variable modification.

7.8. Enzymatic assays

To assay enzymatic activities, cells from bacterial cultures were suspended in PBS (50 mM NaH_2PO_4, 0.3 mM EDTA, pH 7.4) and sonicated with a Branson Sonifier (c=4, 20%, 3–6 times for 30 s). Specific enzymatic activities were calculated considering the molar extinction coefficient (ε) of NADH and NADPH (6.22 and 6.30, respectively) and the total protein quantity in the sample. The quantification of total protein in the bacterial extracts was conducted using the Bradford method (Bradford, 1976).

7.8.1. GAPDH glycolytic activity

GAPDH glycolytic activity was quantified following a previously described method by Pancholi and Fischetti (1992). The assay buffer was composed of 50 mM Na_2HPO_4 pH 8.6, 40 mM triethanolamine, 5 mM EDTA, 1 mM NAD^+ or $NADP^+$ and 4 mM DL-glyceraldehyde-3-phophate (Cayman Chemical 17865) to which 20 µg of total protein from cell extract were added. The reaction was performed in a final volume of 1 ml and absorbance was measured at 340 nm to monitor NADH or NADPH formation for 15 min every 30 s in a Shimadzu UV-1800 spectrophotometer.

7.8.2. GAPDH gluconeogenic activity

GAPDH gluconeogenic activity was measured by monitoring the decrease of NADH as described by Q. Wang et al. (2010). The substrate, 1,3-biphosphoglycerate, was generated by an initial reaction from D-3-phosphoglyceric acid (Sigma-Aldrich P8877), and then a second reaction was performed to measure the activity of interest. The initial reaction mixture consisted of 40 mM triethanolamine pH 8.5, 8.0 mM $MgSO_4$, 200 pg/ml 3-phosphoglyceric phosphokinase (Sigma-Aldrich P7634), 12 mM 3-phosphoglycerate, 2.4 mM ATP, and 0.15 mM NADH. This reaction was incubated for 1 h and stopped by heating at 90°C for 5 min. Then, to initiate the second reaction, 0.1 mM of the appropriate cofactor (NADH or NADPH) was added, as well as 20 µg of total protein from cell extracts to a final reaction volume of 1 ml. Absorbance at 340 nm was measured to monitor NADH or NADPH decrease as described above.

7.8.3. Erythrose-4-phosphate dehydrogenase (Epd) activity

Epd activity was quantified as described by Zhao et al. (1995). The assay buffer was composed of 50 mM sodium pyrophosphate pH 8.6, 1 mM dithiothreitol, 1 mM NAD^+ and 2 mM D-Erythrose-4-phosphate (Sigma-Aldrich E0377). 100 µg of total protein from cell extract were added to assay the activity. The reaction was performed at 50°C for 10 min and OD_{340} was measured every 2 min to monitor NADH formation.

8. MICROSCOPY TECHNIQUES

8.1. Nodule histology and microscopy

Samples were prepared at the microscopy unit of Estación Experimental del Zaidín - CSIC (Granada, Spain) and the microscopy unit of the CIC-University of Granada. Fresh nodules were collected from 21 and 28 days-old bean plants (*Phaseolus vulgaris* cv. Contender). Larger nodules were cut in half for better penetration of the fixing solution, nodules were then fixed in 4% paraformaldehyde, 2% glutaraldehyde, 0.05 M Na-cacodylate buffer (pH 7.2) under vacuum for 2 h at 4ºC. After a second fixation overnight at 4ºC, the samples were washed 3 times with 0.05 M cacodylate buffer for 30 min at room temperature. The nodules were postfixed in 1% osmium tetroxide in the same buffer (overnight at 4ºC). Samples were dehydrated in ethanol series and embedded in Epoxi EMbed 812 resin and polymerized for 48 h at 60ºC. Semithin (1 µm) sections were sliced with a Reichert Ultracut S ultramicrotome. Sections microscopy were stained with 1% (w/v) toluidine blue in aqueous 1% sodium borate for direct observation under optical microscopy.

8.2. Transmission electron microscopy immunolabeling

Samples were prepared at the Electron Cryomicroscopy Unit from the CCiTUB, University of Barcelona. They were cryoimmobilized using a Leica HPM100 High-Pressure Freezer (Leica Microsystems, Vienna, Austria). Planchettes containing the frozen samples were transferred to cryo-tubes containing 0.5% uranyl acetate (EMS, Hatfield, PA, USA) in acetone under liquid nitrogen and were freeze substituted at -90ºC for 80 h in an EM AFS2 (Leica Microsystems, Vienna, Austria). Samples were warmed up to -50ºC at a 5ºC/h slope and kept at -50ºC. They were rinsed with acetone and infiltrated in Lowicryl HM20 resin (EMS, Hatfield, PA, USA) at -50ºC. Samples were polymerized under UV light at -50ºC for 24 h, during the warming up at 5ºC/h slope until 22ºC and at 22ºC for 48 h. Sections 60 nm in thickness were obtained using a UC6 ultramicrotome (LeicaMicrosystems, Vienna, Austria). They were washed sequentially in 10 mM PBS, glycine 10 mM and 10 mM PBS. Then, they were incubated on drops of 5% bovine serum albumin (BSA) in 10 mM PBS for 15 min and they were changed to 1% BSA in 10 mM PBS , followed by incubation with the polyclonal anti-*R. etli* Gap antibody 1:35 in 1% BSA 10 mM PBS for 1 h. Then, they were washed in 0.25% Tween 20 in PBS 10 mM and they were changed to 1% BSA in 10 mM PBS, followed by incubation with anti-rabbit 12 nm colloidal gold-conjugated antibody 1:30 (Jackson) in 1% BSA 10 mM PBS for 30 min. Samples were washed in PBS, incubated in 1% glutaraldehyde in PBS for 5 min and rinsed in milliQ water. As a negative control for non-specific binding of the colloidal gold-conjugated antibody, the primary antibody was omitted. Sections were stained with 2% uranyl acetate and lead citrate and were

observed in a Tecnai™ Spirit TWIN microscope (FEI, Eindoven, The Netherlands) equipped with a tungsten cathode from the Electron Cryomicroscopy Unit from the CCiTUB. Images were acquired at 120 kV with a CCD Megaview 1 k × 1 k.

9. IN SILICO ANALYSES

9.1. Databases and Bioinformatics software

9.1.1. Databases

Genetic sequences were obtained from the National Center for Biotechnology Information (NCBI) and the Kyoto Encyclopedia of Genes and Genomes (KEGG).

The Universal Protein database UniProt was used for protein biological and molecular functions, to retrieve sequences and IDs, and other searches of protein information.InterPro (EMBL-EBI) (Paysan-Lafose et al., 2023) and PSORTb version 3.0.3 tools (https://www.psort.org/psortb) were used for domain and subcellular localization prediction respectively. To retrieve moonlighting proteins information, the databases MoonProt (Mani *et al*., 2015; Chen *et al*., 2021), and MultitaskProtDB (Franco-Serrano *et al*., 2018) were used.

9.1.2. Sequence Management

Multiple sequence alignment was performed using the software MUSCLE (MUltiple Sequence Comparison by Log-Expectation) by the EMBL-EBI (Madeira *et al*., 2022). DNA sequence visualization, annotation, editing and cloning, as well as plasmid maps were performed using the Snapgene® software (Dotmatics). For oligonucleotice design the softwares Oligo 6 (Molecular Biology Insights), Primer-BLAST (NIH-NCBI) and OligoAnalyzerTM Tool (IDT) were used.

9.2. Statistical analysis

Statistical analysis for comparison among different strains or conditions was performed by one-way ANOVA with post-hoc Tukey HSD test (Tukey, 1949). Statistical analysis and graph generation were performed using the softwares Graphpad Prism 9.0, Microsoft Excel 16.16 (Microsoft Corporation) and RStudio 1.3 software (R Core Team, 2020). When evaluating significant differences among diverse datasets the different categories were designated using a letter or symbol code, with different letters or symbols for statistically significant different groups.

9.3. Image analysis

ImageJ image analysis software (Schneider *et al*., 2012) was used to measure irregular areas and length in culture plate photographs.

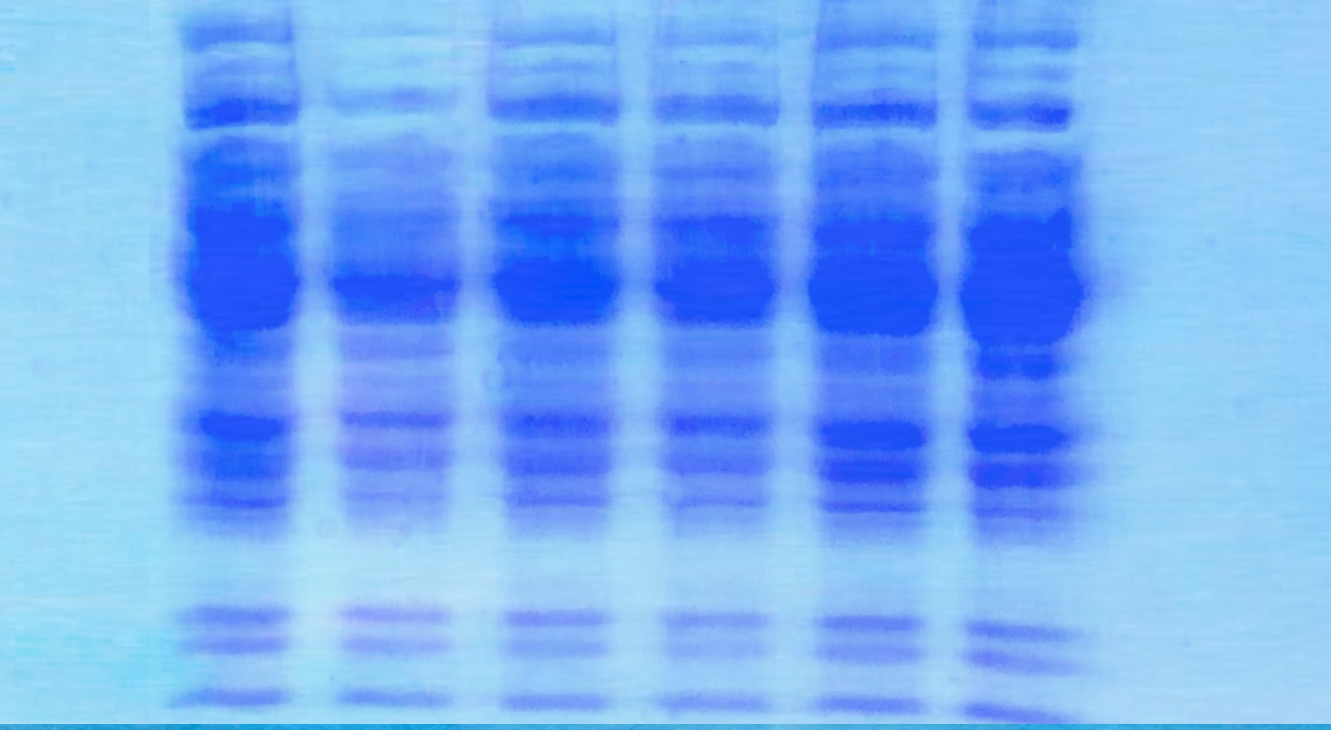

CHAPTER I

Analysis of *Pseudomonas syringae* proteomic profiles modulated by c-di-GMP

CHAPTER I

Keywords:
Cyclic-digualylate
Pseudomonas syringae
Proteome
Exported proteins
Moonlighting proteins
Rhizobium etli

Analysis of *Pseudomonas syringae* proteomic profiles modulated by c-di-GMP

ABSTRACT

Cyclic diguanylate (c-di-GMP, cdG) is a bacterial second messenger well known for orchestrating transitions between distinct lifestyles, notably playing a pivotal role in biofilm formation. The production and secretion of the biofilm matrix, composed of polysaccharides, lipids and proteins, undergoes regulation by c-di-GMP. Building upon previous investigations into the extracellular proteome of *Rhizobium etli* under high c-di-GMP conditions (Lorite *et al*., 2023), our study delved into the impact of this second messenger on the intracellular and extracellular proteome of the phytopathogen *Pseudomonas syringae* pv. tomato DC3000 by quantitative proteomics. The identification of differentially abundant (DA) proteins reinforced its involvement in biofilm formation, exopolysaccharide production and motility. However, a great number of these proteins appeared related to an array of cellular processes. Moreover, the trends observed in the export of proteins were markedly different compared to *R. etli*, where c-di-GMP promoted the export of cytoplasmic moonlighting proteins. In contrast, the export of a large number of cytoplasmic metabolic enzymes was downregulated in Pto, underscoring the importance of exporting potential moonlighting cytoplasmic proteins outside the cell. Gene expression analyses corroborated the proteomic data, although deviations were noted in some cases. Immunodetection analyses were specifically conducted on Gap proteins, as its exportation appeared promoted by c-di-GMP in *R. etli*. However, the export of Gap1 and Gap2 did not experience significant changes under high c-di-GMP levels. Nonetheless, its study remained interesting, since both Gap proteins were found to be exported under different culture conditions, suggesting potential moonlighting roles in this bacterium.

BACKGROUND

Bis-(3′,5′)-cyclic diguanosine monophosphate (c-di-GMP) is a widespread bacterial second messenger which acts as a lifestyle-switch molecule. It is involved in numerous processes including cell to cell signalling, virulence or cell cycle progression, but its primary and most prominent role lies in orchestrating the transition from a unicellular planktonic form of life to multicellular communities like biofilms (Junkermeier & Hengge, 2023; Römling, 2023). In biofilms, bacteria reside within a self-produced extracellular matrix, composed of exopolysaccharides, nucleic acids, and proteins. Beyond immobilizing bacteria, this matrix also enhances liquid retention, contribute to nutrient acquisition, and provide protection against mechanical stress and toxic compounds, with biofilm bacteria exhibiting higher antibiotic resistance (Römling & Balsalobre, 2012; Krol *et al*., 2020). C-di-GMP serves as a key regulator, both directly and indirectly, in the secretion of numerous biofilm biopolymers, but also in the secretion of proteins crucial for maintaining biofilm structural integrity, like adhesins, and motility organelles, such as flagella and pili. Additionally, c-di-GMP has been shown to impact the expression and/or activity of diverse protein secretion systems (López-Baena *et al*., 2019). It is noteworthy that cytoplasmic proteins have been also detected in bacterial extracellular matrices, albeit their origins are unclear and often explained as contaminants due to cell lysis or to protein-containing membrane vesicles shedding during cell growth (Jiao *et al*., 2011; Fong & Yildiz, 2015).

Pseudomonas syringae pv. tomato (Pto) is a phytopathogenic bacteria known to cause speck disease on tomato and crucifers (Lamichhane *et al*., 2015). To exert its virulence, Pto utilizes a sophisticated strategy involving the release of an array of effectors through a type III secretion system (T3SS). Additionally, it produces coronatine, a phytotoxin that induces stomatal opening, thereby facilitating bacterial entry into the apoplast (Xin *et al*., 2018). Complementing these mechanisms, flagella and biosurfactants facilitate movement, and exopolysaccharides provide protection against desiccation (Burch *et al*., 2012; Duque *et al*., 2013). Protein secretion also plays a crucial role in the interaction of Pto with the host plant. The Hrp T3SS releases proteins, known as effectors that either interact with the host cell wall and plasma membrane or are directly translocated into the cytoplasm. Besides their involvement in disease development, certain secreted proteins are also implicated in nutrient acquisition, stress responses, or metabolic adaptation (Petnicki-Ocwieja *et al*., 2002; Filloux, 2011; Schumacher *et al*., 2014). In the extracellular fraction of Pto DC3000 grown in a T3SS-inducing medium, the prevailing proteins detected were closely linked to the T3SS. Additionally, the translation elongation factor Tu (EF-Tu),

the coronafacic acid and coronafacic acid polyketide synthases, both essential for coronatine synthesis, certain ribosomal proteins, and different metabolic enzymes were also found (Elkhalfi *et al*., 2014; Schumacher *et al*., 2014).

In *P. syringae* strains, c-di-GMP intricately modulates virulence by inhibiting the T3SS, leading to the downregulation of numerous genes critical for pathogenicity. Additionally, c-di-GMP suppresses bacterial motility by inhibiting several flagellar operons, and represses pathogen-associated molecular patterns (PAMPs) by downregulating *fliC* transcription (Wang *et al*., 2019; Wang *et al*., 2023). Moreover, the production of EPS in *P. syringae* is subject to regulation by multiple environmental signals. Factors such as nutrient availability, temperature, and surface association strongly influence the expression of various polysaccharides controlled by c-di-GMP and the signaling proteins LadS and CbrB (Krishna *et al*., 2022). For instance, overexpressing the DGC PleD* in Pto and *P. savastanoi* pv. phaseolicola (Pph) caused significant alterations in phenotypes such as motility or EPS production (Pérez-Mendoza *et al*., 2014).

In a quantitative proteomics study of the extracellular proteome of another plant-interacting bacteria, *Rhizobium etli*, Lorite *et al*. (2023) observed that artificially elevated intracellular levels of c-di-GMP facilitated the secretion of various extracellular proteins potentially involved in adhesion and biofilm formation. Notably, these included the rhizobial adhesion protein RapA, as well as previously undescribed putative adhesins, and different flagellins. Nevertheless, high c-di-GMP levels also promoted the selective export of cytoplasmic proteins (ECPs) to the extracellular milieu. Remarkably, approximately 50% of these exported cytoplasmic proteins had been previously characterized as multifunctional proteins in other organisms, often found extracellularly or associated with the bacterial cell surface. The differential exportation of two of these cytoplasmic proteins, the translation elongation factor (EF-Tu) and glyceraldehyde 3-phosphate dehydrogenase (Gap), was confirmed by immunoblot assays.

In this study, we aimed to identify intracellular and extracellular proteins regulated by c-di-GMP in the phytopathogenic bacterium Pto DC3000, employing an approach similar to the one used in the study conducted with *R. etli*. By doing so, we aimed to elucidate the regulatory mechanisms governed by c-di-GMP in *P. syringae* and to compare the responses of these two contrasting plant-interacting bacteria to elevated c-di-GMP conditions. Through this comparative analysis, we aimed to gain insights into the diverse strategies employed by these bacteria in response to c-di-GMP signalling, potentially uncovering novel aspects of bacterial adaptation and pathogenicity in plant-microbe interactions.

SPECIFIC MATERIALS AND METHODS

Bacterial strains and sample collection

The bacterial strain Pto Δ*wssBC* (strain details in Table M.1) was employed to prevent excessive cellulose production under elevated c-di-GMP levels. The plasmid pJB3pleD* (Table M.2) was used to induce high c-di-GMP levels, whereas the strain with physiological c-di-GMP levels bore the plasmid vector pJB3Tc19.

Samples were obtained from 250 ml cultures grown in T3SS-inducing minimal media with mannitol and pyruvate as carbon sources (MMPM), described in *Materials and Methods*. Cultures were grown overnight at 20ºC with continuous shaking (180 rpm), to an OD_{600}=0.7-0.9 and centrifuged 2× 30 min at 7500×*g* at 4ºC to separate cell pellets and culture supernatants. Cell pellets were resuspended in 1 ml extraction buffer (0.7 M sucrose, 0.5 M Tris-HCl pH 8.2, 0.1 M KCl, 50 mM EDTA, 2% β-mercaptoethanol and 12 g/l (w/v) polyvinylpolypyrrolidone), sonicated for 5 cycles of 30 s (C = 4, 20%) in a Branson Sonicator 250, centrifuged at 15,000×*g* for 2 min, and the supernatant extract was collected. Culture supernatants were concentrated from 250 ml to 300 µl using Amicon® Ultra-15 Centrifugal Filter Devices with 3000 MWCO cut-off. Samples were obtained from three independent culture replicates.

Immunodetection by Western blot

For Western blots, protein samples (20-40 µg) were loaded onto 10% SDS-PAGE gels, and electrophoresis and membrane transfer were performed following standard procedures as described in *Materials and Methods*.

Rabbit polyclonal anti-Pto Gap1 and anti-Pto Gap2 antibodies were obtained (Davids Biothecnologie GMBH, Germany) against synthetic peptides (DLGDSEMNAHLLRFDTVHG and KAHRFARHRQSDAVELSVHE) derived from the Pto DC3000 Gap1 (PSPTO_1287) and Gap2 (PSPTO_2102) primary sequences, respectively. These anti-Gap antibodies were diluted to a working concentration of 2.5 µg/ml. A monoclonal mouse anti-*E. coli* Elongation Factor EF-Tu antibody (LSBio Inc., Seattle, WA, USA) was used in a 1:2000 dilution, following manufacturer's recommendation. This antibody recognizes the N-terminus (SKEKFE sequence) of the EF-Tu from *E. coli* and other bacteria. FliC was detected using a mouse anti-FliC antibody from *P. fluorescens* (De Weger *et al*., 1987) in a 1:10000 dilution.

Gene expression quantification by real-time PCR

Specific oligonucleotides (Table SI.1) were used for each qRT-PCR reaction. As the *wssB* gene was selected as representative of the cellulose synthase operon, the wild type

strain (non-mutant in the *wssBC* genes) was used in this case. Cultures were grown in MMPM for 24 h at 20ºC with continuous shaking (180 rpm), to an OD_{600}=0.7-0.9. PCR reactions and quantification were performed following standard procedures as described in *Materials and Methods*.

Functional classification

A functional classification of the differentially abundant proteins was conducted establishing 12 main categories encompassing different functions. The *Extracellular function and Structural* category included proteins involved in aggregation and adhesion, flagella and motility, peptidoglycan and polysaccharide production and structural proteins. The second category, *Protein synthesis and modification*, included chaperones, proteases, ribosomal and other proteins involved in translation and in protein modification processes. Four metabolic categories were arranged: *Carbon metabolism*, with proteins involved in the glycolysis and tricarboxylic acid cycle; *Nucleic acid metabolism*, with proteins involved in transcription, purin and pyrimidin metabolism, replication and recombination; *Nitrogen metabolism*, including amino acid metabolism and nitrogen assimilation; and *Lipid metabolism* comprising the functions of lipid biosynthesis and degradation. An *Energy production* category was established with enzymes involved in ATP synthesis and electron transfer. The *Cofactors-metals* category included proteins involved in the biosynthesis of cofactors and metal metabolism. In the *Genetic Regulation* category, transcriptional regulators and a sub-group of sensory proteins were included. A *Transport* category was established including transporters and proteins being part of secretion systems. The *Virulence* category included all those proteins involved in T3SS, T6SS, effector and toxin production, considered virulence factors in Pto DC3000. A final category named *Generic Enzymes* was established to encompass enzymes involved in different processes within the cell that could not be included in the other categories. Lastly, a number of proteins that lacked a recognised function or did not fit into any assigned category were classified as *Unknown function*.

Additional methods used in this chapter are previously described in the general *Materials and Methods* section:

- Growth curves
- Total protein samples preparation
- Proteomic analysis
- Gene expression analysis
- Databases and bioinformatics software

RESULTS

We examined the relative abundance of proteins in both the intracellular and extracellular proteome of Pto DC3000 with elevated c-di-GMP levels (pJBpleD* plasmid) compared to its isogenic derivative with physiological c-di-GMP levels (pJB3Tc19 plasmid). Growth curves of the assayed strains in rich media displayed no significant differences between them. In MMPM, the high c-di-GMP strain displayed a lower OD between hours 15 and 30, but then reached the same level as the wild type strain throughout the rest of the growth curve (Fig. SI.1). It is worth mentioning that the high c-di-GMP strain still showed slight aggregation/flocculation in minimal media, which may have interfered with the OD reads.

Protein samples were obtained from the intracellular content and supernatants of three independent culture replicates. An SDS-PAGE gel electrophoresis with Coomassie staining of the analysed samples is shown in Fig. SI.2. Interestingly, the protein band pattern appeared consistent with no discernible differences among the samples. This study was performed using quantitative MS-based proteomics.

C-di-GMP-dependent intracellular proteome of *P. syringae* pv. tomato

The MS-based proteomic analysis of the intracellular proteome identified 784 differentially abundant (DA) proteins that met the criteria of statistically likely (q-value≤0.05 and ±1.5-fold change), from which 296 proteins qualified as statistically confident (p-value≤0.01 and ±2-fold change) (Fig. 1A). Due to the large number of proteins in the statistically likely protein group for the intracellular proteome, further analysis focused solely on the statistically confident protein candidates. This subset comprised 116 proteins showing increased abundance (IA) and 180 proteins displaying reduced abundance (RA) in the high c-di-GMP strain.

An interesting finding in the analysis of the intrasome was the presence of an ISPsy5 transposase among the RA proteins. Proteome analyses identified the peptides as belonging to two proteins: PSPTO_0035 and PSPTO_5304, which are 99.8% identical. Surprisingly, PSPTO_0035 is 100% identical to other 32 proteins putatively present in Pto DC3000: PSPTO_0039, PSPTO_0196, PSPTO_0670, PSPTO_1020, PSPTO_1098, PSPTO_1189, PSPTO_1227, PSPTO_2437, PSPTO_2460, PSPTO_2840, PSPTO_2971, PSPTO_3213, PSPTO_3216, PSPTO_3613, PSPTO_3651, PSPTO_3996, PSPTO_3999, PSPTO_4251, PSPTO_4389, PSPTO_4567, PSPTO_4693, PSPTO_4737, PSPTO_4764, PSPTO_4994, PSPTO_5212, PSPTO_5215, PSPTO_5368, PSPTO_5411, PSPTO_5443, PSPTO_5445, PSPTO_5543, PSPTO_5591. Since it was not possible to unambiguously assign the peptides to a specific protein, we excluded both PSPTO_0035 and PSPTO_5304 from our analyses. This left 295 proteins of the intrasome for further analyses, of which 116 proteins showed IA and 179 displayed RA in the high c-di-GMP strain.

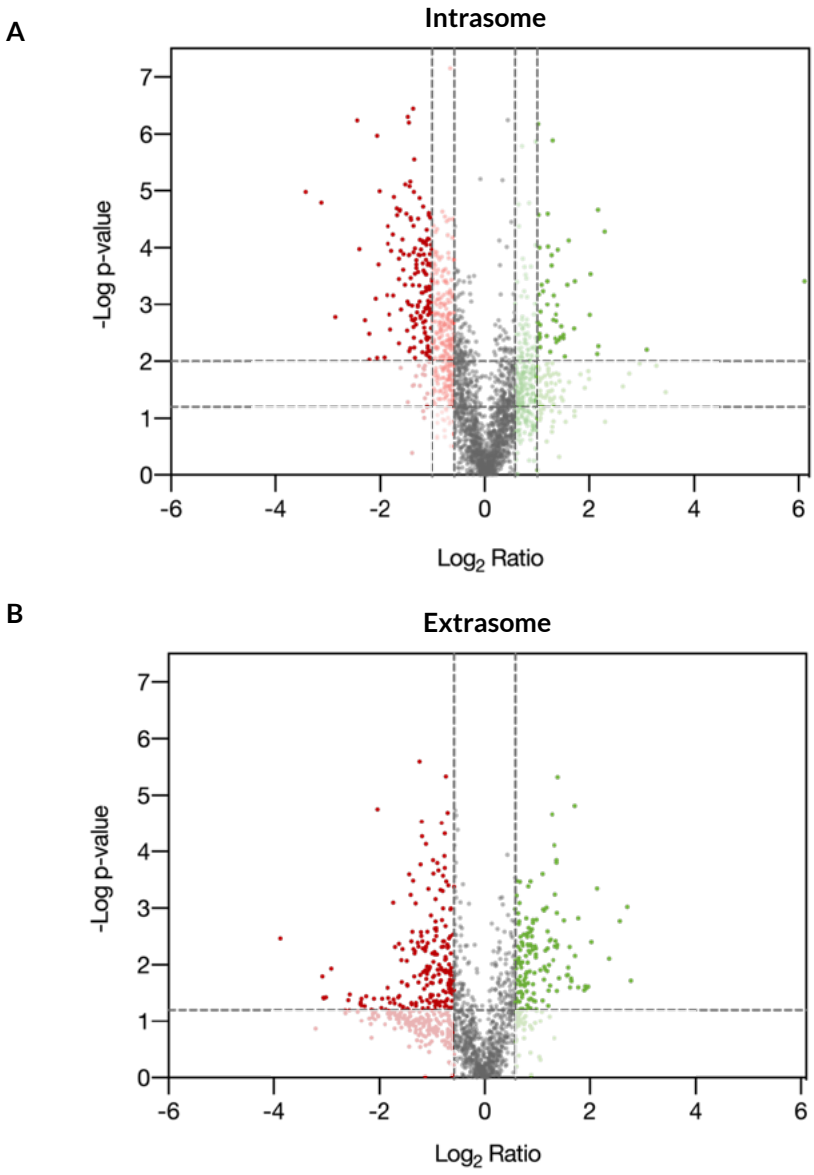

Figure RI.1. Volcano plots of the differentially abundant proteins comparing Pto strains with physiological and high levels of c-di-GMP.
Each differentially expressed protein is represented by a dot. Red dots represent statistically likely proteins (q-value≤0.05 and ±1.5-fold change), with increased or reduced abundance.
A. Intracellular proteome. Dark red and green dots represent proteins qualified as statistically confident (p-value≤0.01 and ±2-fold change) that were considered for the analysis, whereas light red and green dots represent statistically likely proteins (q-value≤0.05 and ±1.5-fold change) that were not considered in the analysis.
B. Extracellular proteome. Dark red and green dots represent proteins qualified as statistically likely proteins (q-value≤0.05 and ±1.5-fold change), which were all considered in the analysis.

The predicted subcellular localization and likely function of each DA protein were examined based on sequence homologies, analysis of protein domains, and literature reports. Regarding subcellular localization, the majority of proteins were cytoplasmic, accounting for 52% and 60% of the IA and RA proteins, respectively. Membrane-associated proteins represented 15% and 32%, whereas periplasmic and extracellular proteins were only represented in the IA group, comprising 8% and 2%, respectively (Fig. RI.2A).

Gene Ontology (GO) functional analysis revealed DA proteins across various functional groups (Fig. RI.2B). Apart from those of unknown function, the larger groups of proteins were those categorised as extracellular function, generic enzymes (enzymes involved in diverse pathways), nucleic acid metabolism, transporters, and genetic regulation. DA proteins were also observed in the functional groups of nitrogen metabolism, protein synthesis and modifications, cofactors and metal metabolism, and virulence (Fig. RI.2B and Table RI.1).

The most abundant DA proteins in the intrasome were those associated with extracellular and structural functions. Intriguingly, no putative or known protein adhesins regulated by c-di-GMP were identified in this experiment. Among the IA proteins at high c-di-GMP levels were those involved in peptidoglycan formation and cellulose biosynthesis, such as WssA, WssE, WssF, WssG or WssI, which are known to be regulated by c-di-GMP and play roles in adhesion/aggregation and biofilm formation (Pérez-Mendoza *et al*., 2014). In contrast, PSPTO_3530/PslB, involved in Psl exopolysaccharide biosynthesis (Heredia-Ponce *et al*., 2020; Krishna *et al*. 2022), was found RA, as well as three LPS related proteins (HtrB, KdtA, WaaG). Regarding motility, one protein related with type IV pili production (PilJ), many proteins from the flagellar basal body (FliG, FliH, FliI, FliM, FlhF, MotB), as well as several proteins involved in chemotaxis (e.g., PSPTO_0117, PSPTO_1334, PSPTO_2616, PSPTO_4531, PSPTO_5159) constituted one of the largest RA functional groups, which agrees with the known downregulation of bacterial motility by c-di-GMP (Römling, 2005; Pérez-Mendoza *et al*., 2014). However, the flagellar L-ring protein FlgH and the hook capping protein FlgD appeared IA under this condition (Table RI.1), whereas other proteins from the external flagellar apparatus such as the flagellin FliC or the hook protein FlgE remained unchanged.

A significant number of DA proteins in the intrasome were classified as generic enzymes, as they would catalyse reactions involved in unclassified pathways or routes. In the IA group, five enzymes presented oxidoreductase activity (PSPTO_2949, PSPTO_4082, PSPTO_4263, PSPTO_4914 and PSPTO_5060), whereas others were hydrolases (PSPTO_0162, PSPTO_0675, PSPTO_5171), or transferases (PSPTO_1331, PSPTO_3856). Some other present enzymes were involved in the biosynthesis of secondary metabolites (PSPTO_0659 or PSPTO_0730/UbiX) or in the degradation of aromatic compounds (PSPTO_3138). Proteins with diverse activities were also present among the RA generic

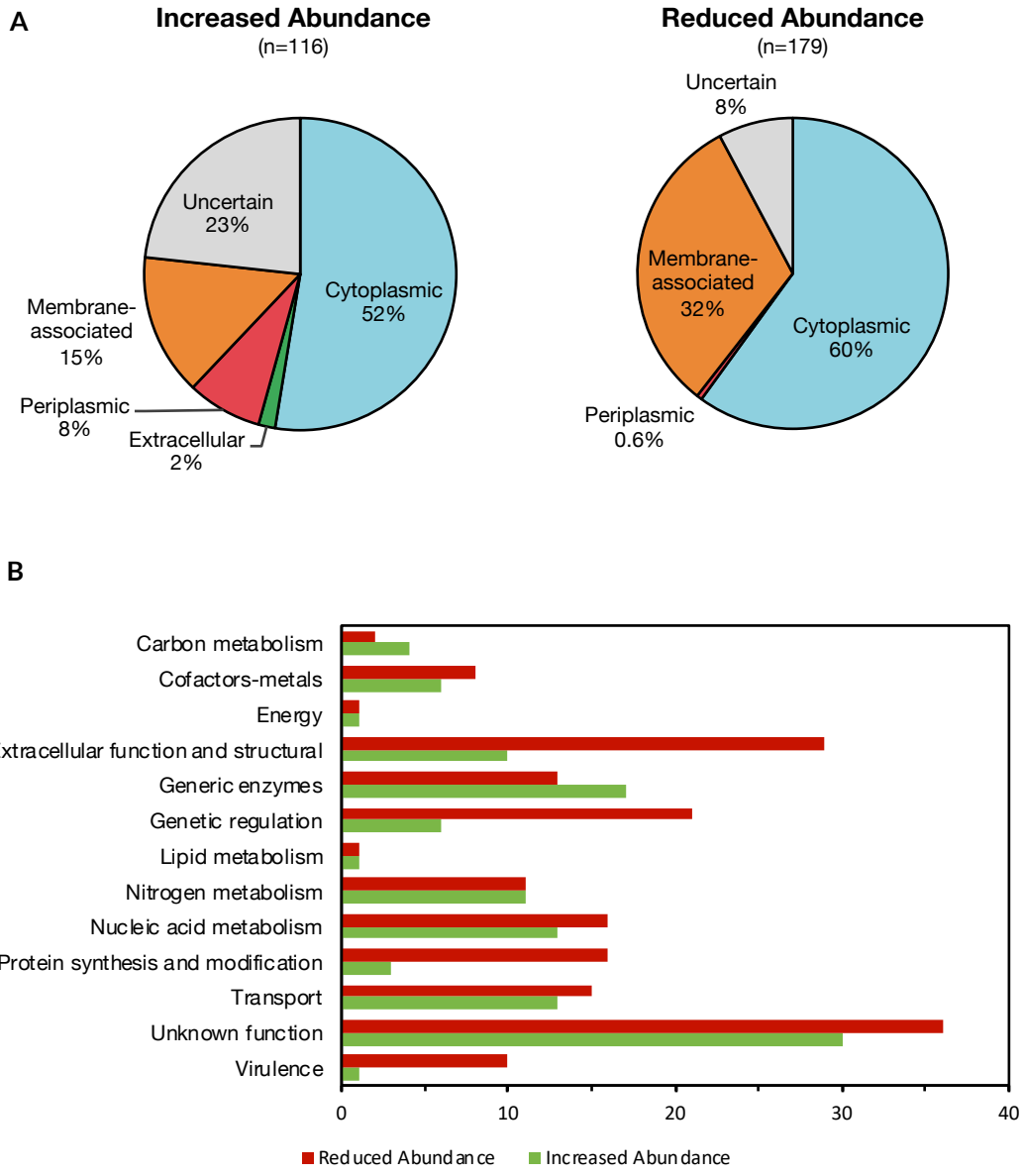

Figure RI.2. Subcellular localization and function of intracellular proteins with differential abundance under high c-di-GMP.
A. Predicted subcellular localization of the increased and reduced abundance proteins under high c-di-GMP.
B. Likely function classification of the proteins exhibiting differential abundance under high c-di-GMP.

enzymes. There were four glycosyltransferases (PSPTO_1067, PSPTO_1918, PSPTO_1946, PSPTO_2710), one acetyltransferase (PSPTO_5506) and three oxidoreductases (Qor, PSPTO_2672, PSPTO_2722). Other enzymes that appeared as RA were PchA, involved in biosynthesis of the siderophore yersiniabactin, PSPTO_5222/UbiH, involved in biosynthesis of a ubiquinone that functions in the respiratory electron transport chain, and VanA involved in vanillate degradation. Curiously, PSPTO_2673, a putative dehydrogenase and PSPTO_2672, containing a flavin-reductase like domain, displayed opposite trends despite being encoded in the same operon. UbiX and UbiH likely involved in a common route of ubiquinone synthesis also exhibited diverging trends.

Concerning nucleic acids metabolism, a histone-like protein (PSPTO_1266), a putative oligoribonuclease (Orn/PSPTO_4950), a putative exodeoxyribonuclease III (PSPTO_0079), and several proteins involved in nucleotide metabolism showed IA. Interestingly, the alarmone (p)ppGpp metabolizing protein SpoT/PSPTO_0073, along with putative cytidine deaminase (Cdd/PSPTO_1602) and adenosine deaminase (PSPTO_0757), displayed RA in the high c-di-GMP strain. Also, many proteins involved in DNA repair and recombination (*i.e.*, Rec proteins) appeared RA.

Among DA transporter proteins, mostly importers but also exporters and putative porins were found. IA transport proteins were mainly ABC transporters (ModA, PSPTO_2775, abP/PSPTO_2638, PSPTO_5358, PSPTO_5562), but also others such as SecG which is a component of the membrane translocase of the general Sec protein secretory pathway. It is interesting to note that in Pto the *secG* gene seems transcriptionally coupled to *tpiA*, encoding the triose-P isomerase protein TpiA that was also found IA (Table RI.1, Carbon metabolism, Glycolysis/TCA/PP). RA transport proteins included ABC transporters (CysA, FtsX, GltK, LolC, PotA, PSPTO_0462), but also the dicarboxylate uptake protein DctA-1. Other RA proteins were involved in type IV pilus formation, T2SS, and T4SS (PilB, PilC, PSPTO_0319, PSPTO_4853), a putative T5SS (PSPTO_3230) and T6SS (PSPTO_5425, PSPTO_5427), also involved in virulence (as classified in Table RI.1). Regarding components of ABC transporters, it is worth to mention that the majority of the IA corresponded to ligand-binding periplasmic proteins whereas most RA proteins were membrane associated components of ABC transporters.

Many proteins containing sensor domains and potentially involved in signal transduction and regulation displayed DA. Most of these proteins (EnvZ, NtrB, etc.) were RA, however one was IA, PSPTO_1208 containing a FecR-like domain and probably involved in citrate-mediated iron uptake (Butcher *et al.*, 2011; Llamas *et al.*, 2014). A significant number of DNA-binding transcriptional regulators were also found DA. GlpR, probably involved in glycerol-3-phosphate uptake and metabolism, the virulence regulator TvrR (Preiter *et al.*, 2005), PSPTO_2646, another TetR-like regulator, PSPTO_4027, belonging to the LuxR

family, and the response regulator PSPTO_4553, homologous to RegA of *P. aeruginosa*, all displayed IA. On the other hand, nearly a dozen putative transcriptional regulators appeared RA in the elevated c-di-GMP strain: MltR (an AraC-type regulator), PSPTO_0303 (response regulator with HDOD domain, IPR013976), PSPTO_0378 (response regulator), PSPTO_0384 (regulator with a methyltransferase domain belonging to the ArsR family), PSPTO_0665 (putative repressor), PSPTO_1499 (WspR-like regulator with a GGDEF domain), PSPTO_2395 (putative sugar responsive regulator), PSPTO_5399 (putative DctD regulator), and the putative LysR family transcriptional regulators PSPTO_1618, PSPTO_2447 and PSPTO_5498. Also, the sigma factor RpoS appeared reduced, suggesting that c-di-GMP could potentially affect the expression of numerous stationary-phase genes.

Regarding proteins involved in nitrogen metabolism, some involved in histidine biosynthesis (HisG) and utilization (HutH-2), methionine salvage pathway (MtnB, MtnC and PSPTO_3506), tryptophan biosynthesis (TrpA) and metabolism of other amino acids were found IA. In contrast, diverse proteins involved in either biosynthesis or degradation of amino acids appeared RA.

Few proteins involved in protein synthesis and modification appeared IA, which included the ribosome modification protein RimK, the tRNA modification factor SmtA, or the rRNA modification factor RsmA(PSPTO_0551). Most proteins in this category appeared RA, including multiple proteins involved in protein, tRNA and rRNA modifications, proteases and chaperones.

There were intriguing results regarding proteins involved in the metabolism of cofactors. For instance, CobP and CobC displayed opposite trends (Table 1), despite both being encoded in the same operon and involved in cobalamin biosynthesis. Likewise, PncA and PncB, involved in nicotinate and nicotinamide metabolism although not located in the same operon, displayed contrasting trends. Two proteins encoded in the same operon although with apparently unrelated roles, protein PSPTO_4034 putatively involved in nicotinamide-nucleotide metabolism and PSPTO_4033 (RecA) involved in DNA repair, also displayed opposite trends (Table RI.1). HemF involved in heme biosynthesis, MetF (methylenetetrahydrofolate reductase), and RibE from the riboflavin biosynthesis pathway, all displayed IA. Irp1, Irp4 and PSPTO_2602 encoded in the yersiniabactin biosynthesis operon, and PSPTO_2150 from the pyoverdine pathway were all RA, suggesting that c-di-GMP could reduce production of these two siderophores.

Virulence-related proteins were also prominent among the RA proteins. Specifically, several proteins involved in coronafacic acid (Cfa3, Cfa5, Cfa6, Cfa7, Cfa9) and coronamic acid (CmaA, CmaB) synthesis, required for Pto virulence, appeared RA. The T6SS secreted protein Hcp-2/PSPTO_5435 was IA, whereas PSPTO_5425 and PSPT_5427 displayed RA, despite the fact that the three of them are part of the same T6SS (Chien *et al*., 2020).

Table RI.1. Functional classification of differentially abundant proteins in the intracellular proteome of the high c-di-GMP strain. For more detailed data and unknown fuction proteins see Appendix B.

Category	Function	Differential Abundance Proteins	
		Increased Abundance (IA)	**Reduced Abundance (RA)**
Carbon metabolism	Glycolysis/TCA/PP	Rpe, TpiA, Xfp, PSPTO_0107	PSPTO_3124, PSPTO_3126
Cofactors-metals	Biosynthesis of cofactors and metal metabolism	CobP, HemF, MetF, PncA, RibE, PSPTO_4034	CobC, CobL, Irp1, Irp4, PncB, PSPTO_2150, PSPTO_2602, PSPTO_5526
Energy	ATP synthesis and electron transfer	EtfB-2	NdH
Extracellular function and structural	Aggregation/Adhesion		
	Flagella/Motility	FlgD, FlgH	FlhF, FliG, FliH, FliI, FliM, MotB, PilJ, PSPTO_0117, PSPTO_0916, PSPTO_1039, PSPTO_1323, PSPTO_1334, PSPTO_1495, PSPTO_1927, PSPTO_2441, PSPTO_2442, PSPTO_2472, PSPTO_2616, PSPTO_4531, PSPTO_4541, PSPTO_4936, PSPTO_5159, PSPTO_5553
	Peptidoglycan	MltB, PSPTO_1025, PSPTO_4989	
	Polysaccharide	WssA, WssE, WssF, WssG, WssI	HtrB, KdtA, WaaG, PSPTO_3530
	Structural		ZapE, ZipA
Generic enzymes	Involved in different metabolic processes	UbiX, PSPTO_0162, PSPTO_0659, PSPTO_0675, PSPTO_1331, PSPTO_1529, PSPTO_2673, PSPTO_2949, PSPTO_3138, PSPTO_3802, PSPTO_3856, PSPTO_4082, PSPTO_4263, PSPTO_4549, PSPTO_4914, PSPTO_5060, PSPTO_5171	Qor, PchA, UbiH, VanA, PSPTO_1067, PSPTO_1918, PSPTO_1946, PSPTO_2672, PSPTO_2710, PSPTO_2722, PSPTO_3705, PSPTO_5104, PSPTO_5506
Genetic regulation	Sensory proteins	PSPTO_1208	EnvZ, NtrB, PSPTO_0965, PSPTO_1605, PSPTO_1606, PSPTO_2123, PSPTO_2131, PSPTO_2715, PSPTO_4293
	Transcriptional regulators	GlpR, TvrR, PSPTO_2646, PSPTO_4027, PSPTO_4553	MltR, RpoS, PSPTO_0303, PSPTO_0378, PSPTO_0384, PSPTO_0665, PSPTO_1499, PSPTO_1618, PSPTO_2395, PSPTO_2447, PSPTO_5399, PSPTO_5498

Table RI.1. *Cont.*

Lipid metabolism	Lipid biosynthesis and degradation	PSPTO_2719	Cfa
Nitrogen metabolism	Amino acid Metabolism	AroB, HisG, HutH-2, MtnB, MtnC, TrpA, PSPTO_1335, PSPTO_2261, PSPTO_2281, PSPTO_3506, PSPTO_4526	AroF-1, AruF, DadA, GcvT-2, IscS, ProB, SoxB-1, PSPTO_0401, PSPTO_0873, PSPTO_3190, PSPTO_5460
	Nitrogen assimilation		
Nucleic acid metabolism	Transcription	Orn	
	Purin and pyrimidine metabolism	ApaH, CysH, CysQ, HyuE, PyrE, PyrF, PyrH, SurE, PSPTO_0828, PSPTO_5403	Cdd, SpoT, PSPTO_0757
	Replication/Recombination	PSPTO_0079	HrpB, MutL, RadA, RecA, RecF, RecN, RecR, Rep, RuvB, SbcD, UvrB, UvrD, PSPTO_5344
	Others	PSPTO_1266	
Protein synthesis and modification	Chaperones		HscC, YegD, PSPTO_1065, PSPTO_5052
	Proteases		PSPTO_1350, PSPTO_1541, PSPTO_1822
	Translation	RsmA/PSPTO_0551, SmtA	EttA, MnmA, QueA, RlmF, RluD, Rnd, TrhO, TtcA
	Modifications	RimK	PSPTO_4481
Transport	Transporters/Secretion systems	AbP, ArsB, ModA, SecG, PSPTO_1852, PSPTO_2343, PSPTO_2484, PSPTO_2601, PSPTO_2775, PSPTO_3846, PSPTO_5333, PSPTO_5358, PSPTO_5562	CysA, DctA-1, FtsX, GltK, LolC, PilB, PilC, PotA, TliE, PSPTO_0138, PSPTO_0319, PSPTO_0462, PSPTO_2160, PSPTO_3230, PSPTO_4853
Virulence	Virulence factors	Hcp-2	Cfa3, Cfa5, Cfa6, Cfa7, Cfa9, CmaA, CmaB, IaaL, PSPTO_5425, PSPTO_5427

C-di-GMP-dependent extracellular proteome of *P. syringae* pv. tomato

The MS-based proteomic analysis of the extracellular proteome identified 396 differential proteins meeting the criteria of statistically likely (q-value≤0.05 and ±1.5-fold change), all of which were considered for further analysis (Fig. RI.1B). Of these, 139 proteins were IA proteins while 257 proteins displayed RA in the strain with high c-di-GMP levels. This observation mirrors the trend seen in the intracellular proteome, with a greater number of RA than IA proteins under high c-di-GMP conditions.

The predicted subcellular localization and likely function of each differentially abundant protein were also studied in this case. Concerning subcellular localization, cytoplasmic proteins comprised the largest group, accounting for 30% and 68% of the IA and RA proteins, respectively (Fig. RI.3A). Membrane-associated proteins represented 14% and 12% of the IA and RA proteins, respectively, displaying similar ratios in both groups. In contrast, periplasmic proteins were more prevalent among the IA proteins (21%) compared to only 2% of the RA proteins. Extracellular proteins followed a similar pattern, accounting for 12% of the IA group but only 1% of RA proteins (Fig. RI.3A).

Gene Ontology (GO) functional analysis of the differentially abundant proteins (Fig. RI.3B) showed that the largest groups of IA proteins were involved in transport (29), and extracellular and structural functions (26). On the other hand, RA proteins were predominantly involved in protein synthesis and modification (38), generic enzymes (37), nitrogen metabolism (30), and nucleic acid metabolism (30). A significant number of proteins classified as unknown function were present in both IA and RA groups (Fig. RI.3B and Table RI.2).

The functional classification of differentially abundant proteins in culture supernatants is depicted in Table RI.2. The most abundant DA proteins in the extrasome were those associated with protein synthesis and modification, which was one of the largest groups of RA proteins, a pattern also observed in the intrasome. In this case, RA proteins included many large and small ribosomal proteins (Rpl, Rpm∗, Rps∗), the ribosome recycling factor Frr, the translation initiation and release factors InfA and PrfC, and several aminoacyl t-RNA ligases. There were also several proteases like ClpA, ClpP or PepN that displayed RA, as well as chaperones like GroES and the peptidyl-prolyl isomerases PpiB, PSPTO_0808, PSPTO_1171 and PSPTO_4581. The IA group displayed a few proteins with putative peptidase activity, like Map-2, Prc, PSPTO_0425, PSPTO_3193, PSPTO_3332, PSPTO_3958 and PSPTO_5329, but also the ribosomal protein S8 (RspH), the putative ribosome-binding GTPase YchF or the amidase PSPTO_3192.

Another functional group with a notable number of proteins was the one named generic enzymes, most involved in diverse but unknown catalytic reactions/pathways. There were nearly 10 IA generic enzymes, which have common features like their

A

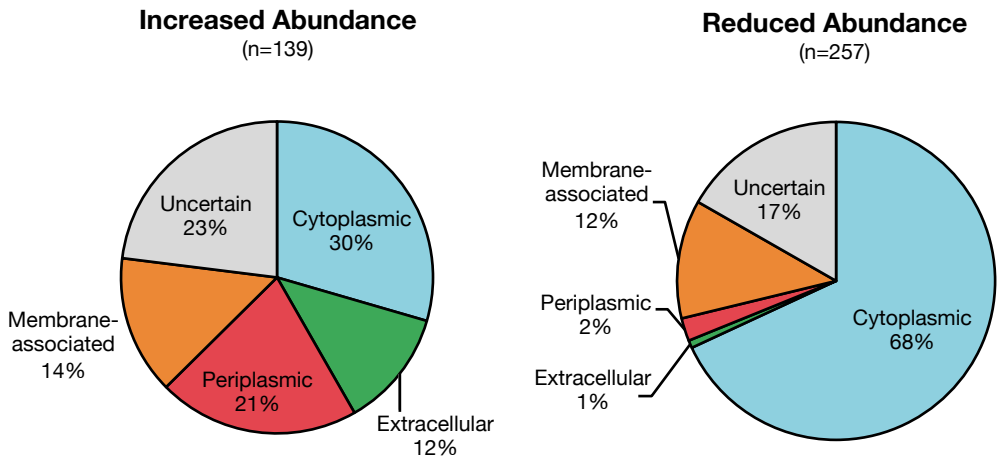

B

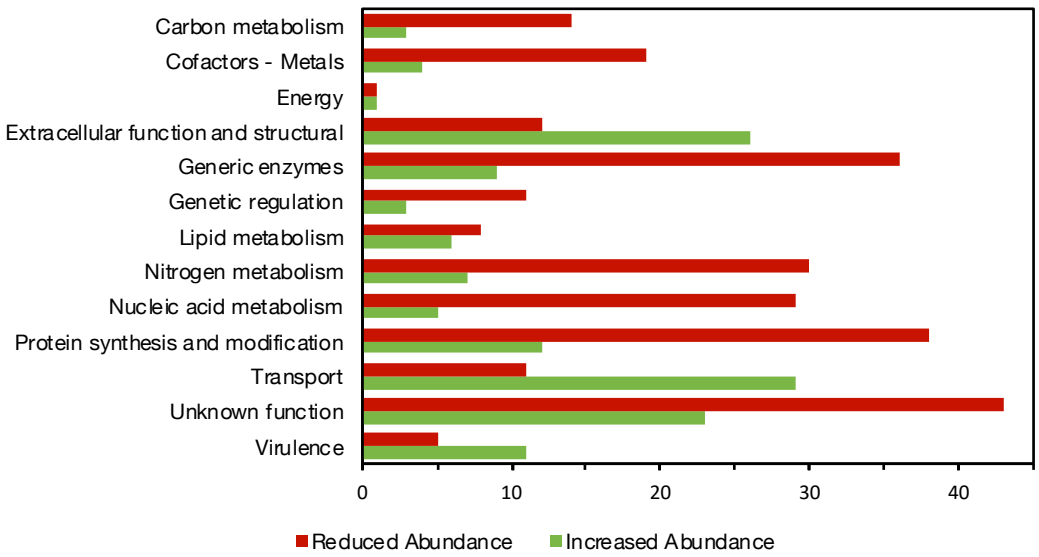

Figure 3. Subcellular localization and function of extracellular proteins with differential abundance under high c-di-GMP.
A.Predicted subcellular localization of the increased and reduced abundance proteins under high c-di-GMP.
B. Likely function classification of proteins displaying differential abundance under high c-di-GMP.

subcellular location (either cytoplasmic or associated to cytoplasmic membrane) and their putative involvement in metabolism of C compounds (acetyltransferases, deacetylases, isomerases, oxidoreductases and hydrolases), including CO_2 (carbonic anhydrase PSPTO_1340). The RA group of generic enzymes included 36 proteins, mostly cytoplasmic, many of which might be involved in secondary oxidoreductase/dehydrogenase activities, often related with antioxidant metabolism. An interesting observation is the presence of CatF, CatI, and CatJ, three proteins encoded by the same operon and participating in the degradation of catechol.

Transporters and secretion proteins were the largest group of IA proteins under high c-di-GMP conditions, consistently with the intrasome profile, where those categories also represented a substantial portion. Similarly, the majority of IA transport proteins were ligand-binding periplasmic proteins of ABC transporters, including FecB, RbsB-2, XylF, ZnuA, PSPTO_0791, PSPTO_2788 or PSPTO_2775 (Table RI.2), the later was also IA in the intracellular proteome (Table RI.1). Other IA periplasmic proteins involved in transport were TolB (from the Tol-Pal translocation system) and DctP (from the TRAP dicarboxylate translocation system). Nevertheless, a few membrane-associated components were also IA, such as PSPTO_1076 which could be involved in LPS biosynthesis or export, or TliF which is an outer membrane protein part of a T1SS involved in secretion of extracellular enzymes (Ahn *et al*., 1999). Intriguingly, another component of this T1SS, TliE, was found RA in the intrasome (Table RI.1). Functional diversity was higher among RA transport proteins (Table RI.2), which included the carbon-starvation responsive, peptide transport protein CstA, the phosphotransferase system protein PtsP, the symporter PSPTO_5500, the proteins PSPTO_4303 and PSPTO_4304/SaxB of the multidrug efflux pump MexAB-OprM (Vargas *et al*., 2011), the putative membrane insertase YidC, or the inner membrane protein PSPTO_5451 which contains the conserved domain of unknown function DUF945 (IPR010352). This group of RA proteins also included ABC-type components such as the pyoverdine transporter PvdE (Swingle *et al*., 2008) the membrane permease PSPTO_2604/YbtP involved in yersiniabactin biosynthesis (Bultreys *et al*., 2006; A. M. Jones *et al*., 2007), and PSPTO_0138 which has unknown role but was also found RA in the intracellular proteome (Table RI.1). Curiously, two components of the phosphotransferase system were identified: PtsN, which exhibited IA, and PtsP, which displayed RA (Table RI.2). It should be also mention that Ffh, a component of the membrane translocase of the general Sec protein secretory pathway exhibited RA in the extrasome. Interestingly, another component of that pathway, SecG, was found to be IA in the intrasome (Table RI.1).

Several IA proteins involved in polysaccharide and peptidoglycan formation, like AlgE, AlgL, DacB, MltB, MltF, OpgG, WssD or WssG, whose functions are related to or known to be regulated by c-di-GMP (Morgan *et al*., 2014; Whitney *et al*., 2015; Kharadi & Sundin, 2020;

Liang *et al*., 2022), were identified in the extracellular function and structural group. Various flagellar and other motility related proteins were also found to be IA in the extracellular proteome (FlgE-1, FlgF, FlgG, FlgK, FlgL, FliC, FliH), all proteins from the most external parts of the flagellum. It is known that high c-di-GMP blocks *P. syringae* motility (Pérez-Mendoza *et al*., 2014), but these results suggest that c-di-GMP may not repress flagellin secretion. Contrarily, FlgH appeared RA despite being encoded in the same operon as the rest of the Flg proteins, and despite having appeared IA in the intracellular compartment (Table RI.1). Surprisingly, few proteins involved in adhesion displayed DA in the extracellular compartment. Only PSPTO_2874, a 653 aa protein containing a central Von Willebrand type A-like domain (IPR002035) putatively involved in adhesion, was IA.

The nitrogen metabolism category included few IA proteins, taking part in amino acid metabolism, and a greater number of RA proteins. The majority of these were also involved in amino acid metabolism (AhcY, ArgH, AroQ, BetA, CarB, IlvN and MetH, among others), but some of them were involved in nitrogen assimilation (CynS, PSPTO_1440, PSPTO_2302). Contrasting behaviours were detected for proteins apparently working in the same pathway, for instance ThrB *vs* ThrC, MtnC *vs* MtnA, or TrpC/D *vs* TrpA (Table RI.2). HisG, MtnC and the phosphorylase PSPTO_3506 were found IA in both intracellular and extracellular proteomes, whereas TrpA displayed IA intracellularly but RA extracellularly (Tables RI.1 and RI.2).

Nucleic acid metabolism was another group with a significant number of RA proteins, many appeared involved in purine and pyrimidine metabolism (Amn, Cdd, Dcd, GuaA, PurA, PurC, PurE, PurF, PurT, PyrC) (Table RI.2). A few appeared involved in transcription efficiency such as GreA and NusG, the sigma-54 transcription factor RpoN, or the oligoribonuclease Orn/PSPTO_4950. Intriguingly, Orn was found IA in the intrasome (Table RI.1). Other RA proteins appeared involved in DNA replication/recombination (DnaE, ParE, TopA) and/or repair (UvrA, Ssb, SbcC), as well as several endoribonucleases (PSPTO_0072, PSPTO_0102, PSPTO_2779, PSPTO_4778). Also, in this RA subgroup was PSPTO_1266, a histone-like protein which curiously appeared IA in the intrasome (Table RI.1). Another histone-like protein HupB was found IA extracellularly, along with a few proteins involved in purine and pyrimidine metabolism (Table RI.2).

The group of proteins involved in biosynthesis of cofactors and metals included also a high number of RA proteins (Table RI.2): BioB involved in biotin metabolism, CobT and CysG involved in porphyrin metabolism, Epd/Gap3 and PdxJ related to vitamin B6 metabolism, MoaB involved in molybdenum cofactor biosynthesis, NudC in nicotinamide-nucleotide metabolism, PanB in panthotenate metabolism, PqqB in coenzyme PQQ, RibH2 in riboflavin biosynthesis, Irp3 and PSPTO_2602 in yersiniabactin biosynthesis, and PSPTO_4193 putatively involved in siderophore utilization.

Table RI.2. Functional classification of differentially abundant proteins in the culture supernatants of the high c-di-GMP strain. In bold are indicated proteins reported as moonlighting in other organisms, underlined are indicated putative moonlighting proteins in other organisms. For more detailed data and unknown fuction proteins see Appendix B.

Category	Function	Differential Abundance Proteins	
		Increased Abundance (IA)	Reduced Abundance (RA)
Carbon metabolism	Glycolysis/TCA/PP	**GlcB2**, Zwf-2, PSPTO_1443	FumC-2, Gcd, Glk, GltA, GpmI, LpdA, Pgm, Rpe, PSPTO_0500, PSPTO_0956, PSPTO_1215, PSPTO_1281, PSPTO_5134, PSPTO_5292
Cofactors-metals	Biosynthesis of cofactors and metal metabolism	CobC, CopA, CopB, PanE-1	Bfr, BioB, CoaD/PSPTO_0417, CobT, CysG, Epd/Gap3, Irp3, MoaB, NudC, PanB, PdxJ, PqqB, RibH2, TerB, TerD, PSPTO_0653, PSPTO_2602, PSPTO_3983, PSPTO_4193
Energy	ATP synthesis and electron transfer	AtpF	CyoB
Extracellular function and structural	Aggregation/Adhesion	PSPTO_2874	
	Motility / Chemotaxis	FlgE-1, FlgF, FlgG, FlgK, FlgL, FliC, FliH, PSPTO_0815	CheB1, FlgH, PSPTO_2616, PSPTO_3237
	Peptidoglycan	DacB, MltB, MltF, OpgG, PSPTO_ 2270, PSPTO_3522, PSPTO_4419, PSPTO_4634	Mpl, PSPTO_0977
	Polysaccharide	AlgE, AlgL, WssD, WssG	GmhA, LpxA
	Structural	AmpC, BamB, MinE, PSPTO_2187, PSPTO_4084	Blc, HflK, GlmU, PSPTO_3403
Generic enzymes	Involved in different metabolic processes	Fnr-2, PSPTO_1245, PSPTO_1340, PSPTO_2290, PSPTO_2697, PSPTO_2847, PSPTO_3495, PSPTO_4161, PSPTO_5507	AcdA, AhpC, CatF, CatI, CatJ, ElbB, GlgB, GloA, Gor-1, GsT, Ppa1, RfbB-2, RfbC-1, SodB, PSPTO_0145, PSPTO_0155, PSPTO_1337, PSPTO_1465, PSPTO_1559, PSPTO_1881, PSPTO_1882, PSPTO_2065, PSPTO_2289, PSPTO_2492, PSPTO_2805, PSPTO_3039, PSPTO_ 3362, PSPTO_3460, PSPTO_3570, PSPTO_3708, PSPTO_3883, PSPTO_3919, PSPTO_3955, PSPTO_4992, PSPTO_5286, PSPTO_5293
Genetic regulation	Sensory proteins		
	Transcriptional regulators	MucB, PyrR, PSPTO_1679	AlgB, CapB, DksA, Hfq, PilH, PSPTO_0066, PSPTO_1274, PSPTO_1433, PSPTO_2376, PSPTO_3980, PSPTO_4427
Lipid metabolism	Lipid biosynthesis and degradation	FabG, IspB, PlcA2, PSPTO_1766, PSPTO_1916, PSPTO_2268	AccA, AccB, FabA, FabB, FabD, FabF, LipA, PSPTO_3857

Table RI.2. *Cont.*

Nitrogen metabolism	Amino acid metabolism	AstE, HisG, MtnC, ThrB, TrpC, TrpD, PSPTO_3506	AhcY, ArgE-2, ArgH, AroQ, BetA, CarB, GabD-3, GltB, GlyA2, IlvA-1, IlvN, LeuA, MetC-1, MetF, MetH, MtnA, ProA, SoxA-1, ThrC, TrpA, PSPTO_0092, PSPTO_0517, PSPTO_1531, PSPTO_1921, PSPTO_3757, PSPTO_5171, PSPTO_5308
	Nitrogen assimilation		CynS, PSPTO_1440, PSPTO_2302
Nucleic acid metabolism	Transcription		GreA, NusG, Orn, RpoN
	Purin and pyrimidine metabolism	CysQ, GuaD, PyrF, PSPTO_2373	Amn, Cdd, Dcd, GuaA, PurA, PurC, PurE, PurF, PurT, PyrC, PSPTO_1909, PSPTO_2331, PSPTO_3665, PSPTO_4973
	Replication/ Recombination		DnaE, ParE, TopA
	Others	HupB	Ssb, SbcC, UvrA, PSPTO_0072, PSPTO_0102, PSPTO_1266, PSPTO_2779, PSPTO_4778
Protein synthesis and modification	Chaperones	HscA	NfuA, GroES, PpiB, PSPTO_0808, PSPTO_1171, PSPTO_4581
	Proteases	Map-2, Prc, PSPTO_0425, PSPTO_3193, PSPTO_3332, PSPTO_3958, PSPTO_5329	ClpA, ClpP, PepN, PSPTO_3437, PSPTO_3911
	Translation	**RpsH**, SelD, YchF, PSPTO_3192	CysS, Der/PSPTO_1438, Frr, InfA, PrfC, **RplD**, RplQ, RplV, RplW, RpmA, RpmE2, RpmF, RpmG, RpmI, RpsF, RpsM, RpsN, RpsQ, RpsR, RpsS, RsfS, HisS, **ThrS**, TyrS, PSPTO_1205
	Modifications		SixA, PSPTO_0412
Transport	Transporters/Secretion systems	DctP, FecB, PtsN, RbsB-2, TliF, TolB, XylF, ZnuA, PSPTO_0364, PSPTO_0791, PSPTO_0889, PSPTO_1054, PSPTO_1076, PSPTO_1159, PSPTO_1255, PSPTO_1600, PSPTO_2141, PSPTO_2667, PSPTO_2775, PSPTO_2785, PSPTO_2788, PSPTO_3049, PSPTO_3058, PSPTO_3256, PSPTO_3335, PSPTO_3490, PSPTO_5245, PSPTO_5306, PSPTO_5316	CstA, Ffh, PtsP, PvdE, SaxB/PSPTO_4304, YidC, PSPTO_0138, PSPTO_2604, PSPTO_2705, PSPTO_4303, PSPTO_5500
Virulence	Virulence factors	Cfa2, Cfl, HopAB2, HopAK1, HopC1, HopD1, HopE1, HopG1, HopI1, HrpK1, PSPTO_5414	Hcp-2, HrpA1, PSPTO_4010, PSPTO_5421, PSPTO_5433

PSPTO_0653 and PSPTO_3983 were putative bacterioferritins, and TerB and TerD are involved in tellurite resistance. IA proteins of this class were the copper resistance proteins CopA and CopB, and PanE-1 and CobC involved in panthotenate and cobalamin metabolism, respectively. It was also noticeable that CobC displayed IA in the extracellular media but was listed as RA in the intrasome (Table RI.1).

Interestingly, certain central metabolic enzymes also exhibited DA in the extracellular media. Several carbon metabolism enzymes (Gcd, Glk, GltA, GpmI, LpdA, Pgm, Rpe) were found with RA, but three displayed IA. One of them, the malate synthase GlcB2 has been described as a moonlighting protein with adhesin functions in *Mycobacterium tuberculosis* (Kinhikar *et al*., 2006).

Among lipid metabolism enzymes, a comparable number of IA and were identified. With IA were FabG, IspB, PlcA2, PSPTO_1916 and the hydrolases PSPTO_1766 and PSPTO_2268. With RA were the acetyl-CoA carboxylase subunits AccA and AccB, the fatty acid biosynthesis proteins FabA, FabB, FabD, FabF, and the putative lipoyl synthase LipA.

A significantly smaller group of regulatory proteins appeared DA compared to the intracellular medium. Still, the majority were RA DNA-binding regulators, including three cold shock proteins (CapB, PSPTO_1274 and PSPTO_2376), two response regulators of two-component systems (AlgB and PilH), the LysR-family regulator OxyR/PSPTO_0066, the AraC family PSPTO_4427, the morphogenic protein RodZ (PSPTO_1433), or the putative regulator of unknown function PSPTO_3980 (Table RI.2). IA proteins includeed the OmpR family regulator PhoB/PSPTO_1679, the pyrimidine operon regulatory protein PyrR, and the anti-anti-sigma factor MucB, which controls AlgU availability (Li *et al*., 2019).

Proteins involved in virulence showed a majority of IA proteins, exhibiting a different trend compared to the intrasome. In this case, besides two coronafacic synthetases Cfa2 and Cfl, the IA proteins were mainly type III effectors, such as HopAB2, HopAK1, HopC1, HopD1, HopE1, HopG1, HopI1, and the helper protein HrpK1. In contrast, HrpA1/PSPTO_1381, the major component of the T3SS-associated pilus, displayed RA, like did two proteins components of the T6SS external filament, Hcp-2 and PSPTO_5433/TssB2 (Table RI.2), despite Hcp-2 or PSPTO_5421/TssJ2 being found IA intracellularly (Table RI.1). Also, RA was the protein PSPTO_4010, a putative bacteriophage protein which displays some homology to the YdaS toxin (IPR031856), and also contains a putative peptidase S24 domain (IPR015927).

Expression of c-di-GMP differentially exported protein-coding genes

Given the unavailability of protein-specific antibodies for many proteins, gene expression analyses were undertaken on select genes encoding proteins identified with DA in the aforementioned proteomic studies. These analyses aimed to provide indirect evidence either supporting or refuting the findings of the proteomic data. Additionally, specific genes were chosen for this qPCR analysis due to their inclusion in large operons and/or the availability of oligonucleotide primers for these genes in the laboratory. For instance, the *wssB* gene was selected as a representative of the cellulose synthase operon. Notably, *wssB* exhibited a significant 21.3-fold increase in expression in the high c-di-GMP strain compared to the wild type (Table RI.3). This rise in gene expression corresponded with the substantial increase of various proteins encoded in the *wss* operon (WssA, WssD, WssE, WssF, WssG), as observed both intracellularly and extracellularly. Indeed, it is well documented that the *wss* operon and cellulose biosynthesis are activated by c-di-GMP in Pto DC3000 (Pérez-Mendoza *et al*., 2014; Prada-Ramírez *et al*., 2016; Pérez-Mendoza *et al*., 2019; Martínez-Rodríguez *et al*., 2023). Similarly, the *algD* gene representative of the alginate operon, displayed increased expression in the c-di-GMP strain. This observation correlated with the IA of proteins AlgE and AlgL, particularly in the extrasome (Table RI.3), and with the reported increase in alginate production under those conditions (Pérez-Mendoza *et al*., 2014).

For other genes, the relationship between gene expression and protein content was not clearly established. In the case of *fliC* and *flgF*, which encode flagellar components, gene expression exhibited a notable decrease with high c-di-GMP levels (Table RI.3), which did not correlate with the non-significant DA observed in the intrasome, neither with its extracellular IA. The unchanged levels of FliC in the cytoplasm were corroborated *via* specific immunoblots, however this method did not corroborate the IA observed for FliC in the extrasome (Fig. RI.4). The IA of these flagellar proteins in the culture medium of the c-di-GMP strain may indicate their release following flagella disintegration.

In the case of the gene encoding the T3SS effector HopAB2, its expression exhibited a slightly increase in the c-di-GMP strain (less than 2-fold), and its intracellular contents remained unchanged; however, it displayed IA extracellularly. In this scenario, it could be argued that HopAB2 synthesis is not significantly enhanced by c-di-GMP, but its secretion is. This observation could also account for the abundance of protein effectors, including HopAB2 and several others, detected with IA in the culture medium of the c-di-GMP strain (Table RI.2). On the contrary, structural components of the T3SS (HrpA1) and T6SS (Hcp-2 and PSPTO_5433) machineries displayed RA extracellularly, albeit Hcp-2 displayed IA intracellularly (Table RI.3).

The transcription of other genes such as *glyA2*, *rpoN* or *mexA* were slightly increased in the c-di-GMP strain, which did not correlate with protein changes observed in the intracellular and extracellular proteomes (Table RI.3).

Table RI.3. Gene expression analysis compared to differentially abundant proteins in the intracellular and extracellular proteome of Pto DC3000 under high c-di-GMP levels. Arrows indicate whether there is increased or decreased abundance of the protein or gene expression levels in the high c-di-GMP strain compared to the physiological level strain. For qRT-PCR gene expression analysis the fold-number variation is indicated next to the arrows.

Proteomics			qRT-PCR	
Protein	**Intracellular**	**Extracellular**	**Gene**	**Differential expression**
WssD WssG	↑ ↑	↑ ↑	*wssB*	↑ ×21.3
AlgE AlgL	- -	↑ ↑	*algD*	↑ ×2.58
FliC FlgF	- -	↑ ↑	*fliC* *flgF*	↓ ×71.9 ↓ ×12.6
HopAB2	-	↑	*hopAB2*	↑ ×1.9
GlyA2	-	↓	*glyA2*	↑ ×1.7
RpoN	-	↓	*rpoN*	↑ ×2.4
SaxA SaxB	↓ ↑	↓ ↓	*mexA* *mexB*	↑ ×2.4 ↑ ×1.3

Comparison of *P. syringae* and *R. etli* c-di-GMP dependent extracellular proteomes

This research into the differential abundance of proteins in the extracellular proteome of Pto under high c-di-GMP conditions follows a similar one previously performed in *R. etli* (Lorite *et al*., 2023). Overall, the total amount of extracellular proteins displaying DA was comparable in both cases, 318 in *R. etli* versus 396 in Pto. However, contrasting behaviours were observed under high c-di-GMP levels between the two bacteria. Specifically, the c-di-GMP dependent extrasome of *R. etli* exhibited much more IA (199, 63%) than RA proteins (119, 37%), whereas the opposite trend was encountered in Pto, with more proteins showing RA (257, 65%) than IA (139, 35%) (Fig. RI.3; Table RI.2).

Comparison of the predicted subcellular localization of proteins also revealed similarities and differences between the extracellular proteomes of Pto and Ret. In both cases, cytoplasmic proteins constituted the larger group of DA proteins, albeit with inverse trends: most cytoplasmic proteins were IA in the Ret extrasome, whereas the majority of cytoplasmic proteins displayed RA in the Pto extrasome. This contrasting trend was also noticeable for other subcellular classifications, especially periplasmic proteins. However, in both extrasomes, extracellular proteins predominantly exhibited IA (compare Fig. RI.1 in this chapter and Fig. 1 of Lorite *et al*. 2023).

In terms of functional analysis, both bacteria exhibited more differences than similarities in the IA of proteins classified in the extracellular function and structural group. However, notable similarities were observed particularly concerning flagellins and other components of the most external parts of the flagellum. In both cases, these proteins displayed high IA in the culture supernatants of the c-di-GMP strains (see Table RI.2 and Table 1 in Lorite *et al*., 2023). Interestingly, the increased presence of flagella components in the extracellular medium contrasts with the demonstrated inhibitory effects that c-di-GMP has on the motility of these two bacteria (Pérez-Mendoza *et al*., 2014). Regarding other functional groups, proteins involved in polysaccharide biosynthesis were found in both cases, although for unrelated molecules. For instance, only the Pto extrasomes presented cellulose synthase components, despite both bacterial species being able to produce c-di-GMP-dependent cellulose. Other exopolysaccharides are species or strain-specific. A striking difference was that several known or hypothetical adhesin proteins appeared DA in the Ret extrasome under high c-di-GMP (e.g., several Raps, *Rhizobium* adhesion proteins), however only one hypothetical adhesin-like (PSPTO_2874) was found for Pto. This is intriguing, since c-di-GMP is known to regulate synthesis and secretion of extracellular adhesion factorscrucial for biofilm formation in most bacteria (Cotter & Stibitz, 2007; Yan *et al*., 2010; Newell *et al*., 2011).

The rest of the functional comparisons revealed differences between Pto and Ret, often with inverted tendencies. For example, transport constituted the main RA group in Ret, whereas in Pto included predominantly IA proteins. Frequently, the opposite trend was observed for exactly the same proteins, like TolB, XylF and ZnuA, which appeared in both exoproteomes. Despite the different trends, it was coincident that most DA proteins belonging to ABC transporters were periplasmic components in both cases. The inverted trend was also observed for ribosomal proteins, which were a significant group of IA proteins in Ret but RA in Pto.

In terms of carbon, nitrogen and lipid metabolism inverted tendencies were also observed, with a high number of metabolic enzymes present with IA in the Ret extrasome but RA in Pto. It is worth noting that many of these IA proteins from Ret had been previously reported as moonlighting proteins. However, this does not seem to be the case for Pto, where a small number of DA moonlighting proteins were detected.

Export of cytoplasmic proteins EF-Tu, Gap1 and Gap2

No significant differential abundance was observed for the Gap1, Gap2 and EF-Tu proteins between the strains with high and physiological c-di-GMP levels in Pto (Fig. SI.3). This contrasts with previous findings in *R. etli*, where the exportation of Gap and EF-Tu was increased under elevated c-di-GMP levels (Lorite *et al*., 2023). Curiously, although not showing DA, Gap1 was detected at significant levels in the extracellular milieu of Pto, unlike Gap2 and EF-Tu, which were barely detected (Fig. SI.3).

Given the continued interest in these proteins based on their behaviour in *R. etli* and the exportation of Gap1 in Pto, immunodetection experiments were conducted using intracellular and extracellular protein samples obtained from cultures grown on two different minimal media: MM with mannitol and pyruvate as carbon sources (the same MM used for proteomic analysis), and M9 with succinate as a carbon source. Consistent with the proteomic results, Gap1 was detected in the culture supernatants with both media, and no discernible difference was appreciated between the wild type and the c-di-GMP strains (Fig. RI.4). Conversely, Gap2 was detected in the culture supernatants of the cells grown in M9 medium with succinate as a carbon source, whereas it remained undetected in minimal media with pyruvate and mannitol. However, no difference was observed in either of the two media tested both under physiological and high c-di-GMP intracellular levels. Furthermore, EF-Tu exhibited a similar pattern, being clearly detected in the supernatant of M9 media, but barely detectable in MM with mannitol and pyruvate as carbon sources (Fig. RI.4). However, it is worth mentioning that initial studies found that exportation of protein EF-Tu to the extracellular compartment was promoted by c-di-GMP in Pto, albeit it was in a growth medium different from the one used here (M.J. Lorite and J. Sanjuán, personal communication).

DISCUSSION

Exported proteins are an important part of the biofilm matrix, and their production and secretion, similar to exopolysaccharides, can be directly or indirectly regulated by c-di-GMP (Cooley *et al*., 2015). The primary aim of this study was to explore the alterations triggered by elevated c-di-GMP levels in both the intracellular and extracellular proteomes of the plant pathogen Pto DC3000 in order to gain new insights into regulatory mechanisms orchestrated by c-di-GMP.

The Pto DC3000 genome encompasses approximately 5600 protein-coding genes. However, only 2251 proteins (around 40%) were identified in the intracellular proteomic analysis. Among these proteins, 784 (35%) displayed significant DA. In the culture supernatants, 1316 proteins were identified, accounting for 23% of the total protein-coding genes in the genome. This proportion mirrors the percentage observed in *R. etli*, which

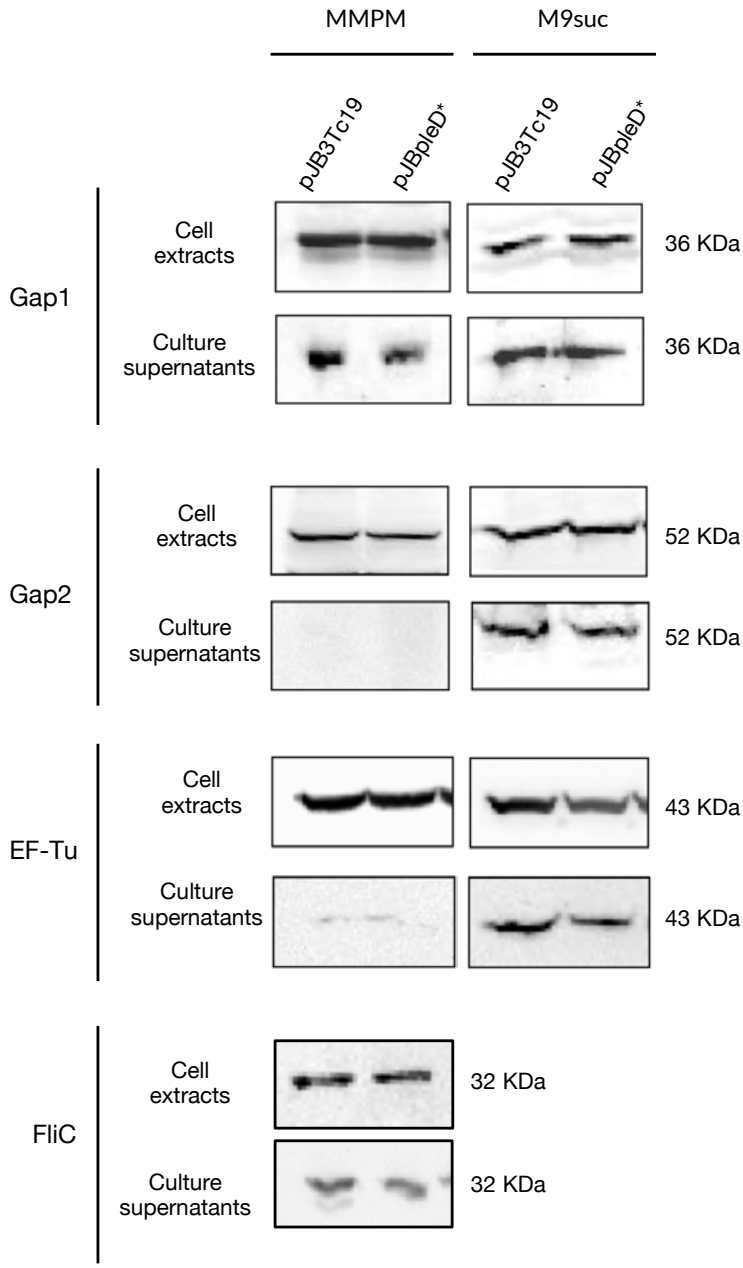

Figure RI.4. Immunodetection of Gap1, Gap2 and EF-Tu proteins.
Pto Δ*wssBC* strains under physiological (pJB3Tc19) and high c-di-GMP conditions (pJB3pleD*) were grown in M9 suc (with succinate as carbon source) and MMPM (T3SS-inducing with pyruvate and mannitol as carbon sources) media. Total protein from cell extracts and supernatants of cultures was analysed. Ten µg of total protein (cell extracts) or 20 µg of total protein (culture supernatants) were loaded into each lane.

was around 27% (Lorite *et al*., 2023). Among the 1316 proteins in the extracellular milieu, 396 (30%) displayed significant DA, a percentage that doubles the 15% of DA proteins observed in *R. etli* despite the total amount being similar (Lorite *et al*., 2023).

The identification of proteins involved in polysaccharide and cellulose biosynthesis among the IA proteins under high c-di-GMP levels, both intra- and extracellularly, corroborates previous results and reinforces the established involvement of c-di-GMP in processes like biofilm formation and exopolysaccharide production (Pérez-Mendoza *et al*., 2014; Morgan *et al*., 2014; Whitney *et al*., 2015; Liang *et al*., 2022). Nonetheless, the finding of certain proteins with RA underscores the complexity of c-di-GMP regulation in biofilm formation.

The utilization of a T3SS-inducing minimal media facilitated the assessment of potential virulence traits linked to c-di-GMP regulation. Previous studies on the Pto extracellular proteome (Schumacher *et al*., 2014), also conducted in T3SS-inducing minimal medium but with fructose as carbon source, identified proteins linked to the T3SS (HrpA1, HrpZ1, HrpW1, HopP1, HrpK1) and T6SS (Hcp2) as the most abundant in the extracellular fraction. Our results revealed that under high c-di-GMP, virulence constitutes one of the extracellular functional groups with predominantly IA proteins. These proteins primarily comprise type III effectors, such as HopAK1, HopC1, HopD1, HopE1, HopG1, HopI1 and HrpK1, along with the coronafacic acid synthetases Cfl and Cfa2 needed for the synthesis of the toxin coronatine. However, an important number of coronafacic acid related proteins appeared with RA intracellularly. From these results, it is intriguing that, while c-di-GMP enhances the export of certain type III effectors involved in virulence, Pto strains overexpressing *pleD** showed no alterations in virulence (Pérez-Mendoza *et al*., 2014). The contrasting behaviours of virulence factors intra- and extracellularly, together with the complex coordination required, may explain the lack of either an increase or decrease in the bacteria's virulence *in planta*.

The c-di-GMP dependent intracellular proteome of Pto diverged significantly from the extracellular proteome. Only some proteins exhibited DA in both proteomes, likely reflecting the multifaceted actions of c-di-GMP, regulating protein abundance intracellularly, as well as influencing protein secretion through multiple mechanisms, including transcriptional and posttranscriptional processes. For instance, numerous flagellar and chemotaxis proteins were DA in both proteomes, often showing IA in the extrasome and RA in the intrasome. This could be attributed to two different events: downregulation of flagellar genes by c-di-GMP, coupled with the simultaneous disassembly of external flagellar components. It was intriguing, however, the behaviour of the FlgH protein, which appeared IA in the intrasome but RA extracellularly. A similar trend was observed for the T6SS effector Hcp-2, which exhibited IA in the intrasome and RA in the extrasome.

The majority of DA proteins in both intra- and exoproteomes were found to be cytoplasmic. However, only a small subset of these proteins appeared DA in both compartments. This observation again suggests that c-di-GMP may be involved in regulating the secretion of certain proteins, regardless of the intracellular mechanisms that modulate gene expression and protein abundance.

As an important part of this study aimed at exploring potential moonlighting proteins, we directed our attention to the behaviour of Gap1 and Gap2, given their documented exportation in other bacterial species (Giménez *et al*., 2014). However, there was no significant DA dependent on c-di-GMP for these proteins in Pto, contrasting with the promoted export of Gap by c-di-GMP observed in *R. etli* (Lorite *et al*., 2023). Elkhalfi *et al.* (2014) had reported the presence of Gap1 in the extracellular media of Pto grown in rich media with glucose and in presence of tomato plant leaflets. Our findings align with this, as we detected Gap1 extracellularly in different media independently of c-di-GMP levels. Interestingly, we also identified Gap2 in the extracellular media, albeit only with certain media composition, specifically with succinate as carbon source. The absence of Gap2 detection extracellularly in T3SS inducing media suggests that its export may not be reliant on the T3SS but on other mechanisms potentially regulated by environmental compound availability. A similar pattern was observed for EF-Tu, with a more pronounced export observed in M9 with succinate as carbon source. However, EF-Tu was abundantly detected in T3SS-inducing media supplemented with fructose as carbon source in the study carried out by Schumacher *et al.* (2014). The primary difference in the media compositions between our study and theirs lies in the carbon sources used (mannitol and pyruvate in our study *versus* fructose in theirs), suggesting that EF-Tu exportation may be modulated by the specific carbon sources present in the media.

In addition to Gap1 and Gap2, Pto also possesses a third putative Gap protein known as Gap3/Epd. This enzyme exhibits a high similarity with Gap enzymes and is classified as a putative bifunctional enzyme for erythrose phosphate dehydrogenase and GAPDH activity (Elkhalfi *et al*., 2013). Interestingly, Gap3/Epd exhibited significant DA in the extracellular media, being detected with RA under high c-di-GMP conditions, therefore positioning it as a compelling candidate as moonlighting protein (Table RI.2). Another potential moonlighting protein detected with IA in the extrasome was the malate synthase GlcB2 (Table RI.2). This enzyme has been described as a laminin-binding adhesin that serves as a virulence-promoting factor in *Mycobacterium tuberculosis* (Kinhikar *et al*., 2006). Furthermore, other possible moonlighting proteins displaying DA were the translational and ribosomal proteins RpsH (IA), ThrS and RplD (RA). They have been implicated in translational regulation in *E. coli* (Yates *et al*., 1980; Springer *et al*., 1985; Zengel & Lindahl, 1996).

Another aim of this study was to compare the responses to elevated c-di-GMP between Pto and a very different plant-interacting bacteria, *R. etli*. Despite their considerable taxonomic distance, substantial genetic disparities, and the contrasting lifestyles, common responses of Ret and Pto extracellular proteomes to elevated intracellular c-di-GMP were observed. For instance, in both studies the great majority of DA extracellular proteins were predicted to have a cytoplasmic localization. Moreover, despite their contrasting trends, additional similarities were drawn at functional level between both c-di-GMP-modulated exoproteomes. Transport, C and N metabolism, and protein synthesis/modification were four of the most represented functional categories among the c-di-GMP regulated extracellular proteins in both cases. This further emphasizes that in these two bacterial species, c-di-GMP modulates (either promoting or reducing) the secretion (by unknown mechanisms) of numerous intracellular housekeeping proteins to the cell exterior.

More precisely, both bacteria exhibited IA of proteins involved in the production of compounds crucial for biofilm formation, like polysaccharides. Additionally, a similar pattern was observed in the behaviour of flagellar proteins. Regardless of the well-documented reduction in bacterial motility under high c-di-GMP (Pérez-Mendoza *et al*., 2014), flagellar proteins were found with IA in the extracellular media. This contrasts with the significant decrease in gene expression observed for *fliC* and *flgF* under high c-di-GMP levels, as well as the intracellular DA of flagellar proteins part of the motor complex. This discrepancy suggests that the IA found in the extracellular media could be due to their disintegration or release from the cell surface. Notably, FlgH was the only flagellar protein found to be downregulated in the extracellular media. Its presence within a membrane lipid bilayer as part of the L-ring, in contrast to the IA status of FlgE-1, FlgF, FlgG, FlgK, FlgL, and FliC, which are located outside the cell or in the intermembrane space, supports the hypothesis of disintegration or release from the cell surface. Furthermore, this observed behaviour aligns with the phenotypes observed, namely the inhibition of motility and increased biofilm formation, which are the primary features identified in c-di-GMP regulation.

Nevertheless, beyond these shared aspects, the remaining DA proteins exhibited notable differences between the two bacteria, with fewer exported proteins potentially functioning as moonlighting proteins in the case of Pto. Additionally, it is worth noting that the minimal media compositions differed between the two bacteria, since Pto was grown in T3SS-inducing MM whereas *R. etli* strains were grown in MMY containing succinate and ammonium chloride as C and N sources, respectively (Lorite *et al*., 2023). Overall, the discrepancies reveal a distinct fine-tuning of the c-di-GMP system and its regulation between the two bacteria, which makes sense given their

opposed modes of interaction with plants. While *R. etli* establishes a symbiotic interaction beneficial for both partners, Pto poses harm to its host plant. As a result, high levels of c-di-GMP elicit varied effects in terms of protein regulation and exportation in these divergent plant-bacteria systems.

SUPPORTING INFORMATION

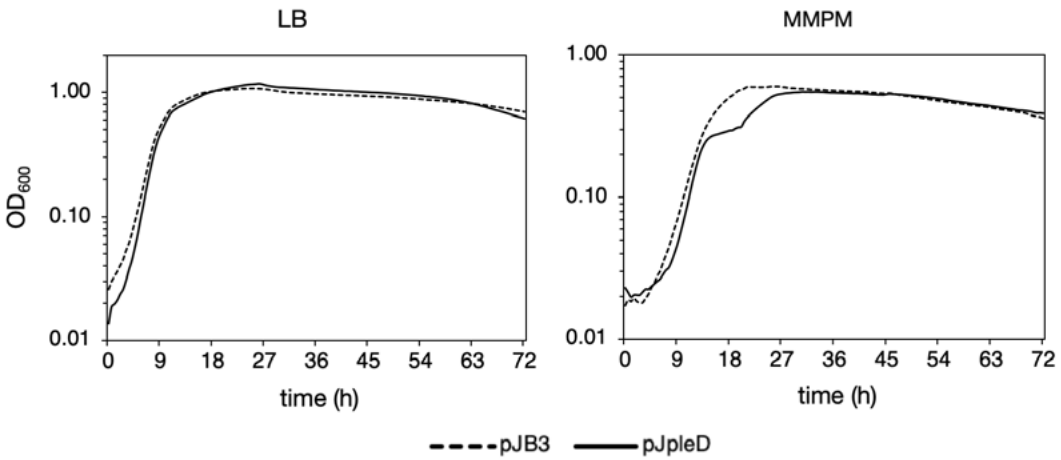

Figure SI.1. Growth curves comparing Pto strains with physiological and high levels of c-di-GMP. Bacteria were grown for 72h at 20°C in rich media and T3SS-inducing minimal media with pyruvate and mannitol as carbon sources with continuous shaking measuring the absorbance at 600 nm every hour in a Bioscreen C system.

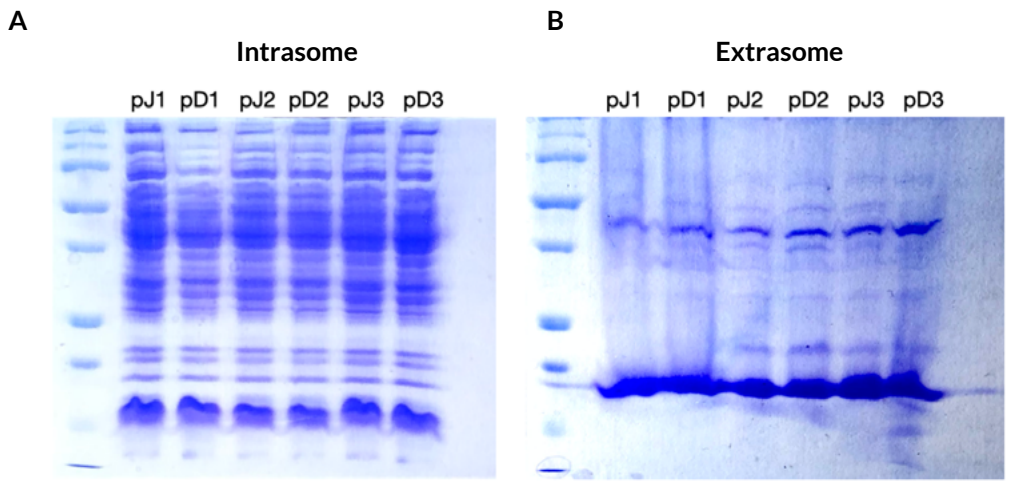

Figure SI.2. SDS-PAGE gel electrophoresis with Coomassie staining of the protein analysed samples.
Samples of three different cell extracts (A. Intrasome) and culture supernatants (B. Extrasome) of Pto strains grown in T3SS-inducing minimal media with physiological c-di-GMP levels (pJB3Tc19, pJ) and high c-di-GMP levels (pJB3pleD*, pD). Ten µg of total protein were loaded into each lane for cell extracts, and 20 µg of total protein were loaded into each lane for culture supernatants.

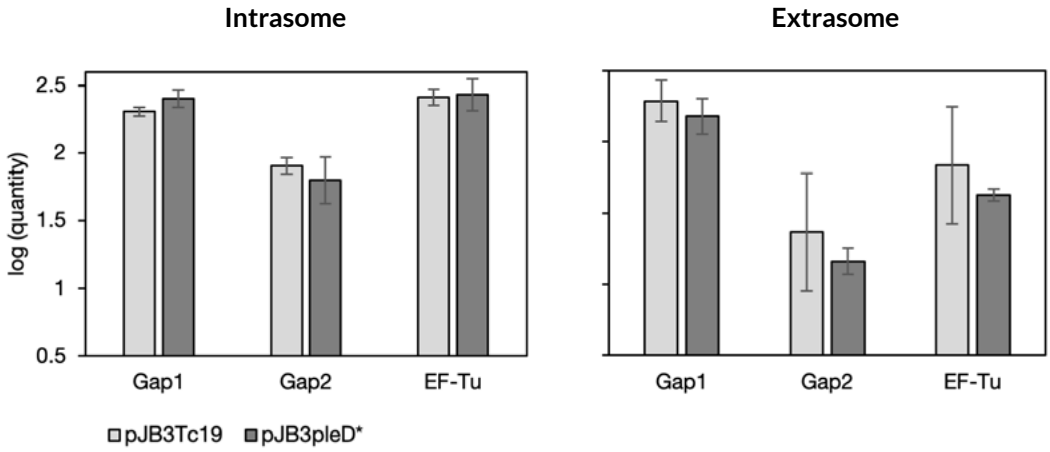

Figure SI.3. Quantification of Gap1, Gap2, and EF-Tu protein levels in both intracellular and culture supernatant samples.
Samples of cell extracts and culture supernatants of Pto strains with physiological c-di-GMP levels (pJB3Tc19) and high c-di-GMP levels (pJB3pleD*) grown in T3SS-inducing minimal media.

Table SI.1. Oligonucleotides used in qRT-PCR.

Gene	Gene ID	Sequence (5' to 3')	Product (bp)
algC	PSPTO_0083	CGAAAGCCTGGCGCAGAACGAACCCA	124
		GACGTCGCTGACATGGCAACCGCTGT	
wssB	PSPTO_1027	GGTGTTCAACGCTGTGACGCAGGA	198
		TGGCGCAGTGAAAGATCATCGAAACG	
algD	PSPTO_1243	CGCTGCTCAATTCCGACTTCGATCAGG	159
		CGTCTTCGGTGGTGGCATTGGTCA	
gyrA	PSPTO_1745	GGCAAGGTCACCCGCTTCAAGGAAT	205
		GACCGCCACGCTTGTACTCAGGGAAC	
flgF	PSPTO_1939	TCGACCAATGGCTTCATGCGTGACCTT	194
		TCGGGAGTCTGCACGGCAATCCAG	
fliC	PSPTO_1949	AAGGCGCACTGCAAGAGTCGACCAAC	197
		GGTGCTGGCGGAACCGTCAAGC	
hopAB2	PSPTO_3087	GTTCAGCCGCGACCCTCGAATACTCC	126
		CATACCCTGCTCCAGCCACTCCCTG	
mexA	PSPTO_4303	CAGGACGACCGCTTTCCGTGTGG	155
		CCTTGGCACTGTTGGCGTTGGCTTC	
mexB	PSPTO_4304	CTGTTGGGCACCTTCGGCATCCTC	107
		ACAATCGCATCGTCCACCAGCAAGC	
rpoN	PSPTO_4453	CAGCGCCGACAACACCTTCATGC	168
		TGCAGGACGAGCGGCTTCATGG	
glyA2	PSPTO_4632	AGAAGAAGCTCAACTCCGCCGTATTCCCT	204
		GGTTTTCAGTACCGCCGGACACCACGT	

CHAPTER II

Two glyceraldehyde-3-phosphate dehydrogenases with distinctive roles in *Pseudomonas syringae* pv. tomato DC3000

CHAPTER II

Keywords:
Glyceraldehyde-3-phosphate dehydrogenase (GAPDH)
Erythrose-4-phosphate dehydrogenase (EPD)
Pseudomonas syringae
Moonlighting proteins
Vitamin B6

Two glyceraldehyde-3-phosphate dehydrogenases with distinctive roles in *Pseudomonas syringae* pv. tomato DC3000

Published in Microbiological Research 278 (2024) 127530.
https://doi.org/10.1016/j.micres.2023.127530
Ariana Casas-Román, María-José Lorite, Juan Sanjuán and María-Trinidad Gallegos
Department of Soil and Plant Microbiology, Estación Experimental del Zaidín (EEZ-CSIC), Granada, Spain.

ABSTRACT

Glyceraldehyde-3-phosphate dehydrogenase (GAPDH or Gap) is a ubiquitously distributed enzyme that plays an essential role in the glycolytic and gluconeogenic pathways. However, additional roles have been described unrelated to its enzymatic function in diverse organisms, often linked to its presence in the cell surface or as a secreted protein. Despite being a paradigm among multifunctional/moonlighting proteins, little is known about its possible roles in phytopathogenic bacteria. In the present work we have studied three putative gap paralogous genes identified in the genome of *Pseudomonas syringae* pv. tomato (Pto) DC3000, an important model in molecular plant pathology, with the aim of determining their physiological and possible non-canonical roles in this bacterium and in the plant infection process. We have established that the Gap1 protein has a predominantly glycolytic activity, whereas the NADPH-dependent Gap2 main activity is gluconeogenic. The third paralogue lacks GAPDH activity in Pto but is indispensable for vitamin B6 metabolism and displays erythrose-4-phosphate dehydrogenase activity, thus referred as *epd*. Both Gap enzymes exhibit distinct functional characteristics depending on the bacterium physiological state, with Gap1 presenting a substantial role in motility, biosurfactant production and biofilm formation. On the other hand, solely Gap2 appears to be essential for growth on tomato plant. Furthermore, Gap1 and Gap2 present a distinctive transcriptional regulation and both have been identified exported outside the cells with different definite media compositions. This serves as compelling evidence of additional roles beyond their central metabolic functions.

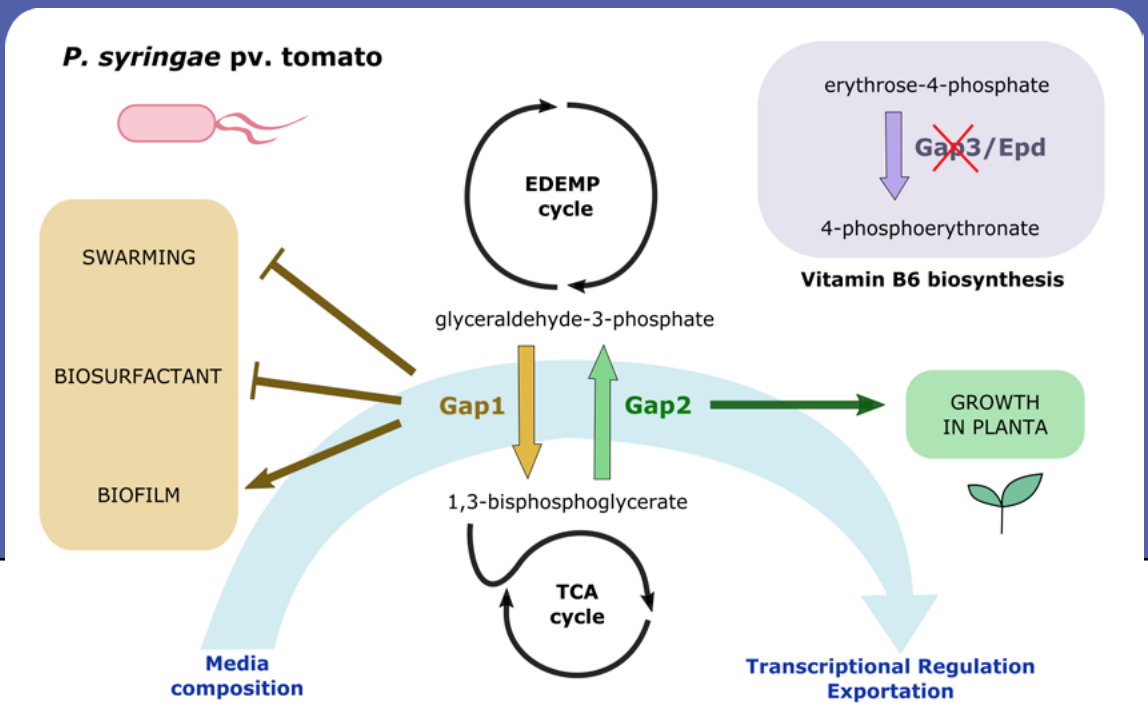

BACKGROUND

Glyceraldehyde-3-phosphate dehydrogenase (GAPDH or Gap) is an ancient and universally distributed enzyme involved in sugar metabolism with pivotal functions in the glycolytic and gluconeogenic pathways. It catalyses the oxidative phosphorylation of glyceraldehyde-3-phosphate (G3P) to 1,3-bisphosphoglycerate (BPG), with NAD^+ or $NADP^+$ acting as a cofactor. The reaction is fully reversible, so BPG becomes the substrate and NAD(P)H the cofactor in gluconeogenesis (Fothergill-Gilmore and Michels, 1993; Seidler, 2013). The GAPDH polypeptide has two main domains: the N-terminal for NAD+ binding, and the C-terminal catalytic domain, which contains a cysteine residue involved in forming a covalent phosphoglycerol thioester intermediate. It exists in the cytoplasm in a hometetrameric form, with four subunits of around 37 KDa each (Segal and Boyer, 1953; Sirover, 2014; Querol-García *et al*., 2017). GAPDH family members can be classified in the ubiquitous class I enzymes, which utilize NAD+ and/or NADP+, class II of archaeal NAD(P)-dependent GAPDHs, and class III bifunctional enzymes (erythrose-4-phosphate dehydrogenase (E4PDH or Epd)/GAPDH) that are predominant in γ-proteobacteria (Figge et al., 1999; Elkhalfi *et al*., 2013). Beyond its well-established

enzymatic functions in bacteria, fungi, mammals, and plants, GAPDH exhibits alternative roles, often dependent on its ability to change its subcellular localization (Giménez *et al*., 2014; Sirover, 2014; Yang and Zhai, 2017). Thus, it has been detected not only in its typical cytosolic position but also on the cell surface or as a secreted protein in various Gram-positive and Gram-negative bacteria. Nevertheless, the mechanism responsible for GAPDH translocation remains uncertain, as it lacks any known motif for extracytosolic trafficking (Kopeckova *et al*., 2020a). The identification of GAPDH on the cell surface has opened new avenues of research, revealing its ability to bind to numerous extracellular matrices, facilitating bacterial adhesion to tissues and contributing to biofilm formation. Additionally, it has been found to play a role in modulating host immune responses and virulence in human and animal pathogenic bacteria (Aguilera *et al*., 2012; Foulston *et al*., 2014; Giménez *et al*., 2014; Ebner *et al*., 2016; Kopeckova *et al*., 2020a). However, little is known about the potential roles of GAPDH in phytopathogenic bacteria.

Pseudomonas syringae pv. tomato (Pto) causes bacterial speck disease, an economically important disease on tomato and crucifers. This disease provokes a decline in the photosynthetic efficiency of infected foliage, defoliation, flower abortion, and fruit/leaves lesions that make them unsuitable for the fresh market (Lamichhane *et al*., 2015; Koike *et al*., 2017; Ahmed, 2022). Pto employs a multifaceted approach to ensure its virulence, possessing an extensive arsenal of effectors that are released through a type III secretion system (T3SS), accompanied by the production of the coronatine phytotoxin, which triggers stomatal opening facilitating its entry into the apoplast (Xin *et al*., 2018). Beyond these mechanisms, Pto is equipped with a range of additional tools that reinforce its pathogenic capabilities. In particular, it possesses flagella and biosurfactants, which facilitate its movement, or exopolysaccharides that protect from desiccation (Roine *et al*., 1997; Berti *et al*., 2007; Burch *et al*., 2010; Burch *et al*., 2012; Vargas *et al*., 2013; Nogales *et al*., 2015). Similarly to *P. putida* KT2440, the genome of Pto DC3000 encodes the enzymes of the Entner-Doudoroff (ED), the Embden-Meyerhof-Parnas (EMP), and the pentose phosphate (PP) pathways for glucose catabolism (Lessie and Phibbs Jr., 1984; del Castillo *et al*., 2007; del Castillo *et al*., 2008; Sudarsan *et al*., 2014; Nikel *et al*., 2015). However, it lacks the glycolytic enzyme 6-phosphofructo-1-kinase (Pfk) (Kohlstedt and Wittmann, 2019), which catalyses the ATP-dependent conversion of fructose-6-phosphate into fructose-1,6-biphosphate. Pseudomonads possess a cyclic metabolism known as the EDEMP cycle, which integrates activities of the EMP, ED, and PP pathways, as it has been evidenced in the case for *P. putida* KT2440 (Nikel *et al*., 2015). This metabolic framework redirects part of the triose phosphates, which would otherwise undergo further oxidation to acetyl-CoA and downwards, to be recycled back into hexose phosphates. Furthermore, the EDEMP cycle functions in both glycolytic

and gluconeogenic regimes, playing a crucial role in distributing carbon throughout the central metabolic pathways (Nikel *et al*., 2015; Kohlstedt and Wittmann, 2019; Wilkes *et al*., 2021).

The Pto DC3000 genome contains three putative gap alleles: *gap1*, *gap2* and *gap3/epd* (Fig. SII.1), which are commonly found in many *Pseudomonas* strains. Alignment of the three GAPDHs revealed a high degree of sequence conservation, particularly between Gap1 and Gap2, which are class I enzymes. In the Gap1 protein (36.26 KDa) the two GAPDH structural domains can be recognised, the N-terminal for NAD+ binding and the C-terminal for catalysis. It is encoded by the PSPT0_1287 gene, which is followed by genes encoding an extracytoplasmic function sigma factor and a putative cell surface signalling system (PSPTO_1286-1285-1284). *gap1* is divergently located to an operon that contains other genes involved in carbon metabolism: *edd* (6-phosphogluconate dehydratase) and *glk* (glucokinase) (Fig. SII.1A). The Gap2 protein (52.73 KDa) possesses an extra N-terminal unstructured region of 130 residues which makes it larger than the canonical GAPDHs. It would belong to the subset of ATP-insensitive class I GAPDHs, which have been proposed to take part in the gluconeogenic pathway (Elkhalfi *et al*., 2013). *gap2* orthologs are present in all Pseudomonas strains and some actinobacteria. The Pto DC3000 *gap2* gene (PSPTO_2102) is surrounded by genes encoding a transcription-repair coupling factor (*mfd*), a hypothetical protein (PSPTO_2103) and a major facilitator family transporter (PSPTO_2104) (Fig. SII.1B). The *gap3/epd* gene (PSPTO_0386) encodes a putative class III bifunctional enzyme of 38.32 kDa which is highly similar to eubacterial orthologs known for their dual substrate specificity, G3P and E4P (Fig. SII.1C). It is usually found as part of an operon that includes *tkt* (transketolase), *gap3/epd*, *pgk* (phosphoglycerate kinase) and fba (fructose-bisphosphate aldolase), which are also enzymes of the central carbon metabolism (Fig. SII.1C). The Epd catalyses the conversion of E4P to 4-phosphoerythronate (4-PE), the first step of the vitamin B6 or pyridoxal 5'-phosphate (PLP) biosynthesis pathway. Epd is required for PLP biosynthesis, making this enzyme essential when uptake of B6 vitamers from the environment is not possible (Richts *et al*., 2019; Nimma *et al*., 2023).

In Pto DC3000 protein secretion plays an important role in the interaction of the bacterium with the host plant, particularly through the T3SS which secretes proteins (effectors) that interact with the cell wall and plasma membrane, or directly translocates them into the cytoplasm of host cells. Those effectors allow bacteria to manipulate plant cell physiology and promote disease by facilitating multiplication and virulence in a susceptible host. However, specific secreted proteins are also involved in processes such as nutrient acquisition, stress responses or metabolic adaptation (Preston, 2000; Petnicki-Ocwieja *et al*., 2002; Filloux, 2011; Rico *et al*., 2011; Schumacher

et al., 2014). The prevalent proteins in the extracellular fraction of Pto DC3000 grown in T3SS-inducing medium were those directly related to T3SS mediated pathogenicity, the translation elongation factor Tu (EF-Tu), the coronafacic acid and coronafacic acid polyketide synthases, both required for the synthesis of the phytotoxin coronatine, some ribosomal proteins, and metabolic enzymes, in particular, the Gap1 isoform (Elkhalfi *et al*., 2014; Schumacher *et al*., 2014).

In the present work we have studied the proteins encoded by the three gap paralogous genes identified in the genome of Pto DC3000 with the aim of establishing their metabolic roles and, particularly, their possible moonlighting functions in the physiology of this bacterium. Exploring new roles of cytoplasmic moonlighting proteins in phytopathogenic bacteria can shed light into previously undiscovered factors and mechanisms involved in the infection process.

Interestingly both Gap1 and Gap2 proteins present distinct functional characteristics depending on the bacterium physiological state. Gap2 seems to be essential for tomato plant infection, whereas Gap1 seems to be dispensable. However, Gap1 plays a substantial role in motility, biosurfactant production, and biofilm formation. Moreover, both proteins exhibit differential expression patterns depending on the media composition and are exported under specific culture conditions, further supporting the hypothesis of their non-canonical roles. The third paralogue, Gap3/Epd lacks significant GAPDH activity but displays specific Epd activity and seems to be essential for PLP biosynthesis in Pto.

SPECIFIC MATERIALS AND METHODS

Bacterial strains and growth conditions

The bacterial strains and plasmids employed in this study can be found in Table M1 and Table M.2 in general Materials and Methods. *E. coli* and Pto DC3000 strains were routinely grown in Luria-Bertani broth (LB) (Sambrook *et al*., 1989) at 37ºC and 20ºC or 28ºC, respectively. Different minimal media were used for Pto DC3000 and derivative strains: M9 (Sambrook *et al*., 1989); the T3SS-inducing minimal medium with modified carbon source MMPM (Huynh *et al*., 1989); and MMR (Robertsen *et al*., 1981). Antibiotics were added when required: rifampicin (10 µg/ml), kanamycin (50 µg/ml), tetracycline (10 µg/ml), or ampicillin (100 µg/ml). All the assays with strains harbouring pJB3Tc19 or its derivative plasmids were carried out in media supplemented with tetracycline to prevent plasmid loss.

Strain and plasmid construction

Δgap mutants were constructed by deleting the genes of interest, PSPTO_1287 (*gap1*), PSPTO_2102 (*gap2*) and PSPTO_0386 (*gap3/edp*). First, the regions bearing the adjacent sequences but lacking the gene in question were amplified by PCR using specific oligonucleotides (Table S1) and subsequently cloned into the suicide pK18*mobsacB* vector, which does not replicate in Pto. The pK18ΔG1 plasmid was constructed by cloning in pK18*mobsacB* a 1239 bp chromosomic sequence from Pto DC3000 with a deletion from nucleotide 10 to 995 of the *gap1* ORF. The pK18ΔG2 plasmid bears a 1175 bp chromosome fragment with a deletion from nucleotide 10 to 1440 of the *gap2* gene. The pK18ΔG3/epd plasmid contains a 1125 bp chromosomal region with a deletion from nucleotide 5 to 1024 in the *gap3/epd* gene. The pK18*mobsacB* derivative plasmids (Km^R $sucrose^S$) were directly electroporated into Pto DC3000, and transformants were selected in kanamycin (50 μg/ml). They were then grown in liquid rich media cultures in the absence of kanamycin to force plasmid loss. Cells were plated on rich medium with sucrose (15% w/v) and the $sucrose^R$ Km^S colonies, potential double-recombinants, were selected and checked by PCR and sequencing. Three mutants were obtained: ΔG1, ΔG2, and Δepd. A double ΔG1/G2 mutant was obtained after introducing the pK18ΔG1 construction into the ΔG2 mutant.

Expression plasmids derived from the pJB3Tc19 bearing the wild type genes were constructed for *in trans* complementation plasmid (Tables M.2 and SII.1). pJG1, pJG2 and pJepd contain *gap1*, *gap2* and *gap3/epd* genes, respectively. For gene expression analysis, two plasmids with transcriptional fusions bearing the *gap1* and *gap2* promoters were contructed using pME6016 (Table M.2).

The introduction of plasmids into Pto DC3000 strains was achieved through electroporation. Transformants were selected by cultivating them on LB agar plates supplemented with the suitable antibiotics.

Western blots

For Western blots (WB), protein samples (20-40 μg) were loaded onto 10% SDS-PAGE gels and electrophoresis and transfer were performed following standard procedures described in General Materials and Methods.

Rabbit polyclonal anti-Pto Gap1 and anti-Pto Gap2 antibodies were obtained (Davids Biothecnologie GMBH, Germany) against synthetic peptides (DLGDSEM–NAHLLRFDTVHG and KAHRFARHRQSDAVELSVHE) derived from the Pto DC3000 Gap1 (PSPTO_1287) and Gap2 (PSPTO_2102) primary sequences, respectively. These anti-Gap antibodies were diluted to a working concentration of 2.5 μg/ml.

Additional methods used in this chapter are previously described in the General Materials and Methods section:

- Growth assays
- Motility and biosrufactant production assays
- Biofilm formation assays
- Tomato plant infection assays
- β-galactosidase assays
- Protein isolation by lyophiization and phenol extraction
- Enzymatic assays
- Statistical analysis

RESULTS

Pto *gap* mutants exhibit different growth deficiencies

To study the role of the Pto *gap* genes in carbon metabolism, single and double *gap* deletion mutants were constructed and growth assays were carried out in both solid (Fig. RII.1A) and liquid M9 minimal media (Fig. RII.1C) using various carbon sources. Glucose was selected as a representative glycolytic carbon source, succinate as a gluconeogenic carbon source, and assays were also performed with both sources simultaneously. Additionally, growth on galactose was evaluated as it enters the metabolism through a different pathway. Unlike the ED pathway, galactose is catabolized *via* an analogous pathway known as the De Ley-Doudoroff pathway, which yields G3P and pyruvate (De Ley and Doudoroff, 1957; Lessie and Phibbs Jr., 1984).

The *gap* mutants showed important growth deficits in both solid and liquid media, but different from one another (Figs. RII.1A and SII.2A). Specifically, ΔG1 was unable to grow on glycolytic carbon sources, but exhibited growth when a gluconeogenic source was used. Conversely, ΔG2 displayed the opposite phenotype: it failed to grow on gluconeogenic carbon sources, but thrived on glycolytic sources. The *in trans* expression of the corresponding wild type genes in the plasmids pJG1 and pJG2 successfully restored growth in both ΔG1 and ΔG2 mutants (Figs. RII.1A and SII.2A).

The ΔG1/2 double mutant was unable to grow on individual carbon sources, either glycolytic or gluconeogenic, and only grew when both types of carbon sources were provided simultaneously (*i.e.*, glucose and succinate). Interestingly, ΔG1/2 (pJG2) could only grow on gluconeogenic carbon sources, mirroring the phenotype of the ΔG1 single mutant and suggesting a presumably gluconeogenic role for the Gap2 enzyme.

However, ΔG1/2 (pJG1) grew on both glucose and succinate as sole carbon sources, did not show the ΔG2 growth deficit, and behaved like the wild type strain (Figs. RII.1A and 1C). This differs from the growth pattern observed with the ΔG2 mutant and the inferred glycolytic function for the Gap1 enzyme.

The mutant lacking the *gap3/epd* gene exhibited important growth deficits on several carbon sources and it was unable to grow when both glycolytic and gluconeogenic carbon sources were provided. However, no significant growth defects were detected with galactose as a single carbon source (Figs. RII.1B and SII.2B). These phenotypes did not correlate with the typical GAPDH activity. Instead, the major growth deficiencies of this mutant suggested the absence of another crucial activity, such as Epd, which catalyses the first step of the vitamin B6 biosynthetic pathway (Zhao *et al*., 1995; Richts *et al*., 2019; Nimma *et al*., 2023). To assess whether the growth deficiencies of the *gap3/epd* mutant were due to the disruption of the vitamin B6 biosynthetic pathway, we conducted growth assays on media supplemented with 20 μM pyridoxine. Interestingly, the previously observed growth deficiencies were alleviated and the mutant displayed normal growth regardless the available carbon source (Figs. RII.1B and SII.2B). These findings suggest that the *gap3/epd* gene is crucial for PLP metabolism. Therefore, we named this mutant as Δepd. In trans expression of the wild type *epd* gene relieved the growth defects of the Δepd strain, except when glucose was the only carbon source (Fig. RII.1B).

Pto Gap proteins present distinctive metabolic activities

GAPDH catalyses the interconversion of BPG to G3P in the presence of NAD(P). In order to characterise the activity of Gap1, Gap2 and Gap3/Epd and elucidate their metabolic functions, we quantified the glycolytic and gluconeogenic GAPDH activities using cellular extracts of the wild type and the mutants cultured in rich media, where all of them grow similarly.

Figure RII.1. Growth of Pto gap mutants on minimal medium containing different carbon sources.

Assays were carried out in both solid (A) and liquid M9 minimal media (B) with different individual carbon sources either glycolytic or gluconeogenic. Carbon sources were glucose (M9 glu) at 10 mM, succinate (M9 suc) at 15 mM, and galactose (M9 gal) at 10 mM when provided simultaneously (M9 glu+suc), glucose was at 5 mM and succinate at 7.5 mM.

A. Growth on solid medium of 10 μl drops of bacterial suspensions at OD_{600}=1. Pictures were taken after incubation for 2 days at 20ºC.

B. Growth on solid medium of the Δepd mutant with the indicated carbon sources, with and without pyridoxine supplementation (20 μM).

C. Growth curves in liquid medium. Bacterial cultures were inoculated at OD_{600}=0.01 and incubated at 20ºC for 72 h with continuous shaking measuring the absorbance at 600 nm every hour in a Bioscreen C.

→

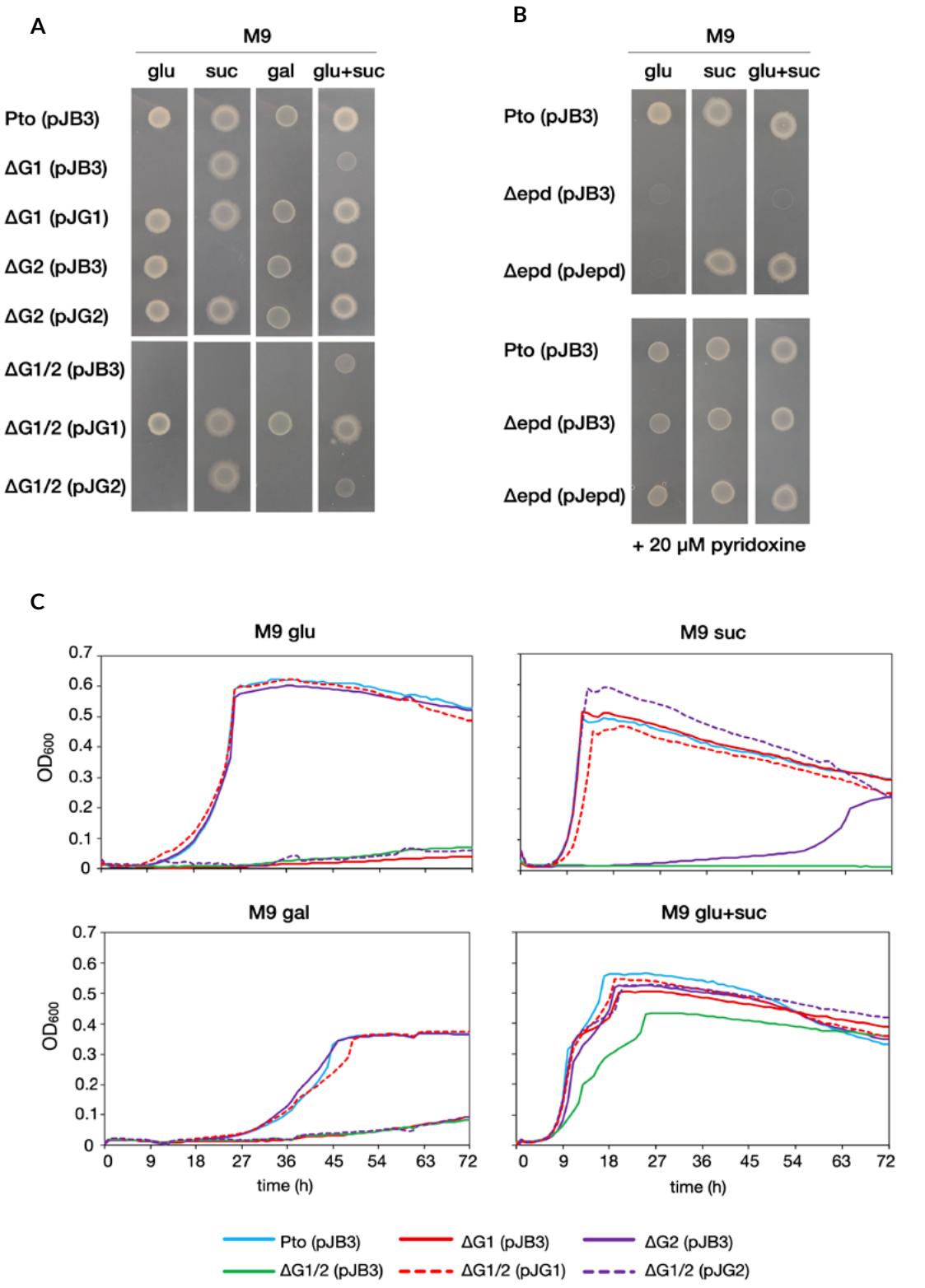
A
M9
glu
suc
gal
glu+suc
Pto (pJB3)
ΔG1 (pJB3)
ΔG1 (pJG1)
ΔG2 (pJB3)
ΔG2 (pJG2)
ΔG1/2 (pJB3)
ΔG1/2 (pJG1)
ΔG1/2 (pJG2)
B
M9
glu
suc
glu+suc
Pto (pJB3)
Δepd (pJB3)
Δepd (pJepd)
Pto (pJB3)
Δepd (pJB3)
Δepd (pJepd)
+ 20 µM pyridoxine
C
M9 glu
M9 suc
M9 gal
M9 glu+suc
OD600
time (h)
0
9
18
27
36
45
54
63
72
Pto (pJB3)
ΔG1 (pJB3)
ΔG2 (pJB3)
ΔG1/2 (pJB3)
ΔG1/2 (pJG1)
ΔG1/2 (pJG2)

Glycolytic activity was measured by monitoring NADH or NADPH formation during the conversion of G3P to BPG (Pancholi and Fischetti, 1992) and was detected in the wild type and the Δepd mutant, but not in the double ΔG1/2 mutant. On the other hand, *in trans* expression of *gap1* or *gap2* in the ΔG1/2 mutant significantly increased the activity compared to that of the wild type (Fig. RII.2A). The ΔG1/2 strain derivative overexpressing the *gap1* gene showed the highest GAPDH activity in the presence of NAD, whereas the strain overexpressing *gap2* displayed a significant activity, albeit lower than that produced by *gap1*, and only in the presence of NADP (Fig. RII.2A). *In trans* expression of *epd* in the Δepd mutant resulted in the same activity level as the wild type, indicating that Gap3/Epd does not possess significant GAPDH activity. This is also supported by the fact that the double ΔG1/2 mutant exhibited no detectable activity despite the presence of the *gap3/epd* gene. Therefore, glycolytic GAPDH enzymatic activity is specific of Gap1 and Gap2 but not of Gap3/Epd.

Gluconeogenic GAPDH activity was measured by monitoring the depletion of NADH or NADPH in the conversion of BPG to G3P (Q. Wang *et al*., 2010). This assay involved two reactions: the first step generated BPG from 3-phosphoglyceric acid, and the second reaction is performed to measure the activity of interest. Consistent with the glycolytic reaction, Gap1 was found to operate with NADH as a cofactor, whereas Gap2 utilized NADPH. Apparent gluconeogenic GAPDH activity was detected in all the strains assayed, including the double ΔG1/2 mutant (Fig. RII.2B), which exhibited a basal activity level probably due to residual substrate still present from the first reaction. In contrast to the glycolytic GAPDH assays, the strain overexpressing the *gap2* gene exhibited the highest gluconeogenic activity, whereas the strain overexpressing *gap1* displayed lower activity, but still significantly higher than the wild type or the *gap3/epd* overexpressing strain (Fig. RII.2B). These results show that Gap1 and Gap2, but not Gap3/Epd, seem to be responsible for the gluconeogenic GAPDH enzymatic activity in Pto DC3000.

Figure RII.2. Gap and Epd enzymatic activities.
Values of enzymatic activity measured in cell extracts obtained from *gap* mutant strains grown in liquid LB. Enzymatic activity was determined by monitoring NADH or NADPH formation or depletion by measuring the absorbance at 340 nm for 30 min. Graphs show the average specific activity in $\mu mol/min^{-1} \cdot mg^{-1}$ of total protein of each strain, and error bars correspond to the standard deviation. Letters a-e denote ANOVA followed by Tukey HSD test categories with significant differences ($p<0.05$).
A. Glycolytic GAPDH activity assays. NAD or NADP were used as cofactors.
B. Gluconeogenic GAPDH activity assays. It should be noticed that NADH was always present in the reaction mixture from the first step reaction. NADPH indicated when added as a co-substrate.
C. Epd activity assays. NAD was used as a cofactor. →

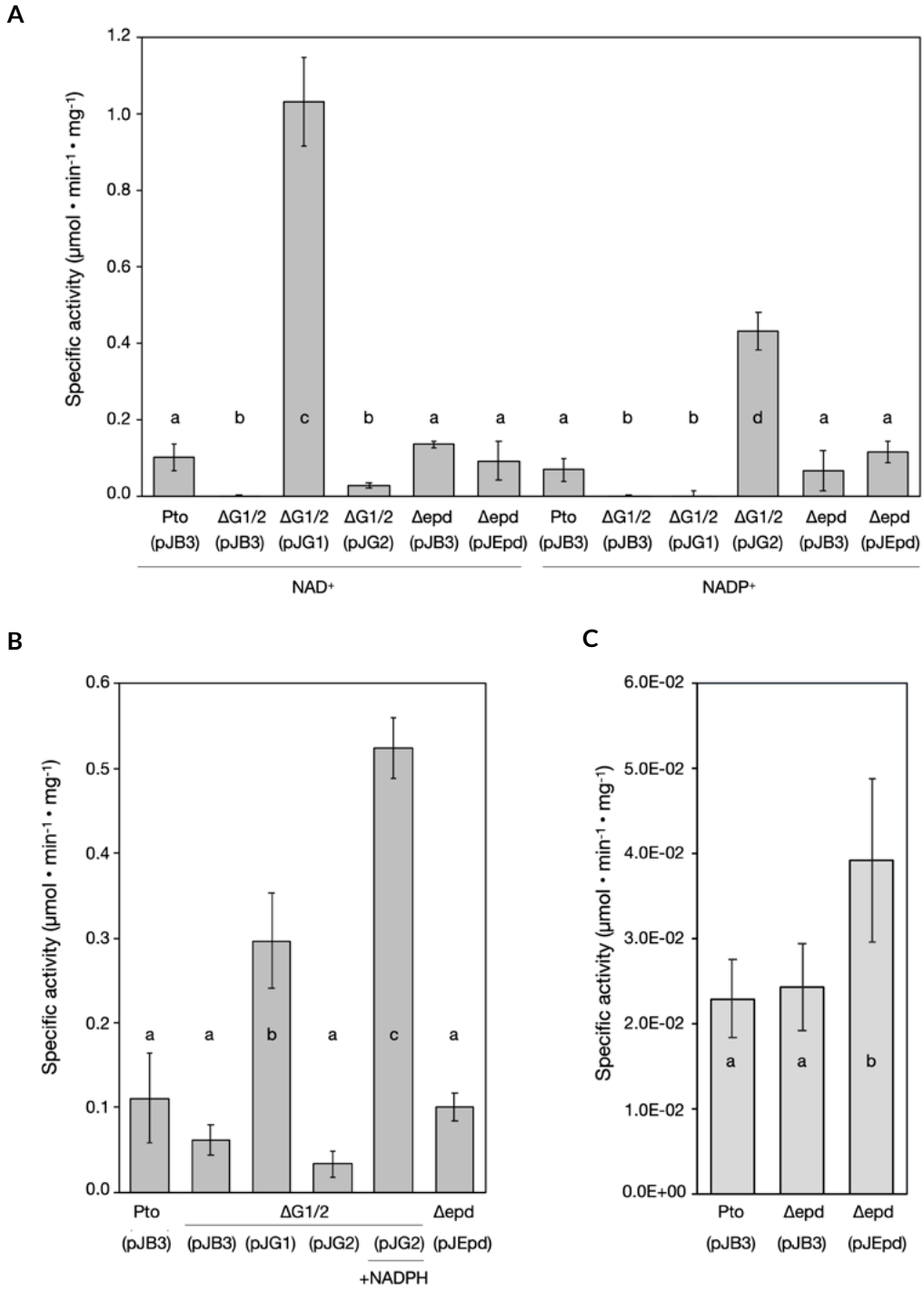
A
Specific activity (µmol • min⁻¹ • mg⁻¹)
1.2
1.0
0.8
0.6
0.4
0.2
0.0
a b c b a a a b b d a a
Pto (pJB3)
ΔG1/2 (pJB3)
ΔG1/2 (pJG1)
ΔG1/2 (pJG2)
Δepd (pJB3)
Δepd (pJEpd)
Pto (pJB3)
ΔG1/2 (pJB3)
ΔG1/2 (pJG1)
ΔG1/2 (pJG2)
Δepd (pJB3)
Δepd (pJEpd)
NAD+
NADP+
B
Specific activity (µmol • min⁻¹ • mg⁻¹)
0.6
0.5
0.4
0.3
0.2
0.1
0.0
a a b a c a
Pto (pJB3)
ΔG1/2 (pJB3)
ΔG1/2 (pJG1)
ΔG1/2 (pJG2)
ΔG1/2 (pJG2)
Δepd (pJEpd)
+NADPH
C
Specific activity (µmol • min⁻¹ • mg⁻¹)
6.0E-02
5.0E-02
4.0E-02
3.0E-02
2.0E-02
1.0E-02
0.0E+00
a a b
Pto (pJB3)
Δepd (pJB3)
Δepd (pJEpd)

In summary, these results suggest that Gap1 has a predominant glycolytic activity and Gap2 a predominantly gluconeogenic activity, despite the fact that both proteins exhibit both activities when overexpressed. Furthermore, Gap1 uses NAD^+ or NADH as cofactors and has no activity when only NADP+ is provided. On the other hand, Gap2 uses $NADP^+$ and NADPH as cofactors and exhibits no significant activity in the presence of NAD^+ or NADH.

As detailed above, Gap3/Epd did not exhibit any detectable GAPDH activity in Pto DC3000. To determine whether it has Epd activity, enzymatic assays were performed with E4P as substrate. Under our experimental conditions, no difference in activity could be detected between the Δepd mutant and the wild type, suggesting a low level of Epd activity. However, the presence of the pJEpd plasmid led to a significant increase in Epd activity (Fig. RII.2C). These results support that Pto DC3000 Epd exhibits E4PDH activity.

Effect of gap deletion in motility and biosurfactant production

Swimming and swarming assays were performed to assess whether deletion of the gap genes caused an impact on motility. The swimming of the four mutants, ΔG1, ΔG2, ΔG1/2 and Δepd was similar to that of the wild type after 48 h (Fig. RII.3A), showing that those mutants did not exhibit defects in flagella production and functioning or growth in LB rich medium.

Regarding swarming motility, the ΔG2 mutant displayed comparable behaviour to the wild type, whereas the ΔG1 and the double ΔG1/2 mutants were faster, showing an increased swarming surface after 24 h (Fig. RII.3B). The Δepd mutant exhibited

---

Figure RII.3. Motility and biofilm formation phenotypes of Pto gap mutants.
A. Swimming assays. Plates were incubated for 48 h at 20°C, then pictures were taken and halos were measured. The graph shows the average diameter of the swimming halos. No significant differences ($p<0.01$) were found among the strains assayed.
B. Swarming assays. Plates were incubated for 24 h at 20°C. The swarming pattern of Δepd without pyridoxine is circled in white as it cannot be clearly appreciated in the photograph due to its transparency. The graph shows the average swarming surface.
C. Comparison of surfactant-induced halos by bacterial colonies. Plates were incubated for 48 h at 20°C and syringafactin halos were detected with atomized oil. The graph shows the average surface of the syringafactin halos.
D. Biofilm formation by the *gap* mutants quantified after growth for 24 h in MMR in a 96-well plate with continuous shaking at 20°C by cristal violet (CV) staining. Represented as the average of 8 wells for each strain for 2 independent plates. OD_{660} was measured to confirm uniform growth among the different strains.
Error bars represent standard deviation. Letters denote Tukey HSD test categories with significant differences ($p<0.01$). →

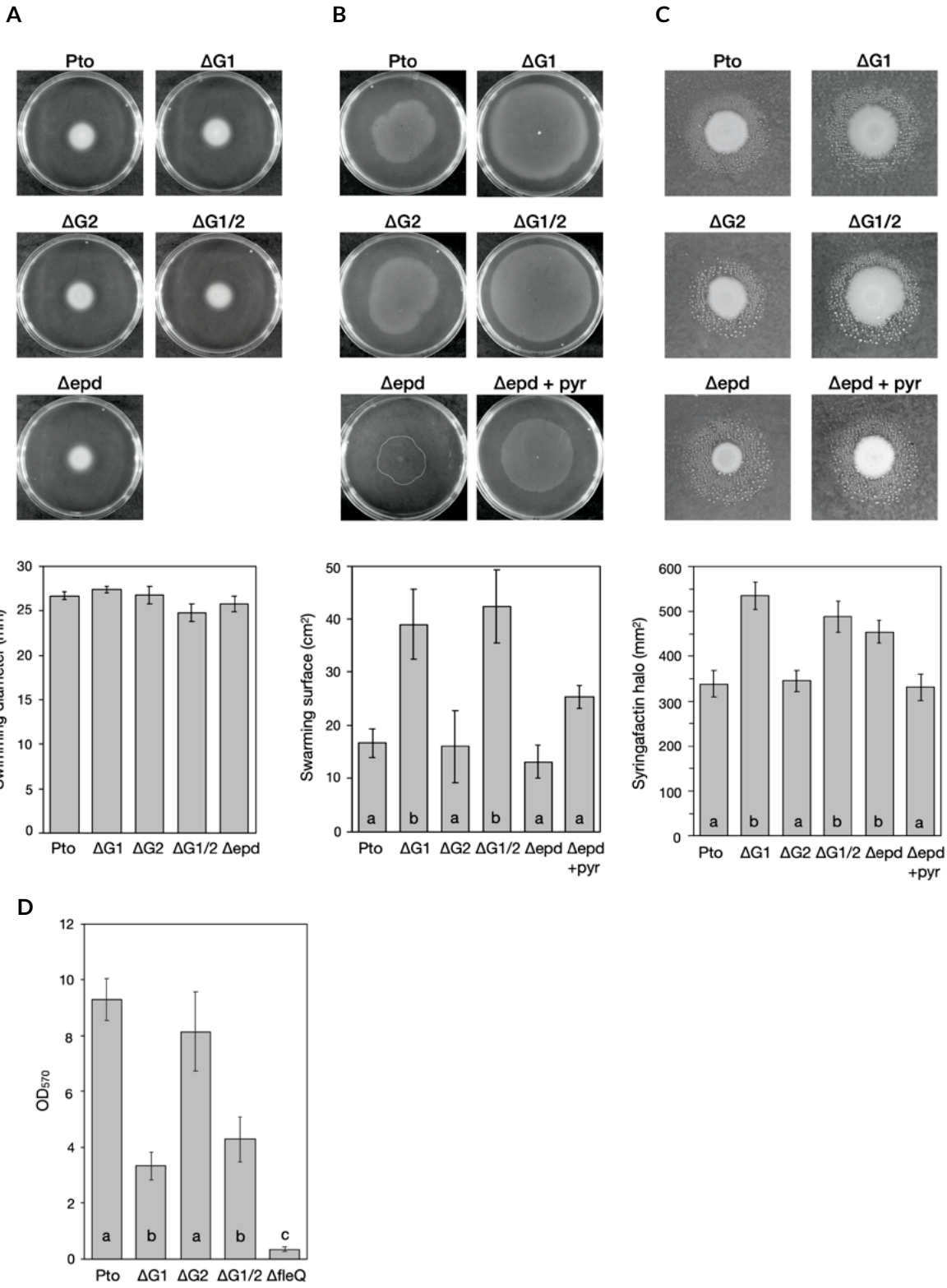
A
B
C
Pto
ΔG1
ΔG2
ΔG1/2
Δepd
Δepd + pyr
Swimming diameter (mm)
Swarming surface (cm²)
Syringafactin halo (mm²)
Pto ΔG1 ΔG2 ΔG1/2 Δepd Δepd +pyr
D
OD570
Pto ΔG1 ΔG2 ΔG1/2 ΔfleQ

a swarming area similar to the wild type, but very faint growth in this medium. Upon pyridoxine supplementation, the swarming surface was clearly appreciated, exhibiting no significant difference in comparison to the wild type.

As flagella synthesis and assembly seemed to remain unaltered in all the mutants, we hypothesized that the increase in their swarming might be linked to a rise in the production of biosurfactants. Therefore, syringafactin production was assessed by measuring the generated surfactant halo. As it has been established that the *gap* mutants present growth deficiencies on specific carbon sources, we performed the syringafactin assays in the same medium as the swarming assays to reduce possible variability caused by metabolic defects. The ΔG2 mutant exhibited a similar syringafactin halo to that of the wild type, whereas the ΔG1 and ΔG1/2 mutants generated a significantly bigger surfactant halo (Fig. RII.3C). These results match the observed swarming behaviour, thus suggesting that the increased syringafactin production by these mutants may be responsible for their enhanced swarming motility. The Δepd biosurfactant production was assessed with and without pyridoxine supplementation. This mutant also increased its syringafactin production, however, the phenotype was reversed when pyridoxine was added to the medium, turning similar to the wild type.

Effect of *gap* deletion in biofilm formation

Pto DC3000 is also able to produce solid-liquid biofilms in the presence of $CaCl_2$ (Fishman *et al*., 2018). As GAPDH has been described involved in adhesion (Jin *et al*., 2005; Lama *et al*., 2009), biofilm formation assays were performed to assess the impact of *gap* gene deletion on this phenotype. Biofilm formation was quantified by CV staining in multi-well plates after growth for 24 h, and a *fleQ* mutant was used as negative control as it is a biofilm deficient strain (Martínez-Rodríguez *et al*., 2023). The amount of biofilm formed by the ΔG1 and double ΔG1/2 mutant significantly decreased compared to the wild type, albeit their levels were still higher than those of the *fleQ* mutant. The ΔG2 mutant, on the other hand, was able to form a higher quantity of biofilm, but still did not reach the levels of the wild type (Fig. RII.3D). It should be noted that the decreased biofilm formation by the ΔG1 and ΔG1/2 mutants was not caused by a lack of growth, since they were able to grow in the provided medium similarly to the other strains.

Gap roles on virulence in planta

To study the impact of the *gap1*, *gap2* and *gap3/epd* genes on virulence, infection assays were carried out in tomato plants comparing the effect of the wild type, the ΔG1, ΔG2, Δepd and ΔG1/2 mutants. In planta growth and virulence ability of those strains was monitored by quantifying the bacterial populations and observing the disease symptoms in tomato leaf tissue for 10 days post inoculation (dpi).

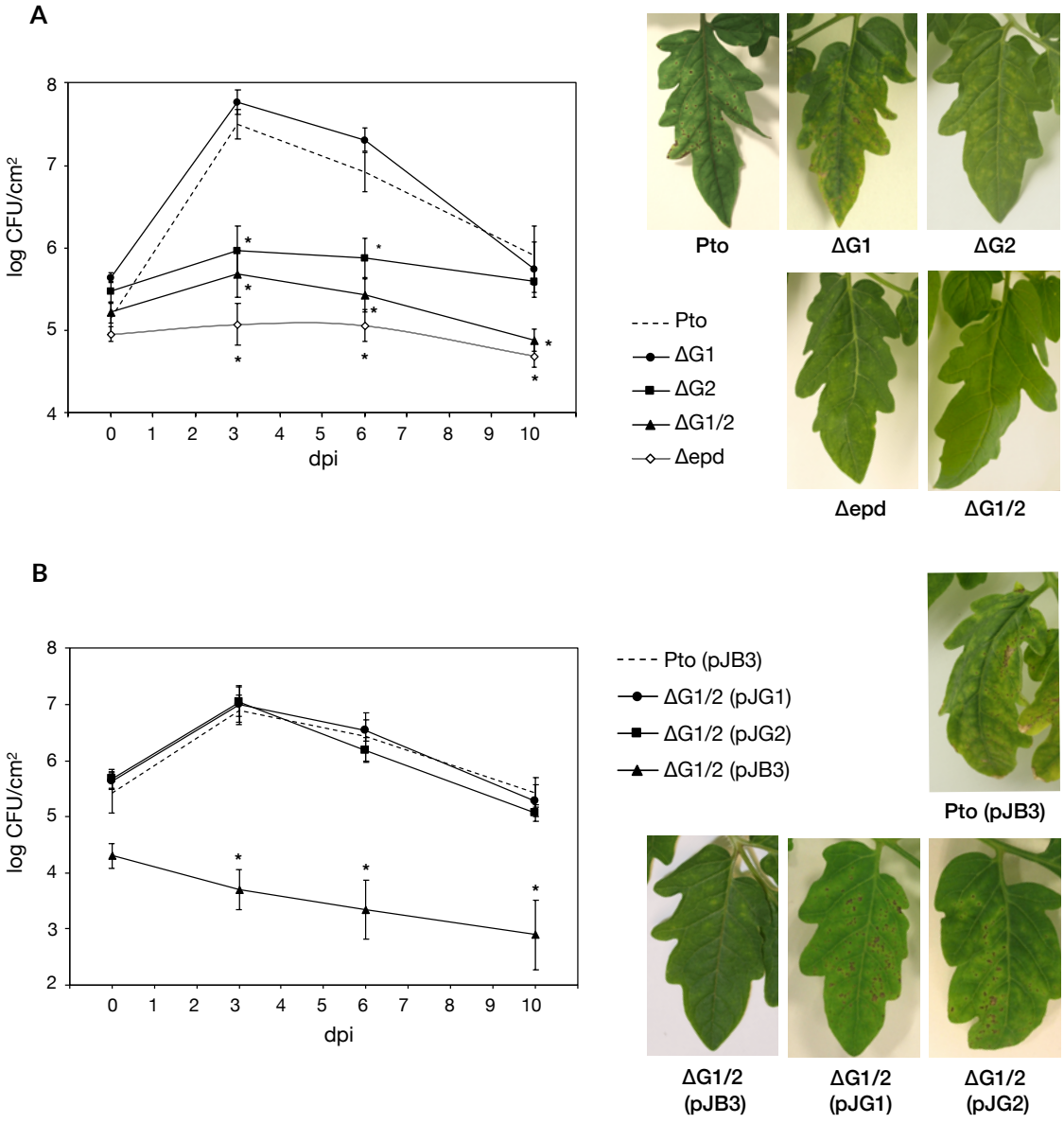

Figure RII.4. Pto bacterial growth and symptom development.
A. Growth and symptom development on tomato leaves inoculated with the deletion mutants.
B. Growth and symptom development inoculated with the double mutant complemented with *gap1* or *gap2*.
Time course of growth of Pto *gap* mutants in the primary leaves of tomato plants (Solanum lycopersicum). Leaves were inoculated with approximately 10^8 CFU/ml by spray and CFUs were quantified at 0, 3, 6 and 10 days post-inoculation (dpi). Error bars indicate standard deviation. Asterisks (*) indicate a statistically significant difference (Tukey HSD test, $p<0.01$). Pictures of the of symptoms induced on tomato leaves 10 dpi with the indicated strains.

The ΔG1 mutant entered the tomato leaves and displayed an analogous apoplast growth pattern to that of the wild type strain. By 3 dpi, both strains reached peak population levels (Fig. RII.4A). The disease symptoms caused by the two strains were similar in severity, with small water-soaked lesions emerging 2-3 days post-inoculation, swiftly transitioning to brown lesions with a surrounding chlorotic halo. These findings suggest that the absence of *gap1* has no discernible impact on *in planta* growth or virulence. In contrast, the ΔG2 and double ΔG1/2 mutants showed important *in planta* growth deficits, exhibiting significantly lower bacterial populations throughout the time of the experiment, with the double mutant almost not being able to increase its population (Fig. RII.4A). The ΔG2 mutant caused reduced disease symptoms, only appearing small water-soaked lesions at 10 dpi, whereas the double mutant ΔG1/2 did not cause any symptoms on the leaves (Fig. RII.4A). *In trans* expression of *gap2* complemented both bacterial population and severity of the plant symptoms in the ΔG2 mutant (Fig. SII.3A). It should be mentioned that the pJG2 plasmid was present in 84.9% of the population at 10 dpi.

The independent effect of *gap1* and *gap2 in trans* expression was studied in the double ΔG1/2 mutant. In both cases, the *in trans* expression of *gap1* or *gap2* in the double mutant triggered growth and symptom development similar to the wild type strain (Fig. RII.4B). This shows that in contrast to the behaviour of the *gap2* mutant, the ectopic expression of *gap1* gene is able to compensate for the loss *gap2* regarding pathogenicity. When inspecting plasmid stability over the course of the experiment, it was observed that at 10 dpi pJG1 and pJG2 were retained by 72.4% and 79.1% of the population, respectively.

In the case of Δepd, the mutant was not able to multiply in the tomato leaves and no population increase was detected during the assays. The disease symptoms observed in the plants were very mild, only appearing very small water-soaked lesions at 10 dpi (Fig. RII.4A). *In trans* expression of the *gap3/epd* gene complemented both bacterial growth and symptom severity of the Δepd mutant (Fig. SII.3B). As before, plasmid stability was monitored showing that pJepd was present in 87.4% of the population at 10 dpi.

Gap1 and Gap2 are differently expressed and exported outside the cells depending on the growth conditions

GAPDH release outside the cells associated to moonlighting functions has been observed in several bacteria (Pancholi and Fischetti, 1992; Aguilera *et al*., 2012; Kainulainen and Korhonen, 2014). Therefore, immunodetection was performed to determine if Gap1 and Gap2 could be found in Pto DC3000 extracellular culture media. Protein samples were obtained from culture supernatants grown in three media with

different carbon sources: M9 with succinate, M9 with glucose and succinate, and T3SS-inducing minimal medium with mannitol and pyruvate. Protein extraction from the cell fraction was also carried out as a control, and Western blot assays were performed to detect both proteins.

Both proteins were immunodetected in cells grown under the three culture conditions (Fig. RII.5). Remarkably, Gap1 seemed to be present at lower levels in cells grown in M9 with succinate as the sole carbon source, compared to M9 supplemented with both glucose and succinate or the T3SS-inducing minimal medium. However, Gap1 was detected at similar levels in the extracellular fractions of the three culture types (Fig. RII.5), which indicates that this protein is consistently exported by Pto DC3000 independently of the medium composition.

As opposed to Gap1, Gap2 was more abundant in the cell fractions of cultures grown on M9 media compared to the T3SS-inducing minimal medium with mannitol and pyruvate as carbon sources (Fig. RII.5). However, Gap2 was only detected in the extra-

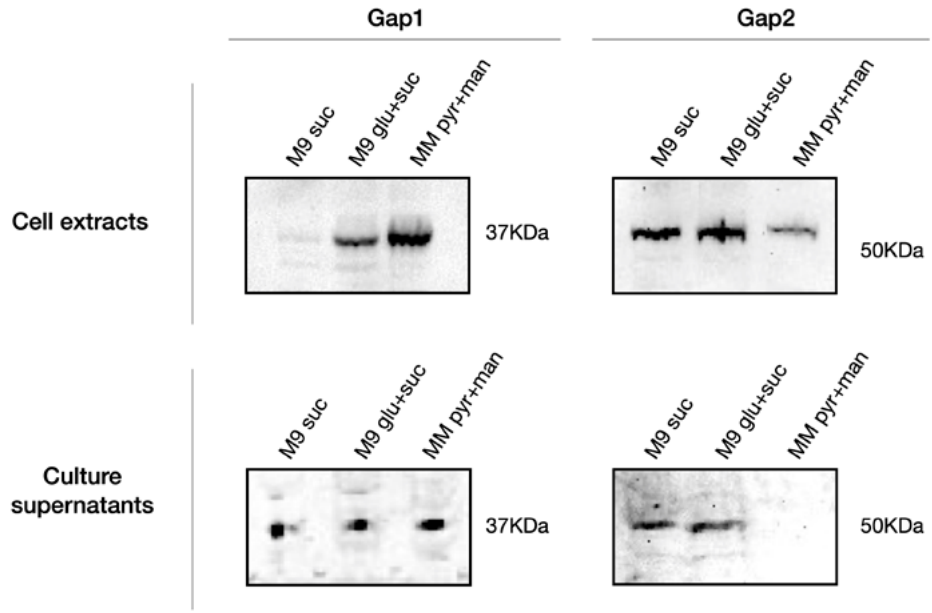

Figure RII.5. Immunodetection of Gap1 and Gap2 in cell extracts and culture supernatants. Pto was grown in different media: M9 suc (with succinate as carbon source), M9 glu+suc (with glucose and succinate as carbon sources) and MM pyr+man (T3SS-inducing with pyruvate and mannitol as carbon sources). Total protein from cell extracts and supernatants of cultures was analysed. 10 µg of total protein were loaded into each lane for cell extracts and 20 µg of total protein were loaded into each lane for culture supernatants.

cellular fraction of cells grown on M9 media, but not when grown on T3SS-inducing medium (Fig. RII.5). These results suggest that the Gap2 protein is only exported under certain conditions, and its extracellular relative abundance seem to correlate with the amounts of protein found intracellularly.

Given the differences appreciated in protein abundance in extracts of cells grown on different media, we studied whether the transcriptional expression of the *gap1* and *gap2* genes changed with the medium composition and/or the carbon source available. β-galactosidase assays were performed using *gap1* and *gap2* gene promoter transcriptional fusions to '*lacZ*. Different media were tested, corresponding to the protein extraction media: M9 with glucose, M9 with succinate, M9 with both glucose and succinate, and T3SS-inducing minimal medium with mannitol and pyruvate. LB was also used as a rich medium control. Expression of pME6016-derived plasmids bearing the P_{gap1} and P_{gap2} transcriptional fusions to *´lacZ* were assessed in the wild type, ΔG1 and ΔG2 strains throughout the growth curve (Fig. SII.4).

The specific β-galactosidase activity from the *gap1* fusion in Pto DC3000 did not significantly change with the medium, although it exhibited higher levels in M9 media with glucose and succinate, and lower levels in T3SS-inducing minimal medium (Fig. RII. 6). Surprisingly, the *gap1* expression profile did not correlate with the Gap1 intracellular protein abundance (Fig. RII. 5). On the other hand, *gap2* expression was higher in the M9 media with succinate compared and to M9 medium with glucose or T3SS-inducing minimal medium, which agrees to the predominantly gluconeogenic activity of the Gap2 enzyme (Fig. RII.6). Furthermore, the detected Gap2 protein abundance in the cell extracts shows a relationship with *gap2* transcriptional expression. Besides, the pattern of expression of P*gap1* and P*gap2* in the ΔG1 and ΔG2 mutants were similar to the wild type strain (Fig. SII.4). Nevertheless, P_{gap2} expression significantly increased at high cell densities, a tendency that was not observed in the case of P_{gap1}, whose expression remained stable throughout the growth curve.

DISCUSSION

GAPDH is recognised as a housekeeping protein prevalent in practically all organisms, since it is an enzyme with a pivotal role in the glycolytic/gluconeogenic pathways, facilitating the interconversion of BPG and G3P (Seidler, 2013). However, GAPDH participates in an array of cellular processes beyond its classic metabolic roles, being considered a paradigm among moonlighting/multifunctional proteins (Seidler, 2013; Sirover, 2014; Jeffery, 2018; Franco-Serrano *et al*., 2021). In some human and animal pathogenic

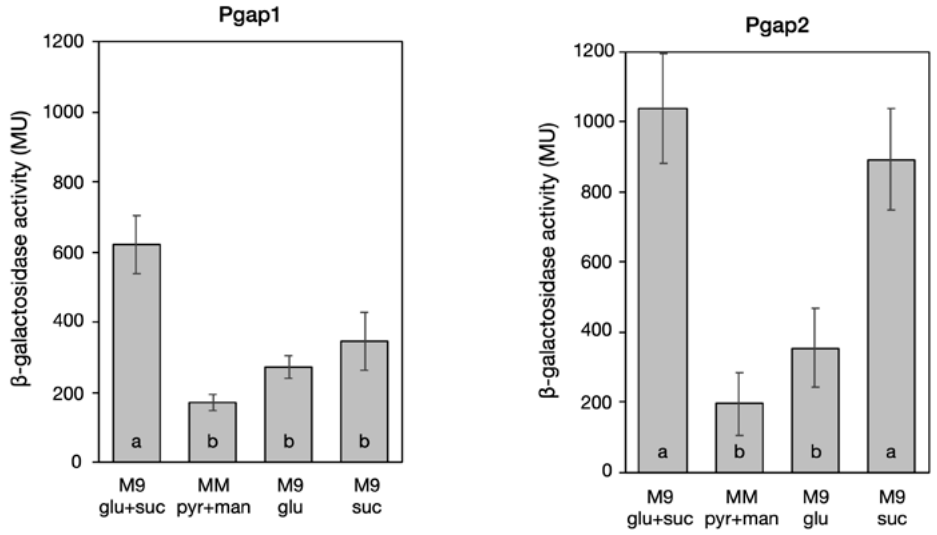

Figure RII.6. Expression of Pto *gap1* and *gap2* genes relative to carbon source availability. β-Galactosidase activities of transcriptional fusions from Pto DC3000 *gap1* and *gap2* promoters to '*lacZ* were masured in the wild type. Different dilutions of cultures in the indicated media were grown for 24 h at 20°C in a microtiter plate at different OD_{660} and β-galactosidase activity was measured. The graph shows the average activity at OD_{660}=1, and error bars correspond to the standard deviation. Letters a to b denote Tukey HSD test categories with significant differences ($p<0.01$). Carbon sources: glucose (glu), succinate (suc), glucose + succinate (glu+suc) and pyruvate + mannitol (pyr+man).

bacteria, GAPDH has been detected surface-associated or shown to be secreted, playing a part in signal transduction to host cells (Aguilera *et al*., 2012; Giménez *et al*., 2014; Ebner *et al*., 2016; Kopeckova *et al*., 2020a). On the other hand, plant pathogenic bacteria establish a multifaceted and close interaction with plant cells which requires the coordinated deployment of diverse virulence factors. Toxins, exopolysaccharides, extracellular proteins, biosurfactants, along with the orchestrated translocation of numerous effectors into plant cells *via* the T3SS collaboratively drive infection and draw nutrients from plants (Petnicki-Ocwieja *et al*., 2002; Cunnac *et al*., 2009; Xin *et al*., 2018). However, little is known about the role of GAPDH in those processes. The genome of Pto DC3000, a significant model in molecular plant pathology, encodes three putative paralogous *gap* genes positioned across distinct regions of the chromosome that are predicted to encode GAPDHs with distinct molecular properties (Elkhalfi e*t al*., 2013). In the present work we explored the physiological and possible non-canonical functions of these three *gap* genes.

The protein encoded by the third paralogue gene, previously referred as *gap3/epd*, is similar to eubacterial orthologs with dual specificity for both G3P and E4P. In *E. coli*, the *gapB* gene, renamed *epd* by Yang *et al*. (1998) encodes a protein with low level phosphorylating and non-phosphorylating GAPDH activities. However, this activity was not sufficient to sustain the growth of *gapA* mutants, which are deficient in the primary *E. coli* GAPDH (Zhao *et al*., 1995; Yang *et al*., 1998). The Pto DC3000 Gap3/Epd protein was reported to display a low GAPDH activity when heterologously expressed in *E. coli* (Elkhalfi *et al*., 2013). However, our Pto double mutant ΔG1/2 was unable to grow on either glycolytic or gluconeogenic carbon sources (Fig. RII.1A), nor did it display significant GAPDH activity (Fig. RII.2). Furthermore, overexpressing *epd in trans* did not significantly augment the GAPDH enzymatic activity compared to the wild type (Fig. RII.2). Therefore, our results support that the Epd protein has no GAPDH activity.

The deoxyxylulose-5-phosphate (DXP)-dependent vitamin B6 biosynthesis pathway is present in α- and γ-proteobacteria. It consists of seven enzymatic steps in which Epd catalyses the first step converting E4P to 4-PE, becoming essential for PLP biosynthesis in organisms that utilize this pathway (Richts *et al*., 2019; Nimma *et al*., 2023). Consistent with a role of Epd in the DXP-dependent PLP biosynthesis pathway, the Pto Δepd mutant exhibited difficulties to grow on both glycolytic and gluconeogenic carbon sources. It was noticeable that the *epd* mutant growth deficit with glucose as carbon source was not reverted by *epd in trans* expression. This could be explained by the accumulation of 4-PE due to the overexpression of *epd*. 4-PE is an inhibitor of 6-phosphogluconate dehydrogenase activity, provoking the accumulation of 6-phosphogluconate, which subsequently acts as a competitive inhibitor of phosphoglucose isomerase (PGI) and other enzymes, ultimately leading to a metabolic gridlock (Sachla and Helmann, 2019). 4-PE is also a potent inhibitor of ribose-5-phosphate isomerase, a crucial enzyme of the PP pathway with essential roles in anabolism and catabolism (Zhang *et al*., 2003). All the observed growth deficits were, however, reverted when the medium was supplemented with the PLP precursor pyridoxine (Figs. RII.1B and SII.2B). Thus, the Pto Δepd strain behaves as a pyridoxine auxotroph and Epd seems to be essential for the PLP-dependent metabolism and bacterial growth when no B6-vitamers are available for intake. This is particularly evident *in planta*. Since B6-vitamers are likely not present in the tomato apoplast, the lack of *epd* impaired bacteria from multiplying (Fig. RII.4A), reinforcing the essential role of *epd* in Pto DC3000. Despite our difficulties to measure Epd enzymatic activity in Pto, a significant Epd activity could be measured when *epd* gene was overexpressed (Fig. RII.2C).

Pto DC3000 enters, multiplies and colonises the tomato leaf apoplast harnessing nutrients from living host cells. Accordingly, Pto activates metabolic pathways that

facilitate the uptake of organic acids, sugars, and amino acids that are abundant in the tomato apoplast, like citrate, succinate, malate, malonate, D-glucuronic acid, GABA, sucrose, D-galactose, fructose, glucose, aspartate and glutamate (Rico and Preston, 2008). However, it lacks an array of metabolic enzymes found in non-plant pathogenic pseudomonads, *i.e.* the oxo-acid dehydrogenase for the assimilation of valine and isoleucine, the glycerate pathway responsible for glyoxylate utilisation, and genes linked to microaerobic and anaerobic metabolism, like NADP-dependent glutamate dehydrogenase, D-lactate dehydrogenase and nitrous-oxide reductase (Rico and Preston, 2008; Rico *et al*., 2011).

The growth assays performed with Pto *gap1* and *gap2* single and double mutants on different carbon sources, together with enzymatic assays evidenced their specialization on glycolytic or gluconeogenic activity, respectively. Furthermore, Gap1 used NAD^+/NADH as cofactors whereas Gap2 used $NADP^+$/NADPH (Figs. RII.1 and 2). Although many bacteria contain a single GAPDH protein capable of performing both glycolytic and gluconeogenic activities, there is no universal layout for this enzymatic activity in bacteria. The separation of those activities into two different enzymes appears to be shared by most *Pseudomonas* species, but occurs in other organisms. The Gram-positive *Bacillus subtilis* and *Staphylococcus aureus* also share the coexistence of NAD-dependent and NADPH-dependent GAPDH enzymes tailored for glycolysis and gluconeogenesis, respectively (Fillinger *et al*., 2000; Purves *et al*., 2010; Commichau *et al*., 2013). This configuration may grant certain advantages for the functioning of particular metabolic pathways in specific environmental conditions and/or the supply of determined metabolites under very different metabolic conditions (Nikel *et al*., 2015). The ΔG1 mutant only grew on gluconeogenic carbon sources, exhibited increased swarming, probably due to elevated syringafactin production, a reduction in biofilm formation, and had no discernible impact on *in planta* growth and symptom development. The lack of Gap1 disrupts the glycolytic pathway, probably leading to the accumulation of pyruvate precursors and a decrease in the production of pyruvate, since its synthesis *via* the PEP pathway is blocked, potentially affecting various metabolic processes that rely on pyruvate as a key intermediate (Fig. RII.7 and Table SII.2). On the other hand, the *gap2* mutant was only able to grow on glycolytic compounds, but did not grow *in planta* and the leaves barely exhibited any symptoms. The lack of Gap2 may impair EDEMP cycle completion, causing the depletion of triose phosphates that prevents them to be recycled back to hexose phosphates and, consequently, NADPH formation (Fig. RII.7). Although both glycolytic and gluconeogenic carbon compounds are present in the tomato leaves, being malate and glucose the main metabolites (Schauer et al., 2005; Zoghlami *et al*., 2011), GAPDH gluconeogenic activity seems to be essential for Pto DC3000 growth *in planta*.

The assay of both glycolitic and gluconeogenic activities in the wild type and in the G1/G2 double mutant complemented *in trans* with each individual gene, allowed us to measure the activity of each enzyme separately (Fig. RII.2). Despite the fact that both proteins exhibited both activities when overexpressed (the main one being nonetheless higher than the other), the growth defects of the single ΔG1 and ΔG2 mutants indicate that the expression of the remaining enzyme was insufficient to compensate for the lacking one. Therefore, Gap1 and Gap2 activities do not seem to be interchangeable under our experimental conditions. Interestingly, Gap1 overexpression in the ΔG1/2 double mutant compensated not only for the missing Gap1 enzyme in the catabolism of glycolytic compounds, but also for Gap2 in the metabolism of gluconeogenic compounds (Figs. RII.1 and 2B). It is possible that the significant gluconeogenic activity displayed by the overexpressed Gap1 (Fig. RII.2B) may be sufficient to compensate for the lack of Gap2 and sustain the functioning of the EDEMP cycle under both glycolytic and gluconeogenic regimes (Fig. RII.7). Gap2 overexpression in the ΔG1/2 double mutant, however, only supported the growth on gluconeogenic compounds, but could not compensate for the absence of Gap1 in the catabolism of glycolytic compounds (Fig. RII.1). Gap2 overexpression together with the absence of Gap1 probably leads to diversion of carbon flux towards gluconeogenesis, since glycolysis is impeded by the absence of Gap1. In that sense, the behaviour of the single and double mutants and ΔG1/2 (pJG1) and ΔG1/2 (pJG2) strains *in planta* paralleled their growth on gluconeogenic carbon sources (Fig. RII.1).

The moonlighting roles of GAPDH in some pathogenic bacteria have been associated with the presence of the protein on the cell surface and in the extracellular media (Pancholi and Fischetti, 1992; Aguilera *et a*l., 2012; Kainulainen and Korhonen, 2014). In Pto DC3000, promoter expression and immunodetection assays revealed that both proteins were present in the bacterial cytoplasm regardless of the culture medium and available carbon source. However, *gap1* expression did not correlate with the intracellular protein abundance: the expression of *gap1* did not significantly change with the medium (Fig. RII.6), whereas the amount of Gap1 protein decreased when only a gluconeogenic carbon source was present (Fig. RII.5). This correlates with its main glycolytic role and suggests that some posttranscriptional and/or postranslational regulatory mechanisms may be responsible for the differences found among the carbon sources used.

Overall, both Gap proteins have been proved to be exported outside the cell under certain conditions, indicating potential additional roles beyond their central metabolic functions. Gap1 is consistently exported in Pto DC3000 independently of the medium composition and intracellular abundance, suggesting that its extracellular location

plays an important role, although it does not appear to be essential for Pto DC3000 interaction with plant cells nor for its virulence. However, the lack of *gap1* resulted in deficiency in biofilm formation, a phenotype observed in the ΔG1 and ΔG1/2 mutants. This suggests that either their metabolic defects impair the synthesis of exopolysaccharides and/or other matrix compounds required for biofilm formation, or Gap1 may have additional role(s) besides its metabolic functions (*i.e.*, in adhesion). Conversely, Gap2 export was correlated with its intracellular abundance, and its requirement for *in planta* growth suggests that its export/secretion may be linked to the infection process.

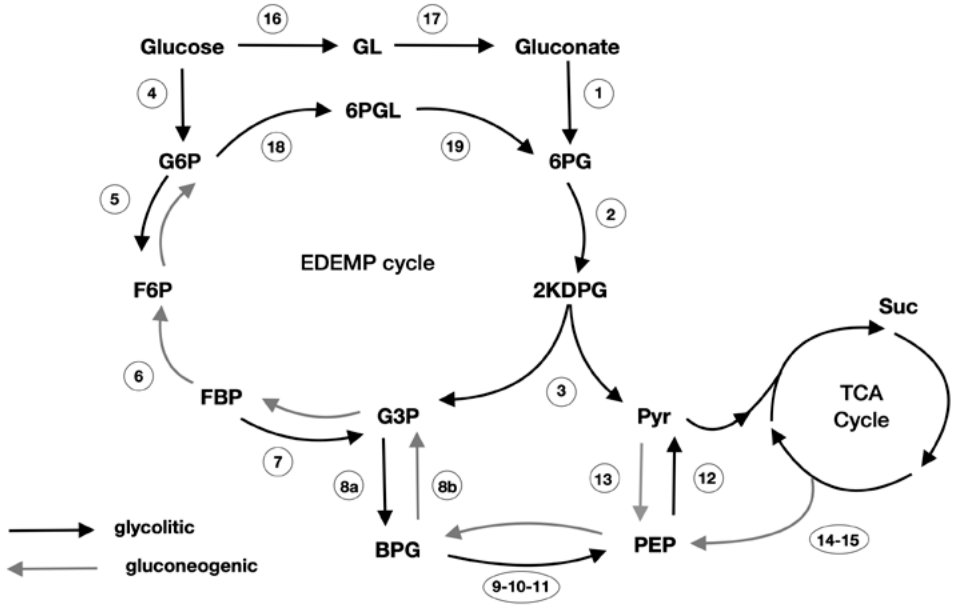

Figure RII.7. Central carbon metabolism in Pto as deduced from gene annotations.
Pseudomonads operate the EDEMP cycle, which integrates activities of the EMP, ED, and PP pathways.
Enzymes: 1. Gluconokinase, 2. 6-phosphogluconato dehydratase, 3. 2-keto-3-deoxy-phosphogluconate aldolase, 4. Glucokinase, 5. Glucose-6-phosphate isomerase, 6. Fructose-1,6-bisphosphatase, 7. Fructose-bisphosphate aldolase, 8a. Gap-1, 8b. Gap-2, 9. Phosphoglycerate kinase, 10. Phosphoglycerate mutase, 11. Enolase, 12. Pyruvate kinase, 13. Phosphoenolpyruvate synthase, 14. Malate quinone oxidoreductase, 15. Phosphoenolpyruvate carboxykinase, 16. Glucose dehydrogenase, 17. Gluconolactonase, 18. Glucose-6-phosphate dehydrogenase, 19. 6-phosphoglucolactonase.
Abbreviations: Glucose-6-phosphate (G6P), fructose-6-phosphate (F6P), fructose-1,6-bisphosphate (FBP), glyceraldehyde-3-phosphate (G3P), 1,3-bisphosphoglycerate (BPG), phosphoenolpyruvate (PEP), 2-keto-3-deoxy-6-phosphogluconate (2KDPG), 6-phosphogluconate (6PG), gluconolactone (GL), 6-phosphogluconolactone (6PGL), pyruvate (pyr), succinate (suc). Entner-Doudoroff (ED), Embden-Meyerhof-Parnas (EMP).

Hence, the possible secretion and membrane association of the two Gap proteins present in Pto DC3000 may be connected to the plant infection process and/or binding to extracellular matrices. Given the pleiotropic effects caused by *gap1* and *gap2* deletions, it becomes challenging to discern between those arising from their critical roles in carbon and energy metabolism and their putative additional extracellular functions. Therefore, further research is required to unveil and differentiate their potential non-metabolic roles (motility, biofilm formation, plant colonisation, virulence, etc.) in the physiology of Pto DC3000.

SUPPORTING INFORMATION

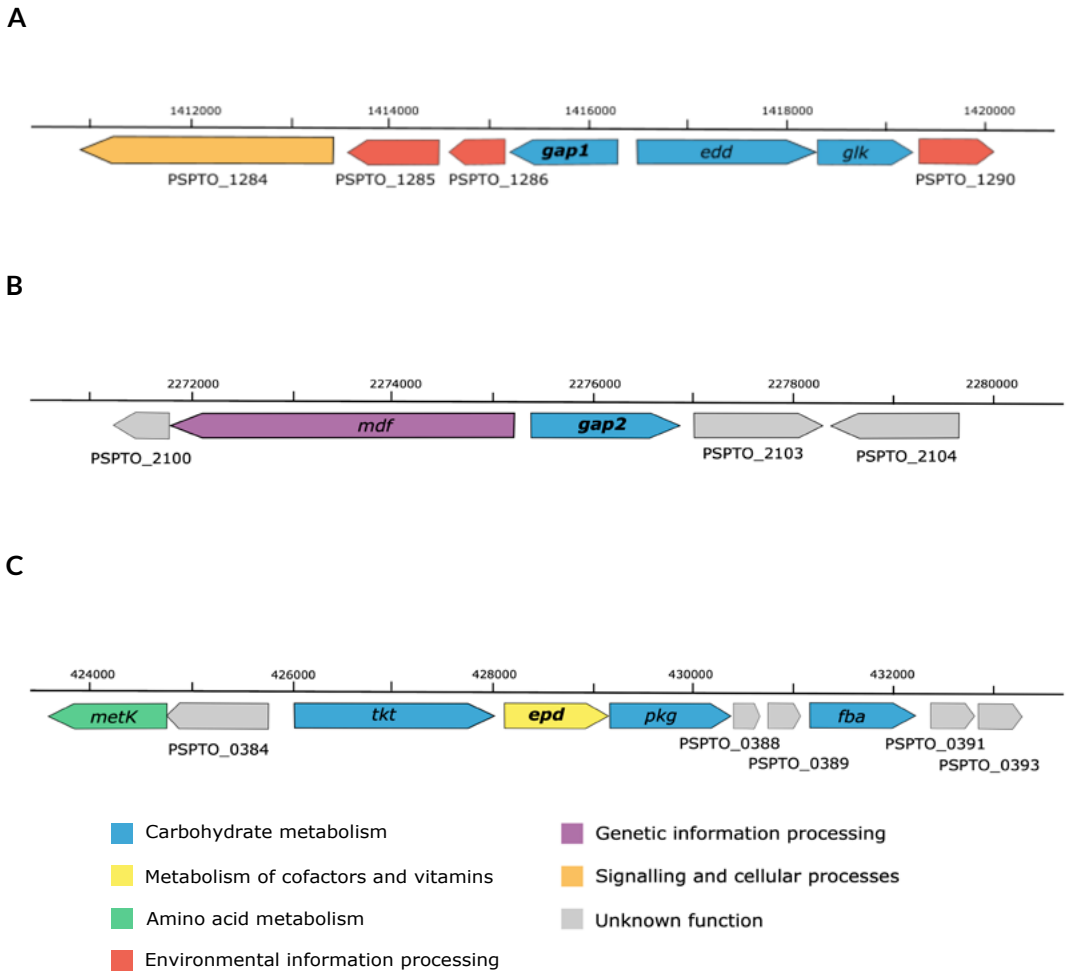

Figure SII.1. Genetic context of the Pto DC3000 gap genes.
A. *gap1* is encoded by the PSPT0_1287 gene, which is followed by genes encoding a sigma ECF factor and a putative cell surface signalling system (PSPTO_1286-1285-1284). It is divergently located to an operon that contains other genes involved in carbon metabolism: *edd* (6-phospho-gluconate dehydratase) and *glk* (glucokinase).
B. *gap2* (PSPTO_2102) is surrounded by a gene encoding a transcription-repair coupling factor (*mfd*), a hypothetical protein (PSPTO_2103) and a major facilitator family transporter (PSPTO_2104).
C. *gap3/epd* is usually found as part of an operon that includes *tkt* (transketolase), *gap3/epd*, *pgk* (phosphoglycerate kinase) and *fba* (fructose-bisphosphate aldolase), which are also enzymes of the central carbon metabolism.

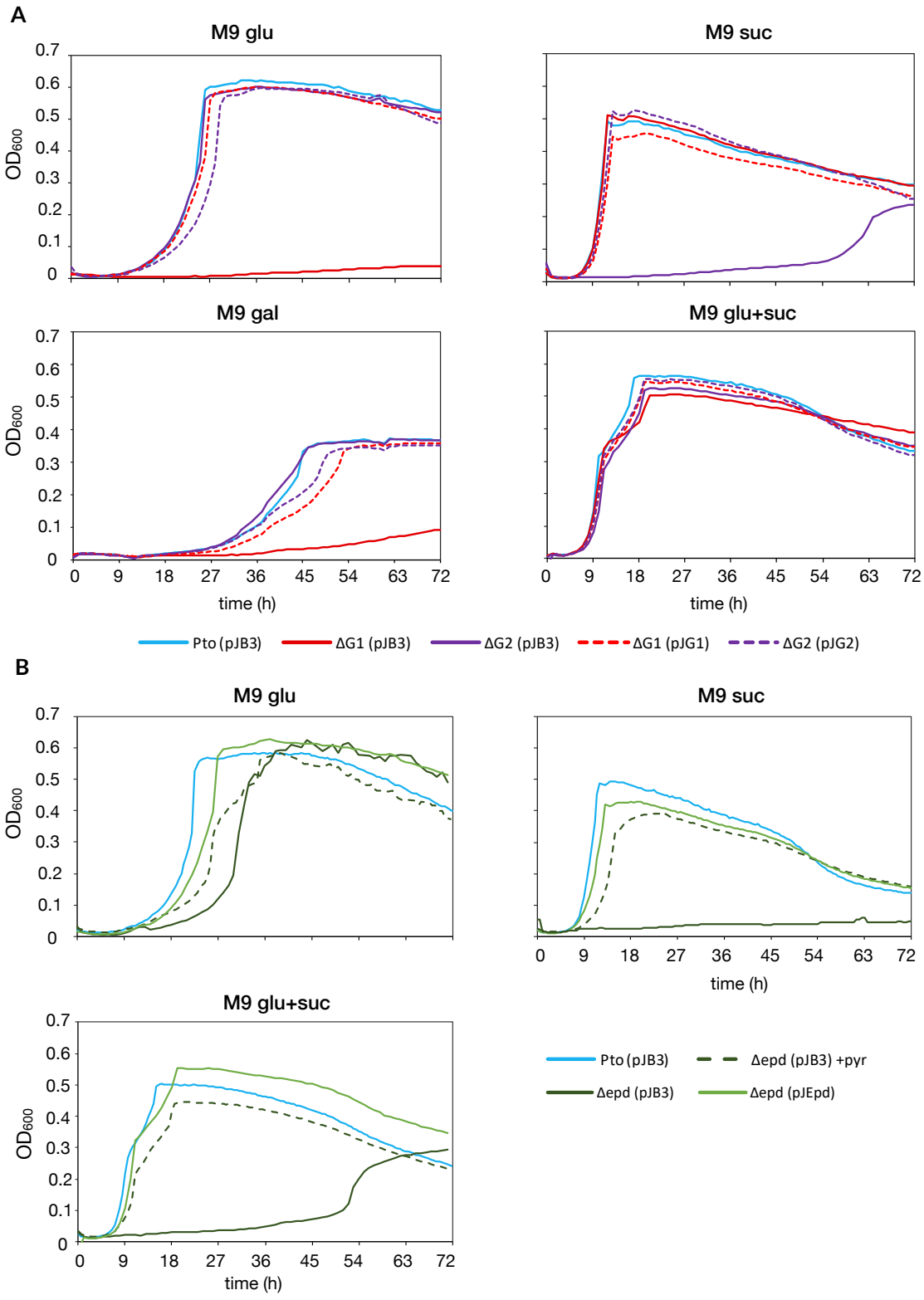
A
M9 glu
M9 suc
M9 gal
M9 glu+suc
OD600
time (h)
Pto (pJB3)
ΔG1 (pJB3)
ΔG2 (pJB3)
ΔG1 (pJG1)
ΔG2 (pJG2)
B
M9 glu
M9 suc
M9 glu+suc
OD600
time (h)
Pto (pJB3)
Δepd (pJB3) +pyr
Δepd (pJB3)
Δepd (pJEpd)

← **Figure SII.2. Growth of Pto gap mutants on minimal medium containing different carbon sources.**
Assays were carried out in liquid M9 minimal media with the indicated individual carbon sources. Glucose (M9 glu), succinate (M9 suc), glucose+succinate (M9 glu+suc) and galactose (M9 gal). Bacterial cultures were inoculated at OD_{600}=0.01 and incubated at 20ºC for 72 h with continuous shaking measuring the absorbance at 600 nm in 1 h periods in a Bioscreen C.
A. Growth of the *gap* deletion mutants with *in trans* expression of *gap1* and *gap2*.
B. Growth of the *epd* deletion mutant with and without pyridoxine supplementation (20 µM) and *in trans* expression of *epd*.

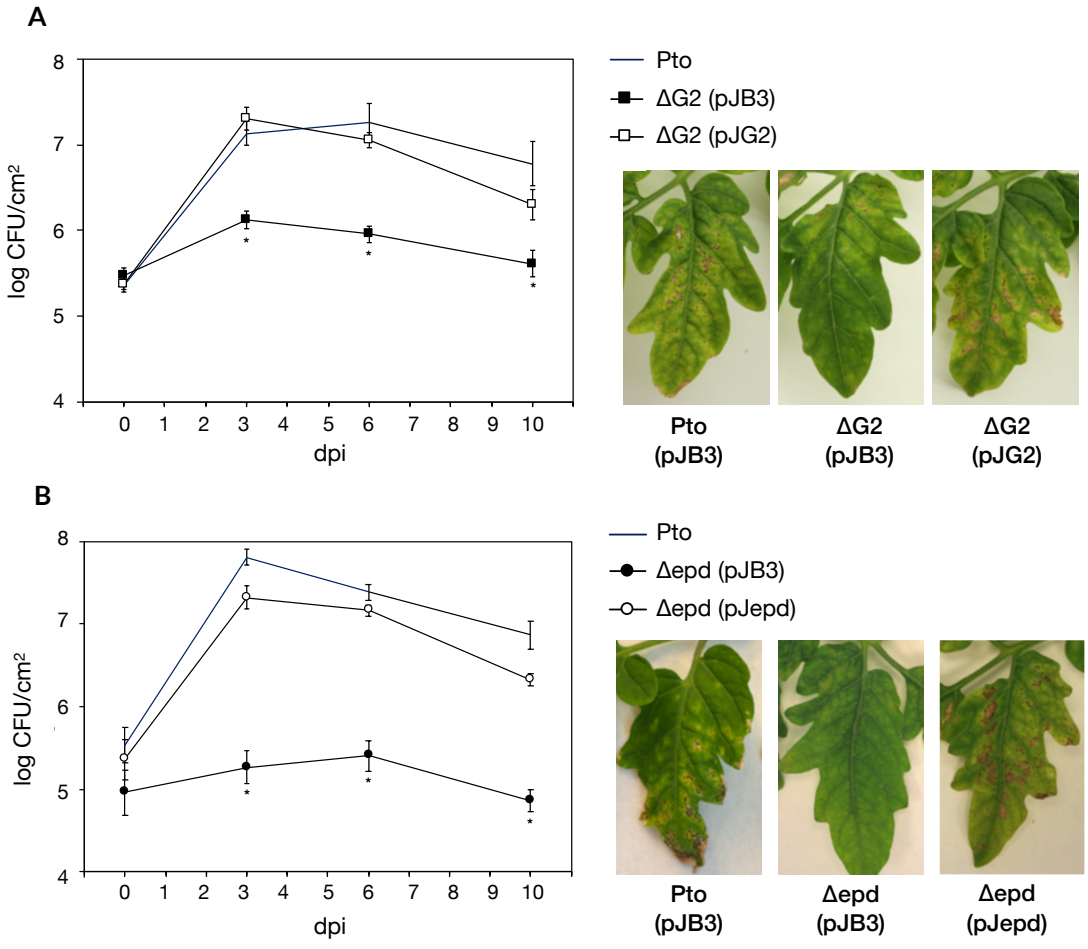

Figure SII.3. Pto bacterial growth and symptom development.
Time course of growth of Pto *gap* mutants in the primary leaves of tomato plants (*Solanum lycopersicum*). Leaves were inoculated with approximately 10^8 CFU/ml by spray and CFUs were quantified at 0, 3, 6 and 10 dpi. Error bars indicate standard deviation. Asterisks (*) indicate a statistically significant difference (One-way ANOVA followed by *post-hoc* Tukey test categories, p<0.01). Symptoms induced on tomato leaves 10 dpi with the indicated strains.
A. pJG2 complementation of the ΔG2 mutant. **B**. pJepd complementation of the Δepd mutant.

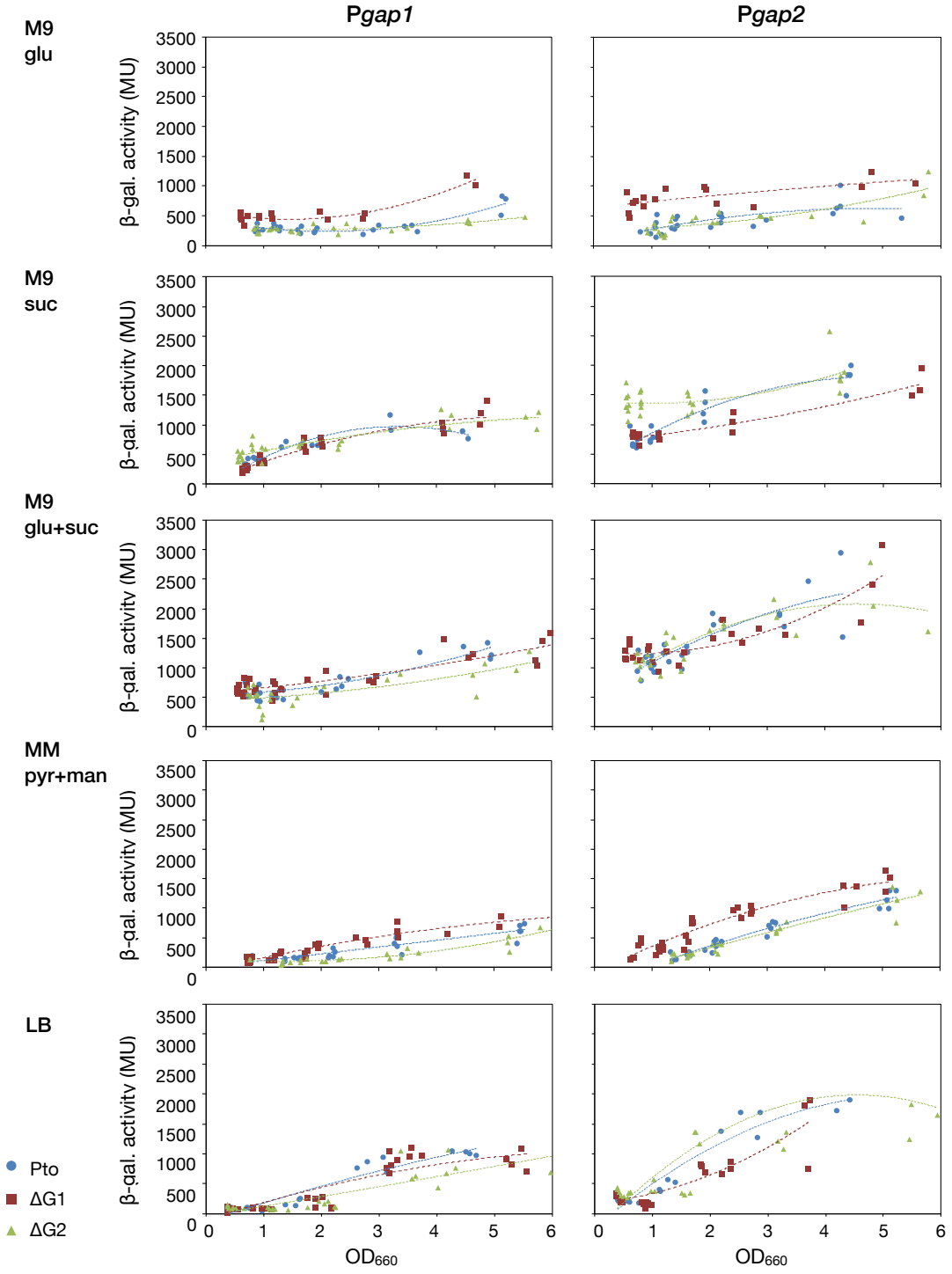
Pgap1
Pgap2
M9 glu
M9 suc
M9 glu+suc
MM pyr+man
LB
β-gal. activity (MU)
0
500
1000
1500
2000
2500
3000
3500
0
1
2
3
4
5
6
OD660
Pto
ΔG1
ΔG2

← **Figure SII.4. Expression of Pto gap1 and gap2 genes in different carbon source cultures.** β-Galactosidase activities of transcriptional fusions from Pto DC3000 *gap1* and *gap2* promoters to '*lacZ* were measured in the wild type (blue dots), ΔG1 mutant (red squares) and ΔG2 mutant (green triangles). Different dilutions of cultures in the indicated media were grown for 24 h (except for LB medium where cultures were grown for 6 h) at 20ºC in a microtiter plate, measured and represented in scatter plots, each strain data is fitted to a nonlinear regression. Carbon sources: glucose (glu), succinate (suc), glucose + succinate (glu+suc), pyruvate + mannitol (pyr+man).

Table SII.1. Oligonucleotides used for Pto *gap* mutants.

Name	Sequence (5'-3')
Directed mutants	
PtG1delA	aaagaattcGCAAACTGACCGACCGAAC
PtG1delB	CGACGCTGAATTTAAGTCATACAGCCGTCCTTC
PtG1delC	GACGGCTGTATGACTTAAATTCAGCGTCGCAGTG
PtG1delD	aaagaattcGATAAGAGTCTGGCGGCTTG
PtG2delA	AAAGAATTCCGTTCACGTCGAGCTTCTGGC
PtG2delB	CTTGATGCTTACTGCGGCCTGAGTCACGGGAACCTTC
PtG2delC	GGTTCCCGTGACTCAGCCGCAGTAAGCATCAAGCG
PtG2delD	aaagaattcGCCACGTCCGATTCAACAGTCC
PtG3delA	aaaggatccATCGCTCGTCGTGGTGGTGGTTATG
PtG3delB	GGTCAGCGACGCGGGGCATGACATTTTCGCCAGG
PtG3delC	GAAAATGTCATGCCCCGCGTCGCTGCCAATAACAG
PtG3delD	tttaagcttGCCCAGCGCTTCCAGTTC
Overexpression plasmids	
SEPtG1F	tttaagcttTGAACTCCAGGCTAACGTCT
SEPtG1R	aaaggatccGACCGGAGATTCAAGCA
SEPTG2F	ttagcatgcATTGTAACGGGGGAAGGTGG
SEPtG2R	aaatctagaCACGCCACAAAACAAAACGG
SEPtG3F	tttaagcttGTCCGCTCCCACATGACTG
SEPtG3R	ttaggatccACACGTTTACCTTGCAGATCG
Promoter constructions	
Pgap1_EcoRI	aaagaattcGTGATGAACTCCAGGCTAACG
Pgap1_PstI	aaactgcagCCGTCCTTCTGAATTTG
Pgap2_EcoRI	aaagaattcGGAAGGTCAGGCTCCAG
Pgap2_PstI	aaactgcagAACCTTCCACATGTAGGGG
Sequencing and verification	
M13U	GTAAAACGACGGCCAGT
M13R	CAGGAAACAGCTATGAC
F2	CTGCGATTCCGACTCGTCC
Z18	TAGCGGAACGTCGTGTAG
PtG1delI	AGCAGGTGCGCGTTCATTTC
PtG2delI	TCGTCAACGATAACCGCGTTGTG
PtG3delI	GTCAAAGCGCGTGAGGTATTCG

Uppercase: hybridization sequence, lowercase: added sequence, underlined: target sequence for a restriction enzyme.

Table SII.2. Enzymes of central carbon metabolism present in Pto as deduced from gene annotations.

Code	Enzyme	Gene name	PSPTO id
Entner-Doudoroff pathway (ED)			
1	Gluconokinase	*gntV*	PSPTO_3564
2	6-phosphogluconate dehydratase	*edd*	PSPTO_1288
3	2-keto-3-deoxy-phosphogluconate aldolase	*eda-1*	PSPTO_1302
Emden-Meyerhoff-Parnas pathway (EMP)			
4	Glucokinase	*glk*	PSPTO_1289
5	Glucose-6-phosphate isomerase	*pgi*	PSPTO_0959
6	Fructose-1,6-bisphosphatase	*fbp*	PSPTO_5168
7	Fructose-bisphosphate aldolase	*fba*	PSPTO_0390
8	Glyceraldehyde-3-phosphate dehydrogenase	*gap-1*, *gap-2*	PSPTO_1287, PSPTO_2102
9	Phosphoglycerate kinase	*pgk*	PSPTO_0387
10	Phosphoglycerate mutase	*gpmA*	PSPTO_5327
11	Enolase	*eno-1*, *eno-2*	PSPTO_1554, PSPTO_4616
12	Pyruvate kinase	*pyk*	PSPTO_4337
13	Phosphoenolpyruvate synthase	*ppsa*	PSPTO_2292
Pentose phosphate pathway (PP)			
18	Glucose-6-phosphate-dehydrogenase	*zwf-1*, *zwf-2*	PSPTO_1300, PSPTO_3121
19	6-phosphoglucolactonase	*pgl*	PSPTO_1301, PSPTO_2765, PSPTO_3768
-	6-phosphogluconate dehydrogenase	*gnd*	PSPTO_3122
-	Ribulose-5-phosphate-3-epimerase	*rpe*	PSPTO_0566
-	Ribose-5-phosphate isomerase	*rpiA*	PSPTO_5289
-	Transketolase	*tkt*	PSPTO_0385, PSPTO_2401, PSPTO_2402
-	Transaldolase B	*tal*	PSPTO_2119
Other pathways			
14	Malate: quinone oxidoreductase	*mqo*	PSPTO_1136
15	Phosphoenolpyruvate carboxykinase	*pckA*	PSPTO_0239
16	Glucose dehydrogenase	*gcd*, *gcd-1*	PSPTO_2492, PSPTO_4196
17	Gluconolactonase	*gnl*	PSPTO_1345

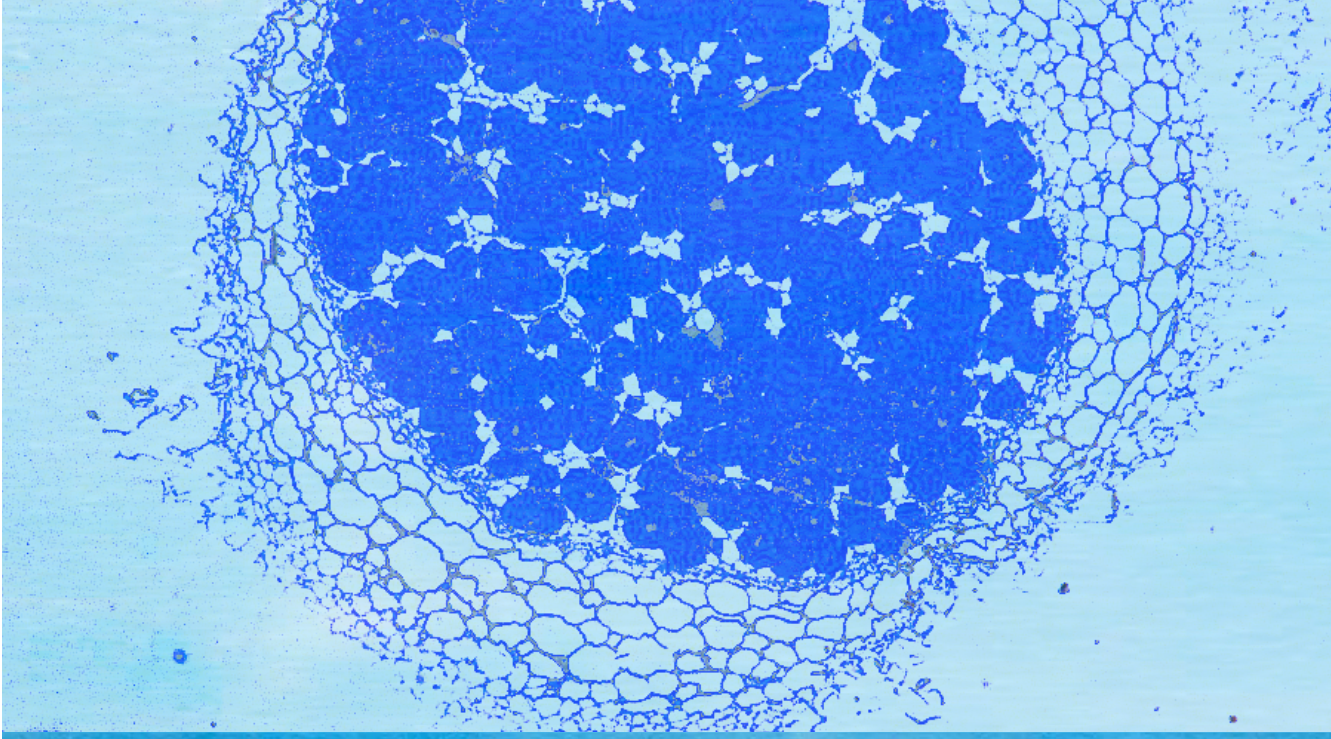

CHAPTER III

The *gap* gene of Rhizobium etli is required for both free life and symbiosis with common beans

CHAPTER III

Keywords:
Glyceraldehyde-3-phosphate dehydrogenase (GAPDH)
Rhizobia
Moonlighting protein
Cyclic diguanylate
Nitrogen fixation
Symbiosis

The *gap* gene of *Rhizobium etli* is required for both free life and symbiosis with common beans

Accepted for publication in Microbiological Research (2024).
https://doi.org/10.1016/j.micres.2024.127737
Ariana Casas-Román, María-José Lorite, Mariana Werner, Socorro Muñoz, María-Trinidad Gallegos and Juan Sanjuán
Department of Soil and Plant Microbiology, Estación Experimental del Zaidín (EEZ-CSIC), Granada, Spain.

ABSTRACT

Glyceraldehyde-3-phosphate dehydrogenase (GAPDH or Gap) is a ubiquitous enzyme essential for carbon and energy metabolism in most organisms. Despite its primary role in sugar metabolism, GAPDH is recognized for its involvement in diverse cellular processes, being considered a paradigm among multifunctional/moonlighting proteins. Besides its canonical cytoplasmic location, GAPDH has been detected on cell surfaces or as a secreted protein in prokaryotes, yet little is known about its possible roles in plant symbiotic bacteria. Here we report that *Rhizobium etli*, a nitrogen-fixing symbiont of common beans, carries a single *gap* gene responsible for both GAPDH glycolytic and gluconeogenic activities. An active Gap protein is required throughout all stages of the symbiosis between *R. etli* and its host plant *Phaseolus vulgaris*. Both glycolytic and gluconeogenic Gap metabolic activities likely contribute to bacterial fitness during early and intermediate stages of the interaction, whereas GAPDH gluconeogenic activity seems critical for nodule invasion and nitrogen fixation. Although the *R. etli* Gap protein is secreted in a c-di-GMP related manner, no involvement of the *R. etli gap* gene in c-di-GMP related phenotypes, such as flocculation, biofilm formation or EPS production, was observed. Notably, the *R. etli gap* gene fully complemented a double *gap1/gap2* mutant of *Pseudomonas syringae* for free life growth, albeit only partially *in planta*, suggesting potential specific roles for each type of Gap protein. Nevertheless, further research is required to unravel additional functions of the *R. etli* Gap protein beyond its essential metabolic roles.

BACKGROUND

Glyceraldehyde-3-phosphate dehydrogenase (GAPDH or Gap) is a housekeeping enzyme of energy metabolism conserved in virtually all organisms, prokaryotes and eukaryotes. Its main role resides in the glycolytic and gluconeogenic pathways, where it catalyses the interconversion of glyceraldehyde-3-phosphate and 1,3-bisphosphoglycerate, using NAD^+/NADH or $NADP^+$/NADPH as cofactors (Seidler, 2013). Typically, GAPDH assumes a homotetrameric configuration within the cytoplasm, each subunit with a mass of approximately 37 KDa. Structurally, the protein comprises two main domains: the N-terminal NAD^+ binding domain and the catalytic domain, which contains a conserved cysteine residue at its active site (Segal & Boyer, 1953; Sirover, 2014; Querol-García *et al*., 2017). GAPDH is often encoded by a single *gap* gene, however some genomes may contain two or more paralogous genes, like in *Bacillus spp*. and *Pseudomonas spp*. (Commichau *et al*., 2013; Elkhalfi *et al*., 2013; Casas-Román *et al*., 2024).

In addition to its primary involvement in glucose metabolism, GAPDH was one of the first proteins to be described as moonlighting or multifunctional. This distinction arises from the discovery of additional activities beyond its canonical role, reported in diverse organisms, including humans (Sirover, 2020), plants (Yang & Zhai, 2017) and bacteria (Gimenez *et al*., 2014; Jeffery, 2018). Moonlighting GAPDH often involves changes in the subcellular localization of the protein. For instance, GAPDH has been observed to be secreted or associated to the surface of both Gram-positive and Gram-negative bacterial cells (Sirover, 2011; Giménez *et al*., 2014; Ebner *et al*., 2016). However, no discernible motifs for extracytosolic trafficking have been identified in its sequence, and its translocation mechanism remains elusive (Kopeckova *et al*., 2020a). Furthermore, GAPDH has been reported to interact with different host components in both pathogens and beneficial bacteria, as well as being involved in adhesion and binding to extracellular matrices (Pancholi & Fischetti, 1992; Jin *et al*., 2005; Aguilera *et al*., 2012; Giménez *et al*., 2014; Ebner *et al*., 2016). However, little is known about the potential roles of GAPDH in plant-interacting bacteria.

Rhizobia are nitrogen-fixing symbiotic microorganisms that face the challenge of adapting to diverse soil environmental conditions while effectively colonizing plant roots. Their ability to perform biological nitrogen fixation is possible thanks to their symbiotic association with legumes (Olivares *et al*., 2013). The dual lifestyle of rhizobia, is greatly influenced by their ability to acquire energy from available carbon compounds (Poole *et al*., 2018). Catabolism of most hexoses in rhizobia takes place through the Entner-Doudoroff (ED) pathway, alternative to the Embden-Meyerhof-Parnas (EMP) route present in *E. coli* (Stowers, 1985). Instead, rhizobia are able to use

the EMP pathway in a gluconeogenic manner, leading to a functional cyclic ED pathway. Galactose catabolism does not follow this scheme nor does it enter glycolysis through the Leloir pathway as in *E. coli*. Galactose is rather catabolized through an analogous route to the ED pathway, known as the De Ley-Doudoroff pathway, ultimately yielding glyceraldehyde-3-phosphate and pyruvate (Arias & Cerveñansky, 1986; Geddes & Oresnik, 2014).

The permanent dialogue between microbes and their eukaryotic hosts during the establishment of an interaction, such as the association of rhizobia with legume plants, triggers a series of physiological, genetic, and cellular adaptive responses that highlight the critical role of bacterial signal transduction. This association entails a lifestyle conversion, necessitating a precisely regulated genetic program for the successful transition from a saprophytic existence in the soil to an intimate symbiotic relationship with the plant host. To facilitate a swift physiological response, it becomes imperative to synchronize the expression of bacterial determinants required for plant colonization and invasion, while adapting to varying environmental conditions. This coordination is made possible through the transduction of signals *via* second messengers, among which bis-(3′,5′)-cyclic dimeric guanosine monophosphate (c-di-GMP, cdG) stands out (Pérez-Mendoza *et al*., 2014; Krol *et al*., 2020). c-di-GMP serves as a pivotal regulator of diverse cellular processes, including cell to cell signalling, cell cycle progression and virulence (Römling *et al*., 2013). However, it is primarily known for its central role in orchestrating the transition between a planktonic/motile and a sessile/biofilm life style in bacteria. To this end, c-di-GMP stimulates the biosynthesis of different extracellular matrix components while inhibiting various forms of motility. It modulates the production of critical proteins for maintaining the structural integrity of bacterial biofilm matrices, including actively secreted proteins, adhesins, and motility organelles, such as flagella and pili. Moreover, c-di-GMP directly or indirectly governs the production and secretion of certain exopolysaccharides (EPS) and other matrix components (Fong & Yildiz, 2015).

A recent study of the extracellular proteome of *Rhizobium etli* revealed that elevated c-di-GMP levels promoted the secretion of various extracellular proteins potentially involved in adhesion and biofilm formation, but, unexpectedly, also promoted the export of cytoplasmic proteins to the extracellular medium (Lorite *et al*., 2023). Remarkably, most of these cytoplasmic proteins had been previously characterised as moonlighting proteins in other organisms. One of these cytoplasmic proteins found in the extracellular medium was GAPDH. Interestingly, c-di-GMP not only promoted

the exportation of the Gap protein but also increased the number of extracellular Gap proteoforms that could be resolved by two-dimensional gel electrophoresis, suggesting a link between c-di-GMP and the posttranslational modification and secretion of this cytoplasmic protein (Lorite *et al*., 2023).

The *Rhizobium etli* Gap protein is a 336 amino acid protein encoded by the *gap* gene (RHE_CH03496, 1011 pb). Located upstream of *gap* is the *tkt* gene, encoding another metabolic protein, transketolase. Downstream of *gap*, an ORF encoding a hypothetical protein that is conserved in other bacteria of the *Rhizobium* genus, is present. Currently, it remains unknown whether these three genes are transcribed as a single operon, and the location or type of promoter regulating their expression. However, it is noteworthy that the genetic tandem *tkt-gap* is conserved not only in many rhizobia, but also in other α- and β-proteobacteria (Fig. SIII.1).

In this study, we investigate the *gap* gene of *Rhizobium etli* CE3, aiming to elucidate its roles in both free-living conditions and during bacterial interaction with the host plant *Phaseolus vulgaris*. Additionally, we endeavour to uncover potential moonlighting roles of the Gap protein encoded by this gene.

SPECIFIC MATERIALS AND METHODS

Bacterial strains and growth conditions

Bacterial strains and plasmids used in this work are listed in Tables M.1 and M.2 in the general Materials and Methods section. *Rhizobium etli* strains were routinely grown in TY broth (Beringer, 1974) at 28°C. Luria-Bertani (LB) broth (Sambrook *et al*., 1989) was used for *Escherichia coli* and *Pseudomonas syringae* strains, which were grown at 37°C and 28°C respectively.

Two minimal media were used for *Rhizobium etli*: MMY medium (Meneses *et al*., 2010) and MMR medium (Robertsen *et al*., 1981). M9 minimal medium was used for Pto DC3000 strains assays (Sambrook *et al*., 1989). When required, antibiotics were added (μg/ml): nalidixic acid (20), streptomycin (100), spectinomycin (100), kanamycin (50), tetracycline (10), rifampicin (10) or ampicillin (100).

Bacterial mutant and genetic constructions

A Δ*gap* mutant was obtained by deleting the *gap* gene (RHE_CH03496) of *R. etli* CE3 (Ret). First, the *gap* gene flanking regions were PCR-amplified using specific primers (Table SIII.1) and cloned into vector pK18*mobsacB*, which does not replicate

and behaves as a suicide plasmid in *Ret*. The pK18Δgap plasmid bears a 1274 bp PstI fragment with a deletion from nucleotide 21 to 1005 of the *gap* gene. This pK18Δgap plasmid was electroporated into *E. coli* S17.1 for posterior conjugation into *R. etli* CE3. Rhizobial transconjugants containing the integrated plasmid were selected in medium with kanamycin. Afterwards, transconjugants were grown in liquid media without antibiotic to allow cointegrate loss, and plated on rich medium supplemented with sucrose (15% wt/vol). To select for double recombinants, colonies were replica plated and Km^s $sucrose^R$ colonies chosen for verification by PCR and sequencing. The *Δgap* mutant named AC1D, was confirmed to carry a deletion of 97% of the *gap* gene.

Expression plasmids bearing different variants of the *gap* gene were constructed for *in trans* complementation of the deletion mutant (Table M.2). A DNA fragment including the *gap* gene was amplified by PCR from chromosomal DNA using specific oligonucleotides (Table SIII.1). The amplified fragment was ligated into pCR2.1-TOPO, sequenced and then cloned into vector pJB3Tc19 to obtain the pJGap plasmid, where the *gap* gene is expressed from the vector borne *lac* promoter. A DNA fragment containing the *gap* gene coding sequence with a single nucleotide change (G461>C), converting Cys154 into a Ser residue of the Gap protein, was synthesized (*Proteogenix*), and cloned into pJB3Tc19 to obtain the pJMCy plasmid. The resulting plasmids were electroporated into *E. coli* S17.1 for posterior conjugation into *R. etli* CE3.

Additional methods used in this chapter are previously described in the general *Materials and Methods* section:

- Growth assays
- *Phaseolus* symbiosis assays
- Nodule histology and microcopy
- Tomato plant infection assays
- Biofilm and flocculation assays
- Exopolysaccharide production determination
- GAPDH enzymatic activity assays
- Statistical analysis

RESULTS

A Rhizobium etli gap mutant is impaired for growth in multiple carbon sources

R. etli growth assays were carried out in media supplemented with defined carbon sources. Glucose and succinate were selected as representative glycolytic and gluconeogenic carbon sources, respectively. Galactose was also evaluated as it is metabolized through the alternative De Ley-Doudoroff pathway (De Ley & Doudoroff, 1957). Fructose and pyruvate were also tested (Fig. SIII.2).

The AC1D *Δgap* mutant exhibited significant growth deficits since it was unable to grow when a single carbon source, either glucose, galactose or succinate, was provided. However, it displayed limited growth when both glycolytic and gluconeogenic pathway carbon sources (i.e., glucose + succinate) were present simultaneously. Yet, the growth rate of the mutant was significantly lower than that of the wild-type (Fig. RIII.1). The plasmid pJGap, which bears the native sequence of the *gap* gene, effectively recovered the wild type phenotype in the AC1D mutant, enabling growth on all carbon sources (Fig. RIII.1). In contrast, the pJMCy plasmid, harboring a site-directed mutated *gap* gene, failed to restore the growth deficiencies of the *gap* mutant, allowing only a slight incrementation in growth compared to the AC1D mutant (Fig. RIII.1A and Fig. SIII.3). This outcome was expected since this specific mutation resulted in the substitution of Cys154 with Ser (Cys154Ser), thereby impacting the active site of the Gap protein (Boschi-Muller *et al*., 1998).

Certain bacteria, such as pseudomonads, possess specialized Gap proteins. In *P. syringae* pv. tomato (Pto) DC3000, Gap1 predominantly fulfills a glycolitic function, whereas Gap2 primarily functions in gluconeogenesis (Casas-Román *et al*., 2024). To gain deeper insights into the metabolic phenotypes of Ret Gap, we introduced the pJG1 and pJG2 plasmids bearing *gap1* and *gap2* genes from Pto DC3000, respectively, into the AC1D mutant. The introduction of the *gap1* gene led to a similar recovery of growth as observed with the pJGap plasmid, as the strain complemented with pJG1 exhibited a growth pattern akin to the wild type in all tested carbon sources.

Figure RIII.1. Growth of *Rhizobium etli gap* strains on different media.
Assays were carried out in (A) solid or (B) liquid MM with defined carbon sources: glucose (glu), succinate (suc), galactose (gal).
A. Growth on solid media. Pictures were taken after incubation for 7 days at 28ºC.
B. Growth curves on liquid media. Bacterial cultures were incubated for 72h at 28ºC with continuos shaking, absorbance was measured every hour in a Bioscreen C.

→

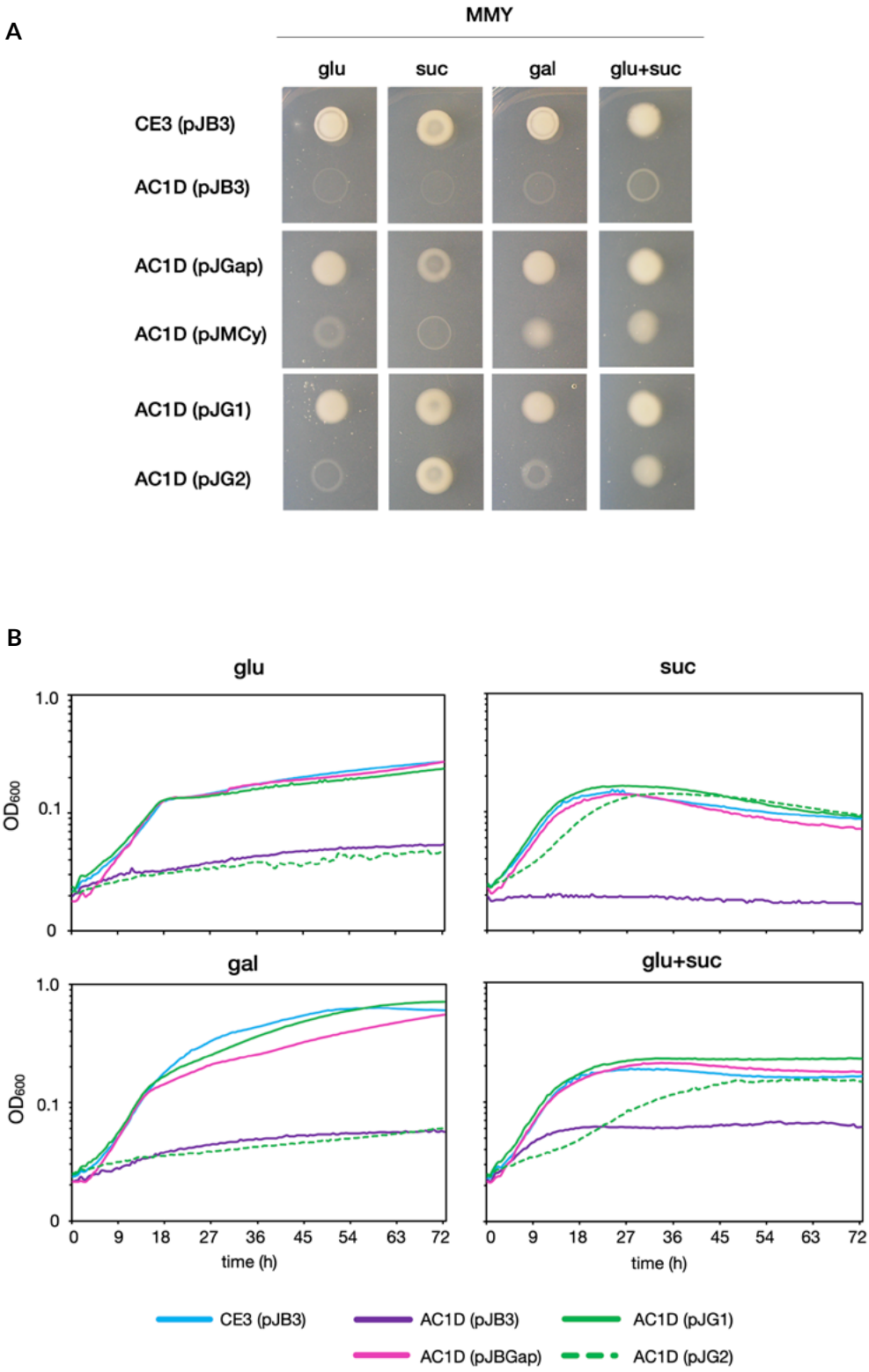
A
MMY
glu
suc
gal
glu+suc
CE3 (pJB3)
AC1D (pJB3)
AC1D (pJGap)
AC1D (pJMCy)
AC1D (pJG1)
AC1D (pJG2)
B
glu
suc
gal
glu+suc
OD600
1.0
0.1
0
0 9 18 27 36 45 54 63 72
time (h)
CE3 (pJB3)
AC1D (pJB3)
AC1D (pJG1)
AC1D (pJBGap)
AC1D (pJG2)

However, upon introduction of the *gap2*, the AC1D mutant only regained growth on gluconeogenic compounds like succinate, but not on glycolytic ones like glucose. Notably, the Gap2 protein was neither able to complement the *R. etli* Gap mutant for growth in galactose (Fig. RIII.1). Galactose metabolism in *R. etli* proceeds through the De Ley-Doudoroff pathway, resulting in the formation of glyceraldehyde-3-phosphate and pyruvate, the same products obtained through the ED pathway (Arias & Cerveñansky, 1986; Geddes & Oresnik, 2014).

R. etli GAPDH catalytic activities

The wild type strain CE3 displayed Gap glycolytic activity only when NAD^+ was provided as a cofactor, and this activity was significantly enhanced when carrying the pJGap plasmid (Fig. RIII.2A). As expected, no Gap glycolytic activity was detected in the AC1D mutant, unless it was complemented with the pJGap plasmid (Fig. RIII.2A). No activity could be detected in the AC1D mutant carrying pJMCy, thus confirming that the substitution of Cys154 with Ser abolishes the activity of the Gap enzyme. Glycolytic Gap activity was also quantifiable in the AC1D mutant carrying *in trans* either the Pto Gap1 or Gap2 genes. However, enzymatic activity levels were markedly higher with the Gap1 gene plasmid (Fig. RIII.2A). Furthermore, Gap1 activity was dependent on NAD^+, whereas Gap2 required NADP as cofactor (Fig. RIII.2A), as previously reported (Casas-Román *et al*., 2024).

Apparent gluconeogenic GAPDH activity was observed in all the strains, wild type and mutants (Fig. RIII.2B). This probably reflects basal activity levels owing to the substrate remaining from the first of the two reactions involved in the assay, as described in materials and methods. Significant gluconeogenic Gap activity was detected in both the wild type and the mutant carrying the pJGap plasmid, demonstrating the expression of the multicopy *R. etli gap* gene. In contrast, the pJMCy plasmid, also in multicopy, did not enhance the basal levels of gluconeogenic Gap activity measured (Fig. RIII.2B).

Figure RIII.2. GAPDH activity assays.
Bacteria were culture in liquid TY and GAPDH activity was determined in cells extracts as described in Materials and Methods. Graphs depict average specific activity of each strain. Error bars correspond to the standard deviation and different letters indicate significant differences (Tukey test, $p<0.05$).
A. Glycolytic GAPDH activity. NAD or NADP were used as cofactors.
B. Gluconeogenic GAPDH activity. NADPH indicated when added as a co-substrate.

→

A

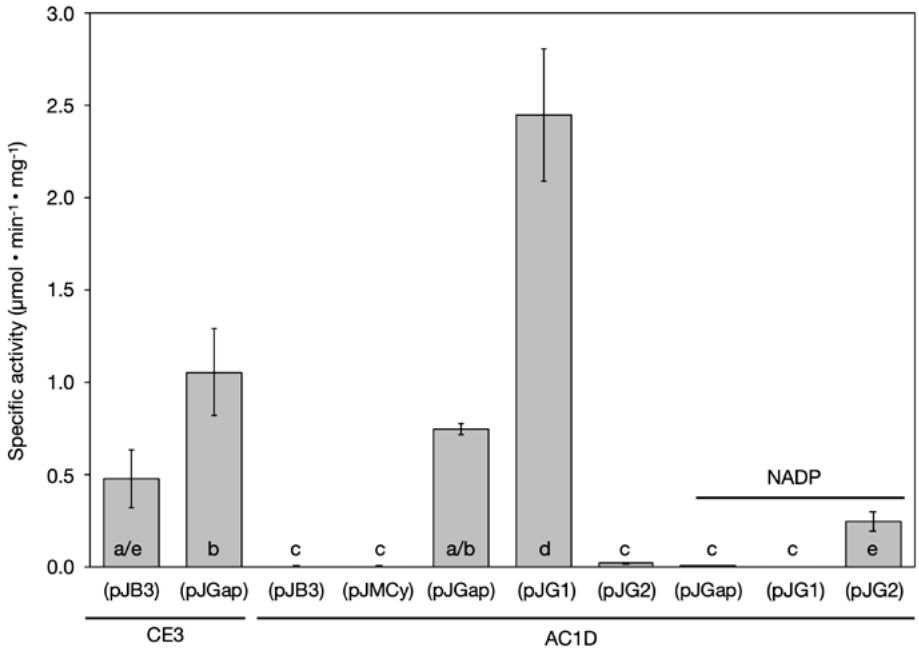
Specific activity (µmol • min-1 • mg-1)
3.0
2.5
2.0
1.5
1.0
0.5
0.0
a/e
b
c
c
a/b
d
c
c
c
e
NADP
(pJB3)
(pJGap)
(pJB3)
(pJMCy)
(pJGap)
(pJG1)
(pJG2)
(pJGap)
(pJG1)
(pJG2)
CE3
AC1D

B

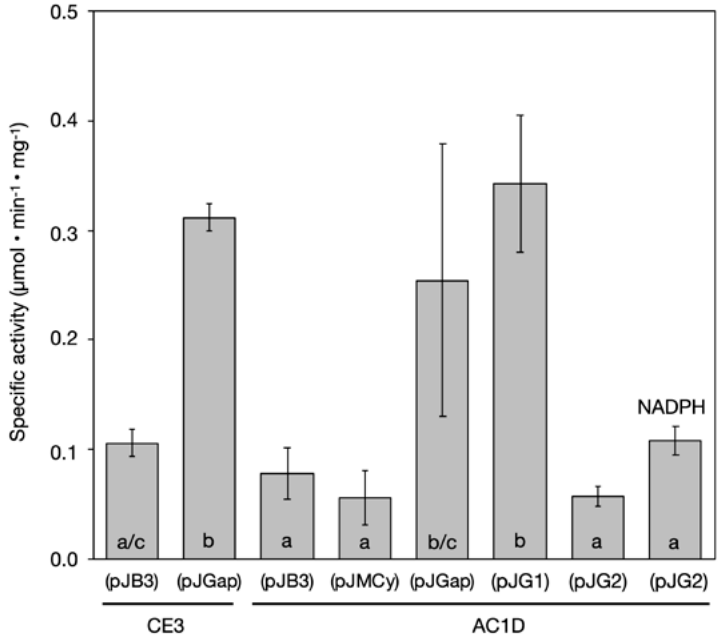
Specific activity (µmol • min-1 • mg-1)
0.5
0.4
0.3
0.2
0.1
0.0
a/c
b
a
a
b/c
b
a
a
NADPH
(pJB3)
(pJGap)
(pJB3)
(pJMCy)
(pJGap)
(pJG1)
(pJG2)
(pJG2)
CE3
AC1D

Furthermore, basal gluconeogenic Gap activity was significantly augmented in the AC1D mutant with the presence of Pto *gap1* and *gap2* genes *in trans*. It is noticeable that Pto Gap2 protein exhibited a lower activity level compared to Gap1 in *R. etli* (Fig. RIII.2B), despite Gap2 being shown to predominantly have GAPDH gluconeogenic activity in Pto (Casas-Román *et al*., 2024).

In summary, these results strongly support that the *R. etli gap* gene encodes a single protein possessing both glycolytic and gluconeogenic GAPDH enzyme activities that require NAD^+/NADH as cofactors. Furthermore, the Cys154 residue of Ret Gap seems to be essential for both activities.

Effect of *gap* mutations in symbiosis

To test the impact of *gap* deletion and overexpression in the symbiotic association between *R. etli* and *P. vulgaris* different assays were performed to assess nodule formation, symbiotic efficiency and nodule invasion.

Nodulation kinetics assays revealed that the AC1D *Δgap* mutant failed to induce nodule formation at the same rate as the wild type (Fig. RIII.3A). Nodules induced by the wild type were observable as early as day 8 after inoculation, with the number of nodules increasing exponentially until 17 dpi. These wild type nodules were predominantly located in the upper part of the root, near the crown, and exhibited a spherical, pink-coloured appearance, indicative of nitrogen-fixing activity. In contrast, the mutant AC1D induced visible bumps or swellings only after 10 dpi, which, however, did not develop into mature nodules. Furthermore, the mutant formed significantly fewer nodules, which were smaller in size and exhibited a white to yellowish coloration, appearing scattered throughout the root system. Expression of the *R. etli* wild type *gap* gene *in trans* (plasmid pJGap) fully restored the nodulation phenotype of the AC1D mutant to wild type nodulation kinetics, in contrast to the pJMCy plasmid carrying the *R. etli gapC154S* mutant gene (Fig. RIII.3A), as expected.

To discern whether glycolytic and/or gluconeogenic Gap activities are indispensable for rhizobia during the symbiotic process, we tested AC1D derivatives carrying the pJG1 and pJG2 plasmids. The *gap1* construct completely restored the AC1D nodulation phenotype, rendering it indistinguishable from the wild type. Similarly, the AC1D mutant expressing the *gap2* gene was able of inducing nitrogen-fixing nodules, albeit at a significantly slower rate than the wild type (Fig. RIII.3A).

The symbiotic efficiency assays conducted in Leonard jars confirmed that the AC1D *Δgap* mutant failed to establish a nitrogen-fixing symbiosis with *P. vulgaris*.

This deficiency was evident from the visual appearance of the plants, which were markedly smaller and exhibited a yellow coloration characteristic of nitrogen deficiency, resembling the non-inoculated control plants (Fig. RIII.3B). Indeed, as seen in Fig. RIII.3C, the shoot dry weight (a), shoot fresh weight (b) and total N per plant (c) were all significantly lower in plants inoculated with the mutant compared to those inoculated with the wild type strain. Introduction of the pJGap plasmid fully complemented the AC1D mutant, restoring it to a wild-type symbiotic phenotype as evidenced by all determined plant and symbiotic parameters. This was not the case, however, with the pJMCy plasmid expressing the GapC154S mutant protein (Fig .RIII.3B and C).

The introduction of plasmids pJG1 or pJG2 also enabled the AC1D mutant to regain its ability to form a nitrogen-fixing symbiosis with its host (Fig. RIII.3B and C). Interestingly, plants inoculated with the mutant bearing *gap1* exhibited similar shoot dry weights and N contents as those inoculated with the wild type, supporting the full complementation of the symbiotic phenotype. In contrast, plants inoculated with the AC1D mutant carrying the *gap2* gene displayed smaller shoot dry weights and reduced N contents compared to those inoculated with the wild type strain (Fig. RIII.3C (a) and (c)). This partial complementation by the pJG2 plasmid was consistent with the results observed in the nodulation kinetics assays described above. It was also noteworthy that the nodules formed by the AC1D (pJG2) strain were generally smaller than those formed by the wild type (Fig. RIII.3C (d)).

To assess whether nodule invasion by the mutant strains was taking place, we conducted observations of the nodule internal structure. At 28 days post-inoculation, the nodules induced by the AC1D mutant showed no infected plant cells, and therefore absence of bacteroids. This was in stark contrast to the nodule invasion pattern induced by the wild type, where the majority of central nodule cells were filled with bacteroids (Fig. RIII.4). We can thus conclude that the AC1D *gap* mutant presents a Nod^{d} Fix^{-} (nodulation deficient and non-fixing) symbiotic phenotype, characterised by a lack of invasion of the nodule cells. Given the significant nodulation delay and decreased shoot biomass and N contents observed for the AC1D (pJG2) strain, we also examined the internal structure of the nodules induced by this strain at both 21 and 28 dpi. At 21 dpi the invaded area appeared much smaller compared to nodules formed by the wild type strain. However, this difference was notably diminished a week later, by 28 dpi (Fig. RIII.4). These observations corroborate that the Pto *gap2* protein can indeed restore the symbiotic capacity in the AC1D mutant, albeit less efficiently than the *gap1* gene.

A

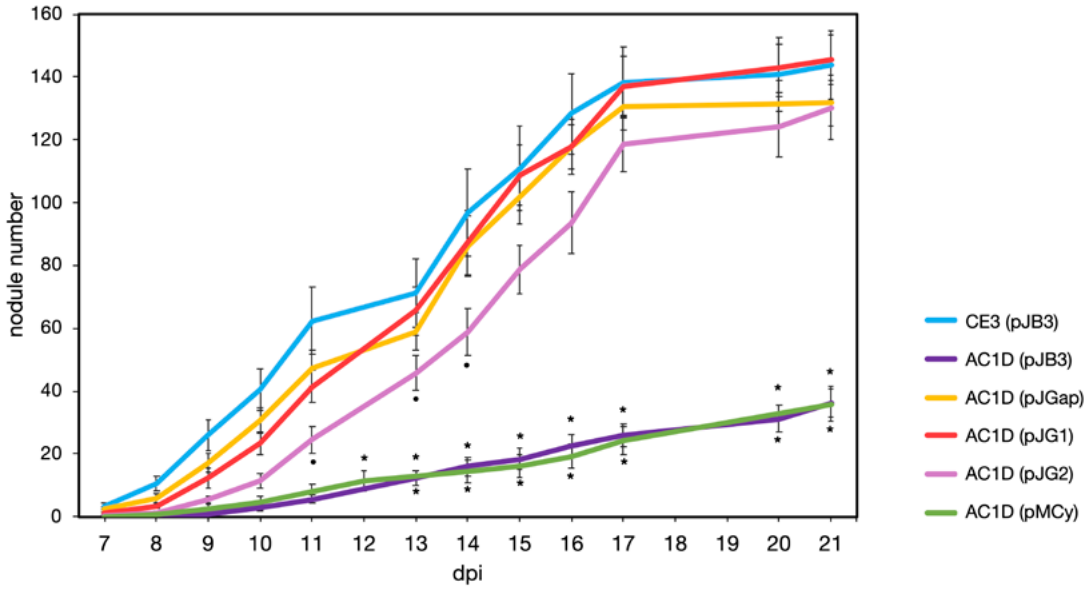
nodule number
dpi
CE3 (pJB3)
AC1D (pJB3)
AC1D (pJGap)
AC1D (pJG1)
AC1D (pJG2)
AC1D (pMCy)

B


CE3 (pJB3)
AC1D (pJGap)
AC1D (pJG1)
AC1D (pJG2)

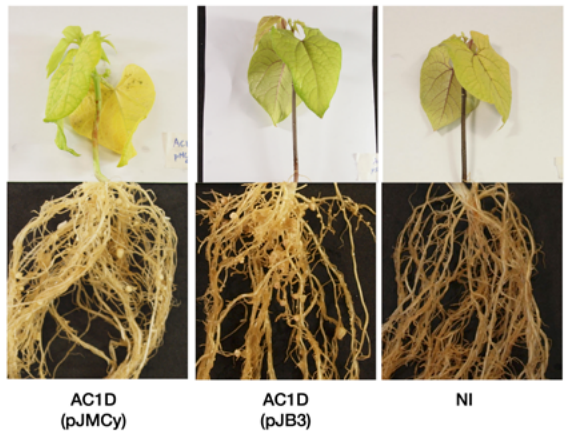
AC1D (pJMCy)
AC1D (pJB3)
NI

C

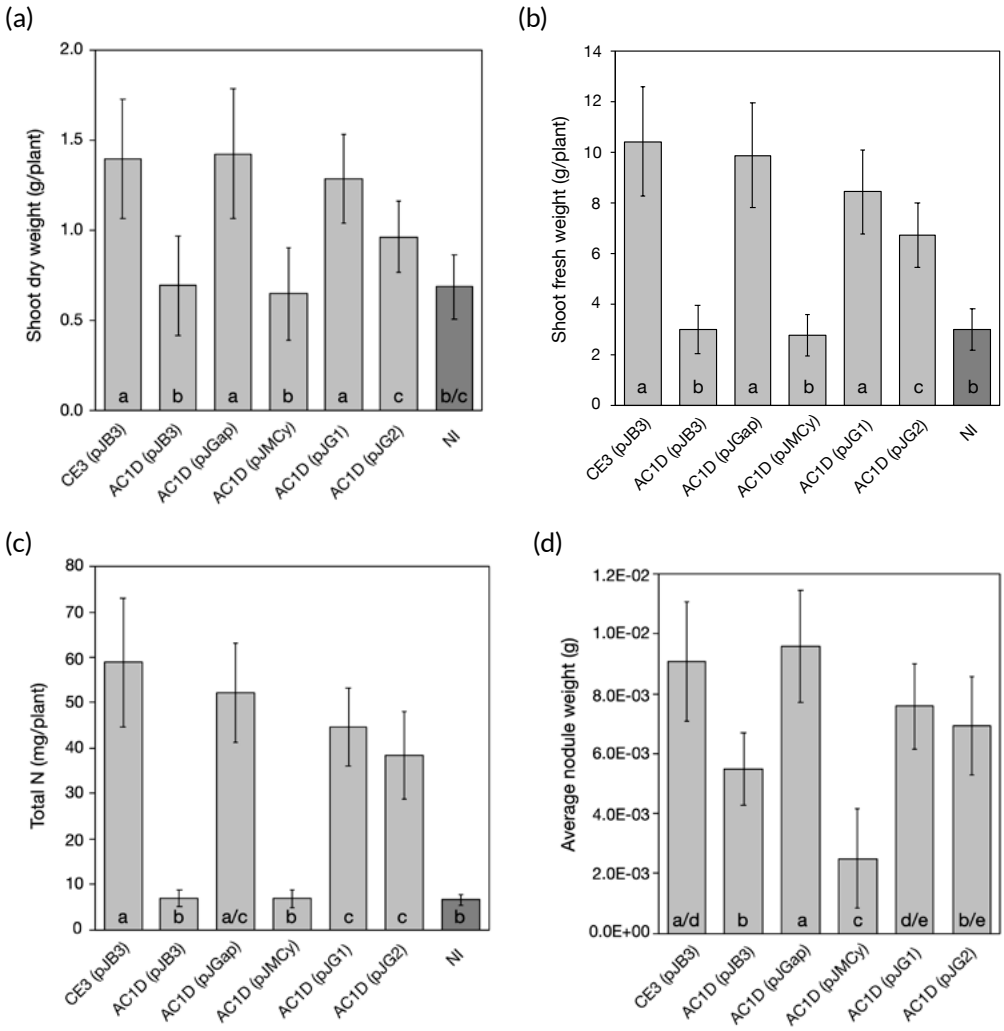

Figure RIII.3. Impact of *gap* mutations on the symbiotic interaction of *R. etli* with *Phaseolus vulgaris*.

A. Nodulation kinetics. Plants were grown in pouches and nodules counted daily. Bars indicate standard error. Dots (•) indicate a statistically significant difference ($p<0.05$) between CE3 (pJB3) and AC1D (pJG2) until 14 dpi. Asterisks (*) indicate significant differences ($p<0.01$) between CE3 (pJB3) and AC1D (pJB3) and AC1D (pJMCys).

B. Pictures of representative plants (shoots and roots) inoculated with the wild-type or mutant strains, taken at 28 dpi.

C. Symbiotic eficiency of *R. etli gap* mutants. Shoot dry weight (a), shoot fresh weight (b), total nitrogen content (c), and average nodule fresh weight (d) of *P. vulgaris* plants grown in Leonard jars, at 28 dpi. NI, non-inoculated. Bars correspond to the standard deviation and different letters indicate significant differences (Tukey test, $p<0.01$).

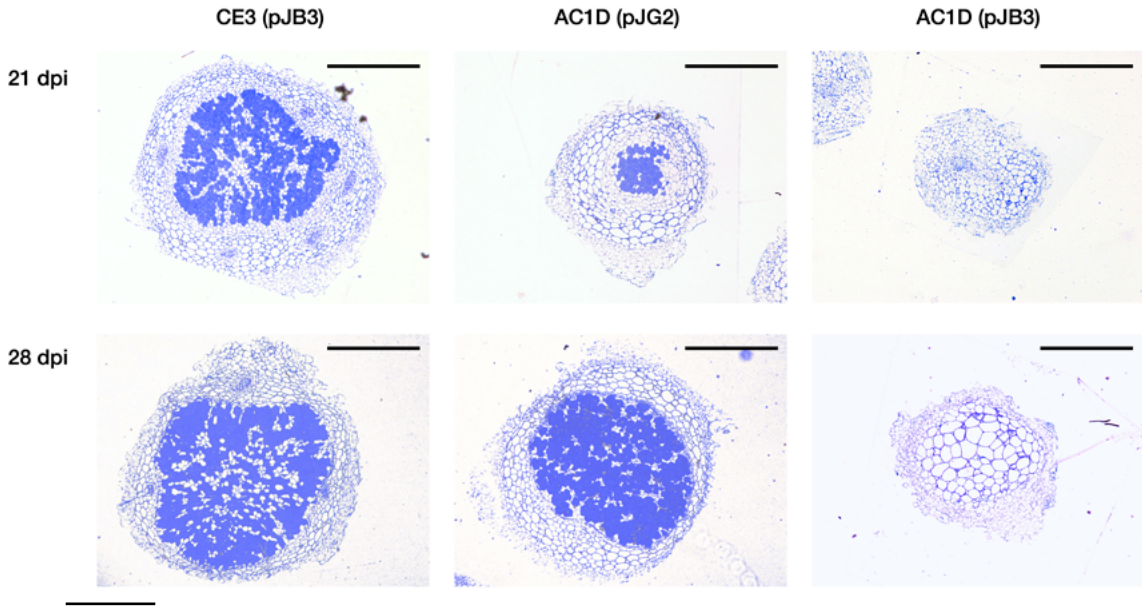

Figure RIII.4. Histology of nodules.
Representative semithin (1 µm) sections stained with 1% (w/v) toluidine blue at 21 and 28 dpi. Scale bars of 500 µm are depicted. Absence of bacteroids in the AC1D mutant, and delayed invasion of the AC1D complemented with the *gap2* gene of P. syringae, are shown.

Expression of the *R. etli gap* gene in other bacteria

We further investigated the capacity of the *R. etli gap* gene to substitute the *gap* genes of other unrelated bacteria. To this end, we used the pJGap plasmid to complement a Pto Gap$^-$ mutant. This bacterium carries two *gap* genes, *gap1* and *gap2*, specialized in glycolytic and gluconeogenic activities, respectively (Casas-Román *et al*., 2024). Upon introduction of pJGap in the Pto ΔG1/2 double mutant, complete recovery of the mutant's growth on all single carbon sources tested was observed (Fig. RIII.5A). This finding confirms that the rhizobial enzyme possesses both Gap activities, even when expressed in a heterologous genetic background.

To evaluate the potential impact of the *R. etli gap* gene on the virulence of Pto, tomato infection assays were performed to determine the virulence of the ΔG1/2 mutant complemented with pJGap. As previously reported, the ΔG1/2 mutant population did not increase and remained significantly lower than that of the wild type (Casas-Román *et al*., 2024), matching the nearly asymptomatic appearance of the tomato leaves (Fig. RIII.5B).

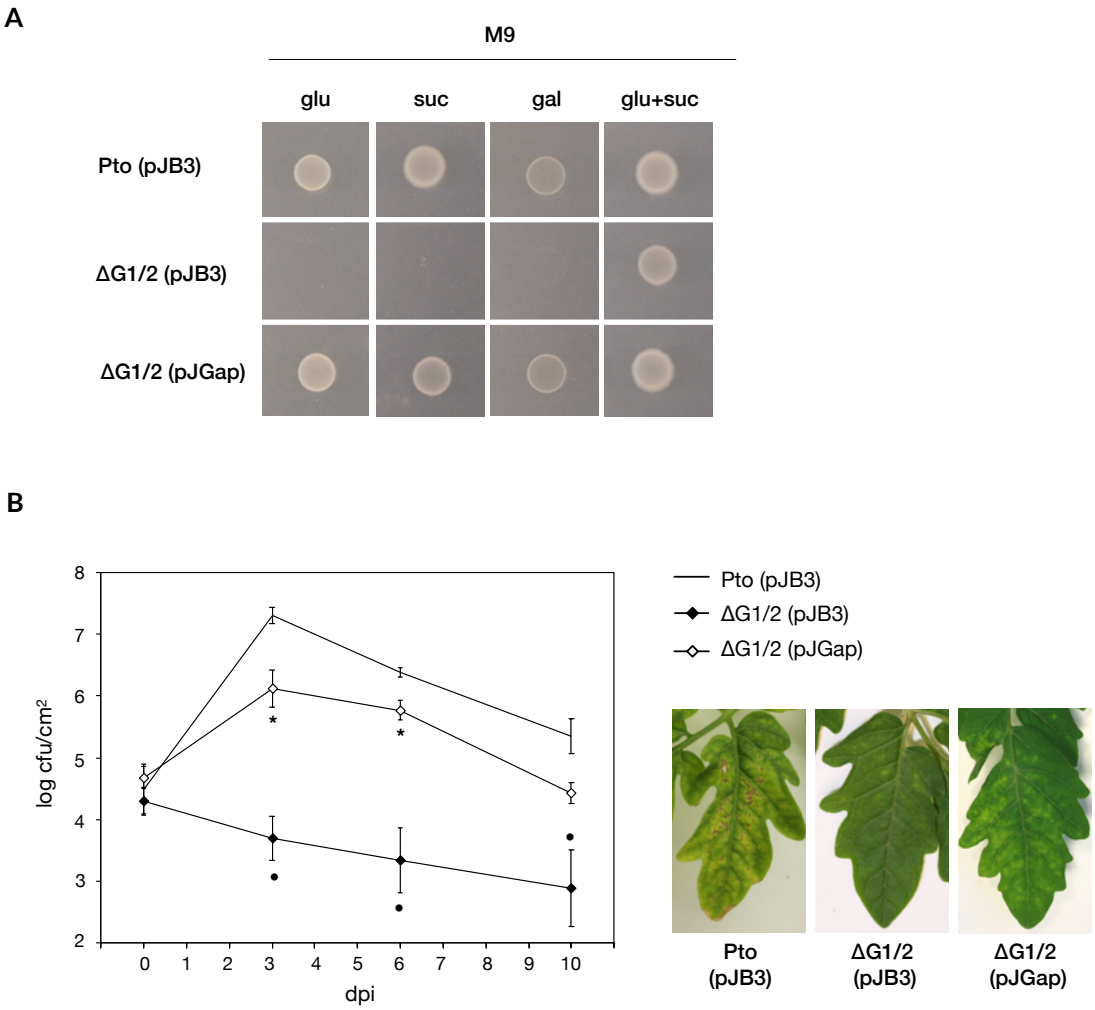

Figure RIII.5. Complementation of a Pto double ΔG1/G2 mutant with the *Rhizobium etli gap* gene.
A. Free-living growth in defined carbon sources: glucose (glu), succinate (suc), galactose (gal). Pictures taken after 2 days at 20°C.
B. Time course of Pto growth in tomato leaves. Bars indicate standard deviation. Statistically significant differences are marked by asterisks (*) and dots(•)(Tukey HSD test, p<0.01). Pictures illustrate visual symptoms on tomato leaves at 10 dpi.

When the pJGap plasmid was introduced, a notable recovery in virulence was observed, as evidenced by the increases in both the population levels and symptoms induced in the leaves. However, this strain did not quite reach the population levels and symptoms induced by the wild type. Evaluation of plasmid stability revealed that at 3 dpi, the point when bacteria reached the highest numbers, pJGap was retained by at least 93.9% of the population.

Involvement of *R. etli gap* gene in biofilm formation and flocculation

To investigate the potential impact of Gap on aggregative behaviour and adhesion in *R. etli*, biofilm formation and flocculation experiments were performed. As these behaviours are known to be enhanced by high levels of c-di-GMP (Pérez-Mendoza *et al*., 2014), both the wild-type and AC1D *Δgap* mutant strains were tested under physiological and elevated c-di-GMP conditions. To accomplish this, strains expressing the *pleD** gene, which increases intracellular c-di-GMP levels, were used (Romero-Jiménez *et al*., 2015).

Biofilm assays were performed for both the wild type and AC1D strains with and without *pleD** overexpression. The assays were carried out in rich medium (TY) supplemented with glucose to ensure suitable growth of the *gap* mutant. The *Δgap* mutant exhibited similar biofilm formation compared to the wild-type under all conditions (Fig. RIII.6A). Furthermore, overexpression of the Gap protein in the wild type did not have any discernible effects on this phenotype. To investigate whether differences in polysaccharide production could be occurring during growth in solid media, Congo Red (CR) and Calcofluor (CF) staining were performed to compare the different strains. Consistent with biofilm formation results, high c-di-GMP conditions enhanced CR and CF staining, indicative of exopolysaccharide production (Romero-Jiménez *et al*., 2015) in both the wild type and the AC1D mutant. This suggests that there is no impairment in polysaccharide production by the mutant strain (Fig. RIII.6B).

Flocculation assays were conducted in glass culture tubes using TY medium supplemented with glucose as well as MMR medium containing glucose and succinate. The *pleD** gene induced a strong aggregative behaviour in the *R. etli* wild type, with significant flocs appearing in liquid culture, (Fig. RIII.7C), in agreement with previous reports (Pérez-Mendoza *et al*., 2014). Likewise, overexpression of *pleD** in the AC1D strain also resulted in aggregative behaviour comparable to that of the wild type (Fig. RIII.7C).

Figure RIII.6. Biofilm formation and flocculation by *R. etli gap* mutant.
A. Biofilm formation by the *R. etli* wild-type and *gap* strains expressing physiological or elevated (PleD*) levels of c-di-GMP. Biofilm quantified after static growth in TY + glucose medium for 72 h. Bars represent standard deviation and different letters indicate significant differences (Tukey test, $p<0.01$).
B. Congo red and Calcofluor staining of the *R. etli gap* mutant. Photographs were taken after growth for 48 h at 28ºC in TY + glucose.
C. Flocculation tests. The bacterial strains were grown in glass tubes with continuous shaking. Tubes were photographed after 24 h in the case of TY supplemented with glucose, and after 48 h of growth in MMR supplemented with glucose and succinate at 28ºC.

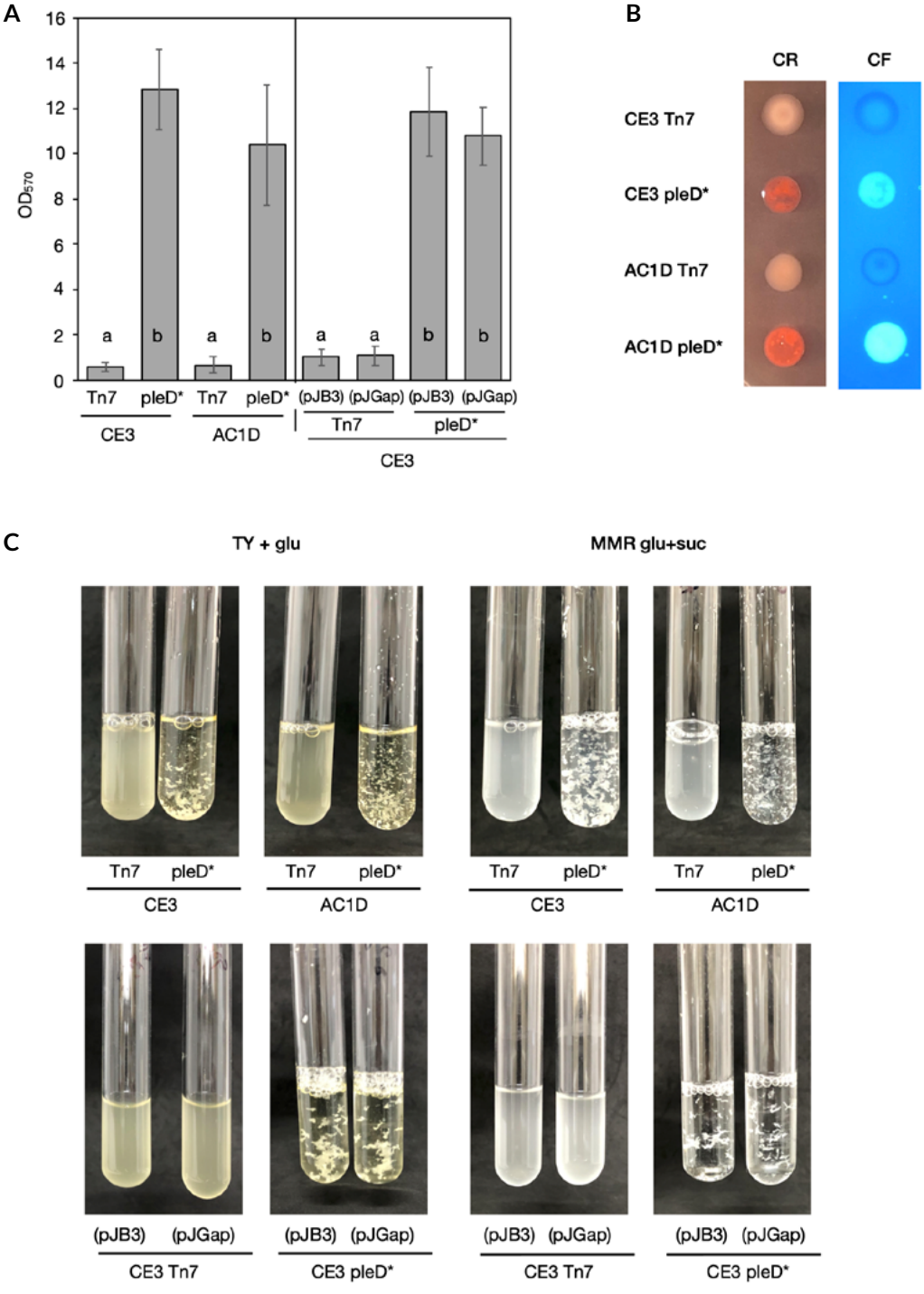
A
16
14
12
10
8
6
4
2
0
OD570
a
b
a
b
a
a
b
b
Tn7
pleD*
Tn7
pleD*
(pJB3)
(pJGap)
(pJB3)
(pJGap)
CE3
AC1D
Tn7
pleD*
CE3
B
CR
CF
CE3 Tn7
CE3 pleD*
AC1D Tn7
AC1D pleD*
C
TY + glu
MMR glu+suc
Tn7
pleD*
CE3
Tn7
pleD*
AC1D
Tn7
pleD*
CE3
Tn7
pleD*
AC1D
(pJB3)
(pJGap)
CE3 Tn7
(pJB3)
(pJGap)
CE3 pleD*
(pJB3)
(pJGap)
CE3 Tn7
(pJB3)
(pJGap)
CE3 pleD*

DISCUSSION

Considered a ubiquitous housekeeping protein, GAPDH is present in nearly all organisms. This enzyme plays a crucial role in cellular metabolism by catalysing the interconversion of glyceraldehyde-3-phosphate and 1,3-bisphosphoglycerate, thereby participating in both the glycolytic and gluconeogenic pathways (Seidler, 2013). In addition to its well-established metabolic roles, GAPDH has emerged as a versatile protein involved in diverse cellular processes unrelated to central carbon metabolism, and thus was recognised as one of the first moonlighting proteins (Seidler, 2013; Sirover, 2014; Jeffery, 2018; Franco-Serrano *et al*., 2021). In various pathogenic and beneficial bacteria, GAPDH has been observed to be secreted to the extracellular milieu or associated to the cell surface, where it often plays roles in adhesion and interaction with different host components (Pancholi and Fischetti, 1992; Aguilera *et al*., 2012; Ebner *et al*., 2016; Kopeckova *et al*., 2020a; Lorite *et al*., 2023). However, our understanding of the extrametabolic functions of GAPDH in plant-associated bacteria is still limited.

Our results underscore that a single *gap* gene governs both glycolytic and gluconeogenic GAPDH activities in *R. etli*. The *gap* deletion mutant AC1D exhibited severe growth deficiencies in the presence of a sole carbon source. However, simultaneous availability of glycolytic and gluconeogenic carbon sources allowed the mutant to proliferate, albeit at a significantly slower rate than the wild type. This indicates that the loss of GAPDH activity is partially compensated for at a metabolic level when bacteria have access to at least one glycolytic and one gluconeogenic carbon source concurrently. Furthermore, mutation of a conserved cysteine residue (C154 in the *R. etli* Gap sequence) rendered the enzyme completely inactive, incapable of rescuing the AC1D mutant phenotype in free life. This is consistent with previous reports highlighting the essential role of this conserved Cys residue for GAPDH activity (Boschi-Muller & Branlant, 1999). In bacteria like *E. coli*, which also carry a single *gap* gene, *gapA* mutants are only able to grow when combined glycolytic and gluconeogenic sources are present (Seta *et al*., 1997). In other bacteria, like *Bacillus subtilis* or *Pseudomonas syringae*, more than one Gap protein are present with a clear specialization on the type of activity (glycolytic or gluconeogenic) and the cofactor (NAD or NADP) used (Commichau *et al*., 2013; Casas-Román *et al*., 2024). In this regard, we have shown that the *R. etli* Gap protein is responsible for both glycolytic and gluconeogenic activities of the enzyme using NAD/NADH as a cofactor. It is unclear what advantages, if any, may be provided by the occurrence of single or multiple *gap* genes.

We have recently demonstrated that elevated c-di-GMP levels in *R. etli* promoted the export of cytoplasmic proteins (ECP) to the external environment, with GAPDH

being one of them (Lorite *et al*., 2023). The second messenger c-di-GMP has an important role in the transition between a planktonic/motile and a biofilm/sessile life style in numerous bacteria, acting as a regulator for the synthesis of various biofilm matrix components, including exopolysaccharides and proteins (Römling *et al*., 2013; Pérez-Mendoza & Sanjuán, 2016). To investigate the potential impact of the Gap protein on aggregation and biofilm formation in *R. etli*, we conducted different experiments under both physiological and high c-di-GMP conditions. Surprisingly, our results revealed that the Δ*gap* mutant formed similar amounts of biofilm compared to the wild type under all conditions tested. We did not observe any significant differences in flocculation or EPS production between the mutant and the wild type strain. Furthermore, overexpression of the Gap protein in the wild type did not lead to notable changes in the aggregative or biofilm phenotypes, regardless the intracellular c-di-GMP levels.

In addition to the presence of the *R. etli* Gap protein in the extracellular milieu, changes in the number and abundance of extracellular Gap proteoforms promoted by c-di-GMP had been observed, suggesting potential roles of Gap beyond central metabolism in *R. etli* (Lorite et al., 2023). Our findings substantiate the pivotal role of the *R. etli gap* gene in nodulation and nitrogen fixation with *P. vulgaris*, since the lack of Gap activity disrupted all key stages of symbiosis, from nodule formation to nodule invasion and nitrogen fixation. The AC1D mutant displayed a Nod^{d} Fix^{-} phenotype (nodulation deficient and non-fixing). The observed delay and reduction in nodule formation by the *Δgap* mutant could be attributed to its inability to effectively utilize the sugars, organic acids and other nutritional compounds secreted by the roots of common beans (Tawaraya *et al*., 2014). Although the availability of both glycolytic and gluconeogenic carbon sources could support some growth of the AC1D mutant in the bean rhizosphere, its inefficient utilization of those carbon sources would hamper its ability to proliferate there, hence explaining the delayed nodulation. Additionally, the nodules induced by the mutant were small and poorly developed. Histological examination of the nodules revealed the absence of a symbiotic central zone, with minimal or no bacterial invasion of plants cells, and lack of nitrogen-fixing bacteroids, accounting for the Fix^{-} phenotype. Bacteria could be readily isolated from the interior of those mutant nodules (data not shown), indicating that these Gap^{-} bacteria were still capable of multiplying within the infection threads, but could not be released into the host cells. The Inf^{-} symbiotic phenotype of the *R. etli* Gap^{-} mutant resembles that described for *S. meliloti* Gap^{-} mutants, which formed nodules lacking a distinctive infection zone and contained few infected cells (Finan *et al*., 1991). Although those *S. meliloti* mutants were not genetically characterized, it is evident that GAPDH activity is indispensable for both types of symbiosis, *S. meliloti*-alfalfa (indeterminate nodules) and *R. etli*-common bean (determinate nodules).

The introduction of the *gap* gene *via* the pJGap plasmid facilitated the restoration of a wild type symbiotic phenotype in the *gap* mutant. Conversely, the pJMCy plasmid, providing an inactive Gap protein, failed to ameliorate the symbiotic phenotypes of the AC1D mutant. This underscores the indispensability of an enzymatically active Gap protein that fulfils the metabolic requirements of the bacterium throughout the different symbiosis stages. However, it remained unclear which of the two enzymatic GAPDH activities, glycolytic or gluconeogenic, might be required at each particular stage. The utilization of specialized Gap proteins helped to answer this question. The *gap1* and *gap2* genes of Pto were separately introduced into the AC1D mutant. In symbiosis, overexpression of *gap1* resulted in a complete recovery of the wild type phenotype. However, only a partial complementation was observed with *gap2*, as the strain still exhibited a delay in nodule formation and invasion, along with reduced symbiosis efficiency. Notably, Pto Gap2 primarily participates in the gluconeogenic pathway (Casas-Román *et al*., 2024). The growth assays in free-living conditions showed that *gap2* overexpression only restored growth of the AC1D mutant on gluconeogenic carbon sources, but not on glycolytic compounds like glucose. This suggest that the absence of glycolytic GAPDH activity in the AC1D mutant complemented with *gap2* accounts for the delayed nodule formation and invasion. These findings support the notion that Gap glycolytic activity is more important during the early and intermediate stages of the symbiosis, whereas gluconeogenic GAPDH activity is necessary for the release of bacteria into the host cells, as well as for bacteroid differentiation and function. Several reports indicate that gluconeogenesis is vital for the synthesis of various metabolites from dicarboxylates in bacteroids (Geddes & Oresnik, 2014). Consistent with our findings, other *R. etli* strains affected in the gluconeogenesis pathway, such as *pckA* (phosphoenolpyruvate carboxykinase) mutants, were reported to induce non-fixing nodule-like structures, where host cells remained uninvaded (Tatè *et al*., 2004).

Gluconeogenic Gap activity also plays a crucial role in the interaction between a very different bacterium and its host plant. We have recently reported that single ΔG2 or double ΔG1/2 mutants of Pto DC3000 exhibited a reduced ability to multiply inside plant tissues, which resulted in diminished virulence (Casas-Román *et al*., 2024). Here, we have shown that the *R. etli gap* gene fully rescued a Pto double ΔG1/G2 mutant for growth in free-living conditions. However, despite the total complementation of the free-living growth phenotype, the capacity of this double mutant to proliferate *in planta* was only partially restored by the rhizobial *gap* gene. Several factors may contribute to this partial restoration *in planta*, including inefficient transcription and/or translation of the *R. etli gap* gene in the *Pseudomonas* genetic background. Additionally, structural differences between the Gap proteins from *R. etli* and Pto may be also relevant, potentially impacting additional functions needed *in planta*. It is worth noting that Pto Gap2

possesses a 130 aa extra N-terminal region of unknown function (Fig. SIII.4) (Elkhalfi *et al.*, 2013), that makes it larger than conventional Gap proteins. This structural variation could influence protein function and/or its role in the interaction with the host.

In summary, our study highlights the essential role of an active Gap protein throughout all the stages of the interaction between *R. etli* and its host plant *P. vulgaris*. Both glycolytic and gluconeogenic Gap metabolic activities are crucial for bacterial fitness during the early and intermediate stages of the interaction, whereas the GAPDH gluconeogenic activity seems essential for nodule invasion and nitrogen fixation. Despite the challenges posed by the essential nature of Gap metabolic activities in identifying putative moonlighting functions, the observed partial interchangeability between *R. etli* and *P. syringae* Gap proteins *in planta* suggest distinct specific tasks for each type of Gap protein. Therefore, further research will be required to unveil any additional roles of the Gap proteins in these plant-associated bacteria beyond their metabolic functions.

SUPPORTING INFORMATION

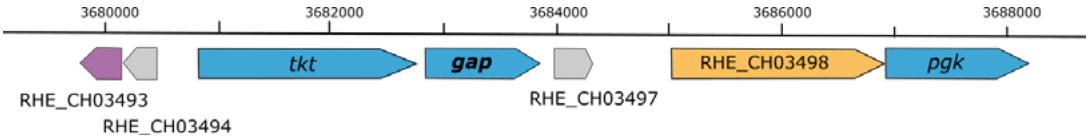

Carbohydrate metabolism

Genetic information processing

Signalling and cellular processes

Unknown function

Figure SIII.1. Genetic context of the Ret gap gene.
Gap is encoded by the RHE_CH03496 gene, which is located downstream of the *tkt* gene, encoding transketolase. Downstream of *gap* is located an ORF coding for a hypothetical protein. It is unknown whether these three genes are transcribed as a single operon.

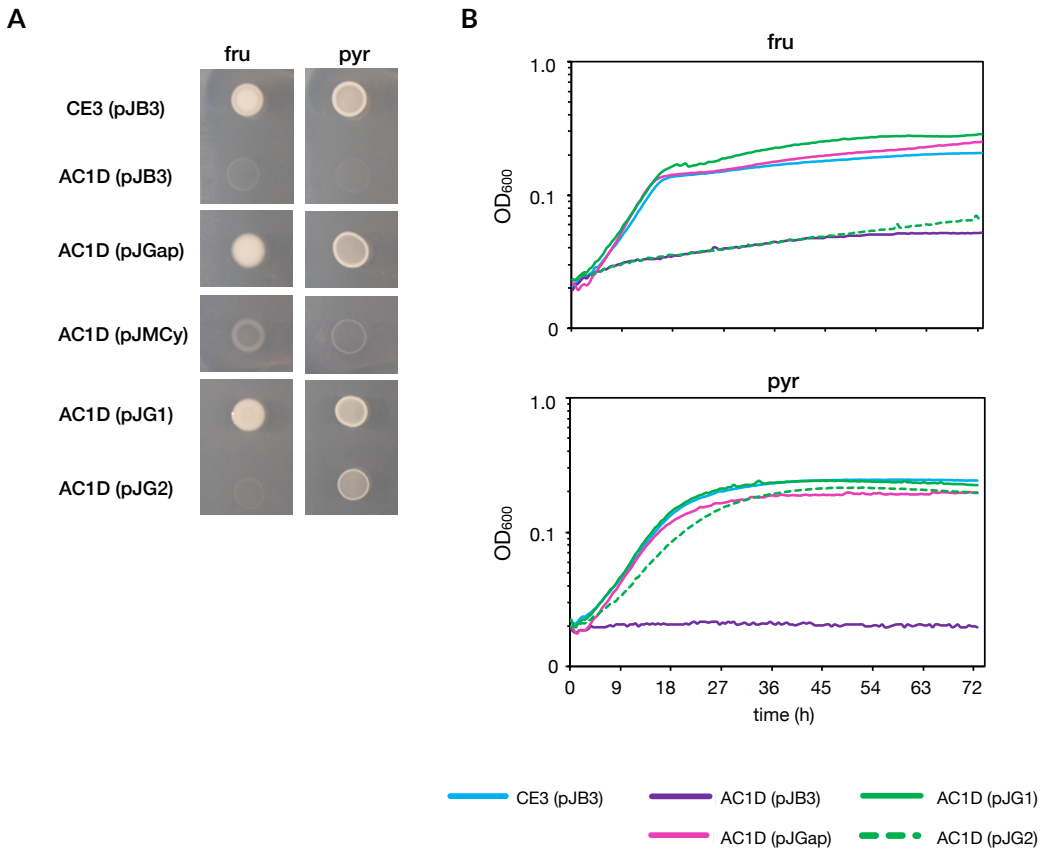

Figure SIII.2. Growth of *R. etli gap* mutants on minimal medium containing different carbon sources.
Assays were carried out in both solid and liquid minimal media with fructose (fru) at 10 mM or pyruvate (pyr) at 20 mM.
A.Growth on solid medium of 20 µl drops of bacterial suspensions at OD_{600}=1. Pictures were taken after incubation for 7 days at 28ºC.
B.Growth curves in liquid medium. Bacterial cultures were inoculated at OD_{600}=0.01 and incubated at 28ºC for 72 h with conFnuous shaking measuring the absorbance at 600 nm every hour in a Bioscreen C.

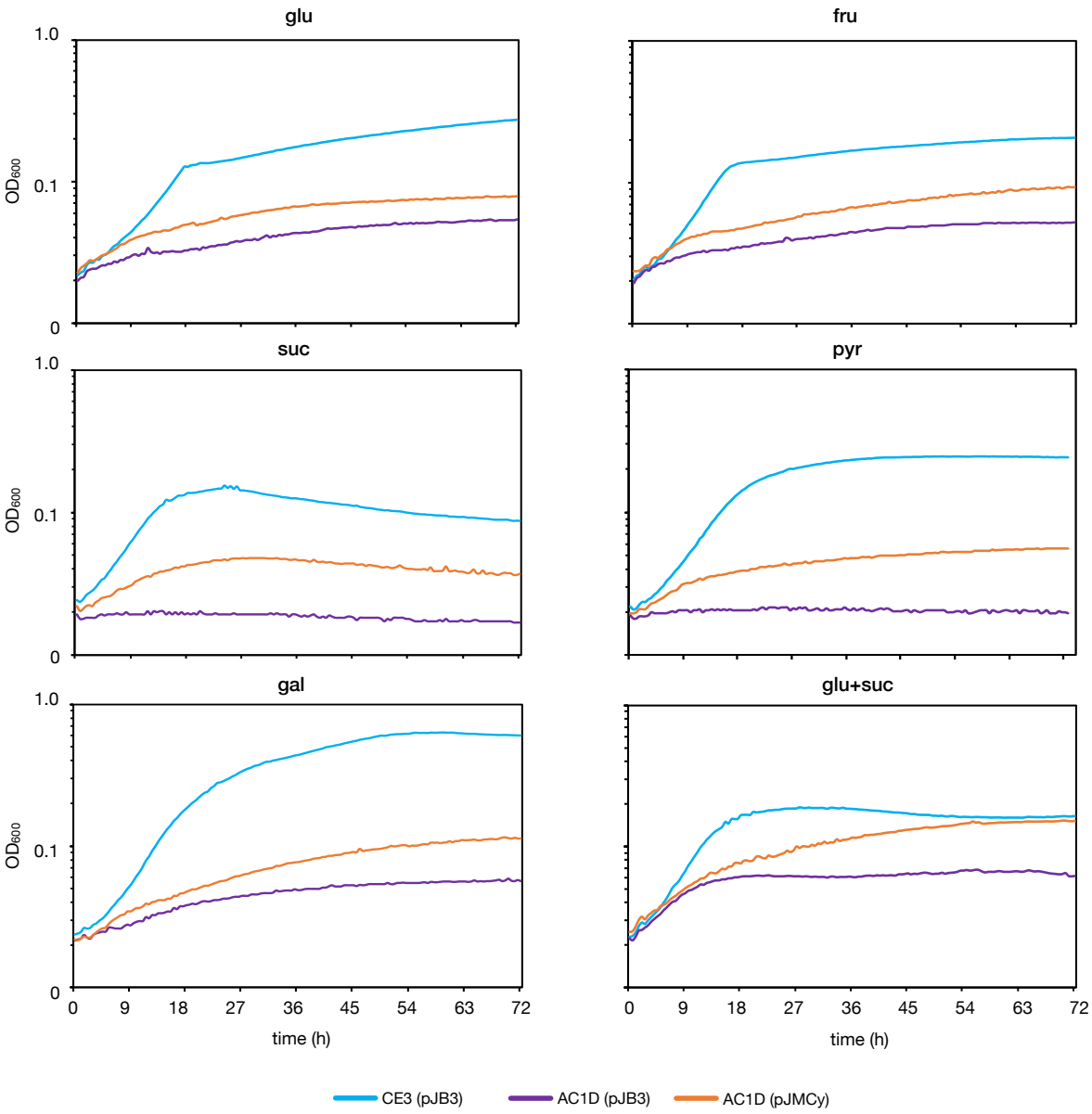

Figure SIII.3. Growth curves of the *R. etli* AC1D (pJMCy) mutant on minimal medium containing different carbon sources.

Carbon sources were glucose (glu) at 10 mM, fructose (fru) at 10 mM, succinate (suc) at 15 mM, pyruvate (pyr) at 20 mM and galactose (gal) at 10 mM. when provided simultaneously (glu+suc), glucose was at 5 mM and succinate at 7.5 mM

Bacterial cultures were inoculated at OD_{660}=0.01 and incubated at 28°C for 72 h with continuous shaking measuring the absorbance at 600 nm every hour in a Bioscreen C.

Figure. SIII.4. Sequence alignment of Gap proteins.
Ret: Gap protein from R. etli. PtoG1: Gap1 protein from *P. syringae*. PtoG2: Gap2 protein from *P.syringae*. Asterisks (*) indicate identical residues in the three proteins, two dots (:) indicate conserved substitutions, and (.) semi-conserved substitutions.

Table SIII.1. Oligonucleotides used for Ret *gap* mutants.

Name	Sequence (5'-3')	Genome position
Directed mutants		
GAPDH.del.A	tctagaCACGGAAACGGCGGAATG	3 682 273 – 3 682 291
GAPDH.del.B	CCCTCAGATGATGGCAACCTTGACTGTC	3 682 855 – 3 682 875
GAPDH.del.C	GGTTGCCATCATCTGAGGGCCTGACGAC	3 683 855 – 3 683 875
GAPDH.del.D	ctgcagGGGTGGTATGGGACAAGC	3 684 500 – 3 684 519
Overexpression plasmids		
GAPDH.compF	ctgcagTTCCAGGCCCTCTCTATCG	3 682 806 – 3 682 824
GAPDH.compR	tctagaGTCAGGCCCTCAGATG	3 683 935 – 3 683 955
Sequencing and verification		
M13U	GTAAAACGACGGCCAGT	
M13R	CAGGAAACAGCTATGAC	
pTn7L	ATTAGCTTACGACGCTACACCC	
pTn7R	CACAGCATAACTGGACTGATTTC	
glmS1etF	CCTGTTATCGTCATTGCTCC	
glmS1etR	CGACAGCAATCAGCAGGC	

Uppercase: hybridization sequence, lowercase: added sequence, underlined: target sequence for a restriction enzyme.
Reference sequence: *Rhizobium etli* CFN 42 GenBank assembly: GCA_000092045.1.

CHAPTER IV

Export mechanisms for cytoplasmic proteins relying on c-di-GMP signalling

CHAPTER IV

Keywords:
Export
Glyceraldehyde-3-phosphate dehydrogenase (GAPDH)
Moonlighting protein
Cyclic diguanylate
Post-translational modifications

Export mechanisms for cytoplasmic proteins relying on c-di-GMP signalling

Part of this chapter has been published in Biology (2023) 12, 44.
https://doi.org/10.3390/biology12010044
María J. Lorite, Ariana Casas-Román, Lourdes Girard, Sergio Encarnación, Natalia Díaz-Garrido, Josefa Badía, Laura Baldomà, Daniel Pérez-Mendoza and Juan Sanjuán
Department of Soil and Plant Microbiology, Estación Experimental del Zaidín (EEZ-CSIC), Granada, Spain.

ABSTRACT

Extracellular matrix components of bacterial biofilms include biopolymers such as polysaccharides, nucleic acids and proteins. Many of the cytoplasmic proteins found in extracellular matrices have been described as moonlighting proteins, exhibiting their canonical function in the cell cytosol and a different one in the extracellular media. Studies of the extracellular proteome of *Rhizobium etli* have revealed that c-di-GMP promotes the secretion of cytoplasmic proteins, among them GAPDH. However, no secretion signals are present in this protein, and like many other moonlighting proteins, the mechanisms enabling its translocation to the cell exterior are unknown. In this chapter, we study different possible mechanisms involved in c-di-GMP promoted secretion of GAPDH in *Rhizobium etli*. High c-di-GMP levels did not significantly impact cell bacterial growth rates or cell lysis, neither the amount of produced membrane vesicles. Transmission electron microscopy immunolabeling located the Gap protein in the cytoplasm, but also associated with cell membranes and extracellularly. It is shown that c-di-GMP increases the number of extracellular Gap proteoforms, what is suggestive of a Gap secretion mechanism involving post-translational modifications (PTMs). Evidence is provided that phosphorylation is one type of PTM present in the *R. etli* Gap protein. This suggests a link between c-di-GMP, post-translational modifications and the export of cytoplasmic proteins.

BACKGROUND

Bacterial biofilms harbour a diverse array of proteins, including cell surface adhesins pili and flagella that facilitate attachment to surfaces, migration and colonization (Absalon *et al*., 2011; Fong & Yildiz, 2015). Secreted proteins further contribute to biofilm structure and stability, with some even remodelling the matrix thanks to their enzymatic activities (Kaplan *et al*., 2003; Nijland *et al*., 2010). Interestingly, a large number of periplasmic, cytoplasmic, inner and outer membrane proteins are also present in the biofilm matrix, which imply the translocation of these proteins to the outside of the cell. Furthermore, many of those cytoplasmic proteins have been described as moonlighting proteins, exhibiting their canonical function in the cell cytosol and a different one in the cell exterior (Jeffery, 2004). However, the mechanisms that regulate and enable their translocation outside the cell remain unknown since the majority of these proteins are secreted without relying on established sorting mechanisms targeting extracellular localization, like signal sequences that guide secretion system pathways (Jeffery, 2018).

One hypothesis posits that these proteins originated from cell lysis and subsequent binding to the surface of neighbouring cells (Oliveira *et al*., 2012; Terrasse *et al*., 2015). However, evidence also point towards active secretion for at least some of them, potentially employing unidentified systems (Ebner *et al*., 2016). Another mechanism involves their packaging into membrane vesicles (MVs), which are spherical nanoparticles surrounded by lipid membranes produced by both Gram-positive and Gram-negative bacteria. These vesicles encapsulate and transport cytoplasmic contents (proteins, DNA, RNA, etc.) away from the cell while providing protection from the external environment (Toyofuku *et al*., 2012; Nagakubo *et al*., 2020). An alternative hypothesis to cell lysis and MVs suggests the secretion of moonlighting proteins onto the cell surface through unknown secretion pathways, described as "non-classical" or "non-canonical". In this scenario, post-translational modifications (PTMs) could render some proteins to be passable substrates through the membranes potentially aided by unidentified chaperones. Although a few mechanisms have been proposed for specific proteins, a comprehensive understanding of these systems remains elusive (Wang *et al*., 2013; Jeffery, 2018).

The second messenger c-di-GMP plays a well-established role in biofilm formation, regulating the transition from motile to sessile life and polysaccharide production. C-di-GMP also directly or indirectly influences the production and secretion of certain proteins like adhesins, and the activity of different protein secretion systems (Pérez-Mendoza *et al*., 2011b; López-Baena *et al*., 2019). As highlighted in Chapter III, the study

of the extracellular proteome of *Rhizobium etli* revealed that high c-di-GMP levels promoted the secretion of many cytoplasmic proteins, including Gap, which lack a recognizable secretion signal (Lorite *et al*., 2023). This finding adds to the mystery surrounding the mechanisms controlling the export of these and other moonlighting proteins to the extracellular environment.

Various hypothesis and mechanisms have been proposed for Gap export in different bacteria: cell lysis in streptococci and staphylococci strains (Pasztor *et al*., 2010; Oliveira et al., 2012; Terrasse et al., 2015), associated to OMV in *R. etli* (Taboada *et al*., 2019), or catalysing OMV membrane fusion in *Myxococcus xanthus* (Whitworth & Morgan, 2015). Additionally, the involvement of specific secretion pathways have been described. Aguilera *et al*. (2012) reported GAPDH secretion through the T3SS in enteropathogenic *E. coli*. Nevertheless, certain probiotic *E. coli* strains lacking T3SS-encoding genes still export Gap, suggesting that there are at least two alternative pathways for Gap secretion in *E. coli* (Wang *et al*., 2013).

This chapter explores potential mechanisms of c-di-GMP promoted secretion of GAPDH in *Rhizobium etli*. Two main proposed mechanisms, cell lysis and export through OMVs, were investigated. Additionally, a study of the involvement of potential PTMs of the Gap protein that might be relevant to its export was initiated.

SPECIFIC MATERIALS AND METHODS

Bacterial strains and growth conditions

R. etli strains LR101 and LR102 (Table M1) were used in this study. LR101 carries a mini-Tn7pleD*Km transposon, which results in elevated intracellular c-di-GMP levels compared with the strain LR102, harbouring a mini-Tn7Km transposon and expressing wild type c-di-GMP levels. Both strains were grown in TY medium and MMY medium (see general *Materials and Methods*) at 28ºC.

Plasmid construction

A pTD-NTwinStrep_Sm (Dammeyer *et al*., 2013) derived plasmid was constructed bearing the *R. etli gap* gene for expression of a tagged recombinant version of this protein. The specific oligonucleotid employed are depicted in Table SIV.1. The pGap12 plasmid (Table M.2) expresses a *R. etli* Gap protein containing an N-terminal Twin-strep tag and a C-terminal 6xHis tag. Expression is driven from a P_{trc} synthetic promoter which responds to IPTG.

Immunodetection by Western blot

Protein immunodetection was carried out as described in *Materials and Methods*. Rabbit polyclonal anti-*R. etli* Gap antibodies were raised (Davids Biothecnologie GMBH, Germany) against a synthetic peptide (DLGPVETNAHLLRYDSIHGK) derived from the *R. etli* CE3 Gap (RHE_CH03496) primary sequence (Lorite *et al*., 2023). This anti-Gap antibody was diluted to a working concentration of 10 µg/ml and used following the previously described standard protocol (7.5. Immunodetection by Western blot).

Mouse monoclonal anti-6x-His epitope tag antibody (MA1-135, ThermoScientific) was diluted 1:2000 times and used following the standard protocol (7.5. Immunodetection by Western blot). This antibody recognizes the 6x-His tag present in the Gap12 recombinant protein.

A rabbit polyclonal anti-phosphoserine/phosphothreonine/phosphotyrosine antibody (Ref. 61-8300, Invitrogen) was used for detection of phosphorylated proteins. This antibody detects phosphorylated serine (pS), threonine (pT) and tyrosine (pY) amino acids with very low cross reactivity to their non-phosphorylated variants (https://www.thermofisher.com/antibody/product/Phosphoserine-threonine-tyrosine-Antibody-Polyclonal/61-8300). It was diluted to a working concentration of 1.0 µg/ml. TBS-T buffer (50 mM Tris-HCl, 140 mM NaCl, 0.1% Tween 20, pH 7.4) and bovin serum albumin (BSA) were used instead of PBS-T and skimmed milk, respectively, with anti-phosphorylation antibodies.

Additional methods used in this chapter are previously described in the general *Materials and Methods* section:

- Growth curves
- Cell viability determination
- Membrane vesicle isolation and quantification
- Protein purification by gravity columns
- Mono-dimensional and two-dimensional protein electrophoresis
- Phos-tag protein electrophoresis
- Protein dephosphorylation
- Transmission electron microscopy immunolabelling
- Statistical analysis

RESULTS

High c-di-GMP levels do not enhance cell lysis

To assess if elevated c-di-GMP levels influenced cell lysis or growth phases of *R. etli*, growth rate and live/dead viability assays were performed.

Growth curves of both *R. etli* strains, LR101 (high c-di-GMP) and LR102 (control), displayed no significant differences in either rich (TY) or minimal (MMY) medium (Fig. RIV.1A). As expected, cell densities were lower in MMY compared to TY for both strains. Notably, despite their inability to produce cellulose, both strains exhibited slight aggregation/flocculation in MMY, especially LR101, which may have affected turbidity measurements. A similar scenario was observed for Pto strains (Chapter I), with no significant growth differences between the strains expressing physiological and high c-di-GMP conditions, either in rich or minimal media.

In addition, fluorescent live/dead viability assays were carried out in minimal media, as described in Materials and Methods, to evaluate the live/dead cell ratios. Cells in the exponential growth phase (DO_{600} = 0.1) served as the control live cells, whereas isopropyl alcohol-treated cells were used as the control dead cells. The live/dead ratio remained above 90% throughout the growth curve, with no significant differences between the two strains (with physiological or high c-di-GMP levels) (Fig. RIV.1B). The live cell percentage only started to decrease in the late stationary phase for both strains.

High c-di-GMP levels do not enhance MV formation in *R. etli*

In order to investigate whether c-di-GMP influenced membrane vesicle (MV) production in *R. etli*, isolation and quantification of MVs from LR101 and LR102 strains were carried out. Direct visualization of MVs was hindered by the high amounts of viscous material, probably extracellular polysaccharides, present in the culture supernatants, particularly from the c-di-GMP strain LR101. Therefore, MV production was indirectly measured by quantifying the total lipid content in the samples with the lipophilic fluorescent probe FM4-64 (Thermofisher, USA), as described in Materials and Methods. Analysis of the relative fluorescence units (RFU) from LR101 and LR102 supernatants revealed no statistically significant differences (Table RIV.1) ($p > 0.05$; Tukey HSD test). This suggests that c-di-GMP does not promote enhanced production of MV by *R. etli*.

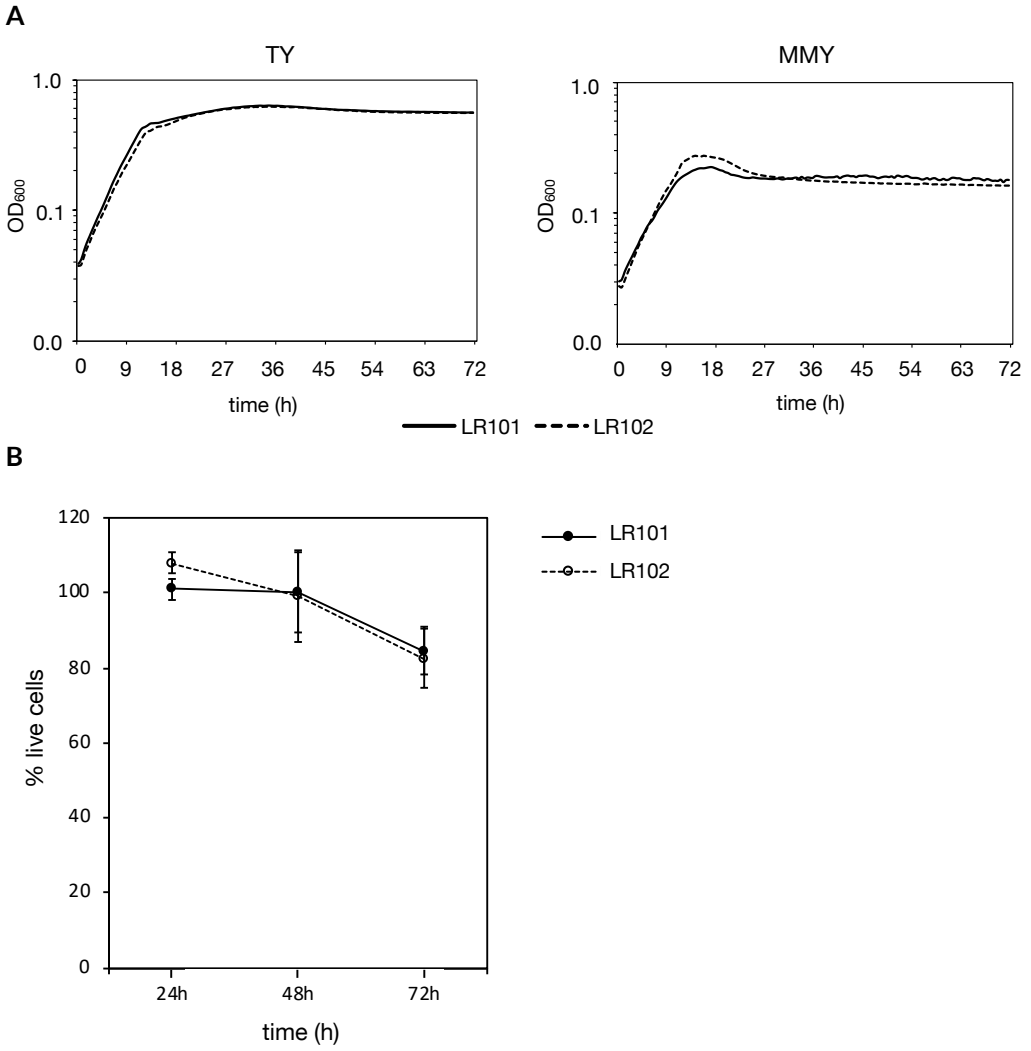

Figure RIV.1. Bacterial growth curves and live/dead ratio under physiological and high c-di-GMP conditions.

LR101 and LR102 present increased and physiological c-di-GMP levels respectively.

A. Growth curves. TY and MMY medium with succinate as the carbon source. The cultures were incubated for 72 h with continuous shaking at 28°C and DO_{600} was measured every 30 minutes in a Bioscreen C.

B. Live/dead quantification based on the PI and SYTO13 fluorescence ratio. Cells were incubated in MMY with succinate as carbon source at 28°C and measures were taken at 24 h, 48 h and 72 h. Graph shows percentage of live cells in the sample at each time point. Error bars indicate standard deviation.

Table RIV.1. MVs quantification by lipid content (FM4-64 probe).
MV samples were incubated with FM4-64 (final concentration of 5 µg/ml in PBS) for 5 min in darkness at room temperature. Emission at 635 nm was measured after excitation at 515 nm. RFU, Relative Fluorescent Units.

	Lipid content (RFU/L culture)
LR101	$2.08 \times 10^3 \pm 3.18 \times 10^2$
LR102	$2.30 \times 10^3 \pm 1.06 \times 10^2$
ΔRFUs	0.909 ± 0.18 ($p>0.05$)

Subcellular localization of *R. etli* Gap protein

Two approaches were used to investigate the subcellular localization of Gap in *R. etl*i: Western blots of MVs and immunocytochemistry. Immunodetection experiments were performed to determine whether Gap was present as part of the cargo or in association with MVs. Therefore, Western blots of the MVs samples as well as the two supernatant wash fractions obtained in the process were carried out. They revealed that Gap could be detected in all samples (Fig. RIV.2A), always with more intensity in the high c-di-GMP strain LR101, corroborating previous results (Lorite *et al*., 2023). However, Gap detection in both MV and supernatant wash samples suggests an association with polysaccharides and/or other molecules in the sample, rather than a direct association with MVs.

To establish the subcellular localization of the *R. etli* Gap protein by another method, immunocytochemistry on ultrathin cryosections from LR101 and LR102 was performed. Anti-Gap specific antibody immunolabelling revealed the presence of Gap mainly in the cytoplasm, but also associated with the inner and outer membranes, periplasm and even outside the cells (Fig. RIV.2B). The finding of Gap in the cytoplasm is consistent with its intracellular metabolic role in sugar metabolism. However, detection of the protein at the inner and outer membranes or outside the cells, suggests that specific Gap export would occur in both strains. Importantly, no gold particles were localised in the observed vesicles (V), indicating these might not be the primary route for export. Unfortunately, although immunocytochemistry confirmed Gap presence outside the cytoplasm, this technique does not allow quantifying potential differences between the LR101 and LR102 strains.

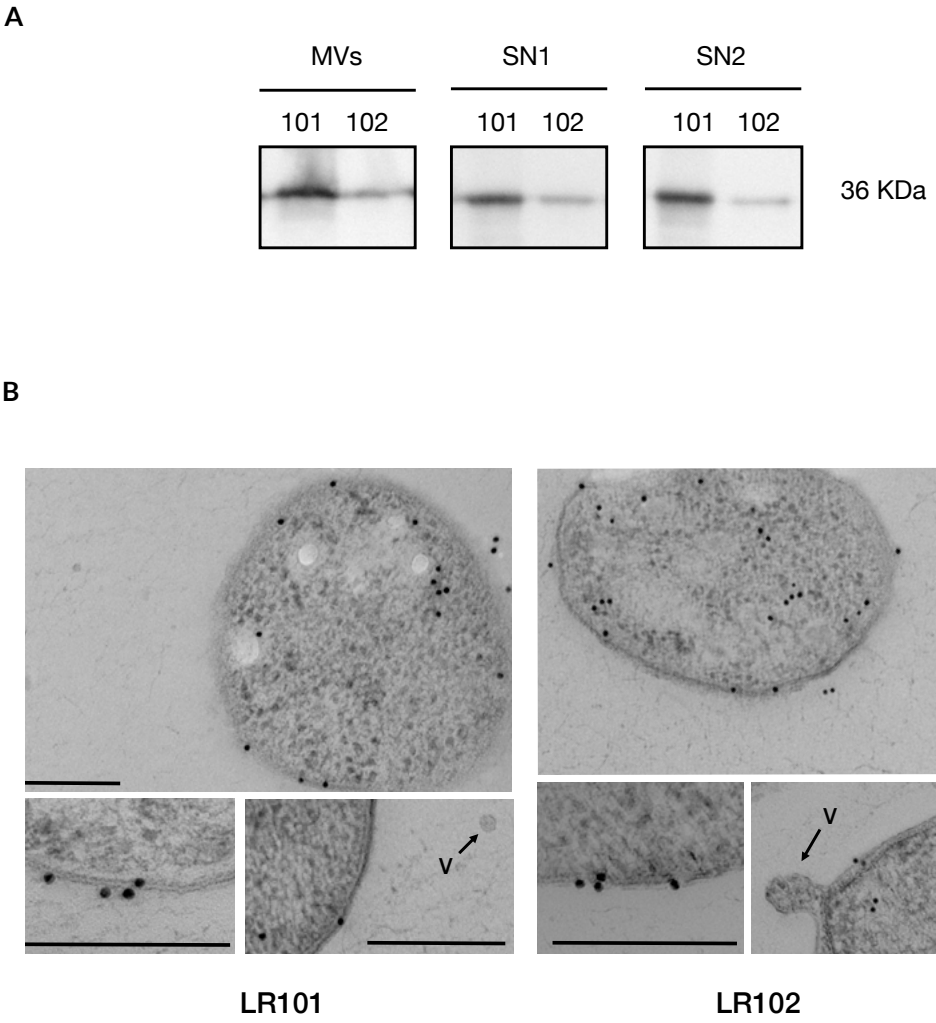

Figure RIV.2. Subcellular localization of Gap in *R. etli*.
A. Immunodetection of Gap in MV samples and supernatant wash fractions (SN) of *R. etli* cultures of strains LR101 and LR102. SN1: supernatant from the first ultracentrifugation; SN2: supernatant of the second ultracentrifugation after washing with PBS. Twenty µg of total protein were loaded into each lane .
B. Immunocytochemistry and electron microscopy. Colloidal gold particles were localised in the cytoplasm, associated with the inner and outer membranes, in the periplasmic space, and outside the cells of both strains, LR101 and LR102. No gold particles were localised in vesicles (V). All scale bars = 200 nm

Post-translational modifications (PTMs) of the *R. etli* Gap protein

Different methodologies associated with immunodetection were performed to identify potential PTMs and/or differences in the Gap proteins of *R. etli* LR101 and LR102 strains.

Two-dimensional separation (2D-GE) of total proteins in both cell-associated and supernatant fractions from LR101 and LR102 cultures, followed by Western blot and specific immunodetection of the Gap protein revealed multiple Gap proteoforms in all samples (Fig. RIV.3). This suggests the presence of PTMs in the Gap polypeptide. Intriguingly, the abundance and especially the number of Gap proteoforms appeared higher in the culture supernatants compared to the cell fractions. This effect was particularly pronounced in supernatants of the c-di-GMP strain LR101, where unique proteoforms with much lower pIs than that predicted for the unmodified Gap (pI=6.87) were revealed (Fig. RIV.3). The absence of these specific proteoforms in the cell fractions suggest that they may be tagged for export. Therefore, these findings suggest that c-di-GMP promotes Gap export to the extracellular environment, and that specific proteoforms carrying certain PTMs may be involved.

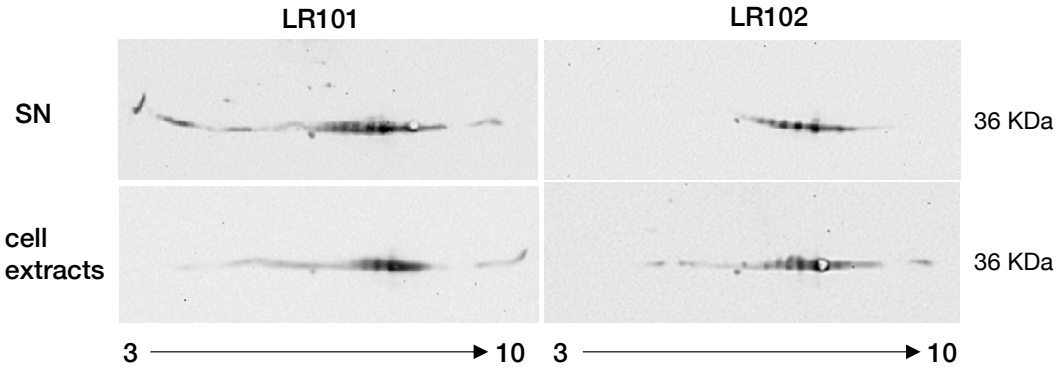

Figure RIV.3. Two-dimensional-GE Western blot and immunodetection of *R. etli* Gap protein. Immunodetection was performed with polyclonal antibodies against *R. etli* Gap. Eighty µg of total protein from supernatants (SN) or cell extracts from cultures of *R. etli* LR101 and LR102 were loaded, except for LR102-SN, for which 100 µg of protein was loaded. The pH gradient (3-10) applied in the first dimension is indicated. Courtesy of M.J. Lorite .

Different PTMs have been described for Gap proteins, like nitrosylation, acetylation or phosphorylation (Sirover, 2014; Ganapathy-Kanniappan, 2017). In the case of rhizobia, the presence of phosphorylated residues was previously reported for the *S. meliloti* Gap protein (Liu *et al*., 2015). Among PTMs, phosphorylations are the most prevalent and are relatively easier to detect compared to other modifications. To investigate the presence of phosphorylated residues in the *R. etli* Gap protein, specific methodologies such as Phos-tag gels and commercial phospho-specific antibodies were employed, facilitating an initial characterization of PTMs for the protein. For both approaches, a tagged version of the Gap protein (Gap12) was expressed from the pGap12 plasmid in the LR101 and LR102 strains. Subsequently, the protein was purified from cell extracts using Strep-Tactin gravity columns, as described in the general *Materials and Methods* section. Two-dimensional GE followed by immunodetection of the supernatant protein fractions overexpressing Gap12 revealed an additional row of spots with higher molecular weight (around 42KDa) but a similar distribution of proteoforms as the wild type protein (Fig. SIV.1). This corresponds with the expected molecular weight for the tagged version of the protein, which confirms that it is also exported outside of the cell and undergoes similar PTMs.

The Phos-tag gel analysis allows visualising potential phosphorylation-induced mobility shifts. The purified proteins were concurrently separated by regular SDS-PAGE and Phos-tag electrophoresis followed by immunodetection with the anti-His tag antibody. A prominent band of the expected molecular weight for Gap12 (around 42 KDa) was observed in the standard SDS-PAGE gel (Fig. RIV.4). In the Phos-tag gel, however, two prominent bands among many smeared bands with a fuzzy appearance were detected. This could be indicative of the presence of multiple Gap12 variants, potentially phosphorylated at distinct residues or with varying degrees of phosphorylation. This PTM could be also present in combination with other types of PTMs, what would increase complexity and number of proteoforms. Notably, no apparent differences were observed between the proteins isolated from the two strains LR101 and LR102. This assay, however, could not be done with Gap12 proteins isolated from the culture supernatants, due to the difficulties encountered to purify sufficient protein amounts from this culture compartment.

We further investigated phosphorylation by immunodetection of the Gap 12 protein using antibodies against phosphoserine (pS), phosphothreonine (pT), and phosphotyrosine (pY) residues. To validate the specificity of those antibodies, they were initially tested on a protein known to be phosphorylated, using the protein BgrV from *S. meliloti*. In wild type *S. meliloti* BgrV exists in two forms, one phosphorylated at residue serine-61, and the other unphosphorylated. Phosphorylation is carried out by

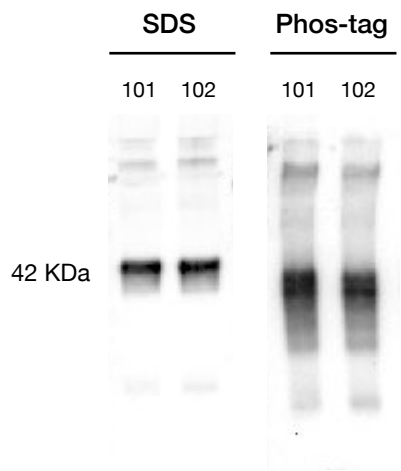

Figure RIV.4. Comparative of standard SDS-PAGE and Phos-tag electrophoreses of the purified Gap12 protein.
Strains LR101 and LR102. Purified protein (2.5 µg) was loaded into each lane. Immunodetection was performed with a His-tag antibody.

the protein kinase BgrW, whereas dephosphorylation depends on the phosphatase BgrU (Baena *et a*l., 2019). A Strep tagged version of BgrV was expressed and purified from a *bgrU* mutant strain IBR503, so that all the Strep-BgrV protein produced was in the phosphorylated state. As illustrated in Fig. SIV.2, the anti-phosphoS/T/Y antibodies successfully detected this phosphorylated BgrV protein. Treatment of the BgrV protein sample with alkaline phosphatase prior to electrophoresis and Western blotting, resulted in the loss of immunodetection of the purified BgrV. This confirmed that the phospho-specific antibodies are able to discriminate between phosphorylated and dephosphorylated proteins.

Next, the phosphorylation profiles of cell extracts and supernatants from *R. etli* strains LR101 and LR102 were analysed after immunodetection with these phospho-specific antibodies (Fig. RIV.5A). The phosphorylated protein profiles in cell extracts displayed a distinct banding pattern compared to the Coomassie-stained whole protein profiles. Notably, no visible differences could be appreciated between the LR101 and LR102 strains in any case (Fig. RIV.5A). The supernatant fractions also exhibited characteristic phosphorylated protein profiles, significantly different from the Coomasie protein profiles. Remarkably, a prominent band around 33 KDa was consistently observed in the supernatants. Interestingly, while some variations could

be appreciated between the LR101 and LR102 strains in the supernatant protein, no such differences were apparent in the phosphorylated profiles (Fig. RIV.5A). The results, however, again provided confidence that the anti-phosphoS/T/Y antibodies could discriminate certain proteins, likely phosphorylated, among a complex pool of proteins.

We conducted similar Western blot assays with the Gap protein purified from LR101 and LR102 cell extracts. Immunodetection of purified Gap12 from both strains using anti-Gap antibodies revealed a similar profile for the proteins purified from both strains (Fig. RIV.5B). Two distinct signals were observed: a broad band composed of two or more polypeptides in the range of 42 KDa, corresponding to the Gap12 polypeptide, and a slightly more defined but yet spread band in the range of 37 KDa, likely corresponding to the wild type Gap polypeptide. Since both LR101 and LR102 bear a wild type *gap* gene in addition to the Gap12 plasmid, it is plausible that Gap12/Gap heterotetramers were retained in the Strep-tactin columns and later eluted. Gap12 and Gap polypeptides differ in the Strep and His tag, resulting in a molecular weight difference of 6.6 KDa. Interestingly, similar protein profiles were revealed when the anti-phosphoS/T/Y antibodies were used instead of the Gap-specific antibodies (Fig. RIV.5B). This result indicates that several Gap12 and wild type Gap proteoforms, which are recognized by the anti-phosphoS/T/Y antibodies, can be separated even by monodimensional electrophoresis. These signals significantly decreased when the Gap samples were treated with phosphatase, providing further evidence for the presence of phosphorylated residues in the purified Gap12 and Gap polypeptides (Fig. RIV.5B). As shown in Fig. RIV.5B, the treatment with the phosphatase cocktail had no effect on the signal intensity of the Gap polypeptides revealed with the anti-Gap antibody.

DISCUSSION

The mechanisms facilitating the export of cytoplasmic proteins outside the cell remain largely unclear, and diverse possibilities have been described, even for similar proteins in different bacteria. Also, the observed enhanced abundance of certain proteins in the extracellular proteome of *R. etli* under high c-di-GMP conditions suggests a potential role for the second messenger in regulating the export of specific proteins.

Our results show that high c-di-GMP levels did not significantly impact cell growth rates in either rich or minimal media (Fig. RIV.1). We also verified that the high c-di-GMP strain LR101 displays similar death rates than the control LR102, discarding stochastic phenomena, such as cell death or lysis that could directly affect the protein contents of the extracellular fractions of the cultures. These observations imply that

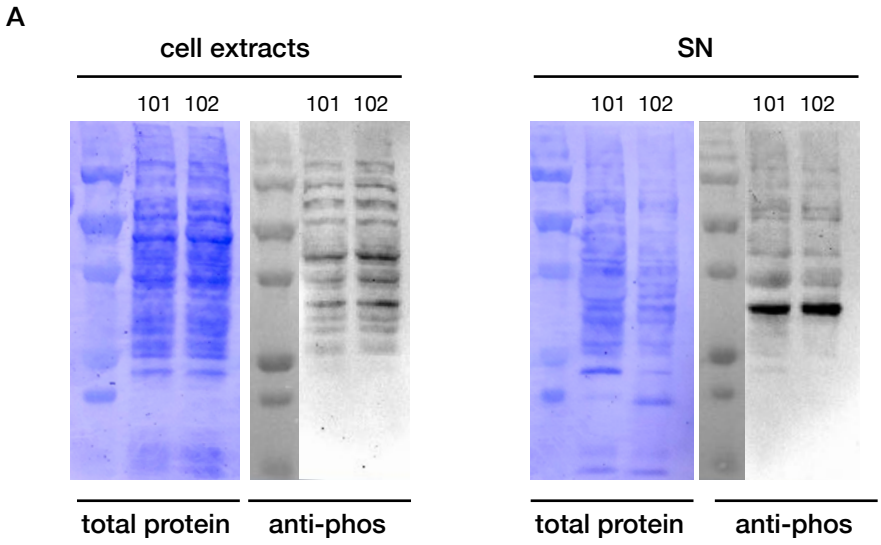

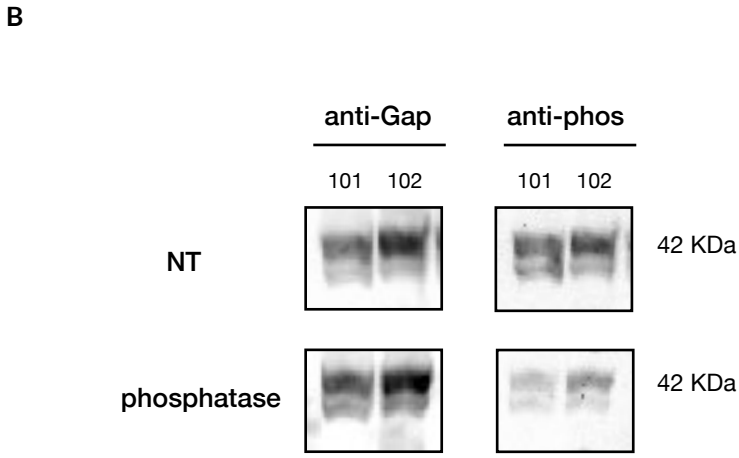

Figure RIV.5. Immunodetection of phosphorylated residues.
A. Total protein profiles of cell extracts and supernatants (SN) of strains LR101 and LR102. Whole protein profiles stained with Coomassie blue (total protein). Immunodetection of phosphorylated residues with anti-phosphoserine/threonine/tyrosine antibodies (anti-phos).
B. Immunodetection of phosphorylated residues of the purified Gap12 protein from cell extracts of LR101 and LR102 strains. Immunodetection with anti-phosphoserine/threonine/tyrosine (anti-phos) and anti-Gap antibodies was performed with non-treated samples (NT) and phosphatase treated samples.

the enhanced Gap contents in the culture supernatants under high c-di-GMP conditions is not triggered by cell lysis. Likewise, *P. syringae* growth curves did neither appear to be impacted by c-di-GMP levels (Chapter I). Since cell lysis does not seem to be responsible for the enhanced appearance of certain cytoplasmic proteins in the culture supernatants under high c-di-GMP conditions, MVs and subcellular immunolocalization analysis were performed to try to elucidate possible transport systems focusing on the Gap protein.

Direct quantification of MVs produced by LR101 and LR102 strains was not possible. However, measurement of lipid contents in the supernatants suggested no significant differences between the amount of vesicles produced by both strains (Table RIV.1). This indicated that elevated c-di-GMP levels do not seem to promote enhanced production of MVs in *R. etli*. However, the possibility of c-di-GMP impacting MV cargo composition remains open for further investigation.

Gap had been previously identified in the proteomic profile of OMVs isolated from *R. etli* (Taboada *et al*., 2019), however this does not necessarily reflect a direct association of Gap and OMVs. In our experiments, Gap was detected in both MVs and wash fractions samples (Fig. RIV.2), what probably suggests that Gap remained associated with polysaccharides and/or other extracellular molecules. Additionally, EM did not reveal any gold particles associated with the observed vesicles. These observation match studies on enterohemorrhagic and enteropathogenic *E. coli*, which determined that Gap export is not mediated by MVs (Egea *et al*., 2007). Consequently, based on the available evidence, it remains inconclusive whether the Gap protein is part of the cargo of MVs produced by *R. etli*, so further investigations dedicated to analyse the specific MV cargo composition are needed.

Electron microscopy analysis revealed the *R. etli* Gap protein in various subcellular localizations. Gap was observed in the cytoplasm, as expected for its role in sugar metabolism. However, the protein was also detected outside the cell, and associated with the inner and outer membranes (Fig. RIV.2). A similar situation was described by Egea *et al.* (2007) for Gap in enterohemorrhagic and enteropathogenic *E. coli* strains using immunogold labelling. This suggests that an active export process for Gap may be functioning in both *E. coli* and *R. etli*. Indeed, a T3SS has been described to be involved in the case of Gap exportation in enteropathogenic *E. coli* (Aguilera *et al*., 2012). However, the late study also highlights the potential existence of an alternative secretion system in probiotic strains, as well as the influence of media compositions. The hypothetical Gap export system of *R. etli* would be expressed in the wild type strain, but potentially upregulated by high c-di-GMP levels. While EM cannot quantify differences between strains, it provides strong evidence for targeted Gap export in both scenarios.

We have shown that c-di-GMP promotes a substantial increase in the number of Gap proteoforms that can be discriminated by 2D-GE (Fig. RIV.3). Particularly striking was the detection of certain proteoforms in the culture supernatants of the elevated c-di-GMP strain, but not in the corresponding cell extracts. This finding suggests that these specific proteoforms might be targeted for secretion outside the cell. The existence of multiple proteoforms for the same protein may be indicative of PTMs, which is consistent with reports of diverse PTMs on Gap from various organisms (Giménez *et al*., 2014; Sirover, 2014). PTMs are chemical modifications that increase the complexity of the proteome by regulating protein activity, localisation and/or interactions with other molecules (Forrest & Welch, 2020; Macek *et al*., 2019). They can be reversible or irreversible, and may occur at any time during a protein's life cycle. Common PTMs include phosphorylation, glycosylation, acylation or methylation, but nearly 300 different types have been described (Leutert *et al*., 2021; Zhao & Jensen, 2009). In the case of moonlighting proteins, there are examples of PTMs acting as a switch, thus serving as a toggle between different functions (Jeffery, 2016). The most common protein PTM is phosphorylation. In a recent report, Yagüe *et al*. (2019) made a compilation of protein phosphorylations in bacteria. They compared 38 bacterial phosphoproteomes and identified 29 orthologues present in at least four phosphoproteomes, being Gap one of them. The *S. meliloti* Gap protein has also been reported to be phosphorylated in at least one residue (Ser-211; Liu *et al*., 2015). Our immunodetection experiments using Phos-tag gels and anti-phosphorylation antibodies also support the presence of phosphorylated residues in the Gap protein of *R. etli* (Fig. RIV.4). No apparent differences in phosphorylated proteoform profiles were observed between the physiological and increased c-di-GMP strains. This study, however, was performed only with Gap proteins purified from cell extracts after monodimensional electrophoresis. Besides, it is likely that phosphorylation(s) of the Gap polypeptide are combined with one or more additional yet unknown PTMs. Such unknown combination of PTMs would be responsible for the great number of Gap proteoforms observed, especially when using bidimensional protein separations. Unfortunately, this methodology could not be applied to discriminate phosphorylated and nonphosphorylated Gap proteoforms. Neither could it be used to study the PTMs in Gap from the extracellular fractions, where the numbers of Gap proteoforms appeared even larger than intracellularly.

The use of antibodies detecting specific protein PTMs is a useful method to recognise the diversity of proteoforms derived from a single protein (Černý *et al*., 2013). However, this approach is only available for certain PTMs (i.e., phosphorylations, methylations, acetylations) and often are unable to detect all the variety of residues that are prone to bear PTMs (for instance, the phosphosite-specific antibodies used here are unable to

detect phosphorylations in residues like histidine, aspartate, etc.). They can neither identify the specific residues bearing the PTM, as do other more sophisticated approaches like mass spectrometry. Related with this, it is worth mentioning that a preliminary study of Gap PTMs by mass spectrometry was carried out by the Proteomics Unit of the Center for Genomic Regulation (CRG, Barcelona), using purified Gap12 protein. Surprisingly, this analysis was unable to detect any PTMs in the Gap12 protein, in spite of all the results presented in this thesis that support the presence of modifications, particularly phosphorylations, in this protein. It is possible that protein sample preparation and/or peptide fragmentations were too aggressive so that PTMs could have been removed. As stated by Macek *et al.* (2019), PTM analysis in bacterial samples may require different treatment and/or tools than eukaryotic samples.

From this study, we can conclude that the c-di-GMP-dependent export of the *R. etli* Gap protein involves an active mechanism and dedicated Gap proteoforms. We have also evidenced that the Gap protein from *R. etli* presents phosphorylations, probably in various residues. Thus, our results reveal a link of c-di-GMP regulation with PTM and export of Gap, and possibly with the phenomenon of protein moonlighting. Although our findings do not support a direct role for c-di-GMP in Gap phosphorylation, it is still possible that c-di-GMP influences Gap export through other PTMs or regulatory pathways. Therefore, further investigation is needed to elucidate the specific mechanisms underlying c-di-GMP-mediated Gap export in *R. etli*.

SUPPORTING INFORMATION

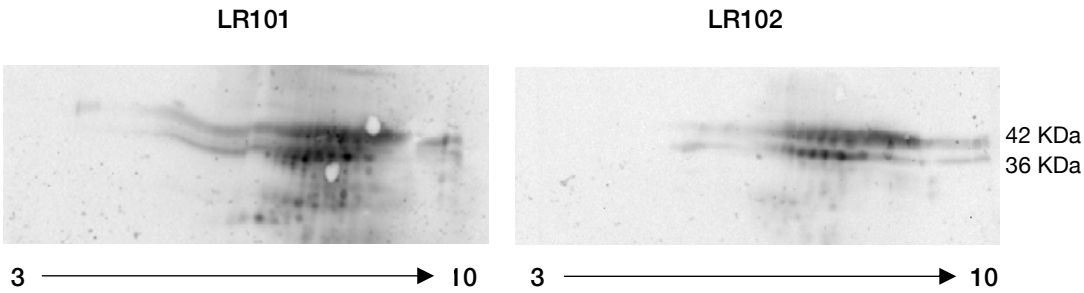

Figure SIV.1. Two-dimensional-GE Western Blot and immunodetection of *R. etli* wild type Gap and recombinant Gap12 proteins.
Immunodetection was performed with polyclonal antibodies against *R. etli* Gap. Eighty µg of total protein from supernatants from cultures of *R. etli* LR101 and LR102 overexpressing Gap12 were loaded. The pH gradient (3-10) applied in the first dimension is indicated. Courtesy of M.J. Lorite.

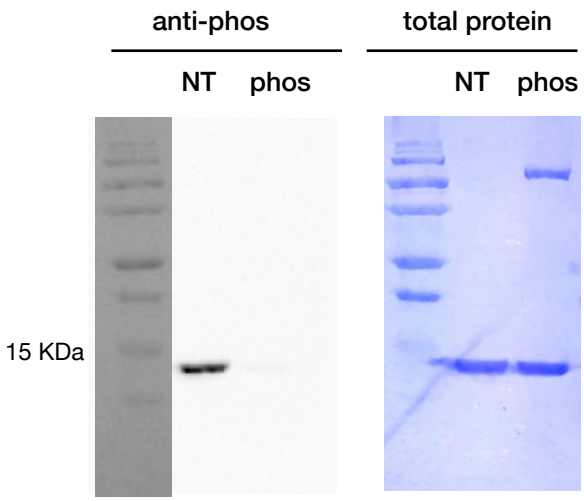

Figure SIV.2. Anti-phosphorylation antibodies specificity.
Immunodetection with anti-phosphoS/T/Y antibodies of the Strep-BrgV protein purified from a *S. meliloti bgrU* mutant, non-treated (NT) or treated with alkaline phosphatase (phos). 2.5 µg of purified protein were loaded into each lane. The membrane was stained with Coomassie blue after immunodetection as a control for both lanes.

Table SIV.1. Oligonucleotides used for the pGap12 plasmid.

Name	Sequence (5'-3')
Protein cloning	
GAP12EF	gcatgcATTTCACACCCTAGGCC
GAP12ER	tctagaACTAGTCGCCAGGGTTT
Sequencing and verification	
pTDF	TGTGTGGAATTGTGAGCGG
pTDR	ACTTTGTTTTAGGGCGACTG
GAPDH2F	GACAGTCAAGGTTGCCATCAATG

GENERAL DISCUSSION

GENERAL DISCUSSION

Plants host a multitude of microorganisms, known as the microbiome, which play vital roles in ecosystem functioning. As the imperative for sustainable agriculture grows, understanding these microbiomes and their impact on plant physiology becomes increasingly important. However, despite the growing recognition of the functional ability of microbial communities in enhancing plant fitness and the rise in pathogen outbreaks, our comprehension of microbial community structures and their mechanisms of interaction with host plant remains incomplete (Plett & Martin, 2018; Santos & Olivares, 2021; Li *et al*., 2024).

Regardless of the outcome of the association, interactions between plants and bacteria involve intricate signal exchanges between both parties. This process is marked by its complexity and multi-layered nature, requiring the coordination of signal perception and regulatory networks in both plants and bacteria. A common aspect of these interactions, whether with harmful or beneficial outputs, is the recognition by the host of specific molecular patterns in the microbes (MAMPs), which trigger the plants' immune system to prevent microbial invasion. As a consequence, microbes have evolved diverse mechanisms to evade plant immune responses and successfully colonise the plant. While these mechanisms may differ, they also share commonalities in signalling molecules and networks that contribute to the establishment of either pathogenic, mutualistic, or neutral associations. In particular, nitrogen-fixing bacterial symbionts of legume plants and phytopathogenic bacteria have adopted similar strategies and genetic characteristics to invade and establish persistent infections within the plant host (Reinhold-Hurek & Hurek, 2011; Soto *et al*., 2011; Tampakaki, 2014).

The continuous exchange of signals between plant and bacteria must be integrated to coordinate the expression of factors essential for colonisation and eventual invasion of the host. Bacterial traits such as motility, chemotaxis, EPS production, biofilm formation, and the secretion of adhesion and effector proteins, are common among plant-interacting bacteria, regardless of their mutualistic or pathogenic nature. Within the intricate regulatory networks governing these traits, the second messenger c-di-GMP assumes a pivotal role, finely tuning bacterial behaviours through both inter- and intracellular signalling pathways (Pérez-Mendoza *et al*., 2014; Martinez-Gil & Ramos, 2018; Krol *et al*., 2020).

The present thesis is focused on proteins that undergo differential regulation by this second messenger in symbiotic and pathogenic bacteria. Building upon a previous study by Lorite *et al*. (2023) about the impact of c-di-GMP on the extracellular proteome of *Rhizobium etli* (Ret), we delve into the proteins found in the intracellular and extracellular environments of *Pseudomonas syringae* pv. tomato (Pto) (Chapter I).

The c-di-GMP dependent intracellular proteome of Pto diverged significantly from the extracellular proteome as only some proteins exhibited DA simultaneously in both cases. This reflects the multifaceted actions of c-di-GMP, regulating protein abundance intracellularly, as well as influencing protein secretion through different processes. For instance, numerous flagellar and chemotaxis proteins were DA in both proteomes, often showing IA in the extrasome and RA in the intrasome. This could be attributed to downregulation of flagellar genes by c-di-GMP, coupled with the simultaneous disassembly of external flagellar components. The identification of proteins involved in polysaccharide and cellulose biosynthesis among the IA proteins under high c-di-GMP levels, both intra- and extracellularly, corroborates previous results and reinforces the established involvement of c-di-GMP in processes like biofilm formation and exopolysaccharide production (Pérez-Mendoza *et al*., 2014; Morgan *et al*., 2014; Whitney *et al*., 2015; Liang *et al*., 2022). Nonetheless, the finding of certain proteins with RA underscores the complexity of c-di-GMP regulation in biofilm formation. Our results also revealed that under high c-di-GMP there is a predominant IA of proteins involved in virulence, however, an important number of coronafacic acid related proteins also appeared with RA intracellularly. From these results, it is intriguing that, while c-di-GMP enhances the export of certain type III effectors involved in virulence, Pto strains overexpressing *pleD** showed no alterations in virulence (Pérez-Mendoza *et al*., 2014). The contrasting behaviours of virulence factors intra- and extracellularly, together with the complex coordination required, may explain the lack of a significant effect in the bacteria's virulence *in planta*.

Despite their considerable taxonomic distance, substantial genetic disparities, and the contrasting lifestyles, common responses of Ret and Pto extracellular proteomes to elevated intracellular c-di-GMP were observed. Both bacteria exhibited IA of proteins involved in the production of compounds crucial for biofilm formation, like polysaccharides, and a similar pattern was observed in the behaviour of flagellar proteins. Moreover, in both studies the great majority of DA extracellular proteins were predicted to have a cytoplasmic localization. Nevertheless, beyond these shared aspects, the majority of the DA proteins exhibited notable differences between the two bacteria. These observations align with the results of studies examining the effect of c-di-GMP on diverse bacterial interactions with their host plants, in which the outcomes vary depending on the specific plant-bacteria system. For instance, they promoted rhizobial attachment to

legume roots, but impaired symbiosis establishment. Similarly, elevated c-di-GMP levels increased the volume of knots induced in olive trees by *P. savastanoi*, while reducing plant tissue necrosis (Pérez-Mendoza *et al*., 2014). Overall, the distinct trends observed between the two bacteria underscore the unique fine-tuning of the c-di-GMP system and its regulation, which makes sense given with the opposing types of interactions despite sharing certain aspects of c-di-GMP regulation.

Moonlighting proteins represent a diverse group of multifunctional proteins that perform multiple, often disparate, roles. A defining feature is their ability to change subcellular localization, thereby acquiring new functionalities. For instance, many cytoplasmic metabolic enzymes and chaperones have been found to undertake non-enzymatic functions when situated outside the cell. These proteins, known as intracellular/surface moonlighting proteins, play significant roles in mediating interactions between bacteria and their hosts by binding to specific host proteins (Jeffery, 2019; Liu & Jeffery, 2020; Nishiyama *et al*., 2023). A notable finding from the study on Ret is that a substantial fraction of the cytoplasmic proteins whose export appeared to be enhanced by c-di-GMP had been previously reported as moonlighting or candidate moonlighting proteins in other organisms (Lorite *et al*., 2023). Interestingly, an opposed contrasting trend emerged in the case of Pto, wherein the export of a larger number of cytoplasmic metabolic enzymes appeared downregulated by c-di-GMP. This further emphasizes that in these two bacterial species, c-di-GMP modulates (either promoting or reducing) the secretion (by unknown mechanisms) of numerous intracellular housekeeping proteins (potentially moonlighting) to the cell exterior.

Glyceraldehyde-3-phosphate dehydrogenase (Gap) appeared as a compelling candidate for potential moonlighting functions with the involvement of c-di-GMP in its regulation, since this second messenger promoted its exportation in *R. etli* (Lorite *et al*., 2023). As a ubiquitous housekeeping protein, Gap is present in most organisms and exhibits a high degree of conservation. Furthermore, moonlighting functions have been described for this protein in a diverse array of bacteria (Dumke *et al*., 2011; Giménez *et al*., 2014; Kopeckova *et al*., 2020). Given this background, Gap seemed to be a promising candidate for similar functional roles in the two bacteria under study. Nevertheless, our results with Pto evidenced that the export of Gap1 and Gap2 did not exhibit significant alterations under high c-di-GMP levels. However, its study remained interesting, as both Gap proteins were found to be exported under different culture conditions, hinting at potential moonlighting roles in this bacterium (Chapters I and II).

The genetic and functional characterization of the Gap proteins present in Pto and Ret uncovered diverse implications for both bacteria (Chapters II and III) (Casas-Román *et al*., 2024). On a metabolic level, there is a clear disparity between the two bacteria since Ret

harbours a single Gap protein responsible for both glycolytic and gluconeogenic activities, whereas Pto possesses distinct enzymes for each activity and they are not interchangeable. Both scenarios for GAPDH enzymatic activity are present across the bacterial realm. For instance, *E. coli* mirrors the Ret setup (Seta *et al*., 1997), whereas *Bacillus subtilis* resembles the Pto arrangement (Commichau *et al*., 2013). The existence of two distinct Gap proteins in Pto underscores the complexity of its metabolic pathways and their regulation, for which gene expression and immunodetection assays have provided indications of posttranscriptional and/or posttranslational regulatory mechanisms. However, the potential advantages, if any, conferred by the presence of either singular or multiple *gap* genes remain uncertain. Interestingly, despite that difference between the two bacteria, the similarity of their *gap* genes enables almost complete regain of the corresponding enzymatic activities when interchangeably complemented .

Moreover, Gap enzymes exhibited distinct functional characteristics depending on the bacteria physiological state. In the case of Pto, Gap1 presented a substantial role in motility, biosurfactant production and biofilm formation; whereas in both bacteria, Gap proteins play crucial roles in their development *in planta*, with Gap2 being particularly significant in the case of Pto. Gap2 exhibits the most notable structural divergence compared to the majority of GAPDHs, as it possesses an additional N-terminal sequence of around 130 residues without specific structural features whose functional role remains undetermined. Interestingly, this Gap2 enzyme only allowed partial complementation of the *R. etli-Phaseolus* symbiosis, whereas the rhizobial *gap* gene only partially complemented a Pto Gap1/Gap2 double mutant *in planta*. In both instances, the Gap proteins present in each bacterium likely play roles beyond their metabolic functions, contributing uniquely to bacterial physiology and interactions with the host. However, due to its status as a housekeeping protein, delineating the effects stemming of the loss of a pivotal enzyme in central carbon metabolism from its potential moonlighting functions poses a challenge.

Delving into the export of Gap presents an intriguing avenue of investigation, particularly due to its translocation outside of the cell, which cannot be solely attributed to its primary metabolic functions, suggesting potential moonlighting roles. In Pto, Gap1 consistently appears to be exported independently of medium composition and c-di-GMP levels, whereas Gap2 does so only when grown in specific media and correlates with its intracellular abundance (Chapter II) (Casas-Román *et al*., 2024). In Ret, Gap is also observed extracellularly under various conditions (Meneses *et al*., 2017), but its exportation is promoted by c-di-GMP (Lorite *et al*., 2023). These findings underscore the likelihood of moonlighting roles for these proteins, yet the mechanisms driving their exportation mechanisms remain elusive. In the case of Ret, previous

research prompted an exploration of potential export mechanisms for Gap in Ret (Chapter IV). Investigations did not yield evidence of Gap export through cell lysis or membrane vesicles. Instead, the observed subcellular localizations of Gap, which was found associated to both the inner and outer membranes, suggest the involvement of non-classical or non-canonical export mechanisms, potentially akin to those described for *E. coli* by Egea *et al*. (2007) and Aguilera *et al*. (2012). Nonetheless, the precise mechanisms facilitating the translocation of cytoplasmic proteins outside the cell remain largely obscure. Various mutations intercepting secretion described for similar proteins in different bacteria such as enolase in *E. coli* and *Bacillus subtilis* (Boël *et al*., 2004; Yang *et al*., 2014) or GAPDH in *Streptococcus pyogenes* (Boël *et al*., 2005), could be investigated. An interesting insight for the future would be to determine the subcellular localization of the Pto proteins Gap1 and Gap2, and even investigate their presence within membrane vesicles.

Post-translational modifications (PTMs) play a pivotal role in the exportation and emergence of moonlighting functions in cytoplasmic proteins. Preliminary investigations on the Ret Gap protein have revealed an increased number of extracellular proteoforms induced by c-di-GMP, indicative of differential PTMs such as phosphorylations (Chapter IV). However, the variety of Gap PTMs as well as a direct relationship between PTMs and protein secretion awaits to be investigated. Nevertheless, this observation opens avenues for further exploration into the number of proteoforms and associated PTMs, which could impact the moonlighting roles of Gap and other cytoplasmic proteins.

As a ubiquitous protein among living organisms, Gap plays a crucial role in carbon metabolism, a function conserved across species. However, as it has been detailed, the genetic organization of *gap* genes varies. Gene duplication is a recurrent occurrence in genome evolution and a major driving force for acquiring new biological functions. Indeed, it has been described to have an important role in the origin and maintenance of moonlighting proteins (Copley, 2014; Espinosa-Cantú *et al*., 2015). Moonlighting roles in a protein can arise when an incidental interaction between a protein and a novel partner enhances the fitness of the organism (Fares, 2014; Jeffery, 2020). The genetic divergence already present in Gap proteins across bacteria may contribute to, or be caused by the diversity of moonlighting functions observed for this enzyme in different organisms.

Indeed, the Gap proteins from Ret and Pto appear to be involved in different cellular processes beyond glucose metabolism. Understanding the distinct regulatory mechanisms governing Gap activities and exportation in Pto and Ret will provide valuable insights into the interplay between bacterial signalling networks and protein trafficking processes. Moreover, c-di-GMP plays a role in modulating Gap activity, but this regulation appears organism-dependent since the specific mechanisms and outcomes seem

to vary with the bacterial species. In Pto and Ret, c-di-GMP plays a role in coordinating biofilm formation, a process crucial for bacterial colonisation and interaction with plant hosts. Additionally, it influences motility-related proteins, which impacts bacterial motility and dispersion within plant tissues. However, beyond these shared traits, the specific protein abundance patterns regulated by c-di-GMP differ markedly between Pto and Ret. Understanding these distinct regulation patterns will shed light on the intricate mechanisms by which bacteria adapt to their environments and interact with plant hosts. Furthermore, this variability most likely extends beyond Gap proteins, so that the organism and its environment influence the regulation of other moonlighting proteins.

CONCLUSIONS

CONCLUSIONS

1. Increased c-di-GMP intracellular levels lead to notable alterations in both the intracellular and extracellular proteomes of Pto, prompting the upregulation and exportation of proteins involved in c-di-GMP regulated processes, such as adhesion and biofilm formation. Additionally, numerous other proteins participating in diverse cellular processes experience either upregulation or downregulation.

2. Despite the phylogenetic distance and the contrasting lifestyles of the two bacterial species Ret and Pto, their extracellular proteomes display common responses to c-di-GMP that involve the differential secretion of many intracellular housekeeping proteins. However, the abundance patterns of other proteins diverge significantly between the two bacterial species.

3. Pto possesses two Gap proteins: Gap1 (PSPT0_1287) primarily exhibits glycolitic activity, whereas the NADPH-dependent Gap2 (PSPTO_2102) participates mainly in gluconeogenesis. The protein encoded by gene PSPTO_0386 (*epd*) lacks GAPDH activity but displays erythrose-4-phosphate dehydrogenase activity and is indispensable for vitamin B6 metabolism.

4. In Pto only Gap2 is essential for growth and colonisation of *Solanum lycopersicum* leaves, whereas Gap1 plays a substantial role in motility, biosurfactant production and biofilm formation. However, both proteins are exported outside the cells: Gap1 appears to be exported under all conditions tested, whereas Gap2 exportation only occurs under certain culture conditions.

5. The genome of the symbiotic bacterium *Rhizobium etli* contains a single *gap* gene (RHE_CH03496) that encodes a Gap protein displaying both glycolytic and gluconeogenic glyceraldehyde 3-phosphate dehydrogenase activities.

6. The *R. etli* Gap protein is essential for free-living growth with single carbon sources, as well as for symbiosis with *Phaseolus vulgaris*. While both Gap metabolic activities likely contribute to the bacterial fitness during early and intermediate stages of the interaction with the plant host, the gluconeogenic activity seems critical for nodule invasion and nitrogen fixation.

7. In both bacteria, Pto and Ret, Gap proteins can be found outside the cell under various growth conditions, suggesting moonlighting roles beyond their central metabolic functions. However, only in *R. etli* Gap exportation appears to be promoted by c-di-GMP.

8. Although the *R. etli* Gap protein is secreted in a c-di-GMP related manner, the *gap* gene does not seem to play a direct role in c-di-GMP related phenotypes, such as flocculation, biofilm formation or EPS production.

9. In *R. etli* c-di-GMP promoted Gap exportation does not seem to involve cell lysis nor quantitative changes in the production of membrane vesicles. Transmission electron microscopy immunolabeling observations support the existence of an active process of Gap exportation that would be enhanced by c-di-GMP .

10. C-di-GMP promoted Gap exportation in *R. etli* involves an increased number of extracellular Gap proteoforms, indicative of several post-translational modifications (PTMs) of the protein, including phosphorylations. This suggests a link between c-di-GMP, post-translational modifications and the export of cytoplasmic proteins.

BIBLIOGRAPHY

BIBLIOGRAPHY

Absalon, C., Dellen, K.V., Watnick, P.I. 2011. A communal bacterial adhesin anchors biofilm and bystander cells to surfaces. PLOS Pathog 7, e1002210. https://doi.org/10.1371/journal.ppat.1002210

Aguilar, O. M., Riva, O., Peltzer, E. 2004. Analysis of *Rhizobium etli* and of its symbiosis with wild *Phaseolus vulgaris* supports coevolution in centers of host diversification. Proc Natl Acad Sci USA 101, 13548–13553. https://doi.org/10.1073/pnas.0405321101

Aguilera, L., Ferreira, E., Giménez, R., Fernández, F.J., Taulés, M., Aguilar, J., Vega, M.C., Badia, J., Baldomà, L. 2012. Secretion of the housekeeping protein glyceraldehyde-3-phosphate dehydrogenase by the LEE-encoded type III secretion system in enteropathogenic *Escherichia coli*. Int J Biochem Cell Biol 44, 955–962. https://doi.org/10.1016/j.biocel.2012.03.002

Ahmed R. 2022. First report of bacterial speck of tomato caused by *Pseudomonas syringae* pv. tomato in AJK, Pakistan. Planta Animalia, 1; 29-30. https://doi.org/10.55627/pa.01.1.0152

Ahn, J.H., Pan, J.G., Rhee, J.S. 1999. Identification of the *tliDEF* ABC transporter specific for lipase in *Pseudomonas fluorescens* SIK W1. J Bacteriol 181, 1847–1852. https://doi.org/10.1128/jb.181.6.1847-1852.1999

Aldridge, P., Paul, R., Goymer, P., Rainey, P., Jenal, U. 2003. Role of the GGDEF regulator PleD in polar development of *Caulobacter crescentus*. Mol Microbiol 47, 1695–1708. https://doi.org/10.1046/j.1365-2958.2003.03401.x

Alfano, J. R., Collmer, A. 2004. Type III secretion system effector proteins: Double agents in bacterial disease and plant defense. Ann Rev Phytopathol 42, 385–414. https://doi.org/10.1146/annurev.phyto.42.040103.110731

Aragón, I. M., Pérez-Mendoza, D., Gallegos, M. T., Ramos, C. 2015a. The c-di-GMP phosphodiesterase BifA is involved in the virulence of bacteria from the *Pseudomonas syringae* complex. Mol Plant Pathol 16, 604–615. https://doi.org/10.1111/mpp.12218

Aragón, I. M., Pérez-Mendoza, D., Moscoso, J. A., Faure, E., Guery, B., Gallegos, M. T., Filloux, A., Ramos, C. 2015b. Diguanylate cyclase DgcP is involved in plant and human *Pseudomonas spp*. Infections. Environ Microbiol 17, 4332–4351. https://doi.org/10.1111/1462-2920.12856

Arias, A., Cerveñansky, C. 1986. Galactose metabolism in *Rhizobium meliloti* L5-30. J Bacteriol 167, 1092–1094. https://doi.org/10.1128/JB.167.3.1092-1094.1986

Baena, I., Pérez-Mendoza, D., Sauviac, L., Francesch, K., Martín, M., Rivilla, R., Bonilla, I., Bruand, C., Sanjuán, J., Lloret, J. 2019. A partner-switching system controls activation of mixed-linkage β-glucan synthesis by c-di-GMP in *Sinorhizobium meliloti*. Environ Microbiol 21, 3379–3391. https://doi.org/10.1111/1462-2920.14624

Bao, Y., Lies, D. P., Fu, H., Roberts, G. P. 1991. An improved Tn7-based system for the single-copy insertion of cloned genes into chromosomes of gram-negative bacteria. Gene 109, 167–168. https://doi.org/10.1016/0378-1119(91)90604-A

Baraquet, C., Harwood, C. S. 2015. FleQ DNA binding consensus sequence revealed by studies of FleQ-dependent regulation of biofilm gene expression in *Pseudomonas aeruginosa*. J Bacteriol 198, 178–186. https://doi.org/10.1128/jb.00539-15

Baraquet, C., Murakami, K., Parsek, M. R., Harwood, C. S. 2012. The FleQ protein from *Pseudomonas aeruginosa* functions as both a repressor and an activator to control gene expression from the *pel* operon promoter in response to c-di-GMP. Nucleic Acids Res 40, 7207–7218. https://doi.org/10.1093/nar/gks384

Barrientos-Moreno, L., Molina-Henares, M. A., Ramos-González, M. I., Espinosa-Urgel, M. 2022. Role of the Transcriptional Regulator ArgR in the connection between arginine metabolism and c-di-GMP signaling in *Pseudomonas putida*. Appl Environ Microbiol 88, e00064-22. https://doi.org/10.1128/aem.00064-22

Bartoli, C., Roux, F. 2017. Genome-wide association studies in plant pathosystems: Toward an ecological genomics approach. Front Plant Sci 8. https://doi.org/10.3389/fpls.2017.00763

Bender, C. L., Alarcón-Chaidez, F., Gross, D. C. 1999. *Pseudomonas syringae* phytotoxins: Mode of action, regulation, and biosynthesis by peptide and polyketide synthetases. Microbiol Mol Biol Rev 63, 266–292. https://doi.org/10.1128/mmbr.63.2.266-292.1999

Berendsen, R. L., Pieterse, C. M. J., Bakker, P. A. H. M. (2012). The rhizosphere microbiome and plant health. Trends Plant Sci 17, 478–486. https://doi.org/10.1016/j.tplants.2012.04.001

Bergmann, S., Rohde, M., Hammerschmidt, S. 2004. Glyceraldehyde-3-phosphate dehydrogenase of *Streptococcus pneumoniae* is a surface-displayed plasminogen-binding protein. Infect Immun 72, 2416–2419. https://doi.org/10.1128/iai.72.4.2416-2419.2004

Beringer, J.E. 1974. R factor transfer in *Rhizobium leguminosarum*. J Gen Microbiol 84, 188–198. https://doi.org/10.1099/00221287-84-1-188

Berti AD, Greve NJ, Christensen QH, Thomas MG. 2007. Identification of a biosynthetic gene cluster and the six associated lipopeptides involved in swarming motility of *Pseudomonas syringae* pv. tomato DC3000. J Bacteriol 189, 6312-6323.

Blanco-Romero, E., Garrido-Sanz, D., Durán, D., Rivilla, R., Redondo-Nieto, M., Martín, M. 2022. Regulation of extracellular matrix components by AmrZ is mediated by c-di-GMP in *Pseudomonas ogarae* F113. Sci Rep 12, Article 1. https://doi.org/10.1038/s41598-022-16162-x

Blatny, J.M., Brautaset, T., Winther-Larsen, H.C., Haugan, K., Valla, S. 1997. Construction and use of a versatile set of broad-host-range cloning and expression vectors based on the RK2 replicon. Appl Environ Microbiol 63, 370–379. https://doi.org/10.1128/aem.63.2.370-379.1997

Boël, G., Jin, H., Pancholi, V. 2005. Inhibition of cell surface export of group A streptococcal anchorless surface dehydrogenase affects bacterial adherence and antiphagocytic properties. Infect Immun 73, 6237–6248. https://doi.org/10.1128/IAI.73.10.6237-6248.2005

Boël, G., Pichereau, V., Mijakovic, I., Mazé, A., Poncet, S., Gillet, S., Giard, J.-C., Hartke, A., Auffray, Y., Deutscher, J. 2004. Is 2-phosphoglycerate-dependent automodification of bacterial enolases implicated in their export? J Mol Biol 337, 485–496. https://doi.org/10.1016/j.jmb.2003.12.082

Boschi-Muller, S., Branlant, G. 1999. The active site of phosphorylating glyceraldehyde-3-Phosphate dehydrogenase is not designed to increase the nucleophilicity of a serine residue. Arch. Biochem. Biophys. 363 259–266. https://doi.org/10.1006/abbi.1998.1080

Boschi-Muller, S., Muller, S., Van Dorsselaer, A., Böck, A., Branlant, G. 1998. Substituting selenocysteine for active site cysteine 149 of phosphorylating glyceraldehyde 3-phosphate dehydrogenase reveals a peroxidase activity. FEBS Lett. 439 241–245. https://doi.org/10.1016/S0014-5793(98)01377-5

Boureau, T., Routtu, J., Roine, E., Taira, S., Romantschuk, M. 2002. Localization of *hrpA*-induced *Pseudomonas syringae* pv. tomato DC3000 in infected tomato leaves. Mol Plant Pathol 3, 451–460. https://doi.org/10.1046/j.1364-3703.2002.00139.x

Bradford, M. M. 1976. A rapid and sensitive method for the quantitation of microgram quantities of protein utilizing the principle of protein-dye binding. Anal. Biochem. 72 248–254. https://doi.org/10.1006/abio.1976.9999

Brassard, J., Gottschalk, M., Quessy, S. 2004. Cloning and purification of the *Streptococcus suis* serotype 2 glyceraldehyde-3-phosphate dehydrogenase and its involvement as an adhesin. Vet Microbiol 102, 87–94. https://doi.org/10.1016/j.vetmic.2004.05.008

Buell, C. R., Joardar, V., Lindeberg, M., Selengut, J., Paulsen, I. T., Gwinn, M. L., Dodson, R. J., Deboy, R. T., Durkin, A. S., Kolonay, J. F., Madupu, R., Daugherty, S., Brinkac, L., Beanan, M. J., Haft, D. H., Nelson, W. C., Davidsen, T., Zafar, N., Zhou, L., Collmer, A. 2003. The complete genome sequence of the Arabidopsis and tomato pathogen *Pseudomonas syringae* pv. Tomato DC3000. Proc Natl Acad Sci USA 100, 10181–10186. https://doi.org/10.1073/pnas.1731982100

Bultreys, A., Gheysen, I., de Hoffmann, E. 2006. Yersiniabactin production by *Pseudomonas syringae* and *Escherichia coli*, and description of a second yersiniabactin locus evolutionary group. Applied and Environ Microbiol 72, 3814–3825. https://doi.org/10.1128/AEM.00119-06

Burch, A. Y., Shimada, B. K., Browne, P. J., Lindow, S. E. 2010. Novel high-throughput detection method to assess bacterial surfactant production. Applied and Environ Microbiol 76, 5363–5372. https://doi.org/10.1128/AEM.00592-10

Burch, A. Y., Shimada, B. K., Mullin, S. W., Dunlap, C. A., Bowman, M. J., Lindow, S. E. 2012. *Pseudomonas syringae* coordinates production of a motility-enabling surfactant with flagellar assembly. J Bacteriol 194, 1287-1298.

Butcher, B.G., Bronstein, P.A., Myers, C.R., Stodghill, P.V., Bolton, J.J., Markel, E.J., Filiatrault, M.J., Swingle, B., Gaballa, A., Helmann, J.D., Schneider, D.J., Cartinhour, S.W. 2011. Characterization of the Fur Regulon in *Pseudomonas syringae* pv. tomato DC3000. J Bacteriol 193, 4598–4611. https://doi.org/10.1128/JB.00340-11

Butterfield, D. A., Hardas, S. S., Lange, M. L. B. 2010. Oxidatively modified glyceraldehyde-3-phosphate dehydrogenase (GAPDH) and Alzheimer's disease: Many pathways to neurodegeneration. J Alzheimer's Dis 20, 369–393. https://doi.org/10.3233/JAD-2010-1375

Campbell, B. M., Beare, D. J., Bennett, E. M., Hall-Spencer, J. M., Ingram, J. S. I., Jaramillo, F., Ortiz, R., Ramankutty, N., Sayer, J. A., Shindell, D. 2017. Agriculture production as a major driver of the Earth system exceeding planetary boundaries. Ecol Soci 22. https://www.jstor.org/stable/26798991

Capela, D., Barloy-Hubler, F., Gouzy, J., Bothe, G., Ampe, F., Batut, J., Boistard, P., Becker, A., Boutry, M., Cadieu, E., Dréano, S., Gloux, S., Godrie, T., Goffeau, A., Kahn, D., Kiss, E., Lelaure, V., Masuy, D., Pohl, T., … Galibert, F. 2001. Analysis of the chromosome sequence of the legume symbiont *Sinorhizobium meliloti* strain 1021. Proc Natl Acad Sci USA 98, 9877–9882. https://doi.org/10.1073/pnas.161294398

Casas-Román, A., Lorite, M. J., Sanjuán, J., Gallegos, M. T. 2024. Two glyceraldehyde-3-phosphate dehydrogenases with distinctive roles in *Pseudomonas syringae* pv. tomato DC3000. Microbiol Res 278, 127530. https://doi.org/10.1016/j.micres.2023.127530

Castaldo, C., Vastano, V., Siciliano, R. A., Candela, M., Vici, M., Muscariello, L., Marasco, R., Sacco, M. 2009. Surface displaced alfa-enolase of *Lactobacillus plantarum* is a fibronectin binding protein. Microb Cell Fact, 8, 14. https://doi.org/10.1186/1475-2859-8-14

Catalano, C. M., Lane, W. S., Sherrier, D. J. 2004. Biochemical characterization of symbiosome membrane proteins from *Medicago truncatula* root nodules. Electrophor 25, 519–531. https://doi.org/10.1002/elps.200305711

Cerný, M., Skalák, J., Cerna, H., Brzobohatý, B. 2013. Advances in purification and separation of posttranslationally modified proteins. J Proteomics 92 2–27. https://doi.org/10.1016/j.jprot.2013.05.040

Chan, C., Paul, R., Samoray, D., Amiot, N. C., Giese, B., Jenal, U., Schirmer, T. 2004. Structural basis of activity and allosteric control of diguanylate cyclase. Proc Natl Acad Sci USA 101, 17084–17089. https://doi.org/10.1073/pnas.0406134101

Chen, C., Liu, H., Zabad, S., Rivera, N., Rowin, E., Hassan, M., Gomez De Jesus, S. M., Llinás Santos, P. S., Kravchenko, K., Mikhova, M., Ketterer, S., Shen, A., Shen, S., Navas, E., Horan, B., Raudsepp, J., Jeffery, C. 2021. MoonProt 3.0: An update of the moonlighting proteins database. Nucleic Acids Res 49, D368–D372. https://doi.org/10.1093/nar/gkaa1101

Chen, C., Zabad, S., Liu, H., Wang, W., Jeffery, C. 2018. MoonProt 2.0: An expansion and update of the moonlighting proteins database. Nucleic Acids Res 46(D1), D640–D644. https://doi.org/10.1093/nar/gkx1043

Chen, J., Zhao, L., Fu, G., Zhou, W., Sun, Y., Zheng, P., Sun, J., Zhang, D. 2016. A novel strategy for protein production using non-classical secretion pathway in Bacillus subtilis. Microb Cell Fact 15, 69. https://doi.org/10.1186/s12934-016-0469-8

Chen, Y., Li, S., Guo, J. 2022. A method for identifying moonlighting proteins based on linear discriminant analysis and bagging-SVM. Front Genet 13. https://www.frontiersin.org/articles/10.3389/fgene.2022.963349

Chien, C.-F., Liu, C.-Y., Lu, Y.-Y., Sung, Y.-H., Chen, K.-Y., Lin, N.-C. 2020. HSI-II gene cluster of *Pseudomonas syringae* pv. tomato DC3000 encodes a functional type VI secretion system required for interbacterial competition. Front Microbiol 11. https://doi.org/10.3389/fmicb.2020.01118

Choi, K.-H., Kumar, A., Schweizer, H.P. 2006. A 10-min method for preparation of highly electrocompetent Pseudomonas aeruginosa cells: Application for DNA fragment transfer between chromosomes and plasmid transformation. J Microbiol Methods 64, 391–397. https://doi.org/10.1016/j.mimet.2005.06.001

Commichau, F.M., Pietack, N., Stülke, J. 2013. Essential genes in *Bacillus subtilis*: a re-evaluation after ten years. Mol. Biosyst. 9, 1068. https://doi.org/10.1039/c3mb25595f

Conway, T. 1992. The Entner-Doudoroff pathway: History, physiology and molecular biology. FEMS Microbiol Rev, 9(1), 1–27. https://doi.org/10.1111/j.1574-6968.1992.tb05822.x

Cooley, R. B., Smith, T. J., Leung, W., Tierney, V., Borlee, B. R., O'Toole, G. A., Sondermann, H. 2015. Cyclic di-GMP-regulated periplasmic proteolysis of a *Pseudomonas aeruginosa* type Vb secretion system substrate. J Bacteriol 198, 66–76. https://doi.org/10.1128/jb.00369-15

Copley, S. D. 2012. Moonlighting is mainstream: Paradigm adjustment required. BioEssays 34, 578–588. https://doi.org/10.1002/bies.201100191

Copley, S. D. 2014. An evolutionary perspective on protein moonlighting. Biochem Soc Trans 42, 1684–1691. https://doi.org/10.1042/BST20140245

Cotter, P.A., Stibitz, S. 2007. c-di-GMP-mediated regulation of virulence and biofilm formation. Curr Opin Microbiol Host-microbe interactions: Bacteria 10, 17–23. https://doi.org/10.1016/j.mib.2006.12.006

Cunnac S, Lindeberg M, Collmer A. 2009. *Pseudomonas syringae* type III secretion system effectors: repertoires in search of functions. Curr Opin Microbiol 12, 53-60.

Cuppels, D.A. 1986. Generation and Characterization of Tn5 Insertion Mutations in *Pseudomonas syringae* pv. tomato. Applied and Environ Microbiol 51, 323–327. https://doi.org/10.1128/aem.51.2.323-327.1986

D'Haeze, W., Leoff, C., Freshour, G., Noel, K. D., Carlson, R. W. 2007. *Rhizobium etli* CE3 bacteroid lipopolysaccharides are structurally similar but not identical to those produced by cultured CE3 Bacteria. J Biol Chem 282, 17101–17113. https://doi.org/10.1074/jbc.M611669200

Dammeyer, T., Timmis, K.N., Tinnefeld, P. 2013. Broad host range vectors for expression of proteins with (Twin-) Strep-tag, His-tag and engineered, export optimized yellow fluorescent protein. Microb Cell Fact 12, 49. https://doi.org/10.1186/1475-2859-12-49

Davies, B. W., Bogard, R. W., Young, T. S., Mekalanos, J. J. 2012. Coordinated regulation of accessory genetic elements produces cyclic di-bucleotides for *V. cholerae* virulence. Cell, 149, 358–370. https://doi.org/10.1016/j.cell.2012.01.053

De Carvalho, K. G., Bambirra, F. H. S., Kruger, M. F., Barbosa, M. S., Oliveira, J. S., Santos, A. M. C., Nicoli, J. R., Bemquerer, M. P., de Miranda, A., Salvucci, E. J., Sesma, F. J. M., Franco, B. D. G. M. 2010. Antimicrobial compounds produced by *Lactobacillus sakei* subsp. Sakei 2a, a bacteriocinogenic strain isolated from a Brazilian meat product. J Ind Microbiol Biotechnol, 37, 381–390. https://doi.org/10.1007/s10295-009-0684-y

De Ley, J., Doudoroff, M. 1957. The metabolism of D-galactose in *Pseudomonas saccharophila*. J. Biol Chem 227, 745–757. https://doi.org/10.1016/S0021-9258(18)70755-2

De Weger, L. A., van der Vlugt, C. I., Wijfjes, A. H., Bakker, P. A., Schippers, B., Lugtenberg, B. 1987. Flagella of a plant-growth-stimulating *Pseudomonas fluorescens* strain are required for colonization of potato roots. J Bacteriol 169 2769–2773. https://doi.org/10.1128/jb.169.6.2769-2773.1987

Del Castillo, T., Duque, E., Ramos, J. L. 2008. A set of activators and repressors control peripheral glucose pathways in *Pseudomonas putida* to yield a common central intermediate. J Bacteriol 190, 2331-2339.

Del Castillo, T., Ramos, J. L., Rodríguez-Herva, J. J., Fuhrer, T., Sauer, U., Duque, E. 2007. Convergent peripheral pathways catalyze initial glucose catabolism in *Pseudomonas putida*: genomic and flux analysis. J Bacteriol 189(14):5142-5152.

Demarre, G., Guérout, A.-M., Matsumoto-Mashimo, C., Rowe-Magnus, D.A., Marlière, P., Mazel, D. 2005. A new family of mobilizable suicide plasmids based on broad host range R388 plasmid (IncW) and RP4 plasmid (IncPalpha) conjugative machineries and their cognate *Escherichia coli* host strains. Res Microbiol 156 245–255. https://doi.org/10.1016/j.resmic.2004.09.007

Dries, L., Hendgen, M., Schnell, S., Löhnertz, O., Vortkamp, A. 2021. Rhizosphere engineering: Leading towards a sustainable viticulture? OENO One, 55, Article 2. https://doi.org/10.20870/oeno-one.2021.55.2.4534

Dumke, R., Hausner, M., Jacobs, E. 2011. Role of *Mycoplasma pneumoniae* glyceraldehyde-3-phosphate dehydrogenase (GAPDH) in mediating interactions with the human extracellular matrix. Microbiology 157 2328–2338. https://doi.org/10.1099/mic.0.048298-0

Duque, E., de la Torre, J., Bernal, P., Molina-Henares, M.A., Alaminos, M., Espinosa-Urgel, M., Roca, A., Fernández, M., de Bentzmann, S., Ramos, J. L. 2013. Identification of reciprocal adhesion genes in pathogenic and non-pathogenic *Pseudomonas*. Environ Microbiol 15, 36–48. https://doi.org/10.1111/j.1462-2920.2012.02732.x

Ebner, P., Götz, F. 2019. Bacterial excretion of cytoplasmic proteins (ECP): Occurrence, mechanism, and function. Trends Microbiol 27, 176–187. https://doi.org/10.1016/j.tim.2018.10.006

Ebner, P., Rinker, J., Nguyen, M.T., Popella, P., Nega, M., Luqman, A., Schittek, B., Di Marco, M., Stevanovic, S., Götz, F. 2016. Excreted cytoplasmic proteins contribute to pathogenicity in *Staphylococcus aureus*. Infect. Immun. 84, 1672–1681. https://doi.org/10.1128/IAI.00138-16

Egea, L., Aguilera, L., Gimenez, R., Sorolla, M.A., Aguilar, J., Badıa, J., Baldomà, L. 2007. Role of secreted glyceraldehyde-3-phosphate dehydrogenase in the infection mechanism of enterohemorrhagic and enteropathogenic *Escherichia coli*: Interaction of the extracellular enzyme with human plasminogen and fibrinogen. Int J Biochem 14. https://doi.org/10.1016/j.biocel.2007.03.008

Elkhalfi, B., Araya-Garay, J.M., Rodríguez-Castro, J., Rey-Méndez, M., Soukri, A., Serrano Delgado, A. 2013. Cloning and heterologous overexpression of three *gap* genes encoding different glyceraldehyde-3-phosphate dehydrogenases from the plant pathogenic bacterium *Pseudomonas syringae* pv. tomato strain DC3000. Protein Expr Purif 89, 146–155. https://doi.org/10.1016/j.pep.2013.02.005

Elkhalfi, B., Serrano, A., Soukri, A. 2014. Identification of an extracellular infection-induced glyceraldehyde-3-phosphate dehydrogenase of the phytopathogenic proteobacterium *Pseudomonas syringae* pv. tomato DC3000. ABB 05 201–208. https://doi.org/10.4236/abb.2014.53026

Elser, J. J., Bracken, M. E. S., Cleland, E. E., Gruner, D. S., Harpole, W. S., Hillebrand, H., Ngai, J. T., Seabloom, E. W., Shurin, J. B., Smith, J. E. 2007. Global analysis of nitrogen and phosphorus limitation of primary producers in freshwater, marine and terrestrial ecosystems. Ecol Lett 10, 1135–1142. https://doi.org/10.1111/j.1461-0248.2007.01113.x

Emerich, D. W., Krishnan, H. B. 2014. Symbiosomes: Temporary moonlighting organelles. Biochem J 460, 1–11. https://doi.org/10.1042/BJ20130271

Erisman, J. W., Galloway, J., Dise, N., Bleeker, A., Grizzetti, B., Leach, A., Vries, W. 2015. Nitrogen, too much of a vital resource. WWF science brief NL. https://doi.org/10.13140/RG.2.1.3664.8163

Espinosa-Cantú, A., Ascencio, D., Barona-Gómez, F., DeLuna, A. 2015. Gene duplication and the evolution of moonlighting proteins. Front Genet 6. https://doi.org/10.3389/fgene.2015.00227

Espinosa-Cantú, A., Ascencio, D., Herrera-Basurto, S., Xu, J., Roguev, A., Krogan, N. J., DeLuna, A. 2018. Protein moonlighting revealed by noncatalytic phenotypes of yeast enzymes. Genetics 208, 419–431. https://doi.org/10.1534/genetics.117.300377

Espinosa-Urgel, M., Ramos-González, M. I. 2023. Becoming settlers: Elements and mechanisms for surface colonisation by *Pseudomonas putida*. Environ Microbiol 25, 1575–1593. https://doi.org/10.1111/1462-2920.16385

Fares, M.A. 2014. The evolution of protein moonlighting: adaptive traps and promiscuity in the chaperonins. Biochem Soc Trans 42, 1709–1714. https://doi.org/10.1042/BST20140225

Farias, G. A., Olmedilla, A., Gallegos, M. T. 2019. Visualization and characterization of *Pseudomonas syringae* pv. tomato DC3000 pellicles. Microb Biotechnol, 12, 688–702. https://doi.org/10.1111/1751-7915.13385

Ferreira, E., Giménez, R., Aguilera, L., Guzmán, K., Aguilar, J., Badia, J., Baldomà, L. 2013. Protein interaction studies point to new functions for *Escherichia coli* glyceraldehyde-3-phosphate dehydrogenase. Res Microbiol, 164, 145–154. https://doi.org/10.1016/j.resmic.2012.11.002

Ferreiro, M. D., Behrmann, L. V., Corral A., Nogales J., Gallegos M. T. 2021. Exploring the expression and functionality of the *rsm* sRNAs in *Pseudomonas syringae* pv. tomato DC3000. RNA Biol, 18,1818-1833.

Figge, R. M., Schubert, M., Brinkmann, H., Cerff, R. 1999. Glyceraldehyde-3-phosphate dehydrogenase gene diversity in eubacteria and eukaryotes: evidence for intra- and inter-kingdom gene transfer. Mol Biol Evol 16, 429-440.

Fillinger, S., Boschi-Muller, S., Azza, S., Dervyn, E., Branlant, G., Aymerich, S. 2000. Two glyceraldehyde-3-phosphate dehydrogenases with opposite physiological roles in a nonphotosynthetic bacterium. J Biol Chem 275, 14031-14037. https://doi.org/10.1074/jbc.275.19.14031

Filloux, A. 2011 Protein secretion systems in *Pseudomonas aeruginosa*: An essay on diversity, evolution, and function. Front Microbiol 2, 155. https://doi.org/10.3389/fmicb.2011.00155

Finan, T. M., McWhInnie, E., Driscoll, B., Watson, R. J. 1991. Complex symbiotic phenotypes result from gluconeogenic mutations in *Rhizobium meliloti*. Mol Plant-Microb. Interact 4, 386–392. https://doi.org/10.1094/MPMI-4-386

Finan, T. M., Oresnik, I., Bottacin, A. 1988. Mutants of *Rhizobium meliloti* defective in succinate metabolism. J Bacteriol 170, 3396–3403. https://doi.org/10.1128/JB.170.8.3396-3403.1988

Fishman M. R., Zhang J., Bronstein P. A., Stodghill P., Filiatrault M. J. 2018. The Ca(2+) induced two-component system, CvsSR regulates the Type III secretion system and the extracytoplasmic function sigma-factor AlgU in *Pseudomonas syringae* pv. tomato DC3000. J Bacteriol 200, e00538-17.

Foley, J. A., Ramankutty, N., Brauman, K. A., Cassidy, E. S., Gerber, J. S., Johnston, M., Mueller, N. D., O'Connell, C., Ray, D. K., West, P. C., Balzer, C., Bennett, E. M., Carpenter, S. R., Hill, J., Monfreda, C., Polasky, S., Rockström, J., Sheehan, J., Siebert, S., … Zaks, D. P. M. 2011. Solutions for a cultivated planet. Nature 478, Article 7369. https://doi.org/10.1038/nature10452

Fong, J. N. C., Yildiz, F. H. 2015. Biofilm matrix proteins. Microbiol Spect, 3, 3.2.28. https://doi.org/10.1128/microbiolspec.MB-0004-2014

Forrest, S., Welch, M. 2020. Arming the troops: Post-translational modification of extracellular bacterial proteins. Sci Prog 103, 003685042096431. https://doi.org/10.1177/0036850420964317

Forsberg, L. S., Bhat, U. R., Carlson, R. W. 2000. Structural Characterization of the O-antigenic polysaccharide of the lipopolysaccharide from *Rhizobium etli* strain CE3: A unique O-acetylated glycan of discrete size, containing 3-O-methyl-6-deoxy-l-talose and 2,3,4-tri-O-methyl-l-fucose. J Biol Chem 275, 18851–18863. https://doi.org/10.1074/jbc.M001090200

Forsberg, L. S., Carlson, R. W. 1998. The structures of the lipopolysaccharides from *Rhizobium etli* strains CE358 and CE359: The complete structure of the core region of *R. etli* lipopolysaccharides. J Biol Chem 273(5) 2747–2757. https://doi.org/10.1074/jbc.273.5.2747

Fothergill-Gilmore, L. A., Michels P. A. 1993. Evolution of glycolysis. Prog Biophys Mol Biol 59, 105-235. https://doi.org/10.1016/0079-6107(93)90001-Z

Foulston L., Elsholz Alexander K.W., DeFrancesco Alicia S., Losick. R. 2014. The extracellular matrix of *Staphylococcus aureus* biofilms comprises cytoplasmic proteins that associate with the cell surface in response to decreasing pH. mBio 5. https://doi.org/10.1128/mbio.01667-14.

Franco-Serrano, L., Hernández, S., Calvo, A., Severi, M. A., Ferragut, G., Pérez-Pons, J., Piñol, J., Pich, Ò., Mozo-Villarias, Á., Amela, I., Querol, E., Cedano, J. 2018. MultitaskProtDB-II: An update of a database of multitasking/moonlighting proteins. Nucleic Acids Res 46, D645–D648. https://doi.org/10.1093/nar/gkx1066

Franco-Serrano, L., Sánchez-Redondo, D., Nájar-García, A., Hernández, S., Amela, I., Perez-Pons, J.A., Piñol, J., Mozo-Villarias, A., Cedano, J., Querol, E. 2021. Pathogen moonlighting proteins: From ancestral key metabolic enzymes to virulence factors. Microorganisms 9, 1300. https://doi.org/10.3390/microorganisms9061300

Frias, A., Manresa, A., de Oliveira, E., López-Iglesias, C., Mercade, E. 2010. Membrane vesicles: A common feature in the extracellular matter of cold-adapted antarctic bacteria. Microb Ecol, 59, 476–486. https://doi.org/10.1007/s00248-009-9622-9

Fuhrer, T., Fischer, E., Sauer, U. 2005. Experimental identification and quantification of glucose metabolism in seven bacterial species. J Bacteriol 187, 1581–1590. https://doi.org/10.1128/JB.187.5.1581-1590.2005

Galán, J. E., Lara-Tejero, M., Marlovits, T. C., Wagner, S. 2014. Bacterial type III tecretion tystems: Specialized nanomachines for protein delivery into target cells. Annu Rev Microbiol 68, 415–438. https://doi.org/10.1146/annurev-micro-092412-155725

Galloway, J. N., Cowling, E. B. 2002. Reactive nitrogen and the world: 200 Years of change. AMBIO: A Journal of the Human Environment, 31, 64–71. https://doi.org/10.1579/0044-7447-31.2.64

Ganapathy-Kanniappan, S. 2017. Analysis of GAPDH Posttranslational Modifications, in: Ganapathy-Kanniappan, S. (Ed.), Advances in GAPDH protein analysis: A functional and biochemical approach. Springer, Singapore, 85–94. https://doi.org/10.1007/978-981-10-7342-7_8

Geddes, B. A., Oresnik, I. J. 2014. Physiology, genetics, and biochemistry of carbon metabolism in the alphaproteobacterium *Sinorhizobium meliloti*. Can J Microbiol, 60, 491–507. https://doi.org/10.1139/cjm-2014-0306

Giménez, R., Aguilera, L., Ferreira, E., Aguilar, J., Baldomà, L., Badia, J. 2014. Glyceraldehyde-3-phosphate dehydrogenase as a moonlighting protein in bacteria. In: Muñoz-Torrero, D., Vázquez-Carrera, M. , Estelrich, J. editors. Recent Advances in Pharmaceutical Sciences IV. Kerala, India: Research Signpost, 165-180.

Gloag, E. S., Turnbull, L., Huang, A., Vallotton, P., Wang, H., Nolan, L. M., Mililli, L., Hunt, C., Lu, J., Osvath, S. R., Monahan, L. G., Cavaliere, R., Charles, I. G., Wand, M. P., Gee, M. L., Prabhakar, R., Whitchurch, C. B. 2013. Self-organization of bacterial biofilms is facilitated by extracellular DNA. Proc Natl Acad Sci USA 110, 11541–11546. https://doi.org/10.1073/pnas.1218898110

González, V., Bustos, P., Ramírez-Romero, M. A., Medrano-Soto, A., Salgado, H., Hernández-González, I., Hernández-Celis, J. C., Quintero, V., Moreno-Hagelsieb, G., Girard, L., Rodríguez, O., Flores, M., Cevallos, M. A., Collado-Vides, J., Romero, D., Dávila, G. 2003. The mosaic structure of the symbiotic plasmid of *Rhizobium etli* CFN42 and its relation to other symbiotic genome compartments. Genome Biol, 4, R36. https://doi.org/10.1186/gb-2003-4-6-r36

González, V., Santamaría, R. I., Bustos, P., Hernández-González, I., Medrano-Soto, A., Moreno-Hagelsieb, G., Janga, S. C., Ramírez, M. A., Jiménez-Jacinto, V., Collado-Vides, J., Dávila, G. 2006. The partitioned *Rhizobium etli* genome: Genetic and metabolic redundancy in seven interacting replicons. Proc Natl Acad Sci USA 103, 3834–3839. https://doi.org/10.1073/pnas.0508502103

Gosselin, I., Wattraint, O., Riboul, D., Barbotin, J.-N., Portais, J.-C. 2001. A deeper investigation on carbohydrate cycling in *Sinorhizobium meliloti*. FEBS Letters, 499, 45–49. https://doi.org/10.1016/S0014-5793(01)02518-2

Götz, F., Yu, W., Dube, L., Prax, M., Ebner, P. 2015. Excretion of cytosolic proteins (ECP) in bacteria. Int J Med Microbiol 305, 230–237. https://doi.org/10.1016/j.ijmm.2014.12.021

Govindarajulu, M., Pfeffer, P. E., Jin, H., Abubaker, J., Douds, D. D., Allen, J. W., Bücking, H., Lammers, P. J., Shachar-Hill, Y. 2005. Nitrogen transfer in the arbuscular mycorrhizal symbiosis. Nature 435, 819–823. https://doi.org/10.1038/nature03610

Grant, S. R., Fisher, E. J., Chang, J. H., Mole, B. M., Dangl, J. L. 2006. Subterfuge and manipulation: Type III effector proteins of phytopathogenic bacteria. Annu Rev Microbiol 60, 425–449. https://doi.org/10.1146/annurev.micro.60.080805.142251

Grenga, L., Little, R. H., Chandra, G., Woodcock, S. D., Saalbach, G., Morris, R. J., Malone, J. G. 2020. Control of mRNA translation by dynamic ribosome modification. PLOS Genetics 16, e1008837. https://doi.org/10.1371/journal.pgen.1008837

Hanahan, D. 1983. Studies on transformation of *Escherichia coli* with plasmids. J. Mol. Biol. 166, 557–580. https://doi.org/10.1016/s0022-2836(83)80284-8

Harvey, K. L., Jarocki, V. M., Charles, I. G., Djordjevic, S. P. 2019. The diverse functional roles of elongation factor Tu (EF-Tu) in microbial pathogenesis. Front Microbiol 10, 2351. https://doi.org/10.3389/fmicb.2019.02351

Hengge, R. 2009. Principles of c-di-GMP signalling in bacteria. Nature Rev Microbiol 7, 263–273. https://doi.org/10.1038/nrmicro2109

Hengge, R. 2021. High-specificity local and global c-di-GMP signaling. Trends Microbiol 29, 993–1003. https://doi.org/10.1016/j.tim.2021.02.003

Hengge, R., Gründling, A., Jenal, U., Ryan, R., Yildiz, F. 2016. Bacterial signal transduction by cyclic di-GMP and other nucleotide second messengers. J Bacteriol 198, 15–26. https://doi.org/10.1128/JB.00331-15

Hengge, R., Pruteanu, M., Stülke, J., Tschowri, N., Turgay, K. 2023. Recent advances and perspectives in nucleotide second messenger signaling in bacteria. microLife 4, uqad015. https://doi.org/10.1093/femsml/uqad015

Heredia-Ponce, Z., Gutiérrez-Barranquero, J. A., Purtschert-Montenegro, G., Eberl, L., Cazorla, F. M., de Vicente, A. 2020. Biological role of EPS from *Pseudomonas syringae* pv. syringae UMAF0158 extracellular matrix, focusing on a Psl-like polysaccharide. NPJ Biofilms Microbi 6, 37. https://doi.org/10.1038/s41522-020-00148-6

Hickman, J. W., Harwood, C. S. 2008. Identification of FleQ from *Pseudomonas aeruginosa* as a c-di-GMP-responsive transcription factor. Mol Microbiol 69, 376–389. https://doi.org/10.1111/j.1365-2958.2008.06281.x

Hirano, S. S., Upper, C. D. 2000. Bacteria in the leaf ecosystem with emphasis on *Pseudomonas syringae*—A pathogen, ice nucleus, and epiphyte. Microbiol Mol Biol Rev 64, 624–653. https://doi.org/10.1128/mmbr.64.3.624-653.2000

Hurkman W. J., Tanaka C. K. 1986. Solubilization of plant membrane proteins for analysis by two-dimensional gel electrophoresis. Plant Physiol 81, 802-806. https://doi.org/10.1104/pp.81.3.802

Hurtado-Rios, J. J., Carrasco-Navarro, U., Almanza-Pérez, J. C., Ponce-Alquicira, E. 2022. Ribosomes: The new role of ribosomal proteins as natural antimicrobials. Int J Mol Sci 23, Article 16. https://doi.org/10.3390/ijms23169123

Huynh T. V., Dahlbeck D., Staskawicz B. J. 1989. Bacterial blight of soybean: regulation of a pathogen gene determining host cultivar specificity. Science 245, 1374-1377. https://doi.org/10.1126/science.2781284

Irigoyen, J. J., Sanchez-Diaz, M., Emerich, D. W. 1990. Carbon metabolism enzymes of *Rhizobium meliloti* cultures and bacteroids and their distribution within alfalfa nodules. Applied and Environ Microbiol 56, 2587–2589. https://doi.org/10.1128/aem.56.8.2587-2589.1990

Jarrell, K. F., McBride, M. J. 2008. The surprisingly diverse ways that prokaryotes move. Nature Rev Microbiol, 6, Article 6. https://doi.org/10.1038/nrmicro1900

Jeffery, C. J. 1999. Moonlighting proteins. Trends in Biochemi Sci 24, 8–11. https://doi.org/10.1016/s0968-0004(98)01335-8

Jeffery, C. J. 2004. Molecular mechanisms for multitasking: recent crystal structures of moonlighting proteins. Current Opinion in Structural Biology 14, 663–668. https://doi.org/10.1016/j.sbi.2004.10.001

Jeffery, C. J. 2009. Moonlighting proteins—An update. Mol Biosyst, 5, 345. https://doi.org/10.1039/b900658n

Jeffery, C. J. 2016. Protein species and moonlighting proteins: Very small changes in a protein's covalent structure can change its biochemical function. J Proteom 134, 19–24. https://doi.org/10.1016/j.jprot.2015.10.003

Jeffery, C. J. 2017. Protein moonlighting: What is it, and why is it important? Phil Trans R Soc B: Biological Sciences, 373, 20160523. https://doi.org/10.1098/rstb.2016.0523

Jeffery, C. J. 2018. Intracellular proteins moonlighting as bacterial adhesion factors. AIMS Microbiol 4, 362–376. https://doi.org/10.3934/microbiol.2018.2.362

Jeffery, C. J. 2019. Intracellular/surface moonlighting proteins that aid in the attachment of gut microbiota to the host. AIMS Microbiol 5, 77–86. https://doi.org/10.3934/microbiol.2019.1.77

Jeffery, C. J. 2020. Enzymes, pseudoenzymes, and moonlighting proteins: diversity of function in protein superfamilies. FEBS J 287, 4141–4149. https://doi.org/10.1111/febs.15446

Jiao, Y., D'haeseleer, P., Dill, B.D., Shah, M., VerBerkmoes, N.C., Hettich, R.L., Banfield, J.F., Thelen, M.P. 2011. Identification of biofilm matrix-associated proteins from an acid mine drainage microbial community. Applied and Environ Microbiol 77, 5230–5237. https://doi.org/10.1128/AEM.03005-10

Jin, H., Song, Y. P., Boel, G., Kochar, J., Pancholi, V. 2005. Group A streptococcal surface GAPDH, SDH, recognizes uPAR/CD87 as its receptor on the human pharyngeal cell and mediates bacterial adherence to host cells. J Mol Biol 350, 27–41. https://doi.org/10.1016/j.jmb.2005.04.063

Jones, A. M., Lindow, S. E., Wildermuth, M. C. 2007. Salicylic acid, yersiniabactin, and pyoverdin production by the model phytopathogen *Pseudomonas syringae* pv. tomato DC3000: Synthesis, regulation, and impact on tomato and *Arabidopsis* host plants. J Bacteriol 189, 6773–6786. https://doi.org/10.1128/JB.00827-07

Jones, K. M., Kobayashi, H., Davies, B. W., Taga, M. E., Walker, G. C. 2007. How rhizobial symbionts invade plants: The *Sinorhizobium–Medicago* model. Nature Rev Microbiol 5, Article 8. https://doi.org/10.1038/nrmicro1705

Jun, S. R., Wassenaar, T. M., Nookaew, I., Hauser, L., Wanchai, V., Land, M., Timm, C. M., Lu, T.-Y. S., Schadt, C. W., Doktycz, M. J., Pelletier, D. A., Ussery, D. W. 2016. Diversity of *Pseudomonas* genomes, including populus-associated isolates, as revealed by comparative genome analysis. Applied and Environ Microbiol 82, 375–383. https://doi.org/10.1128/AEM.02612-15

Junkermeier, E.H., Hengge, R. 2023. Local signaling enhances output specificity of bacterial c-di-GMP signaling networks. microLife 4, uqad026. https://doi.org/10.1093/femsml/uqad026

Kainulainen, V., Korhonen, T. K. 2014. Dancing to another tune-adhesive moonlighting proteins in bacteria. Biology (Basel) 3, 178-204. https://doi.org/10.3390/biology3010178

Kaplan, J. B., Ragunath, C., Ramasubbu, N., Fine, D. H. 2003. Detachment of *Actinobacillus actinomycetemcomitans* biofilm cells by an endogenous β-hexosaminidase activity. J Bacteriol 185, 4693–4698. https://doi.org/10.1128/jb.185.16.4693-4698.2003

Kharadi, R. R., Castiblanco, L. F., Waters, C. M., Sundin, G. W. 2018. Phosphodiesterase genes regulate amylovoran production, biofilm formation, and virulence in *Erwinia amylovora*. Applied and Environ Microbiol 85, e02233-18. https://doi.org/10.1128/AEM.02233-18

Kharadi, R. R., Sundin, G. W. 2020. Cyclic-di-GMP regulates autoaggregation through the putative peptidoglycan hydrolase, EagA, and regulates transcription of the *znuABC* zinc uptake gene cluster in *Erwinia amylovora*. Front Microbiol 11. https://doi.org/10.3389/fmicb.2020.605265

Kim, J., Dang, C. V. 2005. Multifaceted roles of glycolytic enzymes. Trends Biochem Sci, 30, 142–150. https://doi.org/10.1016/j.tibs.2005.01.005

Kinhikar, A. G., Vargas, D., Li, H., Mahaffey, S. B., Hinds, L., Belisle, J. T., Laal, S. 2006. *Mycobacterium tuberculosis* malate synthase is a laminin-binding adhesin. Mol Microbiol 60, 999–1013. https://doi.org/10.1111/j.1365-2958.2006.05151.x

Kinoshita, E., Kinoshita-Kikuta, E., Takiyama, K., Koike, T. 2006. Phosphate-binding Tag, a new tool to visualize phosphorylated proteins. Mol Cel Proteom 5, 749–757. https://doi.org/10.1074/mcp.T500024-MCP200

Kinoshita, H., Uchida, H., Kawai, Y., Kawasaki, T., Wakahara, N., Matsuo, H., Watanabe, M., Kitazawa, H., Ohnuma, S., Miura, K., Horii, A., Saito, T. 2008. Cell surface *Lactobacillus plantarum* LA 318 glyceraldehyde-3-phosphate dehydrogenase (GAPDH) adheres to human colonic mucin. J App Microbiol, 104, 1667–1674. https://doi.org/10.1111/j.1365-2672.2007.03679.x

Kohlstedt, M., Wittmann, C. 2019. GC-MS-based ^{13}C metabolic flux analysis resolves the parallel and cyclic glucose metabolism of *Pseudomonas putida* KT2440 and *Pseudomonas aeruginosa* PAO1. Metab Eng, 54, 35–53. https://doi.org/10.1016/j.ymben.2019.01.008

Koike, S. T., Alger, E. I., Ramos-Sepulveda, L., Bull C. T. 2017. First report of bacterial leaf spot caused by *Pseudomonas syringae* pv. tomato on kale in California. Plant Dis 101, 504-504. https://doi.org/10.1094/PDIS-10-16-1460-PDN

Kopeckova, M., Pavkova, I., Link, M., Rehulka, P., Stulik, J. 2020a. Identification of Bacterial Protein Interaction Partners Points to New Intracellular Functions of Francisella tularensis Glyceraldehyde-3-Phosphate Dehydrogenase. Front Microbiol 11, 576618. https://doi.org/10.3389/fmicb.2020.576618

Kopeckova, M., Pavkova, I., Stulik, J. 2020b. Diverse localization and protein binding abilities of glyceraldehyde-3-phosphate dehydrogenase in pathogenic bacteria: The key to its multifunctionality? Front Cell Infect Microbiol 10. https://doi.org/10.3389/fcimb.2020.00089

Kothary, M. H., Gopinath, G. R., Gangiredla, J., Rallabhandi, P. V., Harrison, L. M., Yan, Q. Q., Chase, H. R., Lee, B., Park, E., Yoo, Y., Chung, T., Finkelstein, S. B., Negrete, F. J., Patel, I. R., Carter, L., Sathyamoorthy, V., Fanning, S., Tall, B. D. 2017. Analysis and characterization of proteins associated with outer membrane vesicles secreted by *Cronobacter spp*. Front Microbiol 8, https://doi.org/10.3389/fmicb.2017.00134

Krishna, P. S., Woodcock, S. D., Pfeilmeier, S., Bornemann, S., Zipfel, C., Malone, J. G. 2022. *Pseudomonas syringae* addresses distinct environmental challenges during plant infection through the coordinated deployment of polysaccharides. Journal of Experimental Botany 73 2206–2221. https://doi.org/10.1093/jxb/erab550

Krol, E., Schäper, S., Becker, A. 2020. Cyclic di-GMP signaling controlling the free-living lifestyle of alpha-proteobacterial rhizobia. Biol Chem 401, 1335–1348. https://doi.org/10.1515/hsz-2020-0232

Kuchma, S. L., Brothers, K. M., Merritt, J. H., Liberati, N. T., Ausubel, F. M., O'Toole, G. A. 2007. BifA, a cyclic-Di-GMP phosphodiesterase, inversely regulates biofilm formation and swarming motility by *Pseudomonas aeruginosa* PA14. J Bacteriol 189, 8165–8178. https://doi.org/10.1128/JB.00586-07

Laemmli, U. K. 1970. Cleavage of structural proteins during the assembly of the head of bacteriophage T4. Nature 227, 680–685. https://doi.org/10.1038/227680a0

Lagitnay, R. B. J. S., Chen, H.-L., Chen, Y.-C., Chuang, D.-Y. 2022. Diguanylate cyclase (DGC) implicated in the synthesis of multiple bacteriocins via the flagellar-type III secretion system produced by *Pectobacterium carotovorum* subsp. carotovorum. Int J Mol Sci 23, Article 10. https://doi.org/10.3390/ijms23105649

Lama A., Kucknoor A., Mundodi V., Alderete J. F. 2009. Glyceraldehyde-3-phosphate dehydrogenase is a surface-associated, fibronectin-binding protein of *Trichomonas vaginalis*. Inf Imm 77, 2703-2711. https://doi.org/10.1128/IAI.00157-09

Lamichhane, J. R., Messéan, A., Morris, C. E. 2015. Insights into epidemiology and control of diseases of annual plants caused by the *Pseudomonas syringae* species complex. J Gen Plant Pathol 81, 331–350. https://doi.org/10.1007/s10327-015-0605-z

Larrainzar, E., Villar, I., Rubio, M. C., Pérez-Rontomé, C., Huertas, R., Sato, S., Mun, J.-H., Becana, M. 2020. Hemoglobins in the legume–*Rhizobium* symbiosis. New Phytol 228, 472–484. https://doi.org/10.1111/nph.16673

Lederberg, E. M., Cohen, S. N. 1974. Transformation of *Salmonella typhimurium* by plasmid deoxyribonucleic acid. J Bacteriol 119, 1072–1074. https://doi.org/10.1128/jb.119.3.1072-1074.1974

Lee, J., Lee, H.-J., Shin, M.-K., Ryu, W.-S. 2004. Versatile PCR-mediated insertion or deletion mutagenesis. BioTechniques 36, 398–400. https://doi.org/10.2144/04363BM04

Lessie T. G., Phibbs Jr. P. V. 1984. Alternative pathways of carbohydrate utilization in pseudomonads. Annu Rev Microbiol 38, 359-388. https://doi.org/10.1146/annurev.mi.38.100184.002043

Leutert, M., Entwisle, S. W., Villén, J. 2021. Decoding post-translational modification crosstalk with proteomics. Mol Cell Proteom 20, 100129. https://doi.org/10.1016/j.mcpro.2021.100129

Li, H., Luo, Y.-F., Williams, B. J., Blackwell, T. S., Xie, C.-M. 2012. Structure and function of OprD protein in *Pseudomonas aeruginosa*: From antibiotic resistance to novel therapies. Int J Med Microbiol 302(2), 63–68. https://doi.org/10.1016/j.ijmm.2011.10.001

Li, M. L., Jiao, J., Zhang, B., Shi, W.-T., Yu, W.-H., Tian, C.-F. 2021. Global transcriptional repression of diguanylate cyclases by MucR1 is essential for *Sinorhizobium*-soybean symbiosis. mBio, 12(5), 10.1128/mbio.01192-21. https://doi.org/10.1128/mbio.01192-21

Li, S., Lou, X., Xu, Y., Teng, X., Liu, R., Zhang, Q., Wu, W., Wang, Y., Bartlam, M. 2019. Structural basis for the recognition of MucA by MucB and AlgU in *Pseudomonas aeruginosa*. FEBS J 286, 4982–4994. https://doi.org/10.1111/febs.14995

Li, X., Zheng, X., Yadav, N., Saha, S., Salama, E.-S., Li, Xiangkai, Wang, L., Jeon, B.-H. 2024. Rational management of the plant microbiome for the second green revolution. Plant Commun 5, 100812. https://doi.org/10.1016/j.xplc.2024.100812

Li, Y., Zhao, J., Liu, Z., Wang, C., Wei, L., Han, S., Du, W. 2021. De novo prediction of moonlighting proteins using multimodal deep ensemble learning. Front Genet 12. https://doi.org/10.3389/fgene.2021.630379

Liang, Z.-X. 2015. The expanding roles of c-di-GMP in the biosynthesis of exopolysaccharides and secondary metabolites. Nat Prod Rep 32, 663–683. https://doi.org/10.1039/c4np00086b

Liang, Z., Rybtke, M., Kragh, K.N., Johnson, O., Schicketanz, M., Zhang, Y.E., Andersen, J.B., Tolker-Nielsen, T. 2022. Transcription of the alginate operon in *Pseudomonas aeruginosa* Is regulated by c-di-GMP. Microbiol Spectr 10, e00675-22. https://doi.org/10.1128/spectrum.00675-22

Lindström, K., Mousavi, S. A. 2020. Effectiveness of nitrogen fixation in rhizobia. Microb Biotechnol 13, 1314–1335. https://doi.org/10.1111/1751-7915.13517

Little, R. H., Grenga, L., Saalbach, G., Howat, A. M., Pfeilmeier, S., Trampari, E., Malone, J. G. 2016. Adaptive remodeling of the bacterial proteome by specific ribosomal modification regulates *Pseudomonas* infection and niche colonisation. PLOS Genetics 12, e1005837. https://doi.org/10.1371/journal.pgen.1005837

Liu, H., Jeffery, C. J. 2020. Moonlighting proteins in the fuzzy logic of cellular metabolism. Molecules 25, 3440. https://doi.org/10.3390/molecules25153440

Liu, J., Miller, S. S., Graham, M., Bucciarelli, B., Catalano, C. M., Sherrier, D. J., Samac, D. A., Ivashuta, S., Fedorova, M., Matsumoto, P., Gantt, J. S., Vance, C. P. 2006. Recruitment of novel calcium-binding proteins for root nodule symbiosis in *Medicago truncatula*. Plant Physiol, 141, 167–177. https://doi.org/10.1104/pp.106.076711

Liu, T., Tian, C. F., Chen, W. X. 2015. Site-specific Ser/Thr/Tyr phosphoproteome of *Sinorhizobium meliloti* at stationary phase. PLOS ONE, 10(9), e0139143. https://doi.org/10.1371/journal.pone.0139143

Liu, Y., Oshima, S., Kurohara, K., Ohnishi, K., Kawai, K. 2005. Vaccine efficacy of recombinant GAPDH of *Edwardsiella tarda* against Edwardsiellosis. Microbiol Immunol,49, 605–612. https://doi.org/10.1111/j.1348-0421.2005.tb03652.x

Livak, K. J., Schmittgen, T. D. 2001. Analysis of relative gene expression data using real-time quantitative PCR and the 2(-Delta Delta C(T)) Method. Methods 25, 402–408. https://doi.org/10.1006/meth.2001.1262

Llamas, M. A., Imperi, F., Visca, P., Lamont, I. L. 2014. Cell-surface signaling in *Pseudomonas*: stress responses, iron transport, and pathogenicity. FEMS Microbiology Reviews 38, 569–597. https://doi.org/10.1111/1574-6976.12078

Lodwig, E., Poole, P. 2003. Metabolism of *Rhizobium* bacteroids. Crit Rev Plant Sci 22, 37–78. https://doi.org/10.1080/713610850

López-Baena, F. J., Vinardell, J. M., Medina, C. 2019. Regulation of protein secretion systems mediated by cyclic diguanylate in plant-interacting bacteria. Front Microbiol 10, 456912. https://doi.org/10.3389/fmicb.2019.01289

Lorite, M. J., Casas-Román, A., Girard, L., Encarnación, S., Díaz-Garrido, N., Badía, J., Baldomá, L., Pérez-Mendoza, D., Sanjuán, J. 2023. Impact of c-di-GMP on the Extracellular Proteome of *Rhizobium etli*. Biology (Basel) 12, 44. https://doi.org/10.3390/biology12010044

Maaz, T. M., Sapkota, T. B., Eagle, A. J., Kantar, M. B., Bruulsema, T. W., Majumdar, K. 2021. Meta-analysis of yield and nitrous oxide outcomes for nitrogen management in agriculture. Glob Change Biol 27, 2343–2360. https://doi.org/10.1111/gcb.15588

Macek, B., Forchhammer, K., Hardouin, J., Weber-Ban, E., Grangeasse, C., Mijakovic, I. 2019. Protein post-translational modifications in bacteria. Nat Rev Microbiol 17, 651–664. https://doi.org/10.1038/s41579-019-0243-0

Madeira, F., Pearce, M., Tivey, A.R.N., Basutkar, P., Lee, J., Edbali, O., Madhusoodanan, N., Kolesnikov, A., Lopez, R. 2022. Search and sequence analysis tools services from EMBL-EBI in 2022. Nucleic Acids Res 50, W276–W279. https://doi.org/10.1093/nar/gkac240

Malay, A. D., Bessho, Y., Ellis, M. J., Antonyuk, S. V., Strange, R. W., Hasnain, S. S., Shinkai, A., Padmanabhan, B., Yokoyama, S. 2009. Structure of glyceraldehyde-3-phosphate dehydrogenase from the archaeal hyperthermophile *Methanocaldococcus jannaschii*. Acta Crystallogr Sect F Struct Biol Cryst 65, 1227–1233. https://doi.org/10.1107/S1744309109047046

Mani, M., Chen, C., Amblee, V., Liu, H., Mathur, T., Zwicke, G., Zabad, S., Patel, B., Thakkar, J., Jeffery, C. J. 2015. MoonProt: A database for proteins that are known to moonlight. Nucleic Acids Res 43, D277-282. https://doi.org/10.1093/nar/gku954

Mann, E. E., Wozniak, D. J. 2012. *Pseudomonas* biofilm matrix composition and niche biology. FEMS Microbiol Rev 36, 893–916. https://doi.org/10.1111/j.1574-6976.2011.00322.x

Martinez-Gil, M., Ramos, C. 2018. Role of Cyclic di-GMP in the bacterial virulence and evasion of the plant Immunity. Curr Issues Mol Biol 25, 199–222. https://doi.org/10.21775/cimb.025.199

Martínez-Granero, F., Redondo-Nieto, M., Vesga, P., Martín, M., Rivilla, R. 2014. AmrZ is a global transcriptional regulator implicated in iron uptake and environmental adaption in *P. fluorescens* F113. BMC Genomics 15, 237. https://doi.org/10.1186/1471-2164-15-237

Martínez-Rodríguez, L., López-Sánchez, A., García-Alcaide, A., Govantes, F., Gallegos, M.-T. 2023. FleQ, FleN and c-di-GMP coordinately regulate cellulose production in *Pseudomonas syringae* pv. tomato DC3000. Front. Mol. Biosci. 10. https://doi.org/10.3389/fmolb.2023.1155579

Masco, L., Crockaert, C., Van Hoorde, K., Swings, J., Huys, G. 2007. *In vitro* assessment of the gastrointestinal transit tolerance of taxonomic reference strains from human origin and probiotic product isolates of bifidobacterium. J Dairy Sci 90, 3572–3578. https://doi.org/10.3168/jds.2006-548

Masson-Boivin, C., Giraud, E., Perret, X., Batut, J. 2009. Establishing nitrogen-fixing symbiosis with legumes: How many rhizobium recipes? Trends Microbiol 17, 458–466. https://doi.org/10.1016/j.tim.2009.07.004

Masson-Boivin, C., Sachs, J. L. 2018. Symbiotic nitrogen fixation by rhizobia—The roots of a success story. Curr Opin Plant Biol 44, 7–15. https://doi.org/10.1016/j.pbi.2017.12.001

Matilla, M. A., Ramos, J. L., Duque, E., de Dios Alché, J., Espinosa-Urgel, M., Ramos-González, M. I. 2007. Temperature and pyoverdine-mediated iron acquisition control surface motility of *Pseudomonas putida*. Environ Microbiol 9, 1842–1850. https://doi.org/10.1111/j.1462-2920.2007.01286.x

Matsuyama, B. Y., Krasteva, P. V., Baraquet, C., Harwood, C. S., Sondermann, H., Navarro, M. V. A. S. 2016. Mechanistic insights into c-di-GMP–dependent control of the biofilm regulator FleQ from *Pseudomonas aeruginosa*. Proc Natl Acad Sci USA 113, E209–E218. https://doi.org/10.1073/pnas.1523148113

Matta, S. K., Agarwal, S., Bhatnagar, R. 2010. Surface localized and extracellular glyceraldehyde-3-phosphate dehydrogenase of *Bacillus anthracis* is a plasminogen binding protein. Biochim Biophys Acta - Proteins and Proteomics, 1804, 2111–2120. https://doi.org/10.1016/j.bbapap.2010.08.004

McDonald, B. A., Stukenbrock, E. H. 2016. Rapid emergence of pathogens in agro-ecosystems: Global threats to agricultural sustainability and food security. Philosophical Trans R Soc B: Biological Sciences 371, 20160026. https://doi.org/10.1098/rstb.2016.0026

Melotto, M., Underwood, W., He, S. Y. 2008. Role of stomata in plant innate immunity and foliar bacterial diseases. Ann Rev Phytopathol 46, 101–122. https://doi.org/10.1146/annurev.phyto.121107.104959

Melotto, M., Zhang, L., Oblessuc, P. R., He, S. Y. 2017. Stomatal defense a decade later. Plant Physiol 174, 561–571. https://doi.org/10.1104/pp.16.01853

Mendes, R., Garbeva, P., Raaijmakers, J. M. 2013. The rhizosphere microbiome: Significance of plant beneficial, plant pathogenic, and human pathogenic microorganisms. FEMS Microbiol Rev 37, 634–663. https://doi.org/10.1111/1574-6976.12028

Meneses, N., Mendoza-Hernández, G., Encarnación, S. 2010. The extracellular proteome of *Rhizobium etli* CE3 in exponential and stationary growth phase. Proteome Sci 8, 51. https://doi.org/10.1186/1477-5956-8-51

Meneses, N., Taboada, H., Dunn, M. F., Vargas, M. del C., Buchs, N., Heller, M., Encarnación, S. 2017. The naringenin-induced exoproteome of *Rhizobium etli* CE3. ArchMicrobiol 199, 737–755. https://doi.org/10.1007/s00203-017-1351-8

Miller, J. H. 1972. Experiments in Molecular Genetics. New York, Cold Spring Harbor Laboratory.

Mills, E., Pultz, I. S., Kulasekara, H. D., Miller, S. I. 2011. The bacterial second messenger c-di-GMP: Mechanisms of signalling. Cell Microbiol 13, 1122–1129. https://doi.org/10.1111/j.1462-5822.2011.01619.x

Morgan, J. L. W., McNamara, J. T., Zimmer, J. 2014. Mechanism of activation of bacterial cellulose synthase by cyclic di-GMP. Nat Struct Mol Biol 21, 489–496. https://doi.org/10.1038/nsmb.2803

Morris, C. E., Monteil, C. L., Berge, O. 2013. The life history of *Pseudomonas syringae*: Linking agriculture to earth system processes. Ann Rev Phytopathol 51, 85–104. https://doi.org/10.1146/annurev-phyto-082712-102402

Mulley, G., Lopez-Gomez, M., Zhang, Y., Terpolilli, J., Prell, J., Finan, T., Poole, P. 2010. Pyruvate is synthesized by two pathways in pea bacteroids with different efficiencies for nitrogen fixation. J Bacteriol 192, 4944–4953. https://doi.org/10.1128/jb.00294-10

Muriel, C., Arrebola, E., Redondo-Nieto, M., Martínez-Granero, F., Jalvo, B., Pfeilmeier, S., Blanco-Romero, E., Baena, I., Malone, J. G., Rivilla, R., Martín, M. 2018. AmrZ is a major determinant of c-di-GMP levels in *Pseudomonas fluorescens* F113. Sci Rep 8, Article 1. https://doi.org/10.1038/s41598-018-20419-9

Nagakubo, T., Nomura, N., Toyofuku, M. 2020. Cracking open bacterial membrane vesicles. Front Microbiol 10, 3026. https://doi.org/10.3389/fmicb.2019.03026

Newell, P. D., Boyd, C. D., Sondermann, H., O'Toole, G. A. 2011. A c-di-GMP effector system controls cell adhesion by inside-out signaling and surface protein cleavage. PLOS Biology 9, e1000587. https://doi.org/10.1371/journal.pbio.1000587

Nicholls, C., Li, H., Liu, J.-P. 2012. GAPDH: A common enzyme with uncommon functions. Clin Exp Pharmacol Physiol 39, 674–679. https://doi.org/10.1111/j.1440-1681.2011.05599.x

Nijland, R., Hall, M. J., Burgess, J. G. 2010. Dispersal of biofilms by secreted, matrix degrading, bacterial DNase. PLOS ONE 5, e15668. https://doi.org/10.1371/journal.pone.0015668

Nikel, P. I., Chavarría, M., Fuhrer, T., Sauer, U., de Lorenzo, V. 2015. *Pseudomonas putida* KT2440 strain metabolizes glucose through a cycle formed by enzymes of the Entner-Doudoroff, Embden-Meyerhof-Parnas, and pentose phosphate pathways. J Biol Chem 290, 25920–25932. https://doi.org/10.1074/jbc.M115.687749

Nimma, R., Kumar, A., Gani, Z., Gahlawat, A., Dilawari, R., Rohilla, R. K., Kumbhar, H., Garg, P., Chopra, S., Raje, M., Iyengar-Raje, C. 2023. Characterization of the enzymatic and multifunctional properties of *Acinetobacter baumannii* erythrose-4-phosphate dehydrogenase (E4PDH). Microb Pathog 175, 105992. https://doi.org/10.1016/j.micpath.2023.105992

Nishimura, A., Morita, M., Nishimura, Y., Sugino, Y. 1990. A rapid and highly efficient method for preparation of competent *Escherichia coli* cells. Nucleic Acids Res 18, 6169. https://doi.org/10.1093/nar/18.20.6169

Nishiyama, K., Yong, C.-C., Moritoki, N., Kitazawa, H., Odamaki, T., Xiao, J.-Z., Mukai, T. 2023. Sharing of moonlighting proteins mediates the symbiotic relationship among intestinal commensals. Applied and Environ Microbiol 89, e02190-22. https://doi.org/10.1128/aem.02190-22

Nogales, J., Vargas, P., Farias, G. A., Olmedilla, A., Sanjuán, J., Gallegos, M. T. 2015. FleQ coordinates flagellum-dependent and independent motilities in *Pseudomonas syringae* pv. tomato DC3000. Applied and Environ Microbiol 81, 7533–7545. https://doi.org/10.1128/AEM.01798-15

Oldroyd, G. E. D. 2013. Speak, friend, and enter: Signalling systems that promote beneficial symbiotic associations in plants. Nat Rev Microbiol 11, Article 4. https://doi.org/10.1038/nrmicro2990

Olivares, J., Bedmar, E. J., Sanjuán, J. 2013. Biological nitrogen fixation in the context of global change. Mol Plant-Microbe Int 26, 486–494. https://doi.org/10.1094/MPMI-12-12-0293-CR

Oliveira, L., Madureira, P., Andrade, E.B., Bouaboud, A., Morello, E., Ferreira, P., Poyart, C., Trieu-Cuot, P., Dramsi, S. 2012. Group B *Streptococcus* GAPDH is released upon cell lysis, associates with bacterial surface, and induces apoptosis in murine macrophages. PLOS ONE 7, e29963. https://doi.org/10.1371/journal.pone.0029963

Ormeño-Orrillo, E., Servín-Garcidueñas, L. E., Rogel, M. A., González, V., Peralta, H., Mora, J., Martínez-Romero, J., Martínez-Romero, E. 2015. Taxonomy of rhizobia and agrobacteria from the *Rhizobiaceae* family in light of genomics. Syst Appl Microbiol 38, 287–291. https://doi.org/10.1016/j.syapm.2014.12.002

Østerås, M., Finan, T. M., Stanley, J. 1991. Site-directed mutagenesis and DNA sequence of pckA of *Rhizobium* NGR234, encoding phosphoenolpyruvate carboxykinase: Gluconeogenesis and host-dependent symbiotic phenotype. Mol Gen Genet 230, 257–269. https://doi.org/10.1007/BF00290676

Pancholi, V., Fischetti, V. A. 1992. A major surface protein on group A streptococci is a glyceraldehyde-3- phosphate-dehydrogenase with multiple binding activity. J Exp Med 176, 415–426. https://doi.org/10.1084%2Fjem.176.2.415

Panter, S., Thomson, R., de Bruxelles, G., Laver, D., Trevaskis, B., Udvardi, M. 2000. Identification with proteomics of novel proteins associated with the peribacteroid membrane of soybean root nodules. Mol Plant-Microbe Int 13, 325–333. https://doi.org/10.1094/MPMI.2000.13.3.325

Pasztor, L., Ziebandt, A.-K., Nega, M., Schlag, M., Haase, S., Franz-Wachtel, M., Madlung, J., Nordheim, A., Heinrichs, D.E., Götz, F. 2010. Staphylococcal major autolysin (Atl) is involved in excretion of cytoplasmic proteins. J Biol Chem 285, 36794–36803. https://doi.org/10.1074/jbc.M110.167312

Paul, K., Nieto, V., Carlquist, W. C., Blair, D. F., Harshey, R. M. 2010. The c-di-GMP binding protein YcgR controls flagellar motor direction and speed to affect chemotaxis by a "backstop brake" mechanism. Mol Cell, 38, 128–139. https://doi.org/10.1016/j.molcel.2010.03.001

Paul, R., Abel, S., Wassmann, P., Beck, A., Heerklotz, H., Jenal, U. 2007. Activation of the diguanylate cyclase PleD by phosphorylation-mediated dimerization. The J Biol Chem 282, 29170–29177. https://doi.org/10.1074/jbc.M704702200

Paysan-Lafosse, T., Blum, M., Chuguransky, S., Grego, T., Pinto, B. L., Salazar, G. A., Bileschi, M. L., Bork, P., Bridge, A., Colwell, L., Gough, J., Haft, D. H., Letunić, I., Marchler-Bauer, A., Mi, H., Natale, D. A., Orengo, C. A., Pandurangan, A. P., Rivoire, C., Sigrist, C. J. A., Sillitoe, I., Thanki, N., Thomas, P. D., Tosatto, S. C. E., Wu, C.H., Bateman, A. 2023. InterPro in 2022. Nucleic Acids Res 51, D418–D427. https://doi.org/10.1093/nar/gkac993

Peix, A., Ramírez-Bahena, M.-H., Velázquez, E. 2009. Historical evolution and current status of the taxonomy of genus *Pseudomonas*. Infect Genet Evolu, 9, 1132–1147. https://doi.org/10.1016/j.meegid.2009.08.001

Peoples, M. B., Herridge, D. F., Ladha, J. K. 1995. Biological nitrogen fixation: An efficient source of nitrogen for sustainable agricultural production? In J. K. Ladha M. B. Peoples (Eds.), Management of biological nitrogen fixation for the development of more productive and sustainable agricultural systems: Extended versions of papers presented at the Symposium on Biological Nitrogen Fixation for Sustainable Agriculture at the 15th Congress of Soil Science, Acapulco, Mexico 1994, 3–28. Springer Netherlands. https://doi.org/10.1007/978-94-011-0055-7_1

Pérez-Cruz, C., Cañas, M.-A., Giménez, R., Badia, J., Mercade, E., Baldomà, L., Aguilera, L. 2016. Membrane vesicles released by a hypervesiculating *Escherichia coli* Nissle 1917 tolR mutant are highly heterogeneous and show reduced capacity for epithelial cell interaction and entry. PLoS ONE 11, e0169186. https://doi.org/10.1371/journal.pone.0169186

Pérez-Mendoza, D., Aragón, I. M., Prada-Ramírez, H. A., Romero-Jiménez, L., Ramos, C., Gallegos, M. T., Sanjuán, J. 2014. Responses to elevated c-di-GMP levels in mutualistic and pathogenic plant-Interacting bacteria. PLoS ONE 9, e91645. https://doi.org/10.1371/journal.pone.0091645

Pérez-Mendoza, D., Bertinetti, D., Lorenz, R., Gallegos, M. T., Herberg, F. W., Sanjuán, J. 2017. A novel c-di-GMP binding domain in glycosyltransferase BgsA is responsible for the synthesis of a mixed-linkage β-glucan. Sci Rep 7, 8997. https://doi.org/10.1038/s41598-017-09290-2

Pérez-Mendoza, D., Coulthurst, S. J., Humphris, S., Campbell, E., Welch, M., Toth, I. K., Salmond, G. P. C. 2011a. A multi-repeat adhesin of the phytopathogen, *Pectobacterium atrosepticum*, is secreted by a Type I pathway and is subject to complex regulation involving a non-canonical diguanylate cyclase. Mol Microbiol 82, 719–733. https://doi.org/10.1111/j.1365-2958.2011.07849.x

Pérez-Mendoza, D., Coulthurst, S. J., Sanjuán, J., Salmond, G. P. C. 2011b. N-Acetylglucosamine-dependent biofilm formation in *Pectobacterium atrosepticum* is cryptic and activated by elevated c-di-GMP levels. Microbiology 157, 3340–3348. https://doi.org/10.1099/mic.0.050450-0

Pérez-Mendoza, D., Felipe, A., Ferreiro, M. D., Sanjuán, J., Gallegos, M. T. 2019. AmrZ and FleQ Co-regulate cellulose production in *Pseudomonas syringae* pv. tomato DC3000. Front Microbiol 10. https://doi.org/10.3389/fmicb.2019.00746

Pérez-Mendoza, D., Romero-Jiménez, L., Rodríguez-Carvajal, M. A., Lorite, M. J ., Muñoz, S., Olmedilla, A., Sanjuán, J. 2022. The Role of Two Linear β-Glucans Activated by c-di-GMP in *Rhizobium etli* CFN42. Biology (Basel) 11, 1364. https://doi.org/10.3390/biology11091364

Pérez-Mendoza, D., Sanjuán, J. 2016. Exploiting the commons: cyclic diguanylate regulation of bacterial exopolysaccharide production. Curr Opin Microbiol 30, 36–43. https://doi.org/10.1016/j.mib.2015.12.004

Petnicki-Ocwieja, T., Schneider, D. J., Tam, V. C., Chancey, S. T., Shan, L., Jamir, Y., Schechter, L. M., Janes, M. D., Buell, C. R., Tang, X., Collmer, A., Alfano, J.R. 2002. Genomewide identification of proteins secreted by the Hrp type III protein secretion system of *Pseudomonas syringae* pv. tomato DC3000. Proc Natl Acad Sci USA 99, 7652–7657. https://doi.org/10.1073/pnas.112183899

Piatigorsky, J., O'Brien, W. E., Norman, B. L., Kalumuck, K., Wistow, G. J., Borras, T., Nickerson, J. M., Wawrousek, E. F. 1988. Gene sharing by delta-crystallin and argininosuccinate lyase. Proc Natl Acad Sci USA 85, 3479–3483. https://doi.org/10.1073/pnas.85.10.3479

Pidutti, P., Federici, F., Brandi, J., Manna, L., Rizzi, E., Marini, U., Cecconi, D. 2018. Purification and characterization of ribosomal proteins L27 and L30 having antimicrobial activity produced by the *Lactobacillus salivarius* SGL 03. J Appl Microbiol, 124, 398–407. https://doi.org/10.1111/jam.13646

Plett, J. M., Martin, F. M. 2018. Know your enemy, embrace your friend: Using omics to understand how plants respond differently to pathogenic and mutualistic microorganisms. Plant J 93, 729–746. https://doi.org/10.1111/tpj.13802

Poole, P., Ramachandran, V., Terpolilli, J. 2018. Rhizobia: from saprophytes to endosymbionts. Nat Rev Microbiol 16, 291–303. https://doi.org/10.1038/nrmicro.2017.171

Portais, J.-C., Tavernier, P., Gosselin, I., Barbotin, J.-N. 1999. Cyclic organization of the carbohydrate metabolism in *Sinorhizobium meliloti*. Eur J Biochem 265, 473–480. Scopus. https://doi.org/10.1046/j.1432-1327.1999.00778.x

Prada-Ramírez, H. A., Pérez-Mendoza, D., Felipe, A., Martínez-Granero, F., Rivilla, R., Sanjuán, J., Gallegos, M. T. 2016. AmrZ regulates cellulose production in *Pseudomonas syringae* pv. tomato DC3000: AmrZ represses cellulose biosynthesis genes. Mol Microbiol 99, 960–977. https://doi.org/10.1111/mmi.13278

Preiter, K., Brooks, D. M., Penaloza-Vazquez, A., Sreedharan, A., Bender, C.L., Kunkel, B. N. 2005. Novel virulence gene of *Pseudomonas syringae* pv. tomato strain DC3000. J Bacteriol 187, 7805–7814. https://doi.org/10.1128/jb.187.22.7805-7814.2005

Preston, G. M. 2000. *Pseudomonas syringae* pv. tomato: The right pathogen, of the right plant, at the right time. Mol Plant Pathol 1, 263–275. https://doi.org/10.1046/j.1364-3703.2000.00036.x

Pueyo, C., Jurado, J., Prieto-Alamo, M. J., Monje-Casas, F., López-Barea, J. 2002. Multiplex reverse transcription-polymerase chain reaction for determining transcriptional regulation of thioredoxin and glutaredoxin pathways. Methods Enzymol 347, 441–451. https://doi.org/10.1016/s0076-6879(02)47044-9

Purves J., Cockayne A., Moody P. C., Morrissey J. A. 2010. Comparison of the regulation, metabolic functions, and roles in virulence of the glyceraldehyde-3-phosphate dehydrogenase homologues *gapA* and *gapB* in *Staphylococcus aureus*. Infect Immun 78, 5223-5232. https://doi.org/10.1128/iai.00762-10

Querol-García, J., Fernández, F. J., Marin, A. V., Gómez, S., Fullà, D., Melchor-Tafur, C., Franco-Hidalgo, V., Albertí, S., Juanhuix, J., Rodríguez de Córdoba, S., Regueiro, J. R., Vega, M. C. 2017. Crystal structure of glyceraldehyde-3-phosphate dehydrogenase from the Gram-positive bacterial pathogen *A. vaginae*, an immunoevasive factor that interacts with the human C5a Anaphylatoxin. Front Microbiol 8. https://doi.org/10.3389/fmicb.2017.00541

Quinto, C., de la Vega, H., Flores, M., Fernández, L., Ballado, T., Soberón, G., Palacios, R. 1982. Reiteration of nitrogen fixation gene sequences in *Rhizobium phaseoli*. Nature 299, 724–726. https://doi.org/10.1038/299724a0

Ramírez-Mata, A., López-Lara, L. I., Xiqui-Vázquez, Ma. L., Jijón-Moreno, S., Romero-Osorio, A., Baca, B. E. 2016. The cyclic-di-GMP diguanylate cyclase CdgA has a role in biofilm formation and exopolysaccharide production in *Azospirillum brasilense*. Res Microbiol 167, 190–201. https://doi.org/10.1016/j.resmic.2015.12.004

Reinhold-Hurek, B., Hurek, T. 2011. Living inside plants: bacterial endophytes. Curr Opin Plant Biol: Biotic interactions 14, 435–443. https://doi.org/10.1016/j.pbi.2011.04.004

Ribeiro, D. M., Briere, G., Bely, B., Spinelli, L., Brun, C. 2019. MoonDB 2.0: An updated database of extreme multifunctional and moonlighting proteins. Nucleic Acids Res 47, D398–D402. https://doi.org/10.1093/nar/gky1039

Richardson, K., Steffen, W., Lucht, W., Bendtsen, J., Cornell, S. E., Donges, J. F., Drüke, M., Fetzer, I., Bala, G., von Bloh, W., Feulner, G., Fiedler, S., Gerten, D., Gleeson, T., Hofmann, M., Huiskamp, W., Kummu, M., Mohan, C., Nogués-Bravo, D., … Rockström, J. 2023. Earth beyond six of nine planetary boundaries. Sci Adv 9, eadh2458. https://doi.org/10.1126/sciadv.adh2458

Richts B., Rosenberg J., Commichau F. M. 2019. A survey of pyridoxal 5'-phosphate-dependent proteins in the Gram-positive model bacterium *Bacillus subtilis*. Front Mol Biosci., 6:32. https://doi.org/10.3389/fmolb.2019.00032

Rico, A., McCraw, S. L., Preston, G. M. 2011. The metabolic interface between Pseudomonas syringae and plant cells. Curr Opin Microbiol 14(1), 31–38. https://doi.org/10.1016/j.mib.2010.12.008

Rico, A., Preston, G. M. 2008. *Pseudomonas syringae* pv. tomato DC3000 uses constitutive and apoplast-induced nutrient assimilation pathways to catabolize nutrients that are abundant in the tomato apoplast. Mol Plant Microbe Interact 21, 269-282. https://doi.org/10.1094/MPMI-21-2-0269

Rigaud, J., Puppo, A. 1975. Indole-3-acetic acid catabolism by soybean bacteroids. J Gen Microbiol 88, 223–228. https://doi.org/10.1099/00221287-88-2-223

Robertsen B. K., Aman P., Darvill A. G., McNeil M., Albersheim P. 1981. Host-symbiont interactions: V. The structure of acidic extracellular polysaccaharides secreted by *Rhizobium leguminosarum* and *Rhizobium trifolii*. Plant Physiol 67, 389-400. https://doi.org/10.1104/pp.67.3.389

Robertson, G. P., Vitousek, P. M. 2009. Nitrogen in agriculture: Balancing the cost of an essential eesource. Ann Rev Environ Resour 34, 97–125. https://doi.org/10.1146/annurev.environ.032108.105046

Rockström, J., Gupta, J., Qin, D., Lade, S. J., Abrams, J. F., Andersen, L. S., Armstrong McKay, D. I., Bai, X., Bala, G., Bunn, S. E., Ciobanu, D., DeClerck, F., Ebi, K., Gifford, L., Gordon, C., Hasan, S., Kanie, N., Lenton, T. M., Loriani, S., … Zhang, X. 2023. Safe and just Earth system boundaries. Nature 619, Article 7968. https://doi.org/10.1038/s41586-023-06083-8

Roine E., Wei W., Yuan J., Nurmiaho-Lassila E. L., Kalkkinen N., Romantschuk M., He S. Y. 1997. Hrp pilus: an hrp-dependent bacterial surface appendage produced by *Pseudomonas syringae* pv. tomato DC3000. Proc Natl Acad Sci USA 94, 3459-3464. https://doi.org/10.1073/pnas.94.7.3459

Romero-Jiménez, L., Rodríguez-Carbonell, D., Gallegos, M. T., Sanjuán, J., Pérez-Mendoza, D. 2015. Mini-Tn7 vectors for stable expression of diguanylate cyclase PleD* in Gram-negative bacteria. BMC Microbiol 15, 190.https://doi.org/10.1186/s12866-015-0521-6

Römling, U. 2005. Characterization of the rdar morphotype, a multicellular behaviour in Enterobacteriaceae. Cell Mol Life Sci 62, 1234–1246. https://doi.org/10.1007/s00018-005-4557-x

Römling, U. 2023. Cyclic di-GMP signaling—Where did you come from and where will you go? Mol Microbiol 120, 564-574. https://doi.org/10.1111/mmi.15119

Römling, U., Balsalobre, C. 2012. Biofilm infections, their resilience to therapy and innovative treatment strategies. J Int Med 272, 541–561. https://doi.org/10.1111/joim.12004

Römling, U., Galperin, M.Y., Gomelsky, M. 2013. Cyclic di-GMP: the First 25 Years of a universal bacterial second messenger. Microbiol Mol Biol Rev 77, 1–52. https://doi.org/10.1128/MMBR.00043-12

Ross, P., Weinhouse, H., Aloni, Y., Michaeli, D., Weinberger-Ohana, P., Mayer, R., Braun, S., de Vroom, E., van der Marel, G. A., van Boom, J. H., Benziman, M. 1987. Regulation of cellulose synthesis in *Acetobacter xylinum* by cyclic diguanylic acid. Nature 325, Article 6101. https://doi.org/10.1038/325279a0

Saad, N., Urdaci, M., Vignoles, C., Chaignepain, S., Tallon, R., Schmitter, J., Bressollier, P. 2009. *Lactobacillus plantarum* 299v Surface-bound GAPDH: A new insight into enzyme cell walls location. J Microbiol Biotechnol 19, 1635–1643. https://doi.org/10.4014/jmb.0902.0102

Saalbach, G., Erik, P., Wienkoop, S. 2002. Characterisation by proteomics of peribacteroid space and peribacteroid membrane preparations from pea (*Pisum sativum*) symbiosomes. Proteomics 2, 325–337. https://doi.org/10.1002/1615-9861(200203)2:3<325::AID-PROT325>3.0.CO;2-W

Sachla, A. J., Helmann, J. D. 2019. A bacterial checkpoint protein for ribosome assembly moonlights as an essential metabolite-proofreading enzyme. Nat Comm 10, 1526. https://doi.org/10.1038/s41467-019-09508-z

Sajid, A., Arora, G., Gupta, M., Singhal, A., Chakraborty, K., Nandicoori, V. K., Singh, Y. 2011. Interaction of *Mycobacterium tuberculosis* Elongation Factor Tu with GTP is regulated by phosphorylation. J Bacteriol 193, 5347–5358. https://doi.org/10.1128/JB.05469-11

Sambrook J., Fritsch E. F., Maniatis T. 1989. Molecular cloning: A laboratory manual. New York, Cold Spring Harbor Laboratory Press.

Sánchez, B., Arias, S., Chaignepain, S., Denayrolles, M., Schmitter, J. M., Bressollier, P., Urdaci, M. C. 2009. Identification of surface proteins involved in the adhesion of a probiotic *Bacillus cereus* strain to mucin and fibronectin. Microbiology, 155, 1708–1716. https://doi.org/10.1099/mic.0.025288-0

Sánchez, B., Schmitter, J. M., Urdaci, M. C. 2009. Identification of novel proteins secreted by *Lactobacillus rhamnosus* GG grown in de Mann-Rogosa-Sharpe broth. Lett Appl Microbiol 48, 618–622. https://doi.org/10.1111/j.1472-765X.2009.02579.x

Santos, L. F., Olivares, F. L. 2021. Plant microbiome structure and benefits for sustainable agriculture. Curr Plant Biol 26, 100198. https://doi.org/10.1016/j.cpb.2021.100198

Savary, S., Willocquet, L., Pethybridge, S. J., Esker, P., McRoberts, N., Nelson, A. 2019. The global burden of pathogens and pests on major food crops. Nat Ecol Evol 3, Article 3. https://doi.org/10.1038/s41559-018-0793-y

Sawana, A., Adeolu, M., Gupta, R. S. 2014. Molecular signatures and phylogenomic analysis of the genus Burkholderia: Proposal for division of this genus into the emended genus *Burkholderia* containing pathogenic organisms and a new genus *Paraburkholderia* gen. nov. harboring environmental species. Front Genet 5, 429. https://doi.org/10.3389/fgene.2014.00429

Schäfer, A., Tauch, A., Jäger, W., Kalinowski, J., Thierbach, G., Pühler, A. 1994. Small mobilizable multi-purpose cloning vectors derived from the *Escherichia coli* plasmids pK18 and pK19: selection of defined deletions in the chromosome of *Corynebacterium glutamicum*. Gene 145, 69–73. https://doi.org/10.1016/0378-1119(94)90324-7

Schäper, S., Krol, E., Skotnicka, D., Kaever, V., Hilker, R., Søgaard-Andersen, L., Becker, A. 2016. Cyclic di-GMP regulates multiple cellular functions in the symbiotic alphaproteobacterium *Sinorhizobium meliloti*. J Bacteriol 198, 521–535. https://doi.org/10.1128/jb.00795-15

Schäper, S., Steinchen, W., Krol, E., Altegoer, F., Skotnicka, D., Søgaard-Andersen, L., Bange, G., Becker, A. 2017. AraC-like transcriptional activator CuxR binds c-di-GMP by a PilZ-like mechanism to regulate extracellular polysaccharide production. Proc Natl Acad Sci USA 114, E4822–E4831. https://doi.org/10.1073/pnas.1702435114

Schauer N., Zamir D., Fernie A. R. 2005. Metabolic profiling of leaves and fruit of wild species tomato: a survey of the *Solanum lycopersicum* complex. J Exp Bot 56, 297-307. https://doi.org/10.1093/jxb/eri057

Schaumburg, J., Diekmann, O., Hagendorff, P., Bergmann, S., Rohde, M., Hammerschmidt, S., Jänsch, L., Wehland, J., Kärst, U. 2004. The cell wall subproteome of *Listeria monocytogenes*. Proteomics 4, 2991–3006. https://doi.org/10.1002/pmic.200400928

Schirmer, T., Jenal, U. 2009. Structural and mechanistic determinants of c-di-GMP signalling. Nat Rev Microbiol 7, 724–735. https://doi.org/10.1038/nrmicro2203

Schmid, J., Sieber, V., Rehm, B. 2015. Bacterial exopolysaccharides: Biosynthesis pathways and engineering strategies. Front Microbiol 6. https://doi.org/10.3389/fmicb.2015.00496

Schneider, C. A., Rasband, W. S., Eliceiri, K. W. 2012. NIH Image to ImageJ: 25 years of image analysis. Nature Methods 9, 671–675. https://doi.org/10.1038/nmeth.2089

Schnider-Keel, U., Seematter, A., Maurhofer, M., Blumer, C., Duffy, B., Gigot-Bonnefoy, C., Reimmann, C., Notz, R., Défago, G., Haas, D., Keel, C. 2000. Autoinduction of 2,4-diacetylphloroglucinol biosynthesis in the biocontrol agent *Pseudomonas fluorescens* CHA0 and repression by the bacterial metabolites salicylate and pyoluteorin. J Bacteriol 182, 1215–1225. https://doi.org/10.1128/JB.182.5.1215-1225.2000

Schumacher, J., Waite, C. J., Bennett, M. H., Perez, M. F., Shethi, K., Buck, M. 2014. Differential secretome analysis of *Pseudomonas syringae* pv tomato using gel-free MS proteomics. Front Plant Sci 5. https://doi.org/10.3389/fpls.2014.00242

Segal, H. L., Boyer P. D. 1953. The role of sulfhydryl groups in the activity of D-glyceraldehyde 3-phosphate dehydrogenase. J Biol Chem 204(1):265-81. https://doi.org/10.1016/S0021-9258(18)66136-8

Seidler, N. W. 2013. GAPDH: Biological properties and diversity, advances in Experimental Medicine and Biology. Springer Netherlands, Dordrecht. https://doi.org/10.1007/978-94-007-4716-6

Seta, F. D., Boschi-Muller, S., Vignais, M. L., Branlant, G. 1997. Characterization of *Escherichia coli* strains with *gapA* and *gapB* genes deleted. J Bacteriol. 179, 5218–5221. https://doi.org/10.1128/jb.179.16.5218-5221.1997

Shanahan, C. A., Strobel, S. A. 2012. The bacterial second messenger c-di-GMP: Probing interactions with protein and RNA binding partners using cyclic dinucleotide analogs. Org Biomol Chem 10, 9113–9129. https://doi.org/10.1039/c2ob26724a

Shirafkan, F., Gharaghani, S., Rahimian, K., Sajedi, R. H., Zahiri, J. (2021). Moonlighting protein prediction using physico-chemical and evolutional properties via machine learning methods. BMC Bioinformatics 22, 261. https://doi.org/10.1186/s12859-021-04194-5

Sierra-Cacho, D., Zamorano-Sánchez, D. S., Xiqui-Vázquez, M. L., Viruega-Góngora, V. I., Ramírez-Mata, A., Baca, B. E. 2021. CdgC, a cyclic-di-GMP diguanylate cyclase of *Azospirillum baldaniorum* is involved in internalization to wheat roots. Front Plant Sci 12. https://doi.org/10.3389/fpls.2021.748393

Silby, M. W., Cerdeño-Tárraga, A. M., Vernikos, G. S., Giddens, S. R., Jackson, R. W., Preston, G. M., Zhang, X.-X., Moon, C. D., Gehrig, S. M., Godfrey, S. A., Knight, C. G., Malone, J. G., Robinson, Z., Spiers, A. J., Harris, S., Challis, G. L., Yaxley, A. M., Harris, D., Seeger, K., … Thomson, N. R. 2009. Genomic and genetic analyses of diversity and plant interactions of *Pseudomonas fluorescens*. Genome Biology 10 R51. https://doi.org/10.1186/gb-2009-10-5-r51

Simon, R., Priefer, U., Pühler, A. 1983. A broad host range mobilization system for *in vivo* genetic engineering: transposon mutagenesis in Gram negative bacteria. Nat Biotechnol 1, 784–791. https://doi.org/10.1038/nbt1183-784

Simonsen, A. C. W., Rosendahl, L. 1999. Origin of *de novo* synthesized proteins in the different compartments of pea-*Rhizobium sp*. symbiosomes. Mol Plant-Microbe Int 12, 319–327. https://doi.org/10.1094/MPMI.1999.12.4.319

Singh, N., Bhalla, N. 2020. Moonlighting Proteins. Annu Rev Genet 54, 265–285. https://doi.org/10.1146/annurev-genet-030620-102906

Sirover, M. A. 2011. On the functional diversity of glyceraldehyde-3-phosphate dehydrogenase: Biochemical mechanisms and regulatory control. Biochim. Biophys. Acta BBA 1810, 741–751. https://doi.org/10.1016/j.bbagen.2011.05.010

Sirover, M. A. 2014. Structural analysis of glyceraldehyde-3-phosphate dehydrogenase functional diversity. Int J Biochem Cell Biol 57, 20–26. https://doi.org/10.1016/j.biocel.2014.09.026

Sirover, M. A. 2020. Moonlighting glyceraldehyde-3-phosphate dehydrogenase: post-translational modification, protein and nucleic acid interactions in normal cells and in human pathology. Crit. Rev. Biochem. Mol. Biol. 55, 354–371. https://doi.org/10.1080/10409238.2020.1787325

Sirover, M. A. 2021. The role of posttranslational modification in moonlighting glyceraldehyde-3-phosphate dehydrogenase structure and function. Amino Acids, 53, 507–515. https://doi.org/10.1007/s00726-021-02959-z

Snapp, S., Sapkota, T. B., Chamberlin, J., Cox, C. M., Gameda, S., Jat, M. L., Marenya, P., Mottaleb, K. A., Negra, C., Senthilkumar, K., Sida, T. S., Singh, U., Stewart, Z. P., Tesfaye, K., Govaerts, B. 2023. Spatially differentiated nitrogen supply is key in a global food–fertilizer price crisis. Nat Sustain 1–11. https://doi.org/10.1038/s41893-023-01166-w

Sondermann, H., Shikuma, N. J., Yildiz, F. H. 2012. You've come a long way: C-di-GMP signaling. Curr Opin Microbiol 15, 140–146. https://doi.org/10.1016/j.mib.2011.12.008

Soto, M. J., Domínguez-Ferreras, A., Pérez-Mendoza, D., Sanjuán, J., Olivares, J. 2009. Mutualism *versus* pathogenesis: The give-and-take in plant–bacteria interactions. Cell Microbiol 11, 381–388. https://doi.org/10.1111/j.1462-5822.2009.01282.x

Soto, M. J., Nogales, J., Pérez-Mendoza, D., Gallegos, M. T., Olivares, J., Sanjuán, J. 2011. Pathogenic and mutualistic plant-bacteria interactions: ever increasing similarities. Open Life Sci 6, 911–917. https://doi.org/10.2478/s11535-011-0069-x

Soto, M. J., Sanjuán, J., Olivares, J. 2006. Rhizobia and plant-pathogenic bacteria: Common infection weapons. Microbiology 152, 3167–3174. https://doi.org/10.1099/mic.0.29112-0

Soumare, A., Diedhiou, A. G., Thuita, M., Hafidi, M., Ouhdouch, Y., Gopalakrishnan, S., Kouisni, L. 2020. Exploiting biological Nitrogen fixation: A route towards a sustainable agriculture. Plants 9, Article 8. https://doi.org/10.3390/plants9081011

Spiers, A. J., Kahn, S. G., Bohannon, J., Travisano, M., Rainey, P. B. 2002. Adaptive divergence in experimental populations of *Pseudomonas fluorescens*. I. Genetic and Phenotypic Bases of Wrinkly Spreader Fitness. Genetics 161, 33–46. https://doi.org/10.1093/genetics/161.1.33

Springer, M., Plumbridge, J. A., Butler, J. S., Graffe, M., Dondon, J., Mayaux, J. F., Fayat, G., Lestienne, P., Blanquet, S., Grunberg-Manago, M. 1985. Autogenous control of *Escherichia coli* threonyl-tRNA synthetase expression *in vivo*. J Mol Biol 185, 93–104. https://doi.org/10.1016/0022-2836(85)90185-8

Steffen, W., Richardson, K., Rockström, J., Cornell, S. E., Fetzer, I., Bennett, E. M., Biggs, R., Carpenter, S. R., de Vries, W., de Wit, C. A., Folke, C., Gerten, D., Heinke, J., Mace, G. M., Persson, L. M., Ramanathan, V., Reyers, B., Sörlin, S. 2015. Planetary boundaries: Guiding human development on a changing planet. Science 347, 1259855. https://doi.org/10.1126/science.1259855

Stevens, C. J. 2019. Nitrogen in the environment. Science 363, 578–580. https://doi.org/10.1126/science.aav8215

Stowers, M. D. 1985. Carbon metabolism in *Rhizobium* species. Annu Rev Microbiol 39, 89–108. https://doi.org/10.1146/annurev.mi.39.100185.000513

Subramanian, S., Gao, X., Dann, C. E., Kearns, D. B. 2017. MotI (DgrA) acts as a molecular clutch on the flagellar stator protein MotA in *Bacillus subtilis*. Proc Natl Acad Sci USA 114, 13537–13542. https://doi.org/10.1073/pnas.1716231114

Sudarsan, S., Dethlefsen, S., Blank, L. M., Siemann-Herzberg, M., Schmid, A. 2014 The functional structure of central carbon metabolism in *Pseudomonas putida* KT2440. Applied and Environ Microbiol 80, 5292-5303. https://doi.org/10.1128/AEM.01643-14

Sudarsan, N., Lee, E. R., Weinberg, Z., Moy, R. H., Kim, J. N., Link, K. H., Breaker, R. R. 2008. Riboswitches in eubacteria sense the second messenger cyclic di-GMP. Science 321, 411–413. https://doi.org/10.1126/science.1159519

Swingle, B., Thete, D., Moll, M., Myers, C. R., Schneider, D. J., Cartinhour, S. 2008. Characterization of the PvdS-regulated promoter motif in *Pseudomonas syringae* pv. tomato DC3000 reveals regulon members and insights regarding PvdS function in other pseudomonads. Mol Microbiol 68, 871–889. https://doi.org/10.1111/j.1365-2958.2008.06209.x

Taboada, H., Dunn, M.F., Meneses, N., Vargas-Lagunas, C., Buchs, N., Andrade-Domínguez, A., Encarnación, S. 2019. Qualitative changes in proteins contained in outer membrane vesicles produced by *Rhizobium etli* grown in the presence of the *nod* gene inducer naringenin. Arch Microbiol 201, 1173–1194. https://doi.org/10.1007/s00203-019-01682-4

Tagua, V. G., Molina-Henares, M. A., Travieso, M. L., Nisa-Martínez, R., Quesada, J. M., Espinosa-Urgel, M., Ramos-González, M. I. 2022. C-di-GMP and biofilm are regulated in *Pseudomonas putida* by the CfcA/CfcR two-component system in response to salts. Environ Microbiol 24, 158–178. https://doi.org/10.1111/1462-2920.15891

Tampakaki, A.P. 2014. Commonalities and differences of T3SSs in rhizobia and plant pathogenic bacteria. Front Plant Sci 5. https://doi.org/10.3389/fpls.2014.00114

Tatè, R., Ferraioli, S., Filosa, S., Cermola, M., Riccio, A., Iaccarino, M., Patriarca, E.J. 2004. Glutamine utilization by *Rhizobium etli*. Mol Plant-Microbe Inter 17, 720–728. https://doi.org/10.1094/MPMI.2004.17.7.720

Tawaraya, K., Horie, R., Saito, S., Wagatsuma, T., Saito, K., Oikawa, A. 2014. Metabolite profiling of root exudates of common bean under phosphorus deficiency. Metabolites 4, 599–611. https://doi.org/10.3390/metabo4030599

Teather, R. M., Wood, P. J. 1982. Use of Congo red-polysaccharide interactions in enumeration and characterization of cellulolytic bacteria from the bovine rumen. Applied and Environ Microbiol 43, 777–780. https://doi.org/10.1128/aem.43.4.777-780.1982

Terrasse, R., Amoroso, A., Vernet, T., Guilmi, A. M. D. 2015. *Streptococcus pneumoniae* GAPDH Is released by cell lysis and interacts with peptidoglycan. PLOS ONE 10, e0125377. https://doi.org/10.1371/journal.pone.0125377

Toyofuku, M., Roschitzki, B., Riedel, K., Eberl, L. 2012. Identification of proteins associated with the *Pseudomonas aeruginosa* biofilm extracellular matrix. J Proteome Res 11, 4906–4915. https://doi.org/10.1021/pr300395j

Tukey, J. W. 1949. Comparing individual means in the analysis of variance. Biometrics, 5, 99-114. https://doi.org/10.2307/3001913

Turnbull, L., Toyofuku, M., Hynen, A. L., Kurosawa, M., Pessi, G., Petty, N. K., Osvath, S. R., Cárcamo-Oyarce, G., Gloag, E. S., Shimoni, R., Omasits, U., Ito, S., Yap, X., Monahan, L. G., Cavaliere, R., Ahrens, C. H., Charles, I. G., Nomura, N., Eberl, L., Whitchurch, C. B. 2016. Explosive cell lysis as a mechanism for the biogenesis of bacterial membrane vesicles and biofilms. Nat Comm 7, Article 1. https://doi.org/10.1038/ncomms11220

Udvardi, M., Poole, P. S. 2013. Transport and metabolism in legume-rhizobia symbioses. Annual Rev Plant Biol 64, 781–805. https://doi.org/10.1146/annurev-arplant-050312-120235

Vargas P., Farias G. A., Nogales J., Prada H., Carvajal V., Baron M., Rivilla R., Martin M., Olmedilla A., Gallegos M. T. 2013. Plant flavonoids target *Pseudomonas syringae* pv. tomato DC3000 flagella and type III secretion system. Environ Microbiol Reports 5, 841-850. https://doi.org/10.1111/1758-2229.12086

Vargas, P., Felipe, A., Michán, C., Gallegos, M. T. 2011. Induction of *Pseudomonas syringae* pv. tomato DC3000 MexAB-OprM multidrug efflux pump by flavonoids is mediated by the repressor PmeR. Mol Plant-Microb Int 24, 1207–1219. https://doi.org/10.1094/MPMI-03-11-0077

Venkateshwaran, M., Volkening, J. D., Sussman, M. R., Ané, J.-M. 2013. Symbiosis and the social network of higher plants. Curr Opi Plant Biol 16, 118–127. https://doi.org/10.1016/j.pbi.2012.11.007

Wang, Q., Zhang, Y., Yang, C., Xiong, H., Lin, Y., Yao, J., Li, H., Xie, L., Zhao, W., Yao, Y., Ning, Z. B., Zeng, R., Xiong, Y., Guan, K. L., Zhao, S., Zhao, G. P. 2010. Acetylation of metabolic enzymes coordinates carbon source utilization and metabolic flux. Science 327, 1004-1007. https://doi.org/10.1126/science.1179687

Wang, D., Griffitts, J., Starker, C., Fedorova, E., Limpens, E., Ivanov, S., Bisseling, T., Long, S. 2010. A nodule-specific protein secretory pathway required for Nitrogen-fixing symbiosis. Science 327, 1126–1129. https://doi.org/10.1126/science.1184096

Wang, G., Chen, H., Xia, Y., Cui, J., Gu, Z., Song, Y., Chen, Y. Q., Zhang, H., Chen, W. 2013. How are the non-classically secreted bacterial proteins released into the extracellular milieu? Curr Microbiol 67, 688–695. https://doi.org/10.1007/s00284-013-0422-6

Wang, G., Xia, Y., Song, X., Ai, L. 2016. Common non-classically secreted bacterial proteins with experimental evidence. Curr Microbiol 72, 102–111. https://doi.org/10.1007/s00284-015-0915-6

Wang, Q., Zhang, Y., Yang, C., Xiong, H., Lin, Y., Yao, J., Li, H., Xie, L., Zhao, W., Yao, Y., Ning, Z.-B., Zeng, R., Xiong, Y., Guan, K.-L., Zhao, S., Zhao, G.-P. 2010. Acetylation of metabolic enzymes coordinates carbon source utilization and metabolic flux. Science 327, 1004–1007. https://doi.org/10.1126/science.1179687

Wang, T., Cai, Z., Shao, X., Zhang, W., Xie, Y., Zhang, Y., Hua, C., Schuster, S.C., Yang, L., Deng, X. 2019. Pleiotropic effects of c-di-GMP content in *Pseudomonas syringae*. Applied and Environ Microbiol 85, e00152-19. https://doi.org/10.1128/AEM.00152-19

Wang, W., Jeffery, C. J. 2016. An analysis of surface proteomics results reveals novel candidates for intracellular/surface moonlighting proteins in bacteria. Molecular BioSystems, 12(5), 1420–1431. https://doi.org/10.1039/C5MB00550G

Wang, Z., Song, L., Liu, X., Shen, X., Li, X. 2023. Bacterial second messenger c-di-GMP: Emerging functions in stress resistance. Microbiol Res 268, 127302. https://doi.org/10.1016/j.micres.2023.127302

Whalen, M. C., Innes, R. W., Bent, A. F., Staskawicz, B. J. 1991. Identification of *Pseudomonas syringae* pathogens of *Arabidopsis* and a bacterial locus determining avirulence on both *Arabidopsis* and soybean. Plant Cell 3 49–59. https://doi.org/10.1105/tpc.3.1.49

Whitney, J. C., Howell, P. L. 2013. Synthase-dependent exopolysaccharide secretion in Gram-negative bacteria. Trends Microbiol 21, 63–72. https://doi.org/10.1016/j.tim.2012.10.001

Whitney, J. C., Whitfield, G. B., Marmont, L. S., Yip, P., Neculai, A. M., Lobsanov, Y. D., Robinson, H., Ohman, D. E., Howell, P. L. 2015. Dimeric c-di-GMP is required for post-translational regulation of alginate production in *Pseudomonas aeruginosa*. J Biol Chem 290, 12451–12462. https://doi.org/10.1074/jbc.M115.645051

Whitworth, D. E., Morgan, B. H. 2015. Synergism between bacterial GAPDH and OMVs: Disparate mechanisms but co-operative action. Front Microbiol 6. https://doi.org/10.3389/fmicb.2015.01231

Widjaja, M., Harvey, K. L., Hagemann, L., Berry, I. J., Jarocki, V. M., Raymond, B. B. A., Tacchi, J. L., Gründel, A., Steele, J. R., Padula, M. P., Charles, I. G., Dumke, R., Djordjevic, S. P. 2017. Elongation factor Tu is a multifunctional and processed moonlighting protein. Sci Rep 7, 11227. https://doi.org/10.1038/s41598-017-10644-z

Wiehlmann, L., Klockgether, J., Hammerbacher, A.-S., Salunkhe, P., Horatzek, S., Munder, A., Peilert, J. F., Gulbins, E., Eberl, L., Tümmler, B. 2023. A VirB4 ATPase of the mobile accessory genome orchestrates core genome-encoded features of physiology, metabolism, and virulence of *Pseudomonas aeruginosa* TBCF10839. Front Cell Infect Microbiol 13, 1234420. https://doi.org/10.3389/fcimb.2023.1234420

Wilkes R. A., Waldbauer J., Aristilde L. 2021. Analogous metabolic decoupling in *Pseudomonas putida* and *Comamonas testosteroni* implies energetic bypass to facilitate gluconeogenic growth. mBio 12, e0325921. https://doi.org/10.1128/mbio.03259-21

Wistow, G. J., Lietman, T., Williams, L. A., Stapel, S. O., de Jong, W. W., Horwitz, J., Piatigorsky, J. 1988. Tau-crystallin/alpha-enolase: One gene encodes both an enzyme and a lens structural protein. J Cell Biol 107, 2729–2736. https://doi.org/10.1083/jcb.107.6.2729

Wouw, M. van de, Kik, C., Hintum, T. van, Treuren, R. van, Visser, B. 2010. Genetic erosion in crops: Concept, research results and challenges. Plant Genet Res 8, 1–15. https://doi.org/10.1017/S1479262109990062

Xin, X.-F., He, S. Y. 2013. *Pseudomonas syringae* pv. tomato DC3000: A model pathogen for probing disease susceptibility and hormone signaling in plants. Ann Rev Phytopathol 51, 473–498. https://doi.org/10.1146/annurev-phyto-082712-102321

Xin, X.-F., Kvitko, B., He, S.Y. 2018. *Pseudomonas syringae*: what it takes to be a pathogen. Nat Rev Microbiol 16, 316–328. https://doi.org/10.1038/nrmicro.2018.17

Xu, Zhaowei, Zhang, H., Zhang, X., Jiang, H., Liu, C., Wu, F., Qian, L., Hao, B., Czajkowsky, D. M., Guo, S., Xu, Zhijing, Bi, L., Wang, S., Li, H., Tan, M., Yan, W., Feng, L., Hou, J., Tao, S. 2019. Interplay between the bacterial protein deacetylase CobB and the second messenger c-di-GMP. EMBO J 38, e100948. https://doi.org/10.15252/embj.2018100948

Yagüe, P., Gonzalez-Quiñonez, N., Fernández-García, G., Alonso-Fernández, S., Manteca, A. 2019. Goals and challenges in bacterial phosphoproteomics. Int J Mol Sci 20, 5678. https://doi.org/10.3390/ijms20225678

Yan, H., Chen, W. 2010. 3′,5′-Cyclic diguanylic acid: A small nucleotide that makes big impacts. Chem Soc Rev 39, 2914–2924. https://doi.org/10.1039/B914942M

Yan, W., Qu, T., Zhao, H., Su, L., Yu, Q., Gao, J., Wu, B. 2010. The effect of c-di-GMP (3′–5′-cyclic diguanylic acid) on the biofilm formation and adherence of *Streptococcus mutans*. Microbiol Res 165, 87–96. https://doi.org/10.1016/j.micres.2008.10.001

Yang, C.-K., Ewis, H. E., Zhang, X., Lu, C.-D., Hu, H.-J., Pan, Y., Abdelal, A. T., Tai, P. C. 2011. Nonclassical protein secretion by *Bacillus subtilis* in the stationary phase is not due to cell lysis . J Bacteriol 193, 5607–5615. https://doi.org/10.1128/JB.05897-11

Yang, S. S., Zhai, Q. H. 2017. Cytosolic GAPDH: a key mediator in redox signal transduction in plants. Biol Plant 61, 417-426. https://doi.org/10.1007/s10535-017-0706-y

Yang, Y., Zhao, G., Man, T. K., Winkler, M. E. 1998. Involvement of the *gapA*- and *epd (gapB)*-encoded dehydrogenases in pyridoxal 5'-phosphate coenzyme biosynthesis in *Escherichia coli* K-12. J Bacteriol 180, 4294-4299. https://doi.org/10.1128/jb.180.16.4294-4299.1998

Yates, J. L., Arfsten, A. E., Nomura, M. 1980. In vitro expression of *Escherichia coli* ribosomal protein genes: autogenous inhibition of translation. Proc Natl Acad Sci USA 77, 1837–1841. https://doi.org/10.1073/pnas.77.4.1837

Young, J. M. 1991. Pathogenicity and identification of the lilac pathogen, P*seudomonas syringae* pv. syringae van Hall 1902. Ann Appl Biol 118, 283–298. https://doi.org/10.1111/j.1744-7348.1991.tb05629.x

Yuan, X., Zeng, Q., Xu, J., Severin, G. B., Zhou, X., Waters, C. M., Sundin, G. W., Ibekwe, A. M., Liu, F., Yang, C.-H. 2020. Tricarboxylic acid (TCA) cycle enzymes and intermediates modulate Intracellular cyclic di-GMP levels and the production of plant cell wall–degrading enzymes in soft rot pathogen *Dickeya dadantii*. Mol Plant-Microb Int 33, 296–307. https://doi.org/10.1094/MPMI-07-19-0203-R

Zaffagnini, M., Fermani, S., Costa, A., Lemaire, S. D., Trost, P. 2013. Plant cytoplasmic GAPDH: Redox post-translational modifications and moonlighting properties. Front Plant Sci 4. https://doi.org/10.3389/fpls.2013.00450

Zakharzhevskaya, N. B., Vanyushkina, A. A., Altukhov, I. A., Shavarda, A. L., Butenko, I. O., Rakitina, D. V., Nikitina, A. S., Manolov, A. I., Egorova, A. N., Kulikov, E. E., Vishnyakov, I. E., Fisunov, G. Y., Govorun, V. M. 2017. Outer membrane vesicles secreted by pathogenic and nonpathogenic *Bacteroides fragilis* represent different metabolic activities. Sci Rep 7. https://doi.org/10.1038/s41598-017-05264-6

Zhan, J., Thrall, P. H., Papaïx, J., Xie, L., Burdon, J. J. 2015. Playing on a pathogen's weakness: Using evolution to guide sustainable plant disease control strategies. Ann Rev Phytopathol 53, 19–43. https://doi.org/10.1146/annurev-phyto-080614-120040

Zhang, R., Andersson, C. E., Savchenko, A., Skarina, T., Evdokimova, E., Beasley, S., Arrowsmith, C. H., Edwards, A. M., Joachimiak, A., Mowbray, S. L. 2003 Structure of *Escherichia coli* ribose-5-phosphate isomerase: a ubiquitous enzyme of the pentose phosphate pathway and the Calvin cycle. Structure, 11, 31-42. https://doi.org/10.1016/s0969-2126(02)00933-4

Zhao, G., Pease, A. J., Bharani, N., Winkler, M. E. 1995. Biochemical characterization of *gapB*-encoded erythrose 4-phosphate dehydrogenase of *Escherichia coli* K-12 and its possible role in pyridoxal 5'-phosphate biosynthesis. J Bacteriol 177 2804–2812. https://doi.org/10.1128/jb.177.10.2804-2812.1995

Zhao, Y., Jensen, O.N. 2009. Modification-specific proteomics: Strategies for characterization of post-translational modifications using enrichment techniques. Proteomics 9, 4632–4641. https://doi.org/10.1002/pmic.200900398

Zoghlami, L., Djebali, W., Abbes, Z., Hediji, H., Maucourt, M., Moing, A., Brouquisse, R., Chaïbi, W. 2011. Metabolite modifications in *Solanum lycopersicum* roots and leaves under cadmium stress. Afr J Biotechnol, 10, 567-579. https://doi.org/10.4314/ajb.v10i4

APPENDICES

APPENDICES

APPENDIX A. Genetic maps of non-commercial plasmids

Genetic maps of the four vectors used to clone DNA fragments. The name and size in bp of each vector are indicated at the center of the map. Genes are depicted with arrows, single (in bold) and double enzyme restriction sites are indicated, as well as oligonucleotide hybridization sites (in purple).

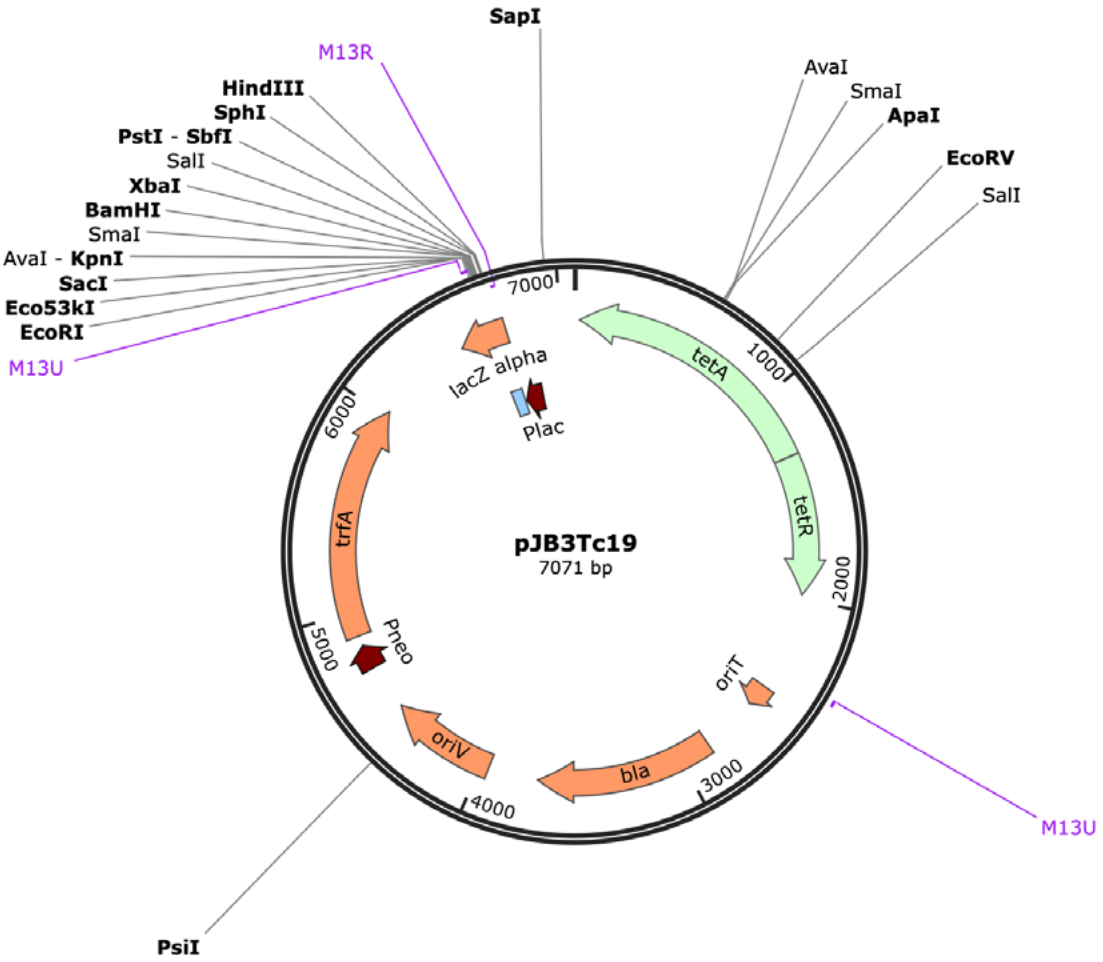

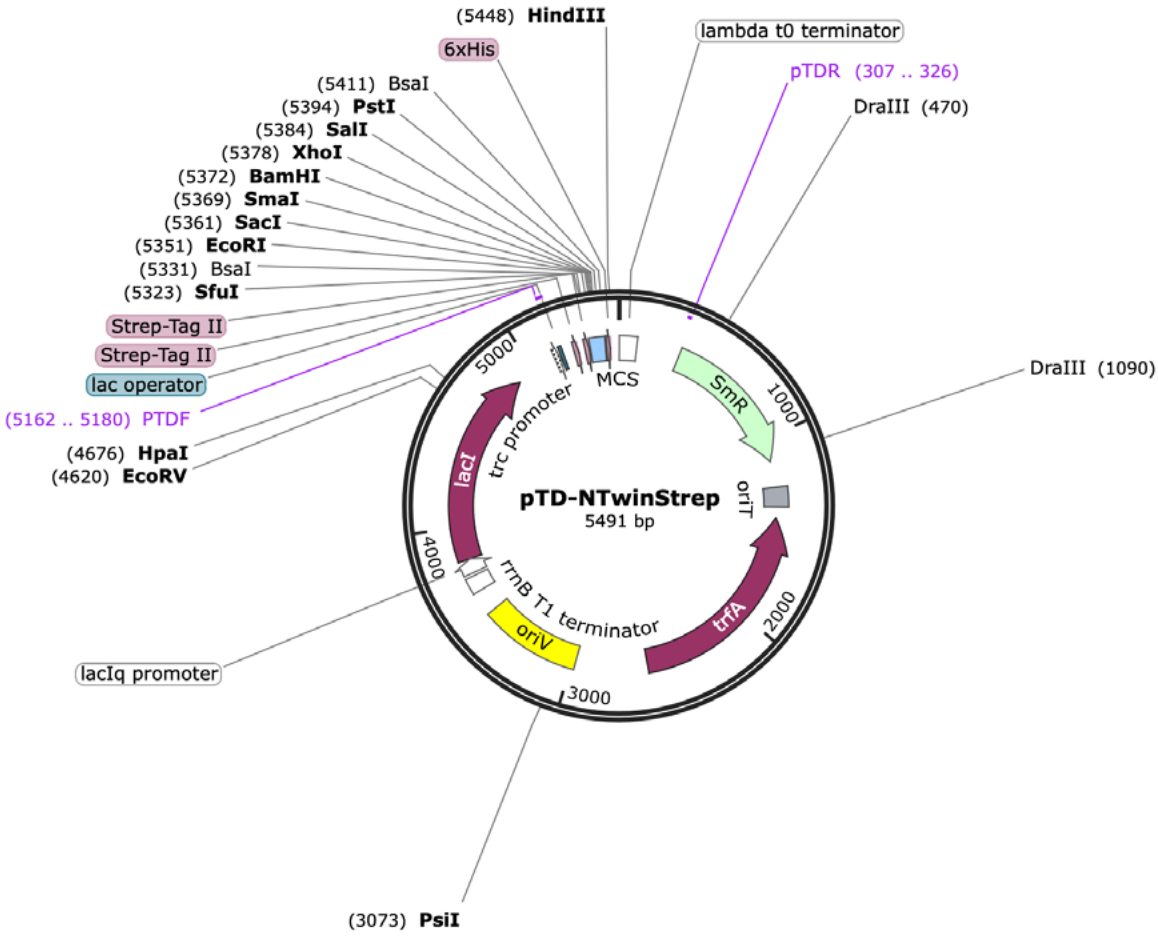
(5448) HindIII
6xHis
lambda t0 terminator
pTDR (307 .. 326)
DraIII (470)
(5411) BsaI
(5394) PstI
(5384) SalI
(5378) XhoI
(5372) BamHI
(5369) SmaI
(5361) SacI
(5351) EcoRI
(5331) BsaI
(5323) SfuI
Strep-Tag II
Strep-Tag II
lac operator
(5162 .. 5180) PTDF
(4676) HpaI
(4620) EcoRV
DraIII (1090)
5000
MCS
SmR
1000
trc promoter
lacI
pTD-NTwinStrep
5491 bp
oriT
4000
rrnB T1 terminator
oriV
trfA
2000
3000
lacIq promoter
(3073) PsiI

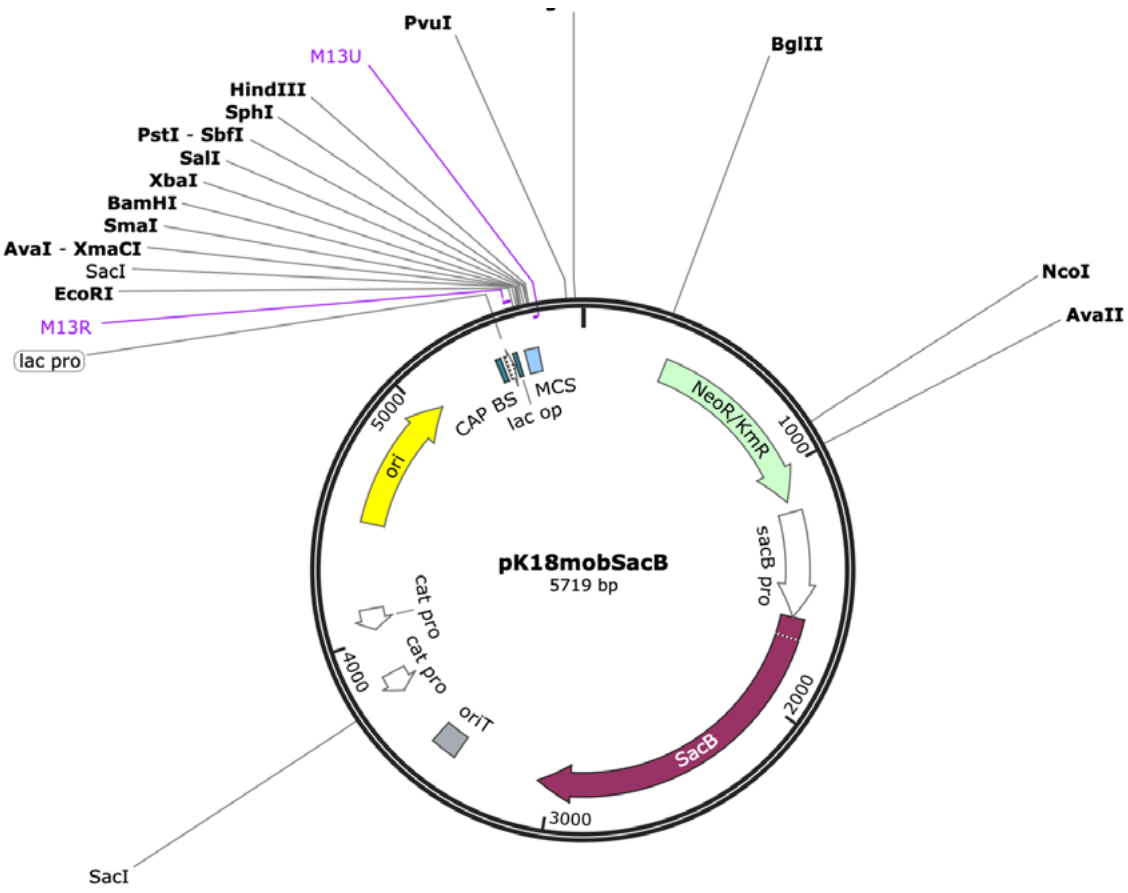
PvuI
BglII
M13U
HindIII
SphI
PstI - SbfI
SalI
XbaI
BamHI
SmaI
AvaI - XmaCI
SacI
EcoRI
M13R
lac pro
NcoI
AvaII
SacI
pK18mobSacB
5719 bp
ori
CAP BS
MCS
lac op
NeoR/KmR
sacB pro
SacB
oriT
cat pro
cat pro
1000
2000
3000
4000
5000

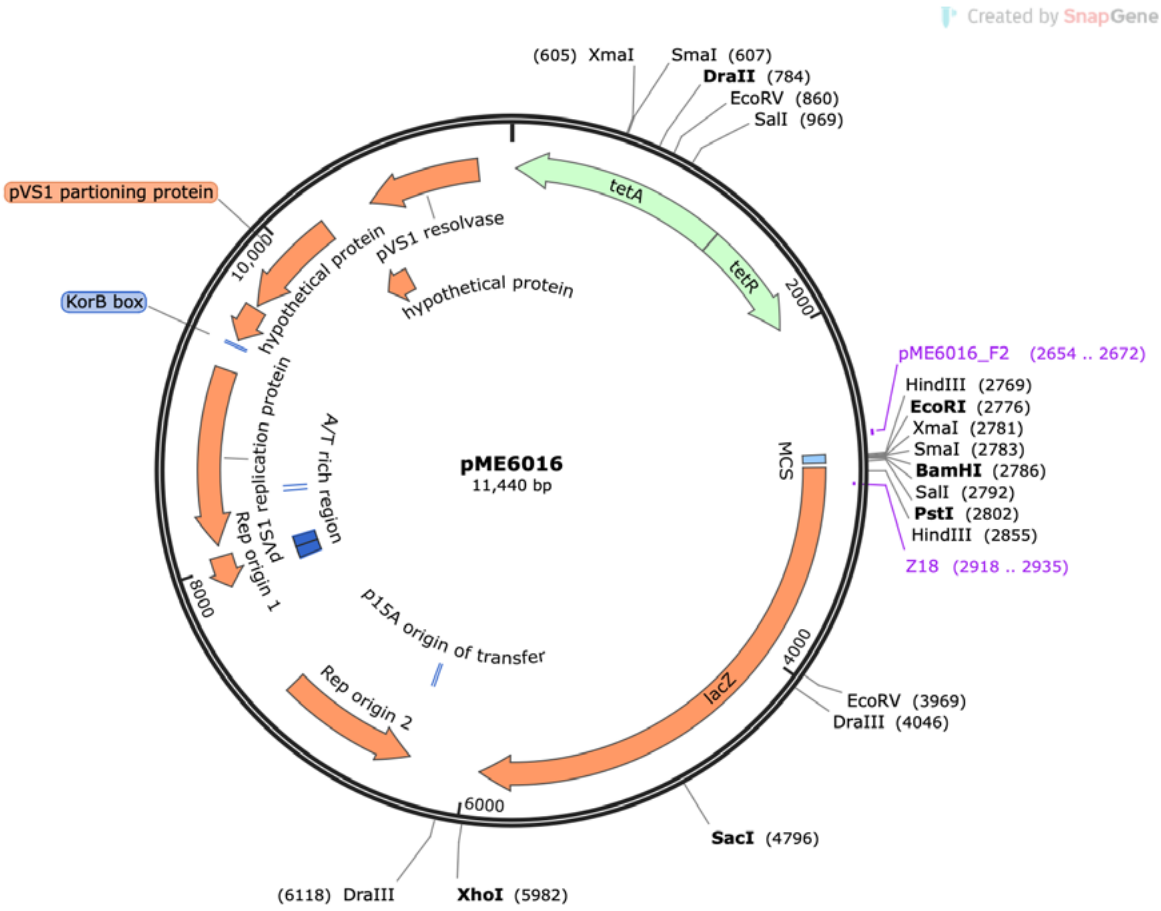
Created by SnapGene
(605) XmaI
SmaI (607)
DraII (784)
EcoRV (860)
SalI (969)
pVS1 partioning protein
KorB box
10,000
hypothetical protein
pVS1 resolvase
hypothetical protein
tetA
tetR
2000
pME6016_F2 (2654 .. 2672)
HindIII (2769)
EcoRI (2776)
XmaI (2781)
SmaI (2783)
BamHI (2786)
SalI (2792)
PstI (2802)
HindIII (2855)
Z18 (2918 .. 2935)
pME6016
11,440 bp
pVS1 replication protein
A/T rich region
Rep origin 1
8000
p15A origin of transfer
Rep origin 2
MCS
lacZ
4000
EcoRV (3969)
DraIII (4046)
6000
SacI (4796)
(6118) DraIII
XhoI (5982)

APPENDIX B. C-di-GMP differentialy abundant proteins in Pto

Intracellular Increased Abundance

UniProt ID	Gene	Function	Localization	Ratio	p-value	q-value
Q88BB0	*PSPTO_0107*	Carbon metabolism	Cytoplasmic	3.30	0.0747	0.0406
Q88A31	*rpe*	Carbon metabolism	Cytoplasmic	2.59	0.0019	0.0043
Q87WQ1	*tpiA*	Carbon metabolism	Cytoplasmic	2.01	0.0189	0.0162
Q886B1	*xfp*	Carbon metabolism	Cytoplasmic	2.32	0.0134	0.0131
Q885W7	*cobP*	Cofactors-metals	Cytoplasmic	2.04	0.0403	0.0269
Q88B49	*hemF*	Cofactors-metals	Cytoplasmic	2.06	0.0001	0.0009
Q87V72	*metF*	Cofactors-metals	Cytoplasmic	2.04	0.0143	0.0137
Q87ZX7	*pncA*	Cofactors-metals	Cytoplasmic	2.07	0.0556	0.0331
Q87XY6	*PSPTO_4034*	Cofactors-metals	Unknown	2.07	0.0033	0.0059
Q889Q8	*ribE*	Cofactors-metals	Cytoplasmic	2.43	0.0323	0.0232
Q884B1	*etfB-2*	Energy	Unknown	2.04	0.0134	0.0131
Q885A1	*flgD*	Extracellular function and structural	Extracellular	2.74	0.0038	0.0065
Q884Z5	*flgH*	Extracellular function and structural	Outer membrane	2.32	0.0166	0.0150
Q87VW2	*mltB*	Extracellular function and structural	Cytoplasmic membrane	2.30	0.0107	0.0116
Q888J9	*PSPTO_1025*	Extracellular function and structural	Periplasmic	9.71	0.0119	0.0124
Q87VE8	*PSPTO_4989*	Extracellular function and structural	Cytoplasmic membrane	7.79	0.0110	0.0117
Q888J8	*wssA*	Extracellular function and structural	Unknown	2.59	0.0161	0.0148
Q888J4	*wssE*	Extracellular function and structural	Membrane	4.91	0.0001	0.0006
Q888J3	*wssF*	Extracellular function and structural	Unknown	4.46	0.0075	0.0094
Q888J2	*wssG*	Extracellular function and structural	Periplasmic	8.56	0.0063	0.0085
Q888J0	*wssI*	Extracellular function and structural	Cytoplasmic membrane	2.29	0.0010	0.0029
Q88B57	*PSPTO_0162*	Generic enzymes	Unknown	2.06	0.0515	0.0315
Q889T8	*PSPTO_0659*	Generic enzymes	Cytoplasmic	2.44	0.0467	0.0297
Q889S4	*PSPTO_0675*	Generic enzymes	Cytoplasmic	2.44	0.0109	0.0117
Q887G5	*PSPTO_1331*	Generic enzymes	Cytoplasmic	2.08	0.0056	0.0080
Q886P8	*PSPTO_1529*	Generic enzymes	Unknown	2.68	0.0042	0.0067
Q882F5	*PSPTO_2673*	Generic enzymes	Cytoplasmic	3.32	0.0004	0.0017
Q881E5	*PSPTO_2949*	Generic enzymes	Unknown	4.03	0.0015	0.0038
Q880L6	*PSPTO_3138*	Generic enzymes	Unknown	3.97	0.0148	0.0140
Q87YJ4	*PSPTO_3802*	Generic enzymes	Cytoplasmic	2.83	0.0481	0.0302
Q87YE4	*PSPTO_3856*	Generic enzymes	Cytoplasmic	4.01	0.0203	0.0168
Q87XU3	*PSPTO_4082*	Generic enzymes	Cytoplasmic	2.48	0.0563	0.0333
Q87XC0	*PSPTO_4263*	Generic enzymes	Cytoplasmic	2.77	0.0433	0.0283
Q87WJ7	*PSPTO_4549*	Generic enzymes	Cytoplasmic	2.26	0.0113	0.0119
Q87VM2	*PSPTO_4914*	Generic enzymes	Cytoplasmic	2.26	0.0036	0.0062
Q87V80	*PSPTO_5060*	Generic enzymes	Cytoplasmic	2.37	0.0334	0.0238
Q87UX1	*PSPTO_5171*	Generic enzymes	Cytoplasmic	2.72	0.0222	0.0179
Q889L9	*ubiX*	Generic enzymes	Cytoplasmic	3.08	0.0232	0.0184
Q87XK9	*glpR*	Genetic regulation	Cytoplasmic	2.07	0.0210	0.0172
Q887S8	*PSPTO_1208*	Genetic regulation	Periplasmic	2.51	0.0434	0.0283
Q882I1	*PSPTO_2646*	Genetic regulation	Cytoplasmic	2.18	0.0687	0.0382
Q87XZ3	*PSPTO_4027*	Genetic regulation	Cytoplasmic	2.42	0.0001	0.0010

Intracellular Increased Abundance

Q87WJ3	*PSPTO_4553*	Genetic regulation	Cytoplasmic	2.11	0.0815	0.0432
Q87Z55	*tvrR*	Genetic regulation	Cytoplasmic	2.58	0.0015	0.0037
Q882B0	*PSPTO_2719*	Lipid metabolism	Cytoplasmic	2.23	0.0432	0.0283
Q87V15	*aroB*	Nitrogen metabolism	Cytoplasmic	2.27	0.0260	0.0200
Q87WV4	*hisG*	Nitrogen metabolism	Cytoplasmic	2.08	0.0023	0.0046
Q87UM2	*hutH-2*	Nitrogen metabolism	Cytoplasmic	2.86	0.0322	0.0231
Q884P3	*mtnB*	Nitrogen metabolism	Cytoplasmic	2.58	0.0046	0.0070
Q884P1	*mtnC*	Nitrogen metabolism	Cytoplasmic	2.42	0.0739	0.0403
Q887G1	*PSPTO_1335*	Nitrogen metabolism	Periplasmic	2.03	0.0225	0.0181
Q883T9	*PSPTO_2261*	Nitrogen metabolism	Unknown	2.15	0.0422	0.0278
Q883R9	*PSPTO_2281*	Nitrogen metabolism	Cytoplasmic	2.26	0.0242	0.0190
Q87ZC3	*PSPTO_3506*	Nitrogen metabolism	Cytoplasmic	2.67	0.0169	0.0152
Q87WM0	*PSPTO_4526*	Nitrogen metabolism	Cytoplasmic	2.15	0.0606	0.0350
Q88B60	*trpA*	Nitrogen metabolism	Cytoplasmic	2.10	0.0392	0.0265
Q88A48	*apaH*	Nucleic acid metabolism	Cytoplasmic	3.78	0.0291	0.0215
Q883S0	*cysH*	Nucleic acid metabolism	Cytoplasmic	2.06	0.0224	0.0180
Q87UA4	*cysQ*	Nucleic acid metabolism	Cytoplasmic	2.05	0.0007	0.0023
Q885G0	*hyuE*	Nucleic acid metabolism	Cytoplasmic	2.42	0.0002	0.0012
Q87VI6	*orn*	Nucleic acid metabolism	Cytoplasmic	2.42	0.0238	0.0187
Q88BD8	*PSPTO_0079*	Nucleic acid metabolism	Cytoplasmic	2.26	0.0391	0.0265
Q889C3	*PSPTO_0828*	Nucleic acid metabolism	Unknown	2.03	<0.0001	0.0005
Q887M5	*PSPTO_1266*	Nucleic acid metabolism	Cytoplasmic	2.49	0.0007	0.0024
Q87UA2	*PSPTO_5403*	Nucleic acid metabolism	Cytoplasmic	2.56	0.0251	0.0195
Q88BD7	*pyrE*	Nucleic acid metabolism	Cytoplasmic	2.55	0.0040	0.0065
Q884R0	*pyrF*	Nucleic acid metabolism	Cytoplasmic	2.65	0.0001	0.0009
Q886P1	*pyrH*	Nucleic acid metabolism	Cytoplasmic	2.31	0.0001	0.0009
Q886L5	*surE*	Nucleic acid metabolism	Unknown	2.78	0.0024	0.0048
Q88AZ9	*rimK*	Protein synthesis and modification	Cytoplasmic	4.07	0.0003	0.0014
Q88A46	*rsmA*	Protein synthesis and modification	Cytoplasmic	2.02	0.0394	0.0266
Q889K9	*smtA*	Protein synthesis and modification	Cytoplasmic	2.10	0.0824	0.0436
Q882I9	*abP*	Transport	Periplasmic	3.28	0.0026	0.0051
Q87YJ7	*arsB*	Transport	Cytoplasmic membrane	6.25	0.0277	0.0207
Q881C3	*modA*	Transport	Periplasmic	2.09	0.0328	0.0235
Q885I1	*PSPTO_1852*	Transport	Cytoplasmic membrane	11.01	0.0345	0.0243
Q883L3 Q888H0	*PSPTO_2343* *PSPTO_1054*	Transport	Outer membrane	2.09	0.0980	0.0494
Q882Y8	*PSPTO_2484*	Transport	Outer membrane	69.21	0.0004	0.0017
Q882M5	*PSPTO_2601*	Transport	Cytoplasmic membrane	6.80	0.0165	0.0150
Q881V7	*PSPTO_2775*	Transport	Outer membrane	2.38	0.0068	0.0088
Q87YF4	*PSPTO_3846*	Transport	Unknown	2.21	0.0180	0.0157
Q87UG5	*PSPTO_5333*	Transport	Unknown	2.13	0.0196	0.0166
Q87UE1	*PSPTO_5358*	Transport	Periplasmic	2.08	0.0037	0.0064
Q87TV8	*PSPTO_5562*	Transport	Unknown	2.36	0.0444	0.0287
Q87WQ2	*secG*	Transport	Cytoplasmic membrane	4.53	0.0054	0.0078
Q88B30	*PSPTO_0201*	Unknown function	Cytoplasmic	2.45	<0.0001	0.0001
Q88B14	*PSPTO_0219*	Unknown function	Unknown	3.58	0.0168	0.0151
Q88A93	*PSPTO_0499*	Unknown function	Unknown	2.05	0.0040	0.0066
Q88A00	*PSPTO_0597*	Unknown function	Cytoplasmic	2.02	0.0123	0.0126
Q889R6	*PSPTO_0683*	Unknown function	Cytoplasmic membrane	2.03	<0.0001	0.0001
Q889L5	*PSPTO_0734*	Unknown function	Cytoplasmic	2.13	0.0004	0.0018
Q887U1	*PSPTO_1195*	Unknown function	Unknown	3.06	0.0001	0.0008

Q887N9	*PSPTO_1252*	Unknown function	Cytoplasmic membrane	2.47	0.0166	0.0150
Q887N0	*PSPTO_1261*	Unknown function	Unknown	2.08	0.0202	0.0168
Q887F2	*PSPTO_1344*	Unknown function	Unknown	2.28	0.0004	0.0017
Q886F9	*PSPTO_1620*	Unknown function	Outer membrane	4.50	<0.0001	0.0005
Q885Y3	*PSPTO_1698*	Unknown function	Periplasmic	2.38	0.0182	0.0158
Q885M9	*PSPTO_1802*	Unknown function	Unknown	2.01	0.0021	0.0044
Q884V0	*PSPTO_1986*	Unknown function	Cytoplasmic membrane	2.86	0.0039	0.0065
Q884R4	*PSPTO_2024*	Unknown function	Cytoplasmic	2.21	0.0432	0.0283
Q884P9	*PSPTO_2039*	Unknown function	Cytoplasmic	2.17	0.0006	0.0022
Q884A7	*PSPTO_2189*	Unknown function	Cytoplasmic membrane	2.62	0.0010	0.0029
Q882F9	*PSPTO_2669*	Unknown function	Unknown	2.71	0.0779	0.0420
Q881E0	*PSPTO_2954*	Unknown function	Cytoplasmic	2.85	0.0034	0.0060
Q880Y0	*PSPTO_3020*	Unknown function	Unknown	2.91	0.0082	0.0099
Q880T4	*PSPTO_3067*	Unknown function	Cytoplasmic	2.03	0.0192	0.0163
Q880S2	*PSPTO_3079*	Unknown function	Cytoplasmic	2.32	0.0337	0.0239
Q880Q1	*PSPTO_3103*	Unknown function	Cytoplasmic	2.02	0.0228	0.0183
Q87Y26	*PSPTO_3986*	Unknown function	Unknown	2.08	0.0713	0.0392
Q87WE1	*PSPTO_4610*	Unknown function	Periplasmic	3.01	0.0004	0.0018
Q87V76	*PSPTO_5064*	Unknown function	Cytoplasmic	2.09	0.0013	0.0036
Q87V70	*PSPTO_5071*	Unknown function	Unknown	2.33	0.0146	0.0139
Q87UW7	*PSPTO_5175*	Unknown function	Unknown	2.30	<0.0001	0.0005
A9H262	*PSPTO_5631*	Unknown function	Unknown	3.31	0.0907	0.0468
D3NQ15	*PSPTO_5635*	Unknown function	Unknown	2.48	0.0019	0.0042
Q87U73	*hcp-2*	Virulence	Extracellular	2.38	0.0493	0.0305

Intracellular Reduced Abundance

UniProt ID	Gene	Function	Localization	Ratio	p-value	q-value
Q880N0	PSPTO_3124	Carbon metabolism	Unknown	0.43	0.0017	0.0040
Q880M8	PSPTO_3126	Carbon metabolism	Cytoplasmic	0.48	0.0038	0.0065
Q885W9	cobC	Cofactors-metals	Cytoplasmic	0.45	0.0442	0.0286
Q87VQ7	cobL	Cofactors-metals	Cytoplasmic membrane	0.43	0.0016	0.0039
Q882M6	irp1	Cofactors-metals	Cytoplasmic membrane	0.33	0.0130	0.0129
Q882M8	irp4	Cofactors-metals	Cytoplasmic	0.43	0.0045	0.0070
Q87VL5	pncB	Cofactors-metals	Cytoplasmic	0.38	0.0016	0.0038
Q884E3	PSPTO_2150	Cofactors-metals	Cytoplasmic membrane	0.40	0.0058	0.0081
Q882M4	PSPTO_2602	Cofactors-metals	Cytoplasmic membrane	0.44	<0.0001	0.0005
Q87TZ1	PSPTO_5526	Cofactors-metals	Cytoplasmic	0.46	0.0077	0.0095
Q888U9	ndH	Energy	Cytoplasmic membrane	0.41	0.0011	0.0031
Q884V9	flhF	Extracellular function and structural	Cytoplasmic membrane	0.38	0.0011	0.0030
Q884X7	fliG	Extracellular function and structural	Cytoplasmic	0.36	<0.0001	0.0005
Q884X6	fliH	Extracellular function and structural	Cytoplasmic	0.44	0.0006	0.0022
Q884X5	fliI	Extracellular function and structural	Cytoplasmic	0.30	0.0007	0.0024
Q884W7	fliM	Extracellular function and structural	Cytoplasmic	0.32	0.0004	0.0016
Q87YC9	htrB	Extracellular function and structural	Cytoplasmic membrane	0.36	0.0029	0.0053
Q87VF9	kdtA	Extracellular function and structural	Cytoplasmic membrane	0.44	0.0001	0.0008

Intracellular Reduced Abundance

Q87VI4	motB	Extracellular function and structural	Cytoplasmic membrane	0.48	0.0102	0.0112
Q87VA8	pilJ	Extracellular function and structural	Outer membrane	0.40	0.0088	0.0102
Q88BA0	PSPTO_0117	Extracellular function and structural	Cytoplasmic membrane	0.44	0.0170	0.0152
Q888V0	PSPTO_0916	Extracellular function and structural	Cytoplasmic membrane	0.33	0.0012	0.0034
Q888I5	PSPTO_1039	Extracellular function and structural	Cytoplasmic	0.49	0.0007	0.0024
Q887H3	PSPTO_1323	Extracellular function and structural	Cytoplasmic	0.49	0.0001	0.0008
Q887G2	PSPTO_1334	Extracellular function and structural	Cytoplasmic membrane	0.45	0.0133	0.0131
Q886T1	PSPTO_1495	Extracellular function and structural	Cytoplasmic	0.33	<0.0001	0.0005
Q885A8	PSPTO_1927	Extracellular function and structural	Cytoplasmic	0.45	0.0003	0.0014
Q883C7	PSPTO_2441	Extracellular function and structural	Cytoplasmic membrane	0.34	0.0002	0.0013
Q883C6	PSPTO_2442	Extracellular function and structural	Cytoplasmic	0.36	<0.0001	0.0001
Q883A0	PSPTO_2472	Extracellular function and structural	Cytoplasmic membrane	0.40	0.0182	0.0158
Q882L0	PSPTO_2616	Extracellular function and structural	Cytoplasmic membrane	0.43	0.0016	0.0038
Q87ZA0	PSPTO_3530	Extracellular function and structural	Cytoplasmic	0.41	0.0002	0.0012
Q87WL5	PSPTO_4531	Extracellular function and structural	Membrane	0.32	0.0048	0.0072
Q87WK5	PSPTO_4541	Extracellular function and structural	Cytoplasmic membrane	0.36	0.0518	0.0316
Q87VK0	PSPTO_4936	Extracellular function and structural	Cytoplasmic membrane	0.47	0.0368	0.0254
Q87UY3	PSPTO_5159	Extracellular function and structural	Membrane	0.42	0.0119	0.0124
Q87TW6	PSPTO_5553	Extracellular function and structural	Cytoplasmic membrane	0.43	0.0269	0.0203
Q87VD8	waaG	Extracellular function and structural	Cytoplasmic	0.48	0.0066	0.0087
Q87WW5	zapE	Extracellular function and structural	Cytoplasmic	0.48	0.0005	0.0020
Q87YY5	zipA	extracellular function and structural	Cytoplasmic membrane	0.50	0.0004	0.0017
Q882N1	pchA	Generic enzymes	Cytoplasmic	0.38	<0.0001	0.0005
Q888F9	PSPTO_1067	Generic enzymes	Cytoplasmic	0.49	0.0002	0.0012
Q885B7	PSPTO_1918	Generic enzymes	Cytoplasmic membrane	0.44	0.0002	0.0012
Q884Z0	PSPTO_1946	Generic enzymes	Cytoplasmic	0.37	0.0001	0.0010
Q882F6	PSPTO_2672	Generic enzymes	Unknown	0.38	0.0003	0.0016
Q882B9	PSPTO_2710	Generic enzymes	Cytoplasmic	0.43	0.0001	0.0009
Q882A7	PSPTO_2722	Generic enzymes	Periplasmic	0.40	0.0001	0.0009
Q87YT7	PSPTO_3705	Generic enzymes	Cytoplasmic	0.49	0.0009	0.0028
Q87V37	PSPTO_5104	Generic enzymes	Unknown	0.39	<0.0001	0.0001
Q87U09	PSPTO_5506	Generic enzymes	Cytoplasmic	0.46	0.0040	0.0066
Q88B47	qor	Generic enzymes	Cytoplasmic	0.47	0.0011	0.0031
Q87US4	ubiH	Generic enzymes	Cytoplasmic membrane	0.35	<0.0001	0.0003
Q881I9	vanA	Generic enzymes	Cytoplasmic	0.35	0.0004	0.0018
Q88AQ7	envZ	Genetic regulation	Cytoplasmic membrane	0.39	0.0025	0.0049
Q882C1	mltR	Genetic regulation	Cytoplasmic	0.46	0.0002	0.0011

Intracellular Reduced Abundance

Q88AN5	ntrB	Genetic regulation	Cytoplasmic membrane	0.28	<0.0001	0.0005
Q88AT3	PSPTO_0303	Genetic regulation	Cytoplasmic	0.32	0.0002	0.0010
Q88AL2	PSPTO_0378	Genetic regulation	Cytoplasmic	0.22	0.0033	0.0059
Q88AK6	PSPTO_0384	Genetic regulation	Cytoplasmic	0.40	0.0018	0.0041
Q889T2	PSPTO_0665	Genetic regulation	Unknown	0.46	0.0003	0.0014
Q888Q1	PSPTO_0965	Genetic regulation	Cytoplasmic membrane	0.47	0.0002	0.0012
Q886S7	PSPTO_1499	Genetic regulation	Cytoplasmic	0.37	<0.0001	0.0003
Q886H4	PSPTO_1605	Genetic regulation	Cytoplasmic membrane	0.09	<0.0001	0.0004
Q886H3	PSPTO_1606	Genetic regulation	Cytoplasmic membrane	0.29	0.0028	0.0052
Q886G1	PSPTO_1618	Genetic regulation	Cytoplasmic	0.49	0.0014	0.0037
Q884H0	PSPTO_2123	Genetic regulation	Cytoplasmic membrane	0.37	<0.0001	0.0001
Q884G2	PSPTO_2131	Genetic regulation	Cytoplasmic membrane	0.11	<0.0001	0.0005
Q883G8	PSPTO_2395	Genetic regulation	Cytoplasmic	0.47	0.0039	0.0065
Q883C1	PSPTO_2447	Genetic regulation	Cytoplasmic	0.47	0.0589	0.0343
Q882B4	PSPTO_2715	Genetic regulation	Cytoplasmic membrane	0.28	0.0007	0.0023
Q87X95	PSPTO_4293	Genetic regulation	Cytoplasmic membrane	0.39	0.0261	0.0200
Q87UA6	PSPTO_5399	Genetic regulation	Cytoplasmic	0.47	0.0038	0.0065
Q87U17	PSPTO_5498	Genetic regulation	Cytoplasmic	0.38	<0.0001	0.0005
G3XDD3	rpoS	Genetic regulation	Cytoplasmic	0.50	0.0002	0.0012
Q888B4	cfa	Lipid metabolism	Cytoplasmic	0.47	0.0015	0.0038
Q883S5	aroF-1	Nitrogen metabolism	Cytoplasmic	0.46	0.0006	0.0022
Q885J9	aruF	Nitrogen metabolism	Cytoplasmic	0.46	0.0020	0.0043
Q88BB6	dadA	Nitrogen metabolism	Cytoplasmic membrane	0.45	0.0985	0.0495
Q887L6	gcvT-2	Nitrogen metabolism	Cytoplasmic	0.43	0.0001	0.0010
Q887A1	iscS	Nitrogen metabolism	Cytoplasmic	0.47	0.0001	0.0008
Q889F0	proB	Nitrogen metabolism	Cytoplasmic	0.50	0.0001	0.0009
Q88AI9	PSPTO_0401	Nitrogen metabolism	Cytoplasmic	0.22	0.0094	0.0107
Q888Z1	PSPTO_0873	Nitrogen metabolism	Cytoplasmic	0.39	0.0004	0.0018
Q880G9	PSPTO_3190	Nitrogen metabolism	Unknown	0.39	<0.0001	0.0005
Q87U54	PSPTO_5460	Nitrogen metabolism	Cytoplasmic	0.39	<0.0001	0.0004
Q88AD2	soxB-1	Nitrogen metabolism	Cytoplasmic	0.47	0.0639	0.0364
Q886H7	cdd	Nucleic acid metabolism	Cytoplasmic	0.45	0.0743	0.0405
Q87W38	hrpB	Nucleic acid metabolism	Unknown	0.47	0.0008	0.0027
Q87VJ2	mutL	Nucleic acid metabolism	Cytoplasmic	0.41	0.0002	0.0011
Q889J2	PSPTO_0757	Nucleic acid metabolism	Cytoplasmic	0.49	0.0014	0.0036
Q87UF4	PSPTO_5344	Nucleic acid metabolism	Cytoplasmic	0.34	0.0001	0.0010
Q87WB3	radA	Nucleic acid metabolism	Unknown	0.48	<0.0001	0.0005
Q87XY7	recA	Nucleic acid metabolism	Cytoplasmic	0.45	0.0001	0.0010
Q88BK1	recF	Nucleic acid metabolism	Cytoplasmic	0.45	0.0014	0.0036
Q87WN8	recN	Nucleic acid metabolism	Cytoplasmic	0.46	0.0011	0.0032
Q87Z00	recR	Nucleic acid metabolism	Cytoplasmic	0.37	0.0066	0.0087
Q88BA4	rep	Nucleic acid metabolism	Cytoplasmic	0.46	0.0001	0.0008
Q87Y35	ruvB	Nucleic acid metabolism	Cytoplasmic	0.49	0.0001	0.0010
Q87YN0	sbcD	Nucleic acid metabolism	Cytoplasmic	0.29	0.0001	0.0009
Q88BE4	spoT	Nucleic acid metabolism	Cytoplasmic	0.46	0.0001	0.0008
Q884C9	uvrB	Nucleic acid metabolism	Cytoplasmic	0.48	0.0001	0.0008
Q87U01	uvrD	Nucleic acid metabolism	Cytoplasmic	0.49	<0.0001	0.0005
Q87WE9	ettA	Protein synthesis and modification	Cytoplasmic	0.48	<0.0001	0.0005
Q87X94	hscC	Protein synthesis and modification	Cytoplasmic	0.48	0.0010	0.0029
Q87ZR6	mnmA	Protein synthesis and modification	Cytoplasmic	0.42	0.0001	0.0010

Intracellular Reduced Abundance

Q888G1	PSPTO_1065	Protein synthesis and modification	Cytoplasmic	0.47	0.0042	0.0067
Q887E6	PSPTO_1350	Protein synthesis and modification	Cytoplasmic	0.44	0.0069	0.0089
Q886N6	PSPTO_1541	Protein synthesis and modification	Cytoplasmic membrane	0.48	0.0012	0.0033
Q885F3	PSPTO_1882	Protein synthesis and modification	Cytoplasmic	0.45	0.0003	0.0013
Q87WR2	PSPTO_4481	Protein synthesis and modification	Cytoplasmic	0.45	0.0138	0.0133
Q87V87	PSPTO_5052	Protein synthesis and modification	Cytoplasmic	0.43	0.0001	0.0008
Q9L6W9	queA	Protein synthesis and modification	Cytoplasmic	0.44	0.0006	0.0022
Q887M4	rlmF	Protein synthesis and modification	Cytoplasmic	0.37	0.0010	0.0029
A0PCI4	rluD	Protein synthesis and modification	Cytoplasmic	0.24	0.0008	0.0025
Q87Y81	rnd	Protein synthesis and modification	Cytoplasmic	0.47	0.0054	0.0078
Q885U7	trhO	Protein synthesis and modification	Cytoplasmic	0.34	0.0001	0.0008
Q885Z7	ttcA	Protein synthesis and modification	Cytoplasmic	0.45	0.0174	0.0154
Q87VN7	yegD	Protein synthesis and modification	Cytoplasmic	0.45	0.0026	0.0050
Q88AS5	cysA	Transport	Cytoplasmic membrane	0.50	0.0013	0.0036
Q885Z9	dctA-1	Transport	Cytoplasmic membrane	0.45	0.0032	0.0058
Q88AG1	ftsX	Transport	Cytoplasmic membrane	0.46	0.0012	0.0033
Q887J7	gltK	Transport	Cytoplasmic membrane	0.45	0.0021	0.0044
Q884I4	lolC	Transport	Cytoplasmic membrane	0.48	0.0084	0.0100
Q888U0	pilB	Transport	Cytoplasmic	0.39	0.0001	0.0010
Q888U1	pilC	Transport	Cytoplasmic membrane	0.49	0.0026	0.0050
Q88A35	potA	Transport	Cytoplasmic membrane	0.42	<0.0001	0.0005
Q88B81	PSPTO_0138	Transport	Cytoplasmic	0.48	0.0005	0.0019
Q88AR7	PSPTO_0319	Transport	Cytoplasmic	0.47	<0.0001	0.0006
Q88AD0	PSPTO_0462	Transport	Cytoplasmic membrane	0.38	0.0019	0.0042
Q884D3	PSPTO_2160	Transport	Cytoplasmic membrane	0.30	0.0001	0.0007
Q880E0	PSPTO_3230	Transport	Outer membrane	0.18	<0.0001	0.0001
Q87VT2	PSPTO_4853	Transport	Cytoplasmic	0.39	0.0039	0.0065
Q87ZU5	tliE	Transport	Cytoplasmic membrane	0.48	0.0002	0.0012
Q88BG6	PSPTO_0048	Unknown function	Cytoplasmic	0.36	0.0009	0.0027
Q88AI4	PSPTO_0406	Unknown function	Cytoplasmic membrane	0.41	0.0002	0.0013
Q88A51	PSPTO_0546	Unknown function	Cytoplasmic	0.46	0.0119	0.0124
Q889A6	PSPTO_0855	Unknown function	Cytoplasmic	0.46	0.0003	0.0014
Q889A5	PSPTO_0856	Unknown function	Cytoplasmic	0.49	0.0002	0.0012
Q888Z0	PSPTO_0874	Unknown function	Cytoplasmic	0.30	<0.0001	0.0004
Q888Y9	PSPTO_0875	Unknown function	Cytoplasmic	0.31	<0.0001	0.0005
Q887P6	PSPTO_1245	Unknown function	Unknown	0.38	0.0059	0.0082
Q887L3	PSPTO_1278	Unknown function	Cytoplasmic membrane	0.39	<0.0001	0.0002
Q887G3	PSPTO_1333	Unknown function	Cytoplasmic	0.49	0.0009	0.0028
Q886E8	PSPTO_1631	Unknown function	Cytoplasmic	0.50	0.0096	0.0108
Q886C3	PSPTO_1656	Unknown function	Unknown	0.40	0.0003	0.0014
Q885B6	PSPTO_1919	Unknown function	Cytoplasmic	0.24	0.0087	0.0102
Q884Q4	PSPTO_2034	Unknown function	Unknown	0.33	<0.0001	0.0005
Q884P7	PSPTO_2041	Unknown function	Cytoplasmic membrane	0.46	0.0005	0.0019

Intracellular Reduced Abundance

Q884M5	PSPTO_2063	Unknown function	Cytoplasmic	0.46	0.0012	0.0033
Q882U5	PSPTO_2527	Unknown function	Cytoplasmic	0.50	0.0004	0.0016
Q881L8	PSPTO_2871	Unknown function	Cytoplasmic	0.42	0.0003	0.0013
Q881L7	PSPTO_2872	Unknown function	Unknown	0.38	<0.0001	0.0003
Q880E1	PSPTO_3229	Unknown function	Outer membrane	0.19	0.0001	0.0009
Q87ZG1	PSPTO_3468	Unknown function	Unknown	0.49	0.0013	0.0036
Q87YW0	PSPTO_3682	Unknown function	Cytoplasmic membrane	0.44	0.0001	0.0008
Q87YA7	PSPTO_3894	Unknown function	Cytoplasmic	0.24	<0.0001	0.0001
Q87Y95	PSPTO_3906	Unknown function	Cytoplasmic	0.47	0.0070	0.0090
Q87Y17	PSPTO_3995	Unknown function	Cytoplasmic	0.41	0.0014	0.0036
Q87XA2	PSPTO_4286	Unknown function	Cytoplasmic	0.24	0.0002	0.0012
Q87W91	PSPTO_4663	Unknown function	Cytoplasmic	0.39	0.0019	0.0042
Q87VU6	PSPTO_4839	Unknown function	Outer membrane	0.37	0.0010	0.0029
Q87VL1	PSPTO_4925	Unknown function	Cytoplasmic	0.25	<0.0001	0.0004
Q87VD0	PSPTO_5009	Unknown function	Cytoplasmic membrane	0.33	0.0001	0.0009
Q87V51	PSPTO_5090	Unknown function	Cytoplasmic	0.42	0.0005	0.0018
Q87UD4	PSPTO_5365	Unknown function	Cytoplasmic	0.49	0.0002	0.0012
Q87UD2	PSPTO_5373	Unknown function	Cytoplasmic	0.28	0.0015	0.0037
D3NQ14	PSPTO_5634	Unknown function	Unknown	0.14	0.0017	0.0039
Q88BV9	PSPTO_B0012	Unknown function	Unknown	0.39	0.0269	0.0203
Q88BV5	PSPTO_B0020	Unknown function	Cytoplasmic	0.20	0.0019	0.0042
Q87W73	cfa3	Virulence	Cytoplasmic membrane	0.42	0.0009	0.0027
Q87W71	cfa5	Virulence	Cytoplasmic membrane	0.45	0.0031	0.0057
Q87W70	cfa6	Virulence	Cytoplasmic membrane	0.27	0.0086	0.0101
Q87W69	cfa7	Virulence	Cytoplasmic membrane	0.31	<0.0001	0.0005
Q87W66	cfa9	Virulence	Cytoplasmic	0.49	0.0086	0.0101
Q87W56	cmaA	Virulence	Cytoplasmic	0.41	0.0023	0.0046
Q87W55	cmaB	Virulence	Cytoplasmic	0.41	0.0010	0.0029
Q88AL8	iaaL	Virulence	Cytoplasmic	0.28	0.0001	0.0008
Q87U82	PSPTO_5425	Virulence	Cytoplasmic	0.42	<0.0001	0.0004
Q87U80	PSPTO_5427	VIrulence	Cytoplasmic	0.37	0.0001	0.0010
Q877T3 Q87UJ2	PSPTO_0035 PSPTO_5304			0.47	0.0059	0.0082

Extracellular Increased Abundance

UniProt ID	Gene	Function	Localization	Ratio	p-value	q-value
Q87Z72	glcB2	Carbon metabolism	Cytoplasmic	2.59	0.0049	0.0121
Q886Y2	PSPTO_1443	Carbon metabolism	Cytoplasmic	1.75	0.0032	0.0104
Q880N3	zwf-2	Carbon metabolism	Cytoplasmic	1.74	0.0134	0.0211
Q885W9	cobC	Cofactors - Metals	Cytoplasmic	3.28	0.0000	0.0007
P59571	copA	Cofactors - Metals	Periplasmic	1.68	0.0040	0.0117
P59572	copB	Cofactors - Metals	Outer membrane	2.86	0.0016	0.0077
Q883S4	panE-1	Cofactors - Metals	Cytoplasmic	2.19	0.0108	0.0193
Q87TT0	atpF	Energy	Cytoplasmic membrane	4.08	0.0040	0.0117
Q887Q2	algE	Extracellular function and structural	Outer membrane	3.93	0.0244	0.0290
Q887Q5	algL	Extracellular function and structural	Periplasmic	3.13	0.0175	0.0245
Q87Z37	ampC	Extracellular function and structural	Periplasmic	2.00	0.0005	0.0042

Extracellular Increased Abundance

Q886Y7	bamB	Extracellular function and structural	Outer membrane	1.68	0.0068	0.0147
Q883N6	dacB	Extracellular function and structural	Periplasmic	1.69	0.0236	0.0286
Q885A0	flgE-1	Extracellular function and structural	Extracellular	1.76	0.0046	0.0121
Q884Z7	flgF	Extracellular function and structural	Periplasmic	1.56	0.0086	0.0168
Q884Z6	flgG	Extracellular function and structural	Extracellular	1.78	0.0022	0.0090
Q884Z2	flgK	Extracellular function and structural	Extracellular	2.43	0.0000	0.0007
Q884Z1	flgL	Extracellular function and structural	Extracellular	2.34	0.0038	0.0116
Q884Y7	fliC	Extracellular function and structural	Extracellular	1.55	0.0063	0.0143
Q884X6	fliH	Extracellular function and structural	Cytoplasmic	1.84	0.0047	0.0121
Q87YC6	minE	Extracellular function and structural	Cytoplasmic	1.59	0.0160	0.0235
Q87VW2	mltB	Extracellular function and structural	Cytoplasmic membrane	3.02	0.0111	0.0196
Q886W7	mltF	Extracellular function and structural	Cytoplasmic	1.58	0.0627	0.0499
Q87UY0	opgG	Extracellular function and structural	Periplasmic	1.62	0.0092	0.0176
Q889D5	PSPTO_0815	Extracellular function and structural	Unknown	1.89	0.0018	0.0081
Q884A9	PSPTO_2187	Extracellular function and structural	Unknown	1.63	0.0075	0.0154
Q883T0	PSPTO_2270	Extracellular function and structural	Unknown	1.86	0.0023	0.0092
Q881L5	PSPTO_2874	Extracellular function and structural	Unknown	1.52	0.0426	0.0413
Q87ZA7	PSPTO_3522	Extracellular function and structural	Periplasmic	1.87	0.0231	0.0282
Q87XU1	PSPTO_4084	Extracellular function and structural	Extracellular	3.73	0.0278	0.0313
Q87WX4	PSPTO_4419	Extracellular function and structural	Cytoplasmic membrane	2.24	0.0138	0.0215
Q87WB9	PSPTO_4634	Extracellular function and structural	Cytoplasmic	2.21	0.0119	0.0199
Q888J5	wssD	Extracellular function and structural	Extracellular	3.14	0.0193	0.0261
Q888J2	wssG	Extracellular function and structural	Periplasmic	2.39	0.0352	0.0365
Q87WB1	fnr-2	Generic enzymes	Cytoplasmic	2.18	0.0011	0.0063
Q887P6	PSPTO_1245	Generic enzymes	Unknown	2.05	0.0078	0.0156
Q887F6	PSPTO_1340	Generic enzymes	Unknown	1.62	0.0047	0.0121
Q883R0	PSPTO_2290	Generic enzymes	Cytoplasmic	2.58	0.0001	0.0023
Q882D1	PSPTO_2697	Generic enzymes	Cytoplasmic	3.43	0.0015	0.0075
Q881P0	PSPTO_2847	Generic enzymes	Outer membrane	2.08	0.0115	0.0197
Q87ZD4	PSPTO_3495	Generic enzymes	Cytoplasmic	1.96	0.0066	0.0144
Q87XL7	PSPTO_4161	Generic enzymes	Unknown	2.25	0.0010	0.0060
Q87U08	PSPTO_5507	Generic enzymes	Cytoplasmic	2.59	0.0002	0.0024
Q87XF6	mucB	Genetic regulation	Periplasmic	1.86	0.0031	0.0104
Q886A2	PSPTO_1679	Genetic regulation	Cytoplasmic	2.67	0.0172	0.0243
Q87VA0	pyrR	Genetic regulation	Cytoplasmic	3.07	0.0048	0.0121
Q87YG7	fabG	Lipid metabolism	Cytoplasmic	1.56	0.0092	0.0177

Extracellular Increased Abundance

Q889F4	ispB	Lipid metabolism	Cytoplasmic	1.59	0.0003	0.0034
Q88BW5	plcA2	Lipid metabolism	Periplasmic	1.82	0.0026	0.0096
Q885R5	PSPTO_1766	Lipid metabolism	Unknown	3.77	0.0032	0.0105
Q885B9	PSPTO_1916	Lipid metabolism	Cytoplasmic	1.83	0.0395	0.0393
Q883T2	PSPTO_2268	Lipid metabolism	Periplasmic	1.51	0.0537	0.0458
Q885J4	astE	Nitrogen metabolism	Cytoplasmic	1.81	0.0062	0.0142
Q87WV4	hisG	Nitrogen metabolism	Cytoplasmic	2.55	0.0038	0.0116
Q884P1	mtnC	Nitrogen metabolism	Cytoplasmic	4.40	0.0004	0.0040
Q87ZC3	PSPTO_3506	Nitrogen metabolism	Cytoplasmic	1.80	0.0573	0.0476
Q88AP1	thrB	Nitrogen metabolism	Cytoplasmic	3.29	0.0069	0.0147
Q88A03	trpC	Nitrogen metabolism	Cytoplasmic	1.54	0.0047	0.0121
Q88A04	trpD	Nitrogen metabolism	Cytoplasmic	1.50	0.0003	0.0033
Q87UA4	cysQ	Nucleic acid metabolism	Cytoplasmic	1.67	0.0187	0.0255
Q87YX9	guaD	Nucleic acid metabolism	Unknown	2.14	0.0426	0.0413
Q87YR9	hupB	Nucleic acid metabolism	Cytoplasmic	1.60	0.0098	0.0180
Q883I4	PSPTO_2373	Nucleic acid metabolism	Unknown	1.52	0.0024	0.0094
Q884R0	pyrF	Nucleic acid metabolism	Cytoplasmic	2.31	0.0529	0.0454
Q886Z7	hscA	Protein synthesis and modification	Cytoplasmic	1.61	0.0598	0.0487
Q883J5	map-2	Protein synthesis and modification	Cytoplasmic	1.62	0.0039	0.0117
Q87YB6	prc	Protein synthesis and modification	Cytoplasmic membrane	1.70	0.0220	0.0277
Q88AG5	PSPTO_0425	Protein synthesis and modification	Unknown	1.58	0.0440	0.0419
Q880G7	PSPTO_3192	Protein synthesis and modification	Cytoplasmic	1.97	0.0016	0.0077
Q880G6	PSPTO_3193	Protein synthesis and modification	Extracellular	2.28	0.0026	0.0096
Q87ZU2	PSPTO_3332	Protein synthesis and modification	Extracellular	2.88	0.0168	0.0242
Q87Y51	PSPTO_3958	Protein synthesis and modification	Unknown	1.72	0.0069	0.0147
Q87UG9	PSPTO_5329	Protein synthesis and modification	Cytoplasmic membrane	1.76	0.0221	0.0277
Q889V7	rpsH	Protein synthesis and modification	Cytoplasmic	1.55	0.0047	0.0121
Q889F7	selD	Protein synthesis and modification	Cytoplasmic	5.15	0.0078	0.0156
Q888C9	ychF	Protein synthesis and modification	Cytoplasmic	1.52	0.0391	0.0391
Q888H3	dctP	Transport	Periplasmic	1.79	0.0062	0.0142
Q889I6	fecB	Transport	Periplasmic	2.41	0.0046	0.0121
Q88AM5	PSPTO_0364	Transport	Periplasmic	1.63	0.0163	0.0238
Q889F9	PSPTO_0791	Transport	Periplasmic	1.56	0.0019	0.0082
Q888X5	PSPTO_0889	Transport	Unknown	1.58	0.0008	0.0054
Q888H0	PSPTO_1054	Transport	Outer membrane	1.69	0.0260	0.0305
Q888F0	PSPTO_1076	Transport	Cytoplasmic membrane	1.57	0.0442	0.0419
Q887X1	PSPTO_1159	Transport	Unknown	1.64	0.0481	0.0435
Q887N6	PSPTO_1255	Transport	Periplasmic	1.51	0.0114	0.0197
Q886H9	PSPTO_1600	Transport	Periplasmic	2.62	0.0000	0.0005
Q884F2	PSPTO_2141	Transport	Cytoplasmic membrane	1.94	0.0047	0.0121
Q882G1	PSPTO_2667	Transport	Periplasmic	1.56	0.0076	0.0154
Q881V7	PSPTO_2775	Transport	Outer membrane	1.70	0.0219	0.0277
Q881U7	PSPTO_2785	Transport	Periplasmic	1.76	0.0028	0.0098
Q881U4	PSPTO_2788	Transport	Unknown	1.61	0.0112	0.0197

Extracellular Increased Abundance

Q880V2	PSPTO_3049	Transport	Cytoplasmic membrane	1.92	0.0116	0.0198
Q880U3	PSPTO_3058	Transport	Periplasmic	2.23	0.0029	0.0101
Q880B6	PSPTO_3256	Transport	Unknown	1.78	0.0004	0.0039
Q87ZT9	PSPTO_3335	Transport	Unknown	1.61	0.0223	0.0277
Q87ZD9	PSPTO_3490	Transport	Periplasmic	1.68	0.0184	0.0254
Q87UQ1	PSPTO_5245	Transport	Periplasmic	1.89	0.0016	0.0077
Q87UJ1	PSPTO_5306	Transport	Periplasmic	5.92	0.0017	0.0078
Q87UI1	PSPTO_5316	Transport	Unknown	1.73	0.0619	0.0495
Q87WT8	ptsN	Transport	Cytoplasmic	1.50	0.0467	0.0429
Q883G4	rbsB-2	Transport	Periplasmic	2.59	0.0041	0.0117
Q87ZU6	tliF	Transport	Periplasmic	1.96	0.0606	0.0489
Q87Y40	tolB	Transport	Cytoplasmic membrane	2.08	0.0123	0.0202
Q880Z3	xylF	Transport	Periplasmic	1.58	0.0036	0.0113
Q87UM8	znuA	Transport	Periplasmic	1.64	0.0600	0.0487
Q88B27	PSPTO_0205	Unknown function	Unknown	1.50	0.0450	0.0425
Q88AQ3	PSPTO_0333	Unknown function	Periplasmic	1.71	0.0066	0.0144
Q88AN3	PSPTO_0355	Unknown function	Unknown	1.89	0.0422	0.0413
Q88AE1	PSPTO_0451	Unknown function	Cytoplasmic membrane	1.82	0.0585	0.0481
Q88A39	PSPTO_0558	Unknown function	Periplasmic	1.50	0.0084	0.0164
Q88A25	PSPTO_0572	Unknown function	Unknown	1.58	0.0195	0.0263
Q886R3	PSPTO_1514	Unknown function	Unknown	2.51	0.0001	0.0017
Q886K2	PSPTO_1577	Unknown function	Unknown	2.16	0.0011	0.0062
Q886J0	PSPTO_1589	Unknown function	Unknown	1.75	0.0514	0.0454
Q886H1	PSPTO_1608	Unknown function	Unknown	1.54	0.0185	0.0255
Q886F8	PSPTO_1621	Unknown function	Unknown	1.86	0.0519	0.0454
Q885Y0	PSPTO_1701	Unknown function	Unknown	1.57	0.0251	0.0296
Q884R4	PSPTO_2024	Unknown function	Cytoplasmic	1.64	0.0324	0.0346
Q883X7	PSPTO_2220	Unknown function	Unknown	1.52	0.0006	0.0043
Q880J1	PSPTO_3166	Unknown function	Cytoplasmic membrane	1.57	0.0230	0.0282
Q87ZM2	PSPTO_3402	Unknown function	Unknown	1.73	0.0290	0.0321
Q87YL2	PSPTO_3783	Unknown function	Unknown	1.65	0.0045	0.0121
Q87XJ0	PSPTO_4188	Unknown function	Cytoplasmic	2.38	0.0036	0.0113
Q87XA0	PSPTO_4288	Unknown function	Cytoplasmic	1.92	0.0139	0.0215
Q87X04	PSPTO_4386	Unknown function	Cytoplasmic	1.77	0.0058	0.0136
Q87VW8	PSPTO_4817	Unknown function	Cytoplasmic membrane	1.56	0.0307	0.0333
Q87VC5	PSPTO_5014	Unknown function	Cytoplasmic membrane	2.60	0.0287	0.0319
Q87UU0	PSPTO_5202	Unknown function	Unknown	1.50	0.0097	0.0180
Q87W74	cfa2	Virulence	Cytoplasmic	1.92	0.0349	0.0364
Q87W76	cfl	Virulence	Cytoplasmic membrane	1.79	0.0407	0.0401
Q8RSY1	hopAB2	Virulence	Extracellular	3.86	0.0272	0.0312
Q87XS5	hopAK1	Virulence	Extracellular	2.32	0.0282	0.0316
Q88A08	hopC1	Virulence	Extracellular	2.35	0.0232	0.0282
Q888Y8	hopD1	Virulence	Extracellular	3.27	0.0267	0.0308
Q87X57	hopE1	Virulence	Extracellular	2.56	0.0330	0.0348
Q87W42	hopG1	Virulence	Extracellular	3.43	0.0251	0.0296
Q87W07	hopI1	Virulence	Extracellular	3.71	0.0239	0.0287
G3XDB3	hrpK1	Virulence	Extracellular	6.82	0.0191	0.0259
Q87U93	PSPTO_5414	Virulence	Unknown	1.82	0.0003	0.0034

Extracellular Reduced Abundance

UniProt ID	Gene	Function	Localization	Ratio	p-value	q-value
Q87WT2	fumC-2	Carbon metabolism	Cytoplasmic	0.39	0.0114	0.0197
Q887K3	glk	Carbon metabolism	Cytoplasmic	0.54	0.0021	0.0088
Q884A2	gltA	Carbon metabolism	Cytoplasmic	0.65	0.0265	0.0308
P52832	gpmI	Carbon metabolism	Cytoplasmic	0.65	0.0000	0.0007
Q883Z5	lpdA	Carbon metabolism	Cytoplasmic	0.62	0.0228	0.0281
Q88A92	PSPTO_0500	Carbon metabolism	Cytoplasmic	0.65	0.0430	0.0416
Q887S1	PSPTO_1215	Carbon metabolism	Cytoplasmic	0.64	0.0590	0.0484
Q887L1	PSPTO_1281	Carbon metabolism	Cytoplasmic	0.50	0.0062	0.0143
Q87V07	PSPTO_5134	Carbon metabolism	Cytoplasmic	0.60	0.0003	0.0034
Q87UK4	PSPTO_5292	Carbon metabolism	Cytoplasmic	0.59	0.0002	0.0027
Q88A31	rpe	Carbon metabolism	Cytoplasmic	0.59	0.0001	0.0022
Q87XI2	gcd	Carbon metabolism	Cytoplasmic membrane	0.28	0.0519	0.0454
Q888R0	PSPTO_0956	Carbon metabolism	Cytoplasmic membrane	0.19	0.0205	0.0270
Q880W5	pgm	Carbon metabolism	Unknown	0.63	0.0105	0.0190
Q87XL8	bfr	Cofactors-metals	Cytoplasmic	0.51	0.0012	0.0069
Q88A98	bioB	Cofactors-metals	Cytoplasmic	0.45	0.0605	0.0489
Q88AH3	coaD	Cofactors-metals	Cytoplasmic	0.63	0.0322	0.0345
Q885W6	cobT	Cofactors-metals	Cytoplasmic	0.56	0.0005	0.0040
Q87ZT0	cysG	Cofactors-metals	Cytoplasmic	0.27	0.0161	0.0236
Q88AK4	epd	Cofactors-metals	Cytoplasmic	0.63	0.0127	0.0205
Q883K5	moaB	Cofactors-metals	Cytoplasmic	0.62	0.0014	0.0073
Q882A9	nudC	cofactors-metals	Cytoplasmic	0.41	0.0473	0.0431
Q87XG4	pdxJ	Cofactors-metals	Cytoplasmic	0.61	0.0000	0.0009
Q88A81	pqqB	Cofactors-metals	Cytoplasmic	0.67	0.0196	0.0263
Q889U4	PSPTO_0653	Cofactors-metals	Cytoplasmic	0.55	0.0022	0.0089
Q87Y29	PSPTO_3983	Cofactors-metals	Cytoplasmic	0.59	0.0000	0.0012
Q87XI5	PSPTO_4193	Cofactors-metals	Cytoplasmic	0.53	0.0017	0.0078
Q885J3	ribH2	Cofactors-metals	Cytoplasmic	0.30	0.0008	0.0054
Q888S2	terD	Cofactors-metals	Cytoplasmic	0.57	0.0010	0.0060
Q882M4	PSPTO_2602	Cofactors-metals	Cytoplasmic membrane	0.57	0.0027	0.0097
Q882M7	irp3	Cofactors-metals	Unknown	0.37	0.0551	0.0465
Q888Q5	panB	Cofactors-metals	Unknown	0.58	0.0529	0.0454
Q888S4	terB	Cofactors-metals	Unknown	0.14	0.0035	0.0113
Q887H0	cyoB	Energy	Cytoplasmic membrane	0.23	0.0109	0.0194
Q884V3	cheB1	Extracellular function and structural	Cytoplasmic	0.37	0.0612	0.0492
Q87TT6	glmU	Extracellular function and structural	Cytoplasmic	0.62	0.0070	0.0147
Q87WX2	gmhA	Extracellular function and structural	Cytoplasmic	0.40	0.0058	0.0136
Q886N1	lpxA	extracellular function and structural	Cytoplasmic	0.57	0.0503	0.0448
Q889M0	mpl	Extracellular function and structural	Cytoplasmic	0.46	0.0612	0.0492
Q888P0	PSPTO_0977	Extracellular function and structural	Cytoplasmic membrane	0.43	0.0474	0.0431
Q882L0	PSPTO_2616	Extracellular function and structural	Cytoplasmic membrane	0.43	0.0380	0.0385
Q880D4	PSPTO_3237	Extracellular function and structural	Cytoplasmic membrane	0.21	0.0537	0.0458
Q87UX2	blc	Extracellular function and structural	Outer membrane	0.45	0.0135	0.0212
Q884Z5	flgH	Extracellular function and structural	Outer membrane	0.61	0.0398	0.0395

Extracellular Reduced Abundance

Q87VJ6	hflK	Extracellular function and structural	Outer membrane	0.49	0.0375	0.0381
Q87ZM1	PSPTO_3403	Extracellular function and structural	Unknown	0.58	0.0127	0.0205
Q87YT6	acdA	Generic Enzymes	Cytoplasmic	0.64	0.0568	0.0474
Q880P6	ahpC	Generic Enzymes	Cytoplasmic	0.62	0.0150	0.0226
Q87X81	catF	Generic Enzymes	Cytoplasmic	0.61	0.0083	0.0163
Q87X79	catI	Generic Enzymes	Cytoplasmic	0.40	0.0160	0.0235
Q87X80	catJ	Generic Enzymes	Cytoplasmic	0.48	0.0041	0.0118
Q87UP3	elbB	Generic Enzymes	Cytoplasmic	0.47	0.0421	0.0412
Q881X0	glgB	Generic Enzymes	Cytoplasmic	0.23	0.0205	0.0270
Q880P8	gloA	Generic Enzymes	Cytoplasmic	0.46	0.0104	0.0189
Q880P2	gor-1	Generic Enzymes	Cytoplasmic	0.66	0.0045	0.0121
Q888T7	gsT	Generic Enzymes	Cytoplasmic	0.55	0.0028	0.0098
Q889M7	ppa1	Generic Enzymes	Cytoplasmic	0.65	0.0217	0.0276
Q88B74	PSPTO_0145	Generic Enzymes	Cytoplasmic	0.46	0.0040	0.0117
Q886W0	PSPTO_1465	Generic Enzymes	Cytoplasmic	0.53	0.0025	0.0096
Q885F4	PSPTO_1881	Generic Enzymes	Cytoplasmic	0.15	0.0099	0.0181
Q885F3	PSPTO_1882	Generic Enzymes	Cytoplasmic	0.44	0.0003	0.0033
Q883R1	PSPTO_2289	Generic Enzymes	Cytoplasmic	0.67	0.0155	0.0231
Q881S7	PSPTO_2805	Generic Enzymes	Cytoplasmic	0.16	0.0543	0.0460
Q880W1	PSPTO_3039	Generic Enzymes	Cytoplasmic	0.27	0.0388	0.0389
Q87ZR2	PSPTO_3362	Generic Enzymes	Cytoplasmic	0.47	0.0107	0.0192
Q87ZG9	PSPTO_3460	Generic Enzymes	Cytoplasmic	0.61	0.0043	0.0121
Q87Z61	PSPTO_3570	Generic Enzymes	Cytoplasmic	0.34	0.0052	0.0128
Q87YT4	PSPTO_3708	Generic Enzymes	Cytoplasmic	0.54	0.0495	0.0442
Q87YB8	PSPTO_3883	Generic Enzymes	Cytoplasmic	0.63	0.0568	0.0474
Q87VE5	PSPTO_4992	generic Enzymes	Cytoplasmic	0.20	0.0492	0.0440
Q87UL0	PSPTO_5286	Generic Enzymes	Cytoplasmic	0.43	0.0026	0.0096
Q87UK3	PSPTO_5293	Generic Enzymes	Cytoplasmic	0.63	0.0181	0.0253
Q87UA9	rfbB-2	Generic Enzymes	Cytoplasmic	0.55	0.0559	0.0470
Q887F9	PSPTO_1337	Generic Enzymes	Cytoplasmic membrane	0.32	0.0212	0.0273
Q882Y0	PSPTO_2492	Generic Enzymes	Cytoplasmic membrane	0.64	0.0031	0.0104
Q87X27	sodB	Generic Enzymes	Periplasmic	0.47	0.0328	0.0348
Q88B64	PSPTO_0155	Generic Enzymes	Unknown	0.66	0.0010	0.0061
Q886L8	PSPTO_1559	Generic Enzymes	Unknown	0.52	0.0037	0.0114
Q884M3	PSPTO_2065	Generic Enzymes	Unknown	0.54	0.0121	0.0200
Q87Y84	PSPTO_3919	Generic Enzymes	Unknown	0.52	0.0044	0.0121
Q87Y54	PSPTO_3955	Generic Enzymes	Unknown	0.44	0.0039	0.0116
Q888E9	rfbC-1	Generic Enzymes	Unknown	0.58	0.0039	0.0116
Q88AQ2	algB	Genetic regulation	Cytoplasmic	0.56	0.0120	0.0199
P0A105	capB	Genetic regulation	Cytoplasmic	0.51	0.0001	0.0022
Q888P8	dksA	Genetic regulation	Cytoplasmic	0.54	0.0065	0.0144
Q87VJ4	hfq	Genetic regulation	Cytoplasmic	0.49	0.0006	0.0043
Q87VA6	pilH	Genetic regulation	Cytoplasmic	0.49	0.0206	0.0270
Q88BF1	PSPTO_0066	Genetic regulation	Cytoplasmic	0.28	0.0014	0.0073
Q887L7	PSPTO_1274	Genetic regulation	Cytoplasmic	0.35	0.0000	0.0005
Q883I1	PSPTO_2376	Genetic regulation	Cytoplasmic	0.43	0.0000	0.0005
Q87Y32	PSPTO_3980	Genetic regulation	Cytoplasmic	0.33	0.0514	0.0454
Q87WW6	PSPTO_4427	Genetic regulation	Cytoplasmic	0.36	0.0000	0.0007
Q886Z1	PSPTO_1433	Genetic regulation	Unknown	0.12	0.0275	0.0312
Q886M7	accA	Lipid metabolism	Cytoplasmic	0.44	0.0183	0.0254
Q883Y6	fabA	Lipid metabolism	Cytoplasmic	0.67	0.0056	0.0135

Q883Y7	fabB	Lipid metabolism	Cytoplasmic	0.49	0.0013	0.0072
Q87YG6	fabD	Lipid metabolism	Cytoplasmic	0.32	0.0049	0.0122
Q87VW7	lipA	Lipid metabolism	Cytoplasmic	0.38	0.0472	0.0431
Q87VS5	accB	Lipid metabolism	Cytoplasmic membrane	0.60	0.0004	0.0040
Q87YG8	fabF	Lipid metabolism	Cytoplasmic membrane	0.57	0.0251	0.0296
Q87YE3	PSPTO_3857	Lipid metabolism	Cytoplasmic membrane	0.20	0.0393	0.0392
Q87V73	ahcY	Nitrogen metabolism	Cytoplasmic	0.52	0.0155	0.0231
Q88AR3	argE-2	Nitrogen metabolism	Cytoplasmic	0.47	0.0228	0.0281
Q88B94	argH	Nitrogen metabolism	Cytoplasmic	0.60	0.0107	0.0192
Q87VS6	aroQ	Nitrogen metabolism	Cytoplasmic	0.24	0.0000	0.0007
Q885A6	cynS	Nitrogen metabolism	Cytoplasmic	0.32	0.0009	0.0060
Q882E8	gabD-3	Nitrogen metabolism	Cytoplasmic	0.59	0.0309	0.0334
Q87WC1	glyA2	Nitrogen metabolism	Cytoplasmic	0.63	0.0094	0.0178
Q87YJ0	ilvA-1	Nitrogen metabolism	Cytoplasmic	0.66	0.0490	0.0440
Q888N5	ilvN	Nitrogen metabolism	Cytoplasmic	0.33	0.0518	0.0454
Q886Y1	leuA	Nitrogen metabolism	Cytoplasmic	0.58	0.0356	0.0366
Q87V72	metF	Nitrogen metabolism	Cytoplasmic	0.42	0.0048	0.0121
Q881Z7	metH	Nitrogen metabolism	Cytoplasmic	0.50	0.0569	0.0474
Q885T7	mtnA	Nitrogen metabolism	Cytoplasmic	0.60	0.0119	0.0199
Q87VV6	proA	Nitrogen metabolism	Cytoplasmic	0.58	0.0001	0.0015
Q88BC5	PSPTO_0092	Nitrogen metabolism	Cytoplasmic	0.55	0.0099	0.0181
Q88A78	PSPTO_0517	Nitrogen metabolism	Cytoplasmic	0.64	0.0278	0.0313
Q886Y5	PSPTO_1440	Nitrogen metabolism	Cytoplasmic	0.58	0.0086	0.0168
Q886P6	PSPTO_1531	Nitrogen metabolism	Cytoplasmic	0.56	0.0201	0.0268
Q885B4	PSPTO_1921	Nitrogen metabolism	Cytoplasmic	0.66	0.0326	0.0347
Q883P8	PSPTO_2302	Nitrogen metabolism	Cytoplasmic	0.39	0.0486	0.0437
Q87YN8	PSPTO_3757	Nitrogen metabolism	Cytoplasmic	0.48	0.0472	0.0431
Q87UX1	PSPTO_5171	Nitrogen metabolism	Cytoplasmic	0.43	0.0150	0.0226
Q87UI9	PSPTO_5308	Nitrogen metabolism	Cytoplasmic	0.36	0.0072	0.0149
Q88AD4	soxA-1	Nitrogen metabolism	Cytoplasmic	0.59	0.0425	0.0413
Q886U5	thrC	Nitrogen metabolism	Cytoplasmic	0.51	0.0435	0.0417
Q88B60	trpA	Nitrogen metabolism	Cytoplasmic	0.53	0.0484	0.0436
Q88AE7	betA	Nitrogen metabolism	Cytoplasmic membrane	0.33	0.0355	0.0366
Q87WP4	carB	Nitrogen metabolism	Periplasmic	0.63	0.0244	0.0290
Q889P8	metC-1	Nitrogen metabolism	Periplasmic	0.66	0.0202	0.0269
Q87V18	gltB	Nitrogen metabolism	Unknown	0.54	0.0464	0.0429
Q87VZ0	amn	Nucleic acid metabolism	Cytoplasmic	0.58	0.0034	0.0109
Q886H7	cdd	Nucleic acid metabolism	Cytoplasmic	0.48	0.0005	0.0040
Q87XN2	dcd	Nucleic acid metabolism	Cytoplasmic	0.54	0.0092	0.0176
Q886M8	dnaE	Nucleic acid metabolism	Cytoplasmic	0.41	0.0549	0.0464
Q87WP5	greA	Nucleic acid metabolism	Cytoplasmic	0.56	0.0010	0.0062
Q886X5	guaA	Nucleic acid metabolism	Cytoplasmic	0.66	0.0174	0.0245
Q889Y3	nusG	Nucleic acid metabolism	Cytoplasmic	0.43	0.0003	0.0034
Q87VI6	orn	nucleic acid metabolism	Cytoplasmic	0.34	0.0014	0.0073
Q87VH3	parE	Nucleic acid metabolism	Cytoplasmic	0.17	0.0331	0.0348
Q88BE5	PSPTO_0072	Nucleic acid metabolism	Cytoplasmic	0.64	0.0019	0.0083
Q88BB5	PSPTO_0102	nucleic acid metabolism	Cytoplasmic	0.37	0.0003	0.0031
Q887M5	PSPTO_1266	Nucleic acid metabolism	Cytoplasmic	0.52	0.0322	0.0345
Q885C6	PSPTO_1909	Nucleic acid metabolism	Cytoplasmic	0.60	0.0017	0.0078
Q883M5	PSPTO_2331	Nucleic acid metabolism	Cytoplasmic	0.24	0.0206	0.0270
Q881V3	PSPTO_2779	Nucleic acid metabolism	Cytoplasmic	0.52	0.0388	0.0389
Q87W05	PSPTO_4778	Nucleic acid metabolism	Cytoplasmic	0.34	0.0064	0.0144

Extracellular Reduced Abundance

Q87VG4	PSPTO_4973	Nucleic acid metabolism	Cytoplasmic	0.44	0.0001	0.0013
Q87VJ9	purA	Nucleic acid metabolism	Cytoplasmic	0.54	0.0538	0.0458
Q87Y59	purC	Nucleic acid metabolism	Cytoplasmic	0.61	0.0582	0.0480
Q87YI6	purF	Nucleic acid metabolism	Cytoplasmic	0.26	0.0530	0.0454
Q87XM1	pyrC	Nucleic acid metabolism	Cytoplasmic	0.39	0.0002	0.0028
Q87WU0	rpoN	nucleic acid metabolism	Cytoplasmic	0.38	0.0456	0.0427
Q87YM9	sbcC	Nucleic acid metabolism	Cytoplasmic	0.50	0.0145	0.0221
Q889U1	ssb	Nucleic acid metabolism	Cytoplasmic	0.42	0.0018	0.0080
Q87ZB5	topA	Nucleic acid metabolism	Cytoplasmic	0.42	0.0037	0.0116
Q889U3	uvrA	Nucleic acid metabolism	Cytoplasmic	0.20	0.0458	0.0428
Q886V7	purT	Nucleic acid metabolism	Cytoplasmic membrane	0.62	0.0004	0.0038
Q87YX7	PSPTO_3665	Nucleic acid metabolism	Unknown	0.58	0.0005	0.0040
Q87U21	purE	Nucleic acid metabolism	Unknown	0.59	0.0156	0.0231
Q87ZS1	clpA	Protein synthesis and modification	Cytoplasmic	0.24	0.0599	0.0487
Q87YR6	clpP	Protein synthesis and modification	Cytoplasmic	0.38	0.0006	0.0043
Q87YQ2	cysS	Protein synthesis and modification	Cytoplasmic	0.37	0.0466	0.0429
Q886P0	frr	Protein synthesis and modification	Cytoplasmic	0.39	0.0053	0.0128
Q87X13	groES	Protein synthesis and modification	Cytoplasmic	0.51	0.0001	0.0023
Q886Y9	hisS	Protein synthesis and modification	Cytoplasmic	0.24	0.0260	0.0305
Q87ZS2	infA	Protein synthesis and modification	Cytoplasmic	0.09	0.0012	0.0068
Q881Z4	nfuA	Protein synthesis and modification	Cytoplasmic	0.47	0.0026	0.0096
Q87YQ0	ppiB	Protein synthesis and modification	Cytoplasmic	0.51	0.0008	0.0054
Q87WH1	prfC	Protein synthesis and modification	Cytoplasmic	0.35	0.0425	0.0413
Q88AH8	PSPTO_0412	Protein synthesis and modification	Cytoplasmic	0.45	0.0264	0.0308
Q889E2	PSPTO_0808	Protein synthesis and modification	Cytoplasmic	0.37	0.0145	0.0221
Q887W2	PSPTO_1171	Protein synthesis and modification	Cytoplasmic	0.56	0.0131	0.0209
Q887T1	PSPTO_1205	Protein synthesis and modification	Cytoplasmic	0.45	0.0002	0.0027
Q87WG9	PSPTO_4581	Protein synthesis and modification	Cytoplasmic	0.53	0.0031	0.0103
Q889X0	rplD	Protein synthesis and modification	Cytoplasmic	0.51	0.0001	0.0022
Q889U5	rplQ	Protein synthesis and modification	Cytoplasmic	0.51	0.0014	0.0073
Q889W6	rplV	Protein synthesis and modification	Cytoplasmic	0.65	0.0063	0.0143
Q889W9	rplW	Protein synthesis and modification	Cytoplasmic	0.56	0.0188	0.0256
Q889F2	rpmA	Protein synthesis and modification	Cytoplasmic	0.63	0.0045	0.0121
Q87XJ5	rpmE2	Protein synthesis and modification	Cytoplasmic	0.36	0.0232	0.0282
Q87YG4	rpmF	Protein synthesis and modification	Cytoplasmic	0.43	0.0002	0.0027
Q88BC7	rpmG	Protein synthesis and modification	Cytoplasmic	0.51	0.0211	0.0273

Extracellular Reduced Abundance

P0A163	rpmI	Protein synthesis and modification	Cytoplasmic	0.57	0.0013	0.0071
Q87VK3	rpsF	Protein synthesis and modification	Cytoplasmic	0.66	0.0149	0.0225
Q889U9	rpsM	Protein synthesis and modification	Cytoplasmic	0.60	0.0073	0.0149
Q889V8	rpsN	Protein synthesis and modification	Cytoplasmic	0.56	0.0170	0.0243
Q889W2	rpsQ	Protein synthesis and modification	Cytoplasmic	0.54	0.0000	0.0007
Q87VK4	rpsR	Protein synthesis and modification	Cytoplasmic	0.58	0.0017	0.0077
Q889W7	rpsS	Protein synthesis and modification	Cytoplasmic	0.38	0.0020	0.0086
Q87VV8	rsfS	Protein synthesis and modification	Cytoplasmic	0.52	0.0238	0.0287
Q883H9	thrS	Protein synthesis and modification	Cytoplasmic	0.44	0.0463	0.0429
Q889Y8	tyrS	Protein synthesis and modification	Cytoplasmic	0.29	0.0466	0.0429
Q886Y6	der	Protein synthesis and modification	Cytoplasmic membrane	0.36	0.0121	0.0200
Q87Y90	PSPTO_3911	Protein synthesis and modification	Periplasmic	0.61	0.0048	0.0121
Q87YK7	pepN	Protein synthesis and modification	Unknown	0.66	0.0221	0.0277
Q87ZJ2	PSPTO_3437	Protein synthesis and modification	Unknown	0.62	0.0004	0.0038
Q883Y2	sixA	Protein synthesis and modification	Unknown	0.60	0.0133	0.0211
Q88B81	PSPTO_0138	Transport	Cytoplasmic	0.59	0.0038	0.0116
Q87UL2	ptsP	Transport	Cytoplasmic	0.32	0.0383	0.0385
Q87WB5	cstA	Transport	Cytoplasmic membrane	0.27	0.0381	0.0385
Q886V3	ffh	Transport	Cytoplasmic membrane	0.59	0.0132	0.0211
Q882M2	PSPTO_2604	Transport	Cytoplasmic membrane	0.17	0.0420	0.0412
Q882C4	PSPTO_2705	Transport	Cytoplasmic membrane	0.28	0.0296	0.0325
Q87X85	PSPTO_4303	Transport	Cytoplasmic membrane	0.11	0.0120	0.0199
Q87U15	PSPTO_5500	Transport	Cytoplasmic membrane	0.28	0.0252	0.0297
Q884E0	pvdE	Transport	Cytoplasmic membrane	0.20	0.0523	0.0454
Q87X84	saxB	Transport	Cytoplasmic membrane	0.12	0.0266	0.0308
Q87TS1	yidC	Transport	Cytoplasmic membrane	0.27	0.0610	0.0492
Q88B54	PSPTO_0165	Unknown function	Cytoplasmic	0.51	0.0165	0.0239
Q88AI2	PSPTO_0408	Unknown function	Cytoplasmic	0.63	0.0057	0.0135
Q888P1	PSPTO_0976	Unknown function	Cytoplasmic	0.35	0.0370	0.0378
Q888M8	PSPTO_0989	Unknown function	Cytoplasmic	0.38	0.0115	0.0197
Q884H7	PSPTO_2116	Unknown function	Cytoplasmic	0.51	0.0132	0.0211
Q883N5	PSPTO_2315	Unknown function	Cytoplasmic	0.31	0.0025	0.0096
Q87ZM9	PSPTO_3395	Unknown function	Cytoplasmic	0.47	0.0072	0.0149
Q87YH7	PSPTO_3821	Unknown function	Cytoplasmic	0.65	0.0095	0.0178
Q87XB5	PSPTO_4272	Unknown function	Cytoplasmic	0.53	0.0433	0.0417
Q87WV9	PSPTO_4434	Unknown function	Cytoplasmic	0.65	0.0069	0.0147
Q87WP6	PSPTO_4499	Unknown function	Cytoplasmic	0.54	0.0005	0.0041
Q87UA1	PSPTO_5404	Unknown function	Cytoplasmic	0.57	0.0064	0.0144
Q88BW6	PSPTO_5633	Unknown function	Cytoplasmic	0.52	0.0040	0.0117
Q889R6	PSPTO_0683	Unknown function	Cytoplasmic membrane	0.45	0.0030	0.0102
Q87ZU1	PSPTO_3333	Unknown function	Cytoplasmic membrane	0.26	0.0274	0.0312
Q87U63	PSPTO_5451	Unknown function	Cytoplasmic membrane	0.32	0.0279	0.0313

Extracellular Reduced Abundance

Q87VU6	PSPTO_4839	Unknown function	Outer membrane	0.23	0.0617	0.0495
Q882W9	PSPTO_2503	Unknown function	Periplasmic	0.31	0.0076	0.0154
Q87WQ9	PSPTO_4484	Unknown function	Periplasmic	0.66	0.0124	0.0202
Q88B25	PSPTO_0208	Unknown function	Unknown	0.64	0.0115	0.0197
Q88AJ9	PSPTO_0391	Unknown function	Unknown	0.33	0.0071	0.0149
Q88A18	PSPTO_0579	Unknown function	Unknown	0.44	0.0031	0.0103
Q888X0	PSPTO_0894	Unknown function	Unknown	0.42	0.0454	0.0427
Q888R9	PSPTO_0947	Unknown function	Unknown	0.49	0.0208	0.0272
Q888P2	PSPTO_0975	Unknown function	Unknown	0.58	0.0287	0.0319
Q888L9	PSPTO_0998	Unknown function	Unknown	0.46	0.0000	0.0007
Q887F2	PSPTO_1344	Unknown function	Unknown	0.59	0.0073	0.0149
Q886D3	PSPTO_1646	Unknown function	Unknown	0.32	0.0376	0.0381
Q885M3	PSPTO_1808	Unknown function	Unknown	0.31	0.0048	0.0121
Q885A5	PSPTO_1931	Unknown function	Unknown	0.58	0.0148	0.0225
Q883J1	PSPTO_2366	Unknown function	Unknown	0.62	0.0357	0.0367
Q882W6	PSPTO_2506	Unknown function	Unknown	0.57	0.0048	0.0121
Q881L7	PSPTO_2872	Unknown function	Unknown	0.48	0.0432	0.0417
Q881L6	PSPTO_2873	Unknown function	Unknown	0.34	0.0599	0.0487
Q87Z85	PSPTO_3545	Unknown function	Unknown	0.65	0.0220	0.0277
Q87YK9	PSPTO_3786	Unknown function	Unknown	0.52	0.0009	0.0060
Q87XZ0	PSPTO_4030	Unknown function	Unknown	0.62	0.0028	0.0098
Q87W03	PSPTO_4780	Unknown function	Unknown	0.56	0.0528	0.0454
Q87V70	PSPTO_5071	Unknown function	Unknown	0.60	0.0000	0.0005
Q87UT9	PSPTO_5203	Unknown function	Unknown	0.58	0.0193	0.0261
Q87US2	PSPTO_5224	Unknown function	Unknown	0.32	0.0066	0.0144
Q87UF7	PSPTO_5341	Unknown function	Unknown	0.28	0.0497	0.0443
D3NQ14	PSPTO_5634	Unknown function	Unknown	0.32	0.0004	0.0036
Q87Y08	PSPTO_4010	Virulence	Cytoplasmic	0.54	0.0170	0.0243
Q87U75	PSPTO_5433	Virulence	Cytoplasmic	0.61	0.0059	0.0138
Q87U73	hcp-2	Virulence	Extracellular	0.56	0.0000	0.0007
Q52473	hrpA1	Virulence	Extracellular	0.55	0.0438	0.0418
Q87U86	PSPTO_5421	Virulence	Unknown	0.59	0.0001	0.0022

APPENDIX C. Copyright Licenses of figures from other publications

Figure	Publication	Journal	Publisher	License
I.1	Campbell et al. (2017)	Ecology and Society	Resilience Alliance	Creative Commons Attribution-NonCommercial 4.0 International License
I.2	Fowler et al. (2013)	Philosophical Transactions of the Royal Society B	The Royal Society	1436479-1
I.3	Grant et al. (2006)	Annual Review of Microbiology	Annual Reviews	1436372-1
I.4	Masson-Boivin et al. (2009)	Trends in Microbiology	ElSevier	5705541229309
I.5	Oldroyd (2013)	Nature Reviews Microbiology	Springer Nature	5705321396519
	K. M. Jones et al. (2007)	Nature Reviews Microbiology	Springer Nature	5705411433842
I.6	Geddes and Oresnik (2007)	Canadian Journal of Microbiology	Canadian Science Publishing	1436406-1
I.7	Jun et al. (2016)	Applied and Environmental Microbiology	American Society for Microbiology	Creative Commons Attribution-NonCommercial 4.0 International License
I.8	Morris et al. (2013)	Annual Review of Phytopathology	Annual Reviews	1436382-1
	Xin and He (2013)	Annual Review of Phytopathology	Annual Reviews	1436384-1
I.9	Kohlstedt and Wittmann (2019)	Metabolic Engineering	ElSevier	Creative Commons CC-BY Attribution-4.0 International License
I.10	Sondermann et al. (2012)	Current Opinion in Microbiology	ElSevier	5705540503497
I.11	Jeffery (2004)	Current Opinion in Structural Biology	ElSevier	5705541082923
I.12	Ebner and Götz (2019)	Trends in Microbiology	ElSevier	5705540190299
I.13	Malay et al. (2009)	Acta Crystallographica Section F Structural Biology and Crystallization Communications	IUCr	n/a
I.14	Seidler et al. (2013)	n/a	Springer	1436486-1

FIGURE INDEX

TABLE INDEX

ABBREVIATION INDEX

°C	degrees celsius
2K6PG	6-phospho-2-ketogluconate
2KDPG	2-keto-3-deoxy-6-phosphogluconate
3PG	3-phosphoglycerate
4-PE	4-phosphoerythronate
6PG	6-phosphogluconate
6PG	6-phosphogluconolactone
Å	Angstrom
Ac-CoA	acetyl-coenzyme A
ADP	adenosine diphosphate
ANOVA	analysis of variance
Ap	ampicillin
APS	ammonium persulfate
ATP	adenosine triphosphate
aux	auxotroph
BCP	1-bromo-3-chloropropane
BNF	biological nitrogen fixation
BPG	1,3-bisphosphoglycerate
BSA	bovin serum albumin
C	carbon
c-di-GMP, cdG	Bis-(3′,5′)-cyclic dimeric guanosine monophosphate
cDNA	complementary DNA
CF	calcofluor
cfu	colony forming unit
cm^2	square centimeter
CP	cytoplasmic protein
CPS	capsular polysaccharide
CR	Congo red
Ct	cycle threshold
CV	column volume
Cys	cysteine
DA	differentially abundant
DAPA	diaminopimelic acid
DEPC	diethyl pyrocarbonate
DGC	diguanylate cyclases
DHAP	dihydroxyacetone-P
DNA	deoxyribonucleic acid
dNTP	deoxynucleotide triphosphate
dpi	days post-inoculation
DTT	dithiothreitol
DXP	1-deoxy-D-xylulose-5-phosphate
E4P	D-erythrose 4-phosphate
E4PDH, Epd	erythrose-4-phosphate dehydrogenase
ECP	exported cytoplasmic protein
ED	Entner-Doudoroff
EDTA	Ethylenediamine tetraacetic acid
EF-Tu	elongation factor Tu
EM	electron microscopy
Em	erythromycin
EMP	Embden-Meyerhof-Parnas
EPS	exopolysaccharide
F6P	fructose-6-phosphate
FbaA	fructose-bisphosphate aldolase
FBP	fructose-1,6-bisphosphate
fru	fructose
g	relative centrifugal force
G3P	glyceraldehyde-3-phosphate
G6P	glucose-6-phosphate
GABA	gamma-aminobutyric acid
gal	galactose

GAPDH, Gap	glyceraldehyde-3-phosphate dehydrogenase
GL	gluconolactone
Glu	glucose
GMP	guanosine monophosphate
GTP	guanosine-5'-triphosphate
h	hour
IA	increased abundance
ID	identifier
IPTG	isopropyl β-D-1-thiogalactopyranoside
kb	kilobases
kDA	kilodalton
KEGG	Kyoto Encyclopedia of Genes and Genomes
Km	kanamycin
kV	kilovolts
l	liter
LB	Luria-Bertani media
LC	liquid chromatography
LC-MS-MS	liquid chromatography with tandem mass spectrometry
LPS	lipopolysaccharide
M	molybdenum
MAMP	microbe associated molecular pattern
mg	milligrams
min	minutes
ml	milliliter
MLG	mixed-linkage β-glucan
mM	millimolar
MM	minimal media
MMPM	minimal media with mannitol and pyruvate
MPA	mobile phase A
MPB	mobile phase B
MS	mass spectrometry
MV	membrane vesicle
MWCO	molecular weight cutoff
N	nitrogen
NAD/H	nicotinamide adenine dinucleotide
NADP/H	nicotinamide adenine dinucleotide phosphate
NBD	nucleotide-binding domain
NCBI	National Center for Biotechnology Information
NI	non-inoculated
nm	nanometer
N_r	reactive nitrogen
Nx	nalidixic acid
OD	optical density
OMV	outer-membrane-vesicle
ONPG	*o*-nitrophenyl-β-D-galactopyranoside
ORF	open reading frame
P5P	pentose-5-phosphate
PAGE	polyacrylamide gel electrophoresis
PAMP	pathogen-associated molecular pattern
PBS	phosphate buffered saline
PCR	polymerase chain reaction
PDE	phosphodiesterase
PEP	phosphoenolpyruvate
PG-agar	peptone-glucose agar
pGpG	5'-phosphoguanylyl-(3'-5')-guanosine
PI	propidium iodide
P_{lac}	lac promoter
PLP	pyridoxal 5'-phosphate

PP	pentose phosphate
pS	phosphoserine
pT	phosphothreonine
PTM	post-translational modification
Pto	*Pseudomonas syringae* pv.tomato
P_{gap*}	*gap* gene promoter
pY	phosphotyrosine
PYR	pyruvate
qRT-PCR	quantitative real-time PCR
^{R}	resistant
R5P	ribose-5-phosphate
RA	reduced abundance
Ret	*Rhizobium etli*
Rif	rifampicin
RNA	deoxyribonucleic acid
RT	room-temperature
s	seconds
^{S}	sensitive
S7P	sedoheptulose-7-phosphate
SDS	sodium dodecyl-sulfate
Ser	serine
Sm	Streptomycin
Spc	Spectinomycin
Suc	succinate
T2SS	type II secretion system
T3SS	type III secretion system
T4SS	type IV secretion system
T6SS	type VI secretion system
TBS	tris-buffered saline
Tc	tetracycline
TCA	tricarboxylix acid
TCA	trichloroacetic acid
TCEP	tris(2-carboxyethyl)phosphine hydrochloride
TEMED	tetramethylethylenediamine
Tmp	trimethoprim
TY	triptone-yeast medium
U	units
UV	ultra-violet
V	vesicle
V	volt
WB	western blot
X-Gal	5-bromo-4-chloro-3-indolyl-β D-galactopyranoside
ε	molar extinction coefficient
µg	microgram
µl	microliter